AN ABSTRACT OF THE THESIS OF

Annapoorna Akella for the degree of Doctor of Philosophy in Chemistry presented on 10 October 1994.

Title: Synthesis and Characterization of New Optical Frequency Converters and Phosphor Hosts

Redacted for Privacy

Abstract approved: _____
Douglas A. Keszler

The emphasis of this work has been in two areas of optical materials - the crystal-chemical development of new optical frequency converters and new hosts for phosphors.

The study encompasses a range of materials - borates, borate fluorides, silicates, silicate fluorides, germanate fluorides, phosphate fluorides, vanadate fluorides, and organic aminoguanidinium salts.

The crystal chemistry of the noncentrosymmetric Nb and Ta oxide pyroborate series was systematically investigated. In the pyroborate series $K_xRb_{1-x}NbOB_2O_5$ and $Rb_{1-x}Cs_xNbOB_2O_5$, the structural variability of the pyroborate group results in materials of differing nonlinearities and birefringence. The crystal structures of $CsNb(Ta)OB_2O_5$ were determined.

The borates $Ba_2Mg(BO_3)_2$ and $K_2Zr(BO_3)_2$ were found to be isostructural to the mineral buetschliite and the borate $Ba_2Ca(BO_3)_2$ crystallizes as a

distorted version of buetschliite. The lanthanide ion Eu^{2+} when doped in $Ba_2Mg(BO_3)_2$ luminesces with a large Stokes shift.

The crystal structures of four aminoguanidinium salts were solved; one of these lead to the structure revision of aminoguanidinium bicarbonate as N-carboxy aminoguanidinium monohydrate.

The solid solution of the noncentrosymmetric borate fluorides $Ba_{7-x}Sr_x(BO_3)_3F_5$ has been investigated. The crystal structures for x = 3 and 4 were determined.

The sub-cell structure of the noncentrosymmetric compound $BaCaBO_3F$ has been solved. It was found by precession methods that this material exists as a 3 × 3 × 3 supercell. The crystallographic site symmetry of the subcell make it an attractive host for lanthanide ions in their +3 oxidation state.

The crystal structure of the new silicate $Li_4SrCa(SiO_4)_2$ and the optical properties of this new silicate host when doped with Eu^{2+} have been studied. The crystal structure of the new silicate fluoride Sr_2LiSiO_4F and an uncommon Eu^{2+} luminescence from this host is described. The crystal structure of the alkaline-earth germanate fluoride $Sr_4Ge_2O_7F_2$, and an unprecedented Eu^{3+} luminescence from the distorted Sr sites is described.

Synthesis and Characterization of New Optical Frequency Converters and Phosphor Hosts

by

Annapoorna Akella

A THESIS

submitted to

Oregon State University

in partial fulfillment of

the requirements for the

degree of

Doctor of Philosophy

Completed 10 October 1994

Commencement June 1995

APPROVED:

Redacted for Privacy

Professor of Chemistry in charge of major

Redacted for Privacy

Head of Department of Chemistry

Redacted for Privacy

Dean of Graduate School

Date thesis is presented 10 October 1994

Typed by Annapoorna Akella for Annapoorna Akella

To,
Sayee, Satyavathi and Sankaram

Acknowledgments

I would like to acknowledge my parents Satyavathi and Sankaram, my brother Sayee, my sisters Lakshmi and Surya for their tremendous support and inspiration. I would like to acknowledge my husband Chris for his friendship and help throughout this period.

I would like to acknowledge my major Professor Doug Keszler, for the assistance and freedom he provided me during my graduate work. It has been very enjoyable to have the opportunity to work with him. I would like to acknowledge my former colleagues Ted Alekel, Kathleen Schaffers and Jim Cox for introducing me to Solid State Chemistry. I would also like to acknowledge the present members of Keszler group Jun-ming Tu, Kimberley Dahm, Anthony Diaz, Ken Vandenberghe, Ki-Seog Chang and Greg Patterson.

I would like to acknowledge Sasirekha Kodialam for the coffee breaks and help with the Seimens.

TABLE OF CONTENTS

LIST OF FIGURES

LIST OF TABLES

Synthesis and Characterization of New Optical Frequency Converters and Phosphor Hosts

CHAPTER 1
Introduction

The study of nonlinear optics undewent a rapid growth in 1960, after the invention of the first laser. It was the laser that provided electric field strengths comparable to interatomic fields, so that spectacular effects such as second harmonic up-conversion of infrared radiation to visible light could be demonstrated. By using crystals, vapours and liquids, new wavelengths extending from the far-infrared to the ultraviolet were soon being created by second harmonic generation, sum and difference mixing, and stimulated Raman scattering. Nonlinear optical effects became available at the milliwatt optical power level in semiconductors, organics, photorefractives, liquid crystals, and glass fibres. These have opened new possibilities for exploiting light in communications, image processing and general purpose computing. The use of lasers is well known - bar code readers, compact disc players, and laser printers. The use of lasers in medical surgery has become more routine in recent times. The standard materials for the generation of new frequencies are high optical quality single crystals that utilize nonresonant 'bound electron' interactions with input and output light in the transparency range of the material. An essentially instantaneous response is necessary for wavelength

conversion since the polarization of the crystal needs to be modulated at the new optical frequency. Nonlinear optics is now a vast and cross-disciplinary subject involving a multitude of different materials, phenomena, and applications. The physics of nonlinear optics imposes severe demands on potential materials allowing the exploration for new materials that meet these demands.

The emphasis of my thesis work involves two areas of optical materials, the crystal-chemical development of new optical frequency converters and hosts for phosphors. Our interest in preparing new phosphor hosts will be discussed in detail in the latter part of the introduction.

A method has been developed in this laboratiory to identify promising frequency-doubling materials by estimation of nonlinear susceptibilities from elementary calculations and visual inspection of crystal structures.[1] A description and application of this method on materials developed in this laboratory are discussed in Chapter 2. In Chapters 3 through 6, the crystal chemistry, structures, and characteristics of six new potential frequency converters are presented. All these materials differ from each other in the chromophores that are reponsible for frequency conversion. In Chapter 7, I describe attempts to produce for new organic nonlinear optical materials in the aminoguanidinium series. The crystal structures of three new aminoguanidinium compounds and the crystal structure revision of the

compound N-carboxy aminoguanidinium hydrate previously reported as aminoguanidinium bicarbonate are discussed. The latter section of the dissertation starting from Chapter 8 is focussed on hosts for luminescent phosphors. The compounds $Ba_2Mg(BO_3)_2$ and $K_2Zr(BO_3)_2$ in Chapters 8 and 10 are the borate derivatives of the mineral buetschliite $K_2Ca(CO_3)_2$. The crystal structures and an unusual Eu^{2+} luminescence in $Ba_2Mg(BO_3)_2$ are discussed in these chapters. In Chapter 8, I discuss the unusual crystal structure of $Ba_2Ca(BO_3)_2$, which is a potential host for Cr^{3+} lasing. In Chapter 11, the structure of the first germanate fluoride $Sr_4Ge_2O_7F_2$ and the unusual luminescence of Eu^{3+} are described. In Chapter 12, the structure of the new silicate fluoride Sr_2LiSiO_4F and an uncommon Eu^{2+} luminescence are detailed. In Chapter 12, the structural and optical features of the silicate $Li_4SrCa(SiO_4)_2$ are presented. The Appendix contains crystal and experimental data on new noncenterosymmetric compounds having formulations similar to that of tentatively identified $Li_2BaCaSi_2O_7$.

Section I. Optical Frequency Converters (SHG)

The optical conversion of light from one frequency to another by crystalline nonlinear optical (NLO) materials (Figure 1.1) has been the primary focus of my research. Frequency conversion of laser light was first witnessed in a quartz crystal in 1961[2] following the discovery of the laser. Laser light can be converted from one frequency to another by using nonlinear optical materials, thus significantly increasing the range of applications. Light generated at shorter wavelengths is necessary for applications in chemical and physical research as well as in a number of industrial applications.

The power ($P_{2\omega}$) in second harmonic generation (SHG) from a crystal of length L, may be approximated by Eq. 1.1,[3]

$$P_{2\omega} \propto P_{\omega}^2 \cdot L^2 \cdot d_{jm}^2 \exp\{-L(\alpha_{\omega}+\frac{1}{2}\alpha_{2\omega})\}\,[\frac{\sin^2 L\cdot\Delta K/2}{(L\cdot\Delta K/2)^2}] \qquad [Eq.\ 1.1]$$

where P_{ω} is the power of the incident beam, d_{jm} is the SHG coefficient, α_{ω} is the absorption coefficient of the crystal at the fundamental wavelength, $\alpha_{2\omega}$ is the absorption coefficient of the crystal at the second harmonic wavelength, and ΔK is the wave vector mismatch between the fundamental and second harmonic waves. The exponential term approximates the absorption characteristics of the NLO crystal and the *sin* term describes the ability to

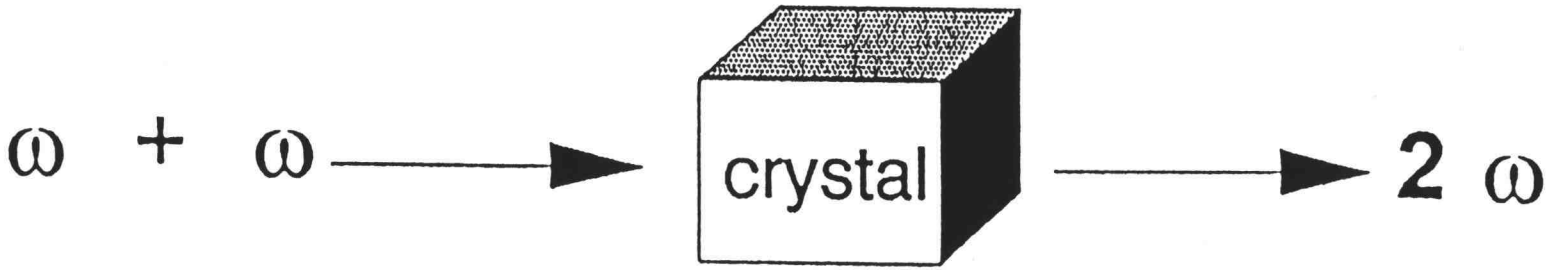

Figure 1.1. Frequency conversion of light via a crystalline medium.

phase match the incoming and doubled waves. It is evident from Equation 1.1. that high powers can be obtained in the second harmonic wave with a large second harmonic coefficient. If the absorption bands of the crystal overlap either the fundamental or second harmonic wavelength, an exponential decrease in the output power will ensue. The phase mismatch between the fundamental and second harmonic waves affects the second harmonic output power.

The macroscopic second harmonic coefficient is defined as

$$d_{jm} \rightarrow \chi^{(2)}_{IJK}(\omega,\omega) = \frac{1}{V}\sum_{ijk} R_{Ii} R_{Jj} R_{Kk} \beta_{ijk}(\omega,\omega) \qquad [Eq.\ 1.2]$$

where V is the volume of the unit cell, the R direction cosines relate molecular coordinates to crystal coordinates, and the coefficients $\beta_{ijk}(\omega,\omega)$ are the microscopic hyperpolarizability tensor components for the relevant anionic groups.

$$\beta_{ijk}(\omega,\omega) = \frac{1}{4}h^2 \sum_{P}\sum_{e,e'} \frac{\langle g|\tilde{\mu}_i|e\rangle\langle e|\tilde{\mu}_j|e'\rangle\langle e'|\tilde{\mu}_k|g\rangle}{(\omega_e-\omega_g-2\omega)(\omega'-\omega_g-\omega)} \qquad [Eq.\ 1.3]$$

In Eq. 1.3. $|g\rangle$ represents a ground electronic state, and $|e\rangle$ and $|e'\rangle$ represent excited electronic states.

An explanation of Equation 1.3. may be gained by considering the *ijk*

subscripts for β; here, *ijk* can be 1, 2, or 3 (= *x*, *y*, or *z*). The subscript *i* indicates the direction of polarization induced by the incoming photons and the subscripts *j* and *k* signify the directions of electric polarization for the incoming photons. The quantity β_{333} describes the magnitude of polarization induced in the *z* direction when two photons also polarized along *z* are incident on a molecule. By permuting over all possible *ijk* values, every possible interaction is described.

For a material to qualify for efficient second harmonic conversion, it should possess a large second harmonic coefficient and the hyperpolarizability tensors must sum constructively. It should be noncentrosymmetric, since in a centrosymmetric crystal each positive β_{ijk} will have a negative partner $-\beta_{ijk}$ that will lead to Equation 1.2 summing to zero. The integrals specified in the numerator of Equation 1.3 represent the transition moments associated with the ground and excited states in the three-photon process. The denominator represents the differences in energies between the energy gaps and the fundamental and second harmonics.

All of these characteristics play an important role in dictating the utility of a new material, but they are only a few of the necessary chemical and mechanical properties that a material must possess to be a useful frequency doubler.

Other conditions that are desirable for applications include the following:

1. Congruent melting
2. Noncentrosymmetric lattice
3. Chemical stability
5. High optical quality
6. High damage threshold
7. Wide transparency range
8. Sufficient birefringence to achieve phase matching
9. Large nonlinear coefficients

An example of a borate that has been used commercially is the low-temperature form of barium borate (β-BaB_2O_4 or BBO) which functions as a frequency converter in the UV region.[4] BBO possesses large nonlinear coefficients (see Table 1.1), 3 to 6 times that of the well-known converter KH_2PO_4.[5] The fifth harmonic generation of 1.06 μm Nd:YAG to 213 nm has been demonstrated in BBO with 11% overall efficiency.[6]

Because of its low threshold power and capabilities as an efficient frequency converter at high powers, the borate LiB_3O_5 (LBO) has recently received considerable attention. LBO can achieve higher second harmonic efficiencies for mode-locked Nd : YAG lasers than $KTiOPO_4$ because of damage limitations in the latter crystal. Crystals of this material are relatively free of inclusions which greatly increases the optical damage threshold, giving

LBO the highest damage threshold of any solid-state frequency converter. Also, it has been shown to exhibit a threshold power for 50% conversion efficiency that is two orders of magnitude lower than that of KDP; it is optically transparent in the range 160 nm to 2.6 μm, making it useful for applications in the UV region.

The 3-dimensional borate framework of LBO is constructed from a condensation of B_3O_7 rings. An example of a similar condensation of B_3O_7 rings is seen in the compounds $BaLi(B_3O_5)_3$ and $BaNa(B_3O_5)_3$ which are presented in Chapter 6.

Table 1.1. Common Nonlinear Optical Materials

	Transmission Range (μm)	Damage Threshold (GW/cm^2)	Nonlinear Coefficient*	Threshold Power (MW)
KDP	0.20-1.5	6	d_{36}= 0.76	75
KTP	0.35-4.5	3	d_{31}= 13.5 d_{32}= 10.4 d_{33}= 28.4	0.1
$YAl_3(BO_3)_4$	0.16-4.5	-	d_{11}= 5.7	-
BBO	0.19-3.5	13.5	d_{11}= 4.1	90
LBO	0.16-2.6	25	d_{31}= 0.15 d_{32}= 2.97 d_{33}= 2.75	0.1

*$d_{mn} \times 10^9$ esu cm^{-3}

We have realized that the length L (eq 1.1.) of the crystal plays a crucial role in enhancing the output power in SHG process. We have predicted that by incorporating fluoride in a borate matrix the viscous borate melts could transform into fluid melts, facilitating preparation of large crystals.

We have examples of several borate fluorides prepared in this laboratory, one noteworthy example is the compound $BaCaBO_3F$. Large single crystals of this compound have been pulled at the rate of 2 mm/hr by Czochoralskii method at the LLNL. This compound when doped with Yb^{3+} has been shown to lase. The presence of fluoride in these materials allows for doping the alkaline-earth metal sites with lanthanides in the +3 oxidation level and achieving charge balance with substitution of O^{2-} for F^-. Such substitutions hardly diminish crystal optical quality, while producing remarkable optical properties. A sample of 2% Yb^{3+}:$BaCaBO_3F$ was initially prepared but due to lack of crystal growth facilities and optical measurement facilities the work was collaborated with Lawrence Livermore National Laboratory. The luminescence of $BaCaBO_3F$ with a variety of lanthanide metal ions is discussed in Chapter 3.

The structural variability of a pyroborate group to produce materials of differing nonlinearities and birefringence is described in Chapter 3. The compounds investigated are the series $K_xRb_{1-x}NbOB_2O_5$ and $Rb_{1-x}Cs_xNbOB_2O_5$. The solid solution of the nonocentrosymmetric borate fluorides $Ba_{7-x}Sr_x(BO_3)_3F_5$, derivatives of the compound $Ba_7(BO_3)_3F_5$,[7] has been systematically investigated

to determine the extent of solubility of Sr. The maximum extent of solubility was found to be at x = 4. The motivation in using Sr was to provide a material which is inexpensive and not hygroscopic, important characteristics for commercialization. A more detailed report pertaining to the crystal structure and solid solution results are presented in Chapter 5. An example of an organic nonlinear optical material aminoguanidinium tartarate is presented in Chapter 7. Noncentrosymmetry in a crystal has been incorporated through a chiral precursor L-tartaric acid.

Section II. Phosphor Hosts

Phosphors can be defined as materials that generate photoluminescence through an excitation energy conversion. Minimization of radiative energy losses, maximization of quantum efficiency, and achieving a desired color rendition are important considerations for phosphor materials. Loss of efficiency through nonradiative pathways can be reduced by isolating the active ions in the structure and by reducing the number of ions in the framework which can lead to quenching. For many types of displays phosphors must have robust UV and thermal stabilities.

The difference in energy between excitation and emission is referred to as the Stokes shift. In the harmonic approximation a large Stokes shift, in general, should lead to a very low quantum efficiency and quenching

temperature. Recently, however, an efficient luminescence has been observed in the material Eu^{2+}:$Ba_2LiB_5O_{10}$,[8] (a compound structurally characterized in this lab[9]) even though the Stokes shift is near 11,000 cm^{-1}. This efficient luminescence has been associated with an off-center occupation of the Ba dopant site by the Eu^{2+} ion and a breakdown of the harmonic model. To develop new materials that may exhibit similar behavior, new compounds containing structurally or electronically anisotropic sites have been identified. We have attempted to systematically analyze this type of Stokes shift in the compound $Ba_2Mg(BO_3)_2$. When doped with Eu^{2+} the compound $Ba_2Mg(BO_3)_2$ emits in the orange-red providing a large Stokes shift. The Eu^{2+}-doped silicate fluoride Sr_2LiSiO_4F exhibits a less dramatic Stokes shift but still emits bright green light, still an uncommon color for Eu^{2+}. The characteristics of this luminescence are presented in Chapter 12. The ion Eu^{3+} has been widely used as a red component in three-color lamps. The emission color of Eu^{3+} is strongly dependent on the site symmetry of the dopant site. For example, emission from Eu^{3+} materials may be orange or red. Blasse and coworkers have shown that for a Eu^{3+} ion occupying a site with a center of symmetry the orange predominates with a maximum intensity near 590 nm. If the Eu^{3+} resides in a site that lacks an inversion center, the red luminescence predominates with a maximum intensity near 610 nm. We have an unprecedented example of a new material $Sr_4Ge_2O_7F_2$; luminescence of Eu^{3+} in this material provides a peak

with maximum intensity in the IR region near 700 nm. We attribute this to the distorted Sr dopant sites. Details are discussed in chapter 12.

Synthesis and Characterization

Solid-state synthesis and solution reactions have been the methods used for the synthesis of new materials. New phases were identified by powder X-ray diffraction by using an automated Philips powder diffractometer. Single crystals of new materials were grown either from the melt or by adding a flux, depending on whether the material melted congruently or incongruently. The structure of the compound was determined by using data from an automated single crystal X-ray diffractometer. Optical properties were investigated for those materials having selected structural features. For noncentrosymmetric structures, a powder second harmonic experiment was performed to determine its approximate efficiency as a frequency converter. Excitation and emission spectra were recorded on suitably doped samples.

References

1. Schaffers, K. I. Ph.D. Thesis Oregon State University **1992**.

2. Franken, P., Hill, A., Peters, C., Weinreich, G. *Phys. Rev. Lett.* **1961**, *7*, 118.

3. Weber, M. J. *CRC Handbook of Laser Science and Technology*, "Section 1: Nonlinear Optical Materials", Boca Raton, Fla.: CRC Press, **1986**.

4. Chen, C., Wu, B., Jiang, A., You, G. *Sci. Sin., Ser B* **1985**, *28*, 235.

5. Eckardt, R. C., Masuda, H., Fan, Y. X., Byer, R. L. *IEEE J. Quantum Electron.* **1990**, *26*, 922.

6. Eimerl, D., Davis, L., Velsko, S., Graham, E. K., Zalkin, A. *J. Appl. Phys.* **1987**, *62*, 1968.

7. Alekel, T. Ph. D. Thesis Oregon State University **1993**.

8. Blasse, G. *Philips Technical Review* **1970**, *31*, 309.

CHAPTER 2
New Borate Structures for NLO Applications

Annapoorna Akella, Douglas A. Keszler,

Kathleen I. Schaffers, and Theodore Alekel III

Oregon State University, Department of Chemistry,

Corvallis, OR 97331-4003

Material Research Society Symposium Proceedings **1994**, *329*, 15.

Abstract

By considering selected examples of new structure types, guidelines are set forth for the synthesis of new solid-state inorganic borates that are likely to have desirable properties for nonlinear optical applications. The structures of two new, noncentrosymmetric orthoborate fluorides $BaCaBO_3F$ and $Ba_7(BO_3)_3F_5$ demonstrate a feasibility for controlling linear optical properties and for producing noncentrosymmetric borates that melt congruently. The structure of $SrLi(B_3O_5)_3$ represents an additional example of a noncentrosymmetric borate resulting from chirality of the B_3O_7 ring. In addition to potential practical value, crystals of the type $AMOB_2O_5$ (A = K, Rb, and Cs; M = Nb and Ta) provide a unique means for examining the structurally dependent interrelationships of linear and nonlinear optical properties.

Introduction

In this contribution, we present an overview of the structural chemistry of selected noncentrosymmetric borates that have been discovered in this lab. These materials have resulted from continuing efforts directed toward the development of new nonlinear optical materials.

Crystals of $YAl_3(BO_3)_4$ (YAB),[1] BaB_2O_4 (BBO),[2] and LiB_3O_5 (LBO)[3] are the commercially available examples of anhydrous borate nonlinear optical materials. Of these crystals, BBO and LBO have found widespread use. While they have rather modest nonlinear susceptibilities in comparison to other materials, their high damage thresholds, UV transparency, and adequate birefringence have made them particularly useful for the production of high-power coherent light over a broad range of wavelengths. Although each material is a simple borate, their applications in laser systems can be quite different. The crystal structure of BBO contains layers of B_3O_6 rings that produce both a larger birefringence and higher nonlinearities than those observed for LBO. The structure of LBO is built from B_3O_7 rings, but these rings are skewed from coplanarity, producing the reduced birefringence and smaller nonlinearities. The higher birefringence of BBO allows phasematched generation of the second through fifth harmonics of a 1.06-μm fundamental, while conversion with LBO is limited to the second and third harmonics where

its smaller birefringence makes it more efficient for these conversion processes. Optical parametric oscillators have been constructed with BBO, and high-power UV radiation has been produced by converting dye, Ti:sapphire, and argon laser light.

Given the commercial success of BBO and LBO and their seemingly complementary properties, one may inquire as to whether there is anything to be gained from the preparation of additional new borates. With the continuing requirements of new laser systems to produce unique wavelengths and higher powers comes a need for specific frequency conversion materials. No single material alone can satisfy the broad spectrum of applications already in existence. Because both BBO and LBO have no derivative chemistry, it is impossible to slightly alter their physical properties to satisfy the demands of a specific application. New structural types that could be chemically derivatized would allow subtle control over both nonlinear and linear properties, i.e., one could manipulate susceptibility coefficients and the magnitude of the birefringence through atomic substitutions within a given structural type. We provide examples of such derivatization with the structures discussed below.

Because BBO is the low-temperature phase of BaB_2O_4, and LiB_3O_5 undergoes a peritectic decomposition, each crystal is grown from a high-temperature solution. (BBO has recently been grown directly from the melt by using steep axial gradients.)[4] The production of BBO boules with a diameter

of 75 mm and LBO boules of 35 mm requires from four to six weeks. For LBO, a core of inclusions along the center of the boule greatly limits the sizes of fabricated crystals. The limitations imposed on the applicability of these materials by the processing conditions may be subverted with the synthesis of new compounds that could be grown as high-quality crystals directly from a stoichiometric melt. We describe below guidelines for the preparation of new borates that are likely to melt congruently and produce fluid melts.

Orthoborates

The structural chemistry of solid-state borates is characterized by a variety of discrete and condensed oxoanions. For example, crystals of YAB contain independent orthoborate BO_3 groups, **1**, those of BBO contain isolated B_3O_6 rings, **2**, and those of LBO contain condensed B_3O_7 rings, **3**. Because orthoborates are in general synthetically accessible in most phase systems and their melts are likely to be less viscous than those of polyborates, we have

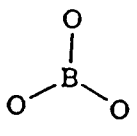

1

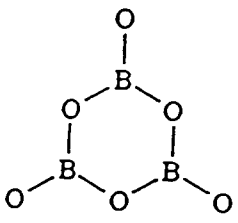

2

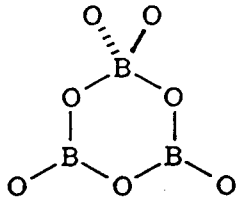

3

Because orthoborates are in general synthetically accessible in most phase systems and their melts are likely to be less viscous than those of polyborates, we have recently examined in the context of the anion group theory[5] the second-order susceptibilities of all noncentrosymmetric compounds containing triangular oxoanions.[6] By modeling each anion with D_{3h} symmetry, we derived the orientational dependencies of the group hyperpolarizability coefficients. The nonlinear susceptibility d_{22} = 2.3 pm/V of BBO can be understood on the basis of the orientations of the B_3O_6 rings, Figure 2.1. These orientations produce a nonlinearity that is 67% of optimum for this number density of rings. If each of the angles with respect to the local z axis were zero, an optimum alignment of B_3O_6 groups would be produced with a resultant nonlinearity of 3.5 pm/V. A similar analysis of the orientations of the BO_3 groups in YAB, Figure 2.2. reveals an alignment that is 49% of optimum. Since the nonlinearity of YAB has been reported to be d_{11} = 1.5 pm/V, we can expect the maximum nonlinearity of an orthoborate crystal to be approximately 3 pm/V. Since the microscopic hyperpolarizability coefficient β_{333} is invariant to rotation about the B-O bond along the z axis, a variety of orthoborate structural arrangements can produce an optimal nonlinearity. From these results, it appears new orthoborate structures could produce useful properties. It should be possible to synthesize an orthoborate with a nonlinearity that is comparable to that of BBO while maintaining a smaller birefringence. Such a material would provide

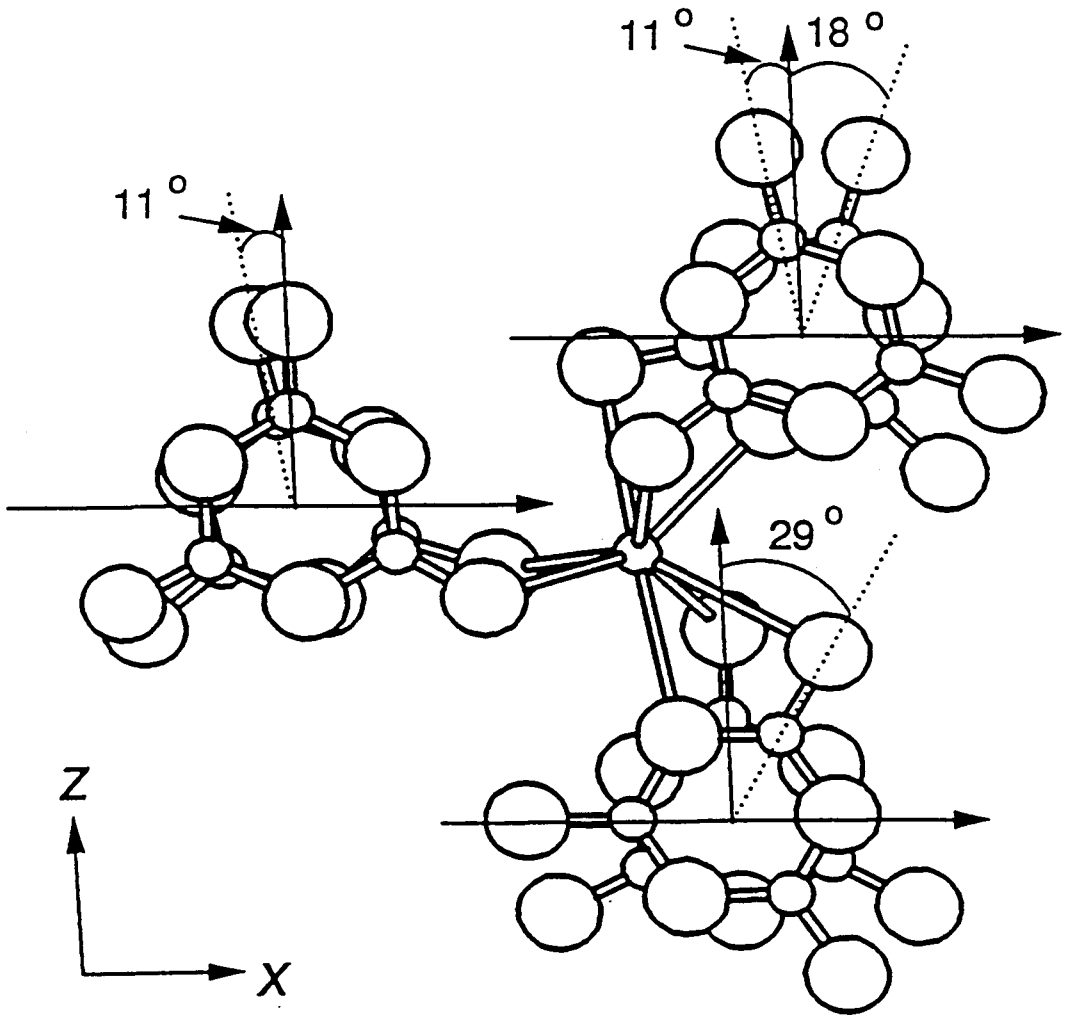

Figure 2.1. Orientation of B_3O_6 groups in low-temperature BaB_2O_4.

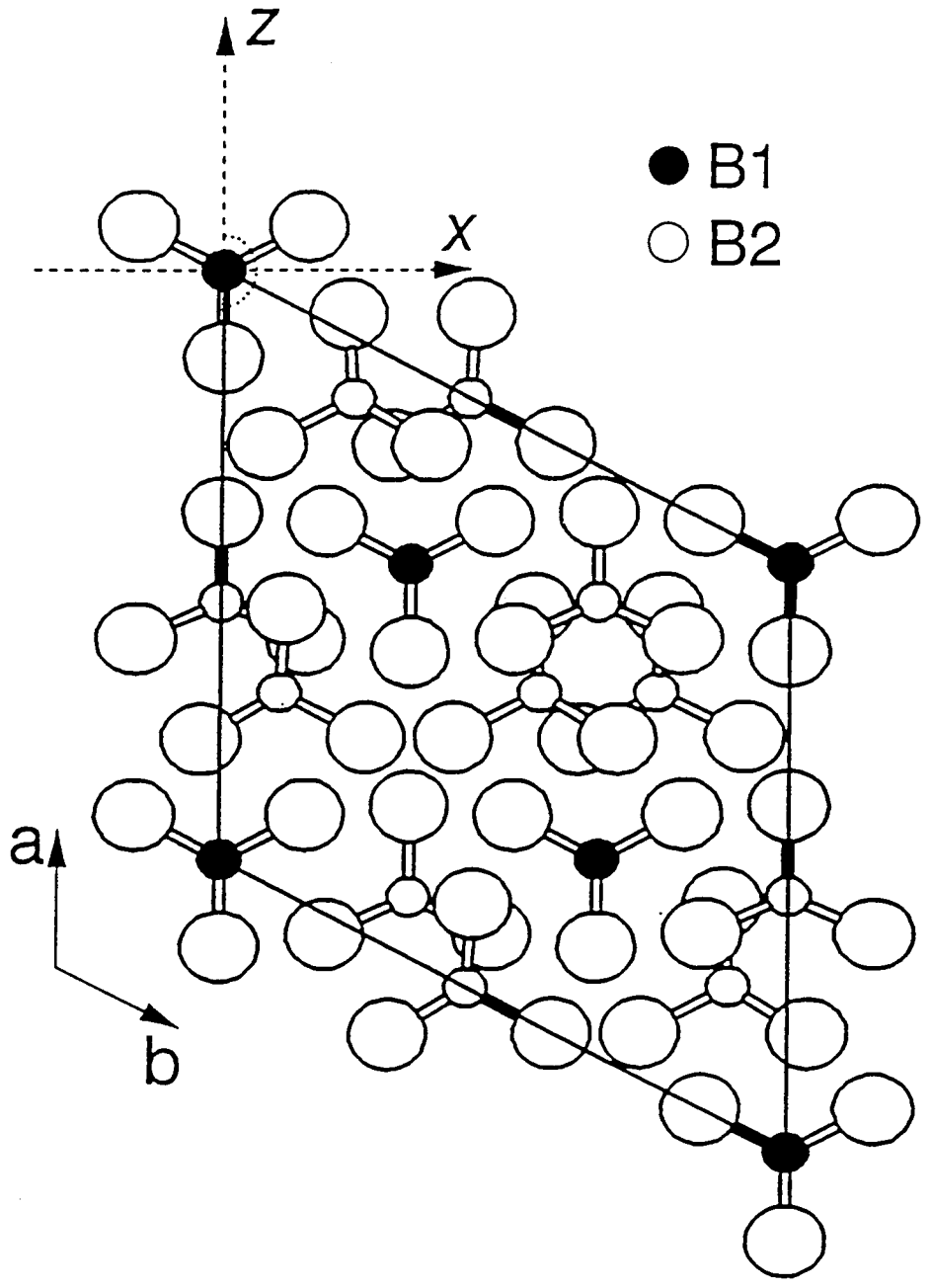

Figure 2.2. Orientation of BO_3 groups in YAB.

a smaller sensitivity to phasematching and an enhanced conversion efficiency for the production of UV light. Additionally, an orthoborate with a birefringence similar to that of LBO, but having higher nonlinearities, is a worthy goal for a synthesis effort. We have recently been examining several borate systems containing a basic oxide and a halide. The combination of basic oxide and acidic B_2O_3 provides favorable conditions for congruent melting, while inclusion of the halide should increase the fluidity of the resulting melt.

One example of a new compound resulting from these investigations is the hexagonal material $BaCaBO_3F$.[7] The structure of this compound contains Ba and Ca atoms disbursed within and between discrete layers of BO_3 groups and F atoms, Figure 2.3.

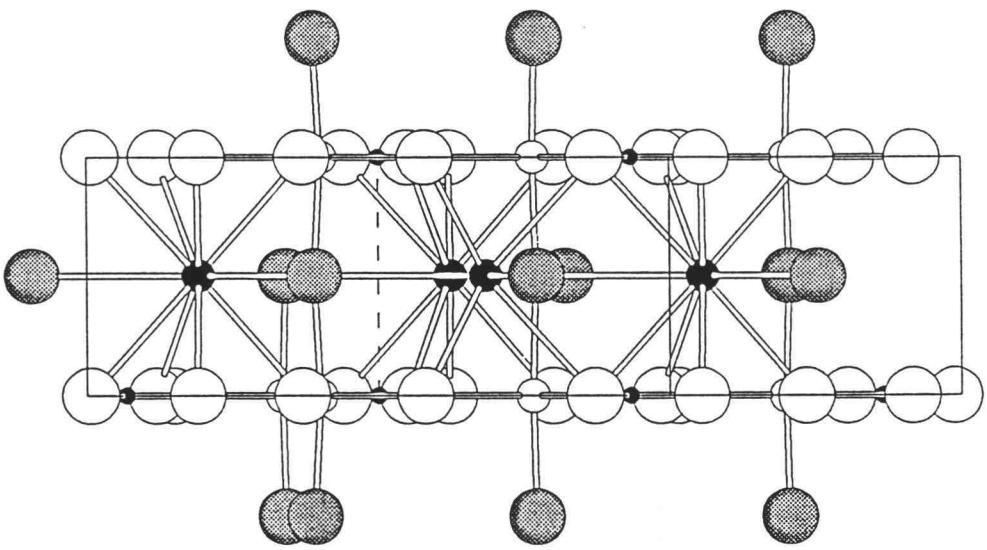

Figure 2.3. Structure of $BaCaBO_3F$. Ba and F atoms are dark and shaded circles.

The relative orientations of the BO_3 groups are depicted in Figure 2.4. From these orientations, the number density of BO_3 groups, and a microscopic susceptibility β_{333} derived from the value of d_{11} = 1.5 pm/V for YAB, we calculate a nonlinearity of d_{11} = 0.4 pm/V for the barium calcium compound. It should be noted that contributions of the Ba-F portion of the matrix to the nonlinearity are neglected in this analysis. Because the BO_3 groups adopt a coplanar arrangement, the birefringence should be similar to that of BBO. For Type I phasematching, θ_m may be expected to be between 20 and 30° which would produce $d_{eff} \approx 0.35$ pm/V.

To realize a smaller birefringence with retention of an intrinsic BO_3 energy gap, the coplanarity of the BO_3 groups must be disrupted. The triangular disposition of groups, **4**, (translated in three dimensions) should produce a crystal having a small birefringence. Because parallel alignment of at least one B-O bond is maintained, this collection of groups represents an optimum nonlinearity. We have observed an arrangement similar to **4** in the compound $Ba_7(BO_3)_3F_5$.[8]

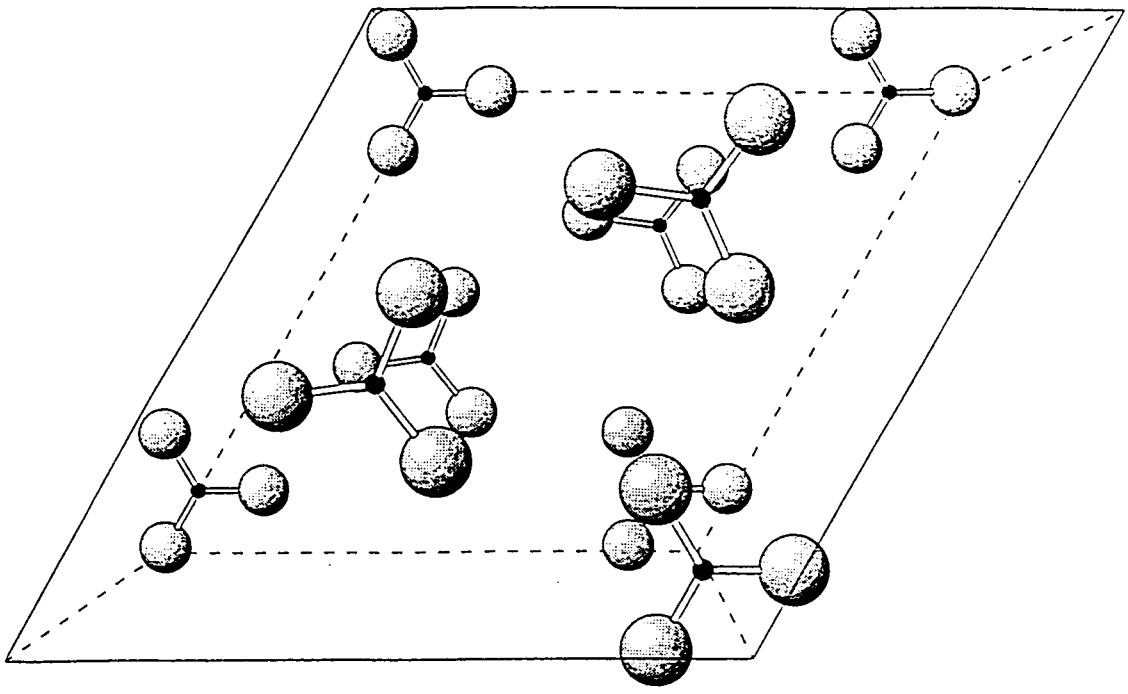

Figure 2.4. BO_3 groups in $BaCaBO_3F$.

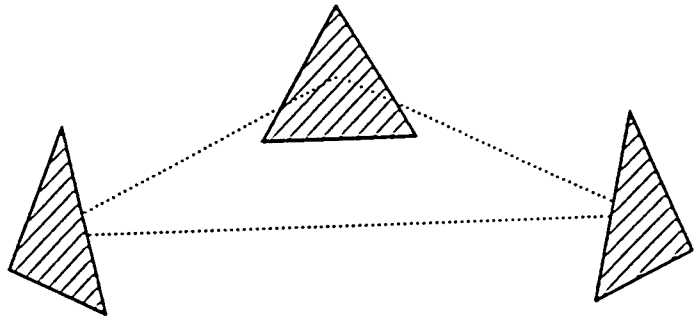

4

The disposition of the BO_3 groups in the structure is illustrated in Figure 2.5. Two levels of triangular arrangements are related by an approximate 6_3 screw axis along the c axis. This produces the apparent C_6 rotation symmetry in the c-axis projection, Figure 2.5. Importantly, each BO_3 group is tilted away from the c axis by 33°. We have also developed a derivative chemistry for this material; Sr atoms may be substituted for the Ba atoms to the solubility limit indicated by the stoichiometry $Ba_3Sr_4(BO_3)_3F_5$.[9] In this structure, the Sr and Ba atoms occupy distinct sites, and the BO_3 groups are now tilted by 40° relative to the c axis. Again, by considering the arrangement of BO_3 groups only, we derive the nonlinear coefficients d_{31} = 0.4 pm/V and d_{33} = 0.8 pm/V. The latter value is similar to the nonlinearity of LBO, but the coefficient d_{31} only is operative in angular phasematching. The lack of a coplanarity among all of the BO_3 groups should produce a small birefringence. The compound $Ba_7(BO_3)_3F_5$ melts congruently, and large crystals have been grown at Virgo Optics.

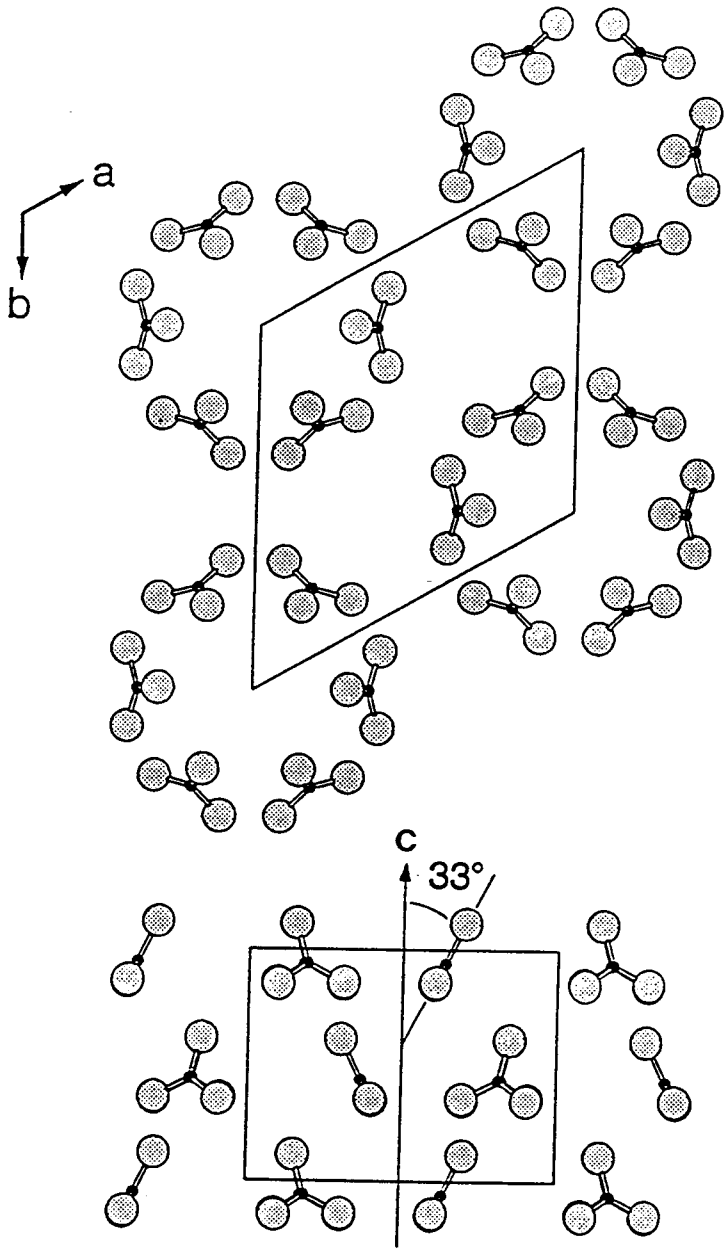

Figure 2.5. Arrangement of BO_3 groups in the structure of $Ba_7(BO_3)_3F_5$. Top) view along the trigonal c axis. bottom) view along [110].

Noncentrosymmetry and B_3O_7 rings

One of the major difficulties in planning the synthesis of new nonlinear optical materials is the inability to predict the occurrence of a noncentrosymmetric structure. We must simply prepare materials and choose those crystals that crystallize in noncentrosymmetric groups for additional studies. We have, however, recently identified a borate stoichiometry where the likelihood of observing noncentrosymmetric structures is greatly enhanced, and this stoichiometry is that of LBO.

LBO contains the B_3O_7 ring system - two BO_3 triangles joined to one BO_4 tetrahedron, **3**. If a compound crystallizes with one of these rings per unit cell, it is likely to crystallize in a noncentrosymmetric space group. The necessary condition for this to occur is the absence of an improper rotation axis in the ring, i.e., the ring must be dissymmetric (chiral). For the compound to be centrosymmetric, the B_3O_7 group minimally would have to contain an S_2 improper rotation axis = a mirror plane of symmetry. This is an unlikely event in a crystal where the associated cations are likely to bind to each of the O atoms in a different manner to satisfy their bonding requirements. Condensation of B_3O_7 rings produces a B:O ratio of 3:5 and compounds of the type LiB_3O_5,[10] CsB_3O_5,[11] and TlB_3O_5,[12] all of which are noncentrosymmetric. The chirality of the B_3O_7 ring systems is well illustrated by consideration of the ring in LBO, **5**.

We have now prepared additional compounds having this 3:5 ratio of B:O. Each compound is noncentrosymmetric and contains one crystallographic type of B_3O_7 ring. The compound $SrLi(B_3O_5)_3$[13] is one example, Figure 2.6. Crystals of this material are uniaxial, space group R3c.

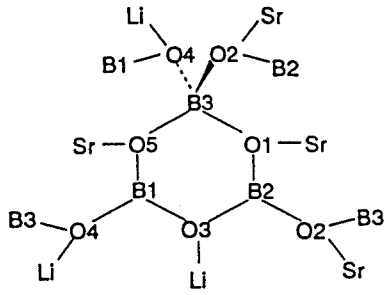

5

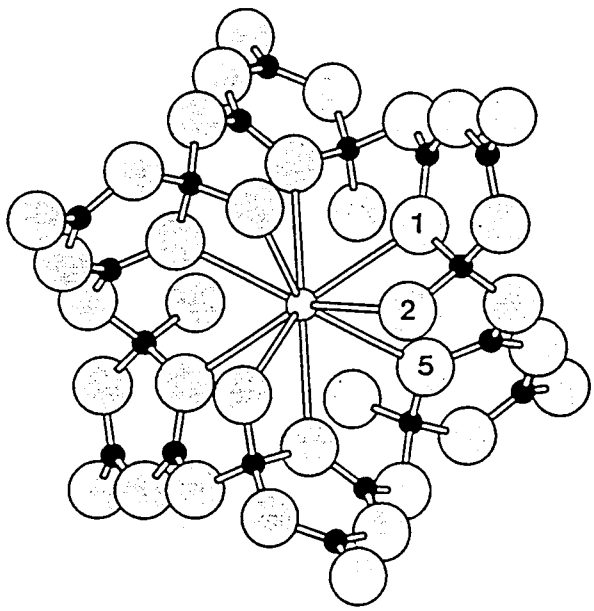

Figure 2.6. Condensed B_3O_7 ring system of $SrLi(B_3O_5)_3$.

Large single crystals have been grown at Stanford University, and attempts were made at Lawrence Livermore National Laboratory[14] to determine phase matching loci, but unfortunately, the material could not be phase matched. Additional studies of the crystal have revealed that it is an unpoled ferroelectric with a dielectric constant of 32, a spontaneous polarization of 10 $\mu C/cm^2$, and a coercivity field of 4.2 kV/cm^2.

Pyroborates

We have also been synthesizing new pyroborates. Rotation about the central B-O bond, **6**, is an important feature of the group. This rotation perturbs the coplanarity of the terminal BO_2 units, resulting in interplanar angles between these units that have ranged up to 86.6°.[15] Variation of this angle within a structural family of materials should provide a means to control birefringence and nonlinearities.

An example of this behavior is given by the series of compounds $AMOB_2O_5$ (A = Cs, Rb, and K; M = Nb and Ta).[16] Complete solid solutions exist in the series $Cs_{1-x}Rb_xNbB_2O_5$ and $Rb_{1-x}K_xNbOB_2O_5$ ($0 < x \leq 1$). The structure of the Cs-Nb derivative[17] is characterized by layers of planar B_2O_5 groups with Nb atoms occupying distorted octahedral sites, Figure 2.7. As the size of the alkali-metal decreases, two important structural changes are observed. The B_2O_5 groups adopt nonplanar geometries by twisting about the central B-O bond and the

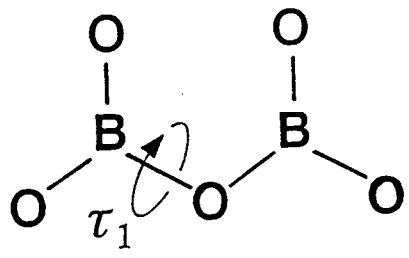

6

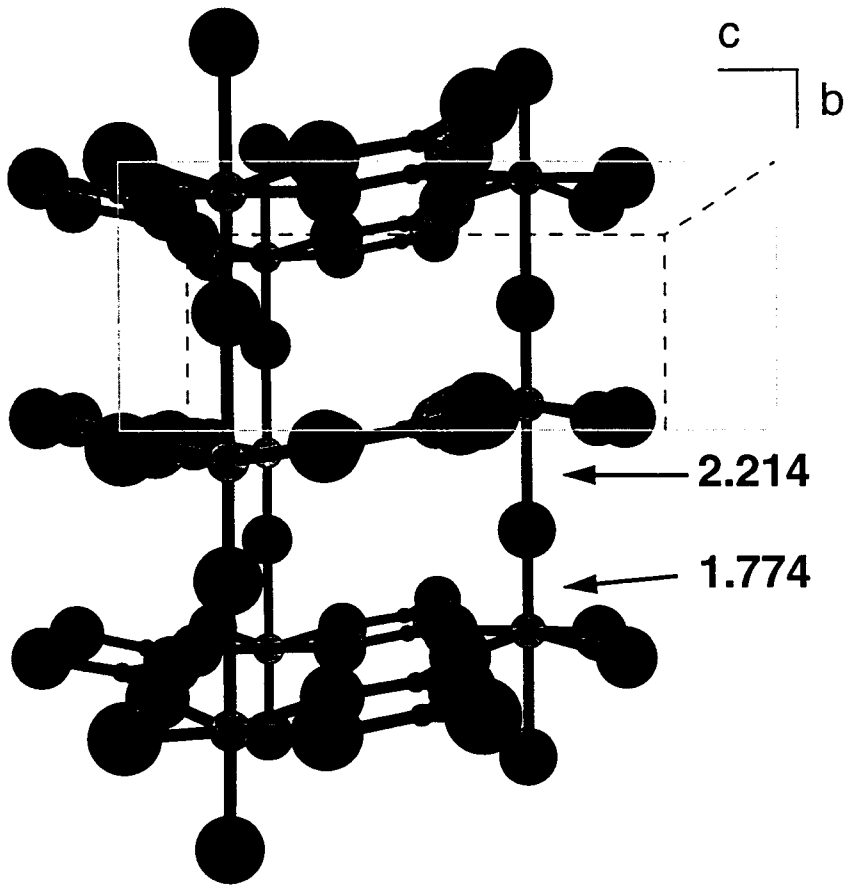

Figure 2.7. Structure of $CsNbOB_2O_5$. Shaded, medium circles are Nb atoms and shaded large circles are O atoms. Here, and in Figure 2.8.

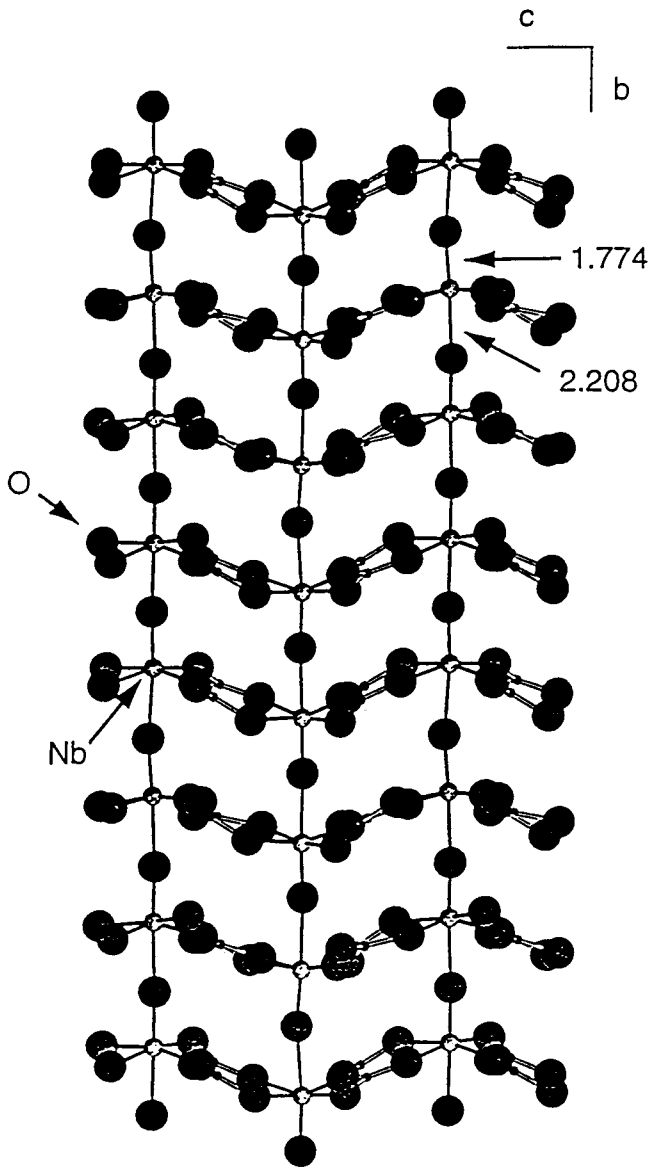

Figure 2.8. Structure of $KNbOB_2O_5$.

results are reflected by the supercells of the Rb and K compounds[18] which are represented as 4 x and 8 x, respectively, the c axis of the Cs derivative. From consideration of the alignment of the B_2O_5 groups, we expect the highest nonlinearity and birefringence to be realized with the Cs derivative. Another

curious feature of these structures is the presence of chains of alternating short, long M-O interactions that extend approximately orthogonal to the B_2O_5 planes. For the Cs-Nb compound these short and long distances are 1.774(6) and 2.214(6) Å, respectively. These chains, of course, are reminiscent of similar alternations of the Ti-O distances in KTP that contribute to its high nonlinearity. In the borate, however, the chains are not expected to contribute significantly to the nonlinearity as pairs of chains are related by an approximate center of symmetry, i.e., the M-O distances in one chain alternate in the manner long-short-long, while in a neighboring chain they alternate as short-long-short.

The distinction between the short, long bond distances in the Ta derivative is much less pronounced.[19] The shorter Ta-O distance is 1.906(2) Å, and the longer is 2.009(2) Å. It is also important to note that the Nb(Ta)-O chains are positioned orthogonal to the polar axis of the crystal. As a result, it is not possible to pole the materials to bring the alternating short, long bond distances of neighboring chains in phase. The displacements of the Nb and Ta atoms from the centers of the octahedra along the polar axis, however, could be an important feature in contributing to the nonlinearity of these materials.

Summary

An overview of selected, new noncentrosymmetric borates has been presented. Emphasis has been placed on the manipulation of linear optical properties. The results indicate that these or other materials yet to be discovered will likely produce optical characteristics that will extend the usefulness of solid-state borates. By applying simple chemical concepts, judicious choices of phase systems can be made that are likely to produce crystals having both desirable optical properties and melt characteristics. The work presented here represents only a small segment of the phase space available for identification of new crystalline borates that may well prove to be the cornerstones of new, emerging optical technologies.

Acknowledgments

This work was supported by the National Science Foundation (DMR-9221372). Acknowledgment is also made to the Donors of the Petroleum Research Fund, administered by the American Chemical Society, for partial support of this research.

References

1. Ballman, A. A. *Amer. Mineral.* **1962**, 47, 1380; Fon, Y. X., Schlecht, R., Qin, M. W., Luo, D., Jiang, A. D., Huang,Y. C. Technical Digest, *Advanced Solid-State Lasers*, **1992**, 311.

2. Eimerl, D., Davis, L., Velsko, S., Graham, E. K., Zalkin, A. *J. Appl. Phys.***1987**, *62*, 1968; D. N. Nikogosyan, *Appl. Phys. A* **1991**, *52*, 359.

3. Chen, C., Wu, Y., Jiang, B., Wu, B., You, G., Li, R., Lin, S. *J. Opt. Soc. Am.* **B 1989**, *6*, 616.

4. Itoh, K., Marumo, F., Kuwano, Y. *J. Cryst. Growth* **1990**, *106*, 728; Kouta, H., Kuwano, Y., Ito, K., Marumo, F. *J. Cryst. Growth* **1991, *114***, 676.

5. Chen, C. T. Sci. Sinica **1979,** *22*, 756; Chen, C. T., Liu, G. Z. *Ann. Rev. Mater. Sci.* **1986,** *16*, 203.

6. Schaffers, K. I. PhD thesis, Oregon State University, **1992**.

7. Crystal data for $BaCaBO_3F$: Rigaku AFC6R diffractometer, a = 9.049(1), c = 4.326(1) Å, V = 306.74(8) $Å^3$, space group P-62m, 511 unique data, R = 0.062, wR = 0.075.

8. Crystal data for $Ba_7(BO_3)_3F_5$: Rigaku AFC6R diffractometer, a = 11.208(5), c = 7.250(2) Å, V = 788.7 (5) Å3, space group P31c, 745 unique data, R = 0.052, wR = 0.068.

9. Crystal data for $Ba_3Sr_4(BO_3)_3F_5$: Rigaku AFC6R diffractometer, a = 10.853(1), c = 6.945 Å, V = 708.5 $Å^3$, space group $P6_3mc$, 1000 unique data, R = 0.043, wR = 0.056.

10. König, H., Hoppe, R., Z. Anorg. Allg. Chem. **1978**, *434*, 71.

11. Krogh-Moe, J. *Acta Crystallogr.*, Sect. B **1973,** *30*, 1025.

12. Touboul, M. *Compt. Rend.*, Sect. C **1973,** *277*, 1025; Gasperin, M., *Acta Crystallogr.*, Sect. B **1974,** *30*, 1181.

13. Crystal data for $SrLi(B_3O_5)_3$: Rigaku AFC6R diffractometer, a = 10.610(1), c = 17,538(2)Å, V = 1709.9(4) $Å^3$, space group R3c, 433 unique data, R = 0.051, wR = 0.067.

14. Eimerl, D., Velsko, S., Davis, L., Wang, F. *Prog. Cryst. Growth Charact.* **1990,** *20*, 59 ; Velsko, S. P. in Materials for Nonlinear Optics: Chemical Perspecties, ACS Symposium Series No. 455, edited by Marder, S., Sohn, J., Stucky, G. (Washington DC: Am. Chem. Soc., **1991**) 343.

15. Alekel, T. A., Keszler, D. A. *J. Solid State Chem.*, in press;Thompson, P. D., Huang, J., Smith, R. W., Keszler, D. A. *J. Solid State Chem.* **1991**, *95*, 126.

16. $RbNbOB_2O_5$: Baucher, A., Gasperin, M., Cervelle, B. *Acta Crystallogr.* **1976,** *32*, 2211.

17. Crystal data for $CsNbOB_2O_5$: Rigaku AFC6R diffractometer, a = 7.527(2), b = 3.988(1), V = 291.7 Å3, space group $Pmn2_1$, 862 unique data, R = 0.023, wR = 0.029.

18. For K derivative: Chai, B. H. T. University of Central Florida (private communcation, June **1993**).

19. crystal data for $CsTaOB_2O_5$: Rigaku AFC6R diffractometer, a = 7.548(1), b = 3.906(1), c = 9.771 (1) Å, V = 288.11(9) $Å^3$, space group $Pmn2_1$, R = 0.057, wR = 0.071.

CHAPTER 3
Crystal Chemistry of Noncentrosymmetric Nb and Ta Oxide Pyroborates

In preparation for submission to *J. Solid State Chemistry*

Abstract

The pyroborate series $Cs_{1-x}Rb_xNbOB_2O_5$ and $Rb_{1-x}K_xNbOB_2O_5$, are noncentrosymmetric compounds containing high densities of chromophores that are aligned to produce significant nonlinear susceptibilities. The compounds $CsNbOB_2O_5$ and $CsTaOB_2O_5$ crystallize with two formula units in the orthorhombic system, space group $Pmn2_1$. The cell parameters from single crystal X-ray data of $CsNbOB_2O_5$ and $CsTaOB_2O_5$ are a = 7.527(2), 7.5479(9) Å; b = 3.988(1), 3.9064(4) Å; c = 9.717(2), 9.7713(9) Å, respectively, and V = 291.7(2), 288.11(9) $Å^3$. The structural variability of the pyroborate group, however, produces materials of differing nonlinearities and birefringence. This variation is clearly observed as one proceeds down the group from K to Cs, i.e. the K derivative exhibits an 8× supercell of the simple structure of $CsNbOB_2O_5$ (space group $Pmn2_1$). Substituting the Nb with Ta and Sb atoms led to the preparation of the compounds $CsTaOB_2O_5$ and $RbSbOB_2O_5$.

Introduction

Because of their structural characteristics, compounds of the type $AMOB_2O_5$ (A = K, Rb, Tl; M = Nb, Ta) have recently been studied as new nonlinear optical materials. The first member of the family, $RbNbOB_2O_5$, was described by Gasperin and co-workers in 1976.[1] The derivatives $TlNbOB_2O_5$, $TlTaOB_2O_5$, and RbTaOB2O5 were described later;[2-4] the K derivative $KNbOB_2O_5$ has also recently been synthesized.[5] Detailed optical studies on large single crystals of $RbNbOB_2O_5$ have revealed that the second-order nonlinear coefficient is 1.5 times larger than that of potassium dihydrogen phosphate (d_{36} = 0.4 pm/V). Moreover, the birefringence is sufficient to phase match 1-μm light. The commercial development of the material, however, has been thwarted by its tendency to delaminate during fabrication processes.[6] During the course of the development of the Rb compound, we also began an investigation of its derivative chemistry.

We describe here the structures of the Cs analogues and solid-solution behavior in the series $Cs_{1-x}Rb_xNbOB_2O_5$ and $Rb_{1-x}K_xNbOB_2O_5$. From these results, we make direct correlations between structural features and optical properties.

Experimental

Powders of the alkali-metal Nb and Ta borates were synthesized by employing high-temperature solid-state methods. Stoichiometric quantities of the starting reagents, alkali-metal precursors (AESAR, nitrates or carbonates ≥99.9%) and Ta or Nb pentoxide (AESAR, ≥99.9%), were mixed with a 5 mol% excess of B_2O_3, ground under hexane, placed in Pt crucibles, and heated at 923 K for 2 h to decompose the reagents and initiate the reactions. The samples were cooled, reground, and heated for 12 h at 1073 K. Compounds in the solid-solution series $K_{1-x}Rb_xNbOB_2O_5$ and $Rb_{1-x}Cs_xNbOB_2O_5$ ($0 \le x \le 1$) were also prepared according to the above prescription. Powder diffraction data were collected on an automated Philips diffractometer, and peak positions were corrected by using NIST Si Standard 640b. The hkl assignment of each reflection was determined by comparison to indexed patterns of the material $RbNbOB_2O_5$. Unit-cell parameters a, b, and c were refined by least -squares analysis (POLSQ) with fourteen peaks in the range $22 \le 2\theta \le 60°$. The results from the solid solution indicated that the end members $CsNbOB_2O_5$ and $KNbOB_2O_5$ do exist and are derivatives of the $RbNbOB_2O_5$ structure type.

Single crystals of $CsNbOB_2O_5$ were grown with a flux of $CsCl:B_2O_3$ (1:1) and a compound to flux ratio of 2:1. The melt was cooled from 1273 to 873 K at 8 K/h and then to room temperature at 50 K/h. The crystals were isolated by

dissolving the flux in hot water. Single crystals of $CsTaOB_2O_5$ were grown from a flux of Cs_2SO_4:CsCl (1:1) with a compound to flux ratio of 2:1, and the same cooling schedule as described above. Crystals of $CsNbOB_2O_5$ and $CsTaOB_2O_5$ with edges near 0.1 mm were selected and mounted on glass fibers with epoxy for structure determination. All measurements were made on a Rigaku AFC6R single crystal diffractometer with graphite-monochromated Mo Kα radiation. Cell constants and the orientation matrix for data collection were obtained from least-squares refinements with 20 automatically-centered reflections in the range $30 \leq 2\theta \leq 36°$. The cell constants correspond to an orthorhombic crystal system, and Laue symmetry mmm was determined on the diffractometer. Extensive, prolonged data collections were conducted on the diffractometer to identify possible supercell reflections; none were found. We note here that crystals of the analogue $RbSbOB_2O_5$ were grown, and the 8×b supercell was readily observed.[6] For each crystal, intensity data were collected over the range of indices $0 \leq h \leq 12$, $0 \leq k \leq 16$, $-6 \leq l \leq 6$ for both $CsNbOB_2O_5$ and $CsTaOB_2O_5$, by using the ω scan technique to a maximum 2θ value of 75°. From 1572 measured reflections for $CsNbOB_2O_5$, a total of 869 were observed $[F_o^2 > 3\sigma(F^2)]$, and from 1570 reflections for $CsTaOB_2O_5$ a total of 927 data were observed. The intensities of three representative reflections measured after every block of 200 data varied by an average of 0.2% for $CsNbOB_2O_5$ and 0.3% for $CsTaOB_2O_5$ during the collection.

The structures were solved by using the *TEXSAN* software package.[7] Each crystal was found to form in the noncentrosymmetric space group $Pmn2_1$. The positions of the Cs and Nb(Ta) atoms were derived from the direct methods program SHELXS,[8] while the remaining atoms O and B were located from difference electron density maps. After full-matrix, least-squares refinements of the models with isotropic displacement coefficients on each atom absorption corrections were applied with the program DIFABS,[9] (transmission factors = 0.92 - 1.12 for $CsNbOB_2O_5$ and 0.86 - 1.26 for $CsTaOB_2O_5$). The data were averaged (R_{int} = 0.032 for $CsNbOB_2O_5$ and 0.043 for $CsTaOB_2O_5$), and the models were then refined with anisotropic displacement coefficients on each atom except for atom O3 in $CsTaOB_2O_5$. Final least squares refinement resulted in the residuals R = 0.022 and *w* R = 0.028 for $CsNbOB_2O_5$ and R = 0.054 and *w* R = 0.066 for $CsTaOB_2O_5$. The final refinement cycle converged in each case with Δ/σ = 0.01, and the maximum peaks in the final electron density maps correspond to 2.37% and 1.97% of a Nb and Ta atom, respectively. Crystal data are outlined in Table 3.1., and atomic positional and displacement parameters are listed in Table 3.2. Anisotropic displacement coefficients are listed in Tables 3.3 and 3.4.

Table 3.1. Crystal data and experimental conditions for $CsNbOB_2O_5$ and $CsTaOB_2O_5$.

	$CsNbOB_2O_5$	$CsTaOB_2O_5$
Diffractomer	---------- Rigaku AFC6R ----------	
Radiation	Graphite monochromated Mo Kα (λ = 0.70926 Å)	
Formula wt., amu	400.92	431.47
Unit cell	---------- Orthorhombic ----------	
a, Å	7.527(2)	7.5479(9)
b, Å	3.988(1)	3.9064(4)
c, Å	9.717(2)	9.7713(9)
V, $Å^3$	291.7(2)	288.11(9)
Space group	---------- $Pmn2_1$ ----------	
D_{calc}, g cm^{-3}	3.910	4.973
F(000)	308	372
Z	2	2
Linear abs. coeff., cm^{-1}	80.471	249.99
No. unique data with		
with $F_o^2 > 3\sigma(F_o^2)$	869	927
$R(F_o)$	0.023	0.057
$R_w(F_o)$	0.029	0.071

Table 3.2. Positional and Thermal Parameters (B_{eq}) for $CsNbOB_2O_5$ and $CsTaOB_2O_5$.

	$CsNbOB_2O_5$				$CsTaOB_2O_5$			
	x	y	z	B_{eq}	x	y	z	B_{eq}
Cs	0	0.4270(1)	0.2262	1.55(2)	0	0.4731	0.3865(2)	1.63(5)
Nb(Ta)	0	0.1148(1)	0.8349	0.52(2)	0	-0.0790	0.7753	0.47(2)
O1	0.1902(6)	0.063(1)	0.9585(5)	1.6(2)	-0.191(3)	-0.046(5)	0.635(2)	2.3(7)
O2	0.1782(6)	0.054(1)	0.6830(4)	1.1(1)	0.177(2)	-0.039(5)	0.923(2)	1.1(4)
O3	0	0.560(1)	0.8358(9)	1.8(2)	0	-0.5658	0.789(3)	2.2(4)
O4	0	0.965(2)	0.4809(6)	1.3(2)	0	0.0176	0.128(2)	1.8(7)
B	0.6633(8)	0.009(1)	0.047796)	1.0(2)	0.335(3)	-0.021(5)	0.561(2)	1.3(5)

$$B_{eq} = 8\frac{\pi^2}{3}\sum_i\sum_j U_{ij} a_i^* a_j^* a_i \cdot a_j$$

Table 3.3. Anisotropic displacement coefficients for $CsNbOB_2O_5$.

Atom	U11	U22	U33	U12	U13	U23
Cs	0.0205(2)	0.0164(2)	0.0220(2)	0	0	-0.003(2)
Nb	0.0054(2)	0.0093(3)	0.0049(2)	0	0	0.0002(2)
O1	0.008(2)	0.030(2)	0.005(1)	-0.001(2)	0.001(1)	-0.004(1)
O2	0.014(2)	0.038(2)	0.010(2)	0.004(2)	-0.006(1)	-0.000(2)
O3	0.031(3)	0.014(2)	0.023(3)	0	0	0.000(3)
O4	0.011(2)	0.031(3)	0.008(2)	0	0	-0.003(2)
B	0.006(3)	0.021(3)	0.012(2)	0.001(2)	0.004(2)	-0.001(2)

Table 3.4. Anisotropic displacement coefficients for $CsTaOB_2O_5$.

Atom	U11	U22	U33	U12	U13	U23
Cs	0.0024(7)	0.0145(5)	0.0251(7)	0	0	-0.0033(6)
Ta	0.0059(2)	0.0065(2)	0.0056(2)	0	0	-0.0001(2)
O1	0.027(9)	0.0145(5)	0.0251(7)	0	0	-0.0033(6)
O2	0.002(4)	0.031(6)	0.011(5)	0.001(4)	0.001(4)	0.008(5)
O3	0.028(5)					
O4	0.013(7)	0.05(1)	0.006(6)	0	0	-0.010(8)
B	0.013(6)	0.021(7)	0.015(7)	-0.001(6)	-0.002(6)	0.005(6)

Results and Discussion

The compounds $CsNbOB_2O_5$ and $CsTaOB_2O_5$ crystallize in the orthorhombic noncentrosymmetric space group $Pmn2_1$. A labeled diagram of the contents of the unit cell is given in Figure 3.1. The structure contains layers that are built from condensation of $Nb(Ta)B_2O_9$ rings, Figure 3.1, where each ring may be described as the conjunction of a Nb(Ta)-centered distorted O octahedron and a B_2O_5 (pyroborate) group. By sharing vertices, these groups fuse to give layers extending in the ac plane, Figure 3.2. The O atoms attached to the Nb(Ta) atom that rest above and below the primary plane of the ring system are also shared between adjacent layers to give linear O··Nb(Ta)··O··Nb(Ta)··O chains that extend along the b axis. The structure is completed by placement of a Cs atom in an 8-coordinate site between the layers.

Interatomic distances and angles are listed in Table 3.5. Average Cs-O distances, 3.20 ± 0.08 Å and 3.18 ± 0.06 Å, and B-O distances, 1.37 ± 0.03 Å and 1.36 ± 0.05 Å, for the Nb and Ta derivatives, respectively, are consistent with the sum of crystal radii.[10] The longer B-O4 distances (cf. Table 3.5.) are consistent with the trend of lengthened B-O interactions about the central O atom of a pyroborate group.[11] As a mirror plane bisects the principal plane of the B_2O_5 group (through the central O atom), the group itself is planar in each

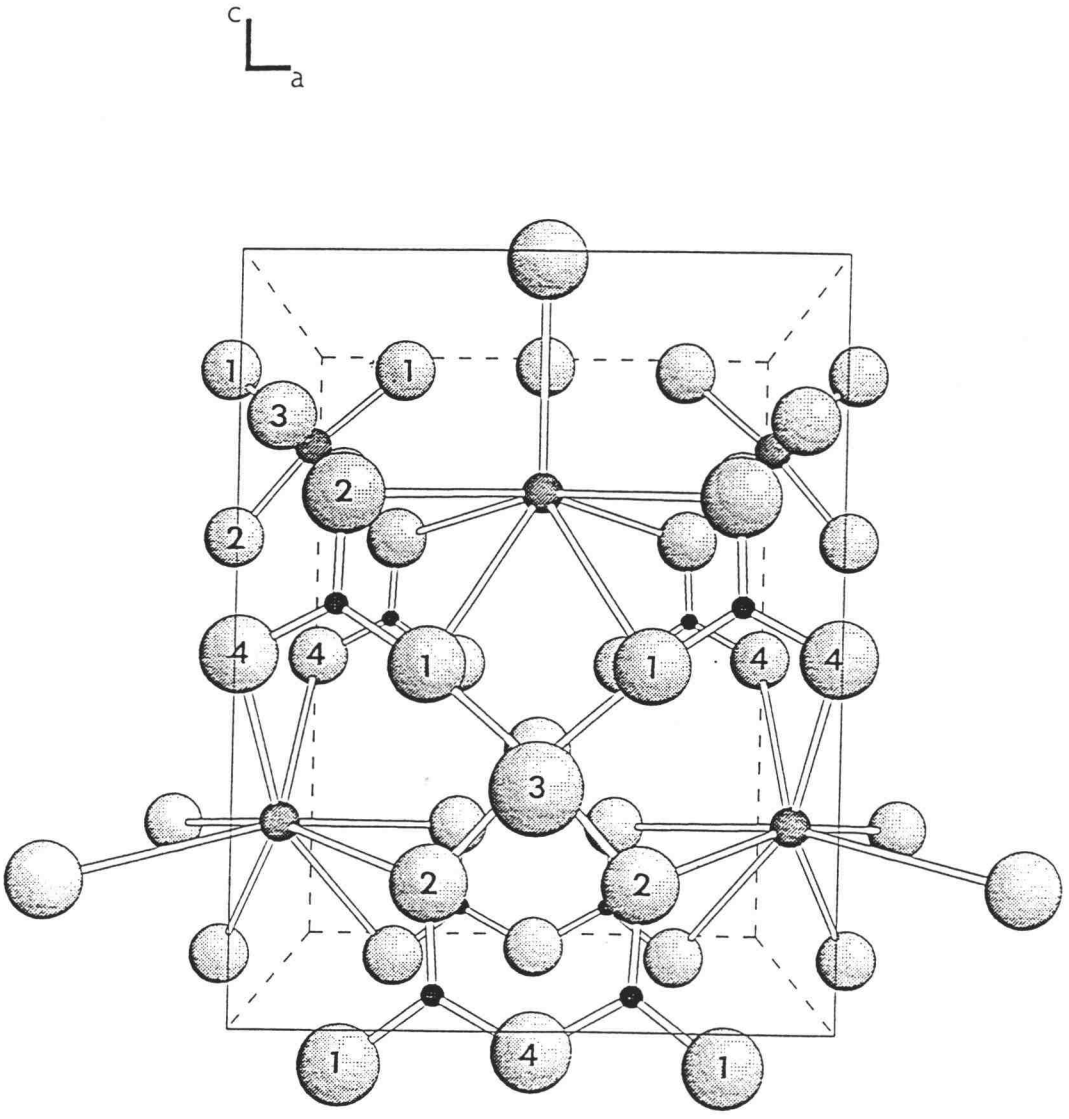

Figure 3.1. Sketch of the unit cell of $CsNbOB_2O_5$ as viewed along the *b* axis. The large shaded atoms represent the O atoms, the medium shaded atoms represent Cs atoms, and the dark circles represent B atoms.

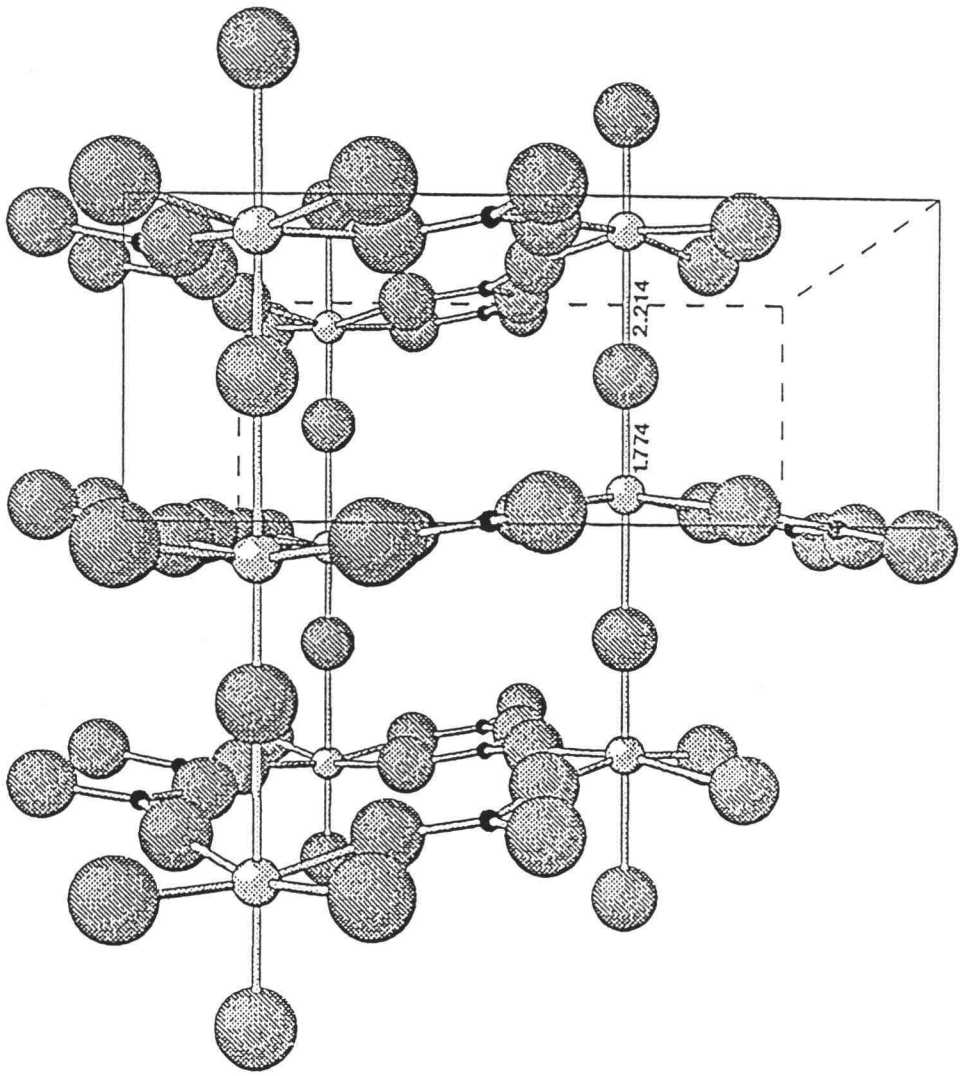

Figure 3.2. Sketch of chains of NbO_6 octahedra with planar pyroborate groups oriented orthogonally in the $CsNbOB_2O_5$ structure.

Table 3.5. Selected Bond Distances (Å) and Angles (°) for $CsNbOB_2O_5$ and $CsTaOB_2O_5$.

	$CsNbOB_2O_5$	$CsTaOB_2O_5$		$CsNbOB_2O_5$	$CsTaOB_2O_5$
Cs -O1 (×2)	3.313(5)	3.28(2)	O1-Cs-O1	51.2(2)	47.2(7)
Cs -O2 (×2)	3.231(5)	3.17(2)	O2-Cs-O2	78.0(1)	76.8(3)
Cs -O2 (×2)	3.101(5)	3.11(2)		97.1(2)	100.3(6)
Cs -O4	3.160(6)	3.17(2)		164.5(1)	166.7(6)
Cs -O4	3.196(7)	3.21(2)		102.7(2)	100.3(6)
			O2-Cs-O1	84.6(1)	81.7(6)
				42.1(1)	39.5(4)
				102.7(2)	90.4(4)
				122.3(1)	124.7(5)
				81.9(1)	83.2(5)
			O1-Cs-O4	153.87(9)	155.8(4)
				105.9(1)	98.3(4)
			O2-Cs-O4	74.2(1)	73.1(3)

Table 3.5. (continued)

	$CsNbOB_2O_5$	$CsTaOB_2O_5$		$CsNbOB_2O_5$	$CsTaOB_2O_5$
				119.38(9)	118.7(3)
			O4-Cs-O4	77.7(1)	75.5(4)
Nb(Ta) -O1(×2)	1.944(4)	1.99(2)	O1-Nb(Ta)-O1	94.9(3)	93(1)
Nb(Ta) -O2(×2)	2.009(4)	1.98(2)	O1-Nb(Ta)-O2	89.2(2)	90.5(7)
Nb(Ta) -O3(×1)	2.214(6)	2.009(2)		165.9(2)	170.9(6)
Nb(Ta) -O3(×1)	1.774(6)	1.906(2)	O1-Nb(Ta)-O3	95.9(2)	96.5(9)
				83.8(2)	88.9(8)
			O2-Nb(Ta)-O2	83.8(2)	85.2(9)
			O2-Nb(Ta)-O3	83.2(2)	82.7(8)
				97.2(3)	91.5(9)
			O3-Nb(Ta)-O3	179.5(5)	172(2)
B -O1	1.343(7)	1.31(3)	O1-B-O2	121.0(6)	120(2)
B -O2	1.362(7)	1.37(2)	O1-B-O4	123.0(6)	118(2)
B -O4	1.394(7)	1.41(2)	O2-B-O4	116.0(5)	121(2)

The pyramidal distortion of the NbO_6 octahedron is evident from the angle O1-Nb-O2 = 165.9(2)°; the distortion is less severe in the Ta analogue where the angle O1-Ta-O2 = 170.9(6)°. The alternation (0.44 Å) of the Nb-O3 short, long distances along the b-axis is also more dramatic than that (0.10 Å) for the corresponding Ta-O3 interactions (cf. Table 3.5.). This result is consistent with the expected magnitude of the dπ -pπ metal-oxygen interactions that should lead to the distortion of the 1-dimensional chain.[12]

These compounds crystallize in the polar point group mm2, and they are expected to have a permanent dipole moments. The B_2O_5 groups pointing in the direction of the polar c axis contribute to the net dipole moment. The other feature of the structure which could contribute to a great extent to the net hyperpolarizability of the material, is the alternating short long polarizable Nb-O chains. In a polar point group the only direction that can accommodate a permanent dipole moment is the c-axis. Since the Nb-O chains are disposed perpendicular to the polar axis, their net contribution to the dipole moment would be zero. A careful examination of Figure 3.2. shows that each Nb-O alternating short long bonded chains have a pseudo centrosymmetrically related long short Nb-O chains. So the dipole moment generated in each of these chains points in opposite directions, thereby leading to the cancellation and a zero contribution to the net dipole moment of the structure.

The only features capable of contributing to the nonlinearity would be the pyroborate functionality and the Nb-O equatorial bonds.

The Cs structure contains planar borate groups in a layered structure, while these groups are quite distorted and nonplanar in the corresponding K analog as shown in Figure 3.3. The structure of the $KNbOB_2O_5$ has been reported by Chai and coworkers.[5] The distortion of the B_2O_5 from the plane is to a greater extent in the K case and to a lesser extent in the Rb analog and barely noticeable in the $CsNbOB_2O_5$. The distortion expresses itself as a repeat unit along the b-axis. The K derivative exhibits an 8× supercell of the simple structure of $CsNbOB_2O_5$ (space group $Pmn2_1$) and the Rb analog a 5× super cell. We speculate the cause of distortion is due to the variation in size of the alkali metal ion. The B_2O_5 groups have to bend out of plane to satisfy the coordination sphere around the smaller K ion. While in the larger Cs ion the B_2O_5 groups continue to satisfy the coordination sphere without having to undergo untoward distortion.

A single crystal X-ray analysis suggests that $RbSbOB_2O_5$ crystallizes in the monoclinic crystal system, same as $RbNbOB_2O_5$ except that it has a repeat unit of 8 along the a axis. The cell constants of $RbSbOB_2O_5$ are a = 3.721(2) × 8, b = 9.477(4), c = 7.176 (3), β = 90.08(6), and V = 1525(2).

The extent of solubility of K and Cs in the $RbNbOB_2O_5$ structure in the range $0 \leq x \leq 1$ was studied by performing a solid solution. The determined cell

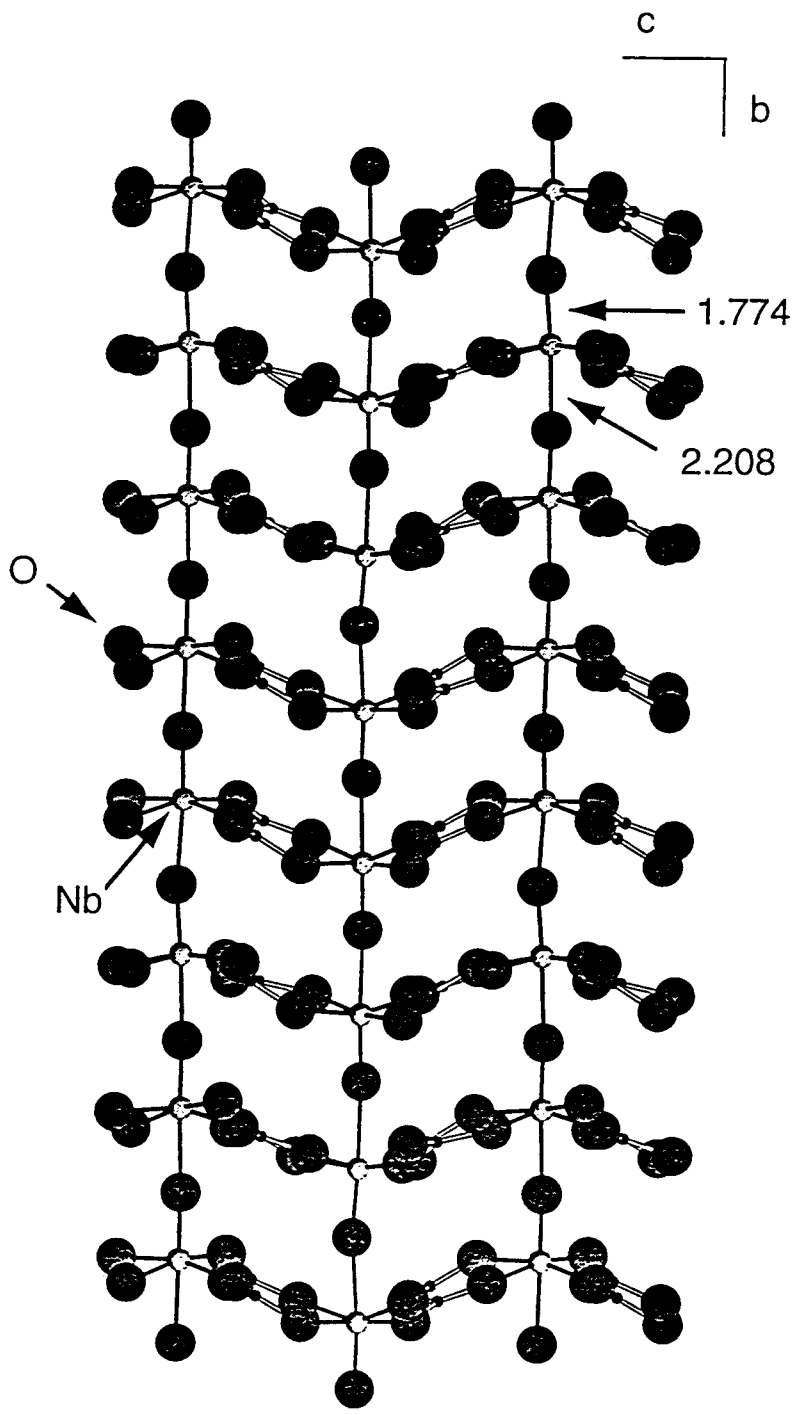

Figure 3.3. Sketch of chains of NbO_6 octahedra with planar pyroborate groups oriented orthogonally in the $KNbOB_2O_5$ structure.

Table 3.6. Lattice Parameters for the $K_{1-x}Rb_xNbOB_2O_5$ solid solutions.

x	a (Å)	b (Å)	c (Å)	V (Å^3)
0[a]	7.315(1)	3.904(4)	9.210(4)	263.1(2)
0.2	7.343(2)	3.866(6)	9.303(7)	264.1(6)
0.4	7.319(8)	3.814(8)	9.300(1)	265.7(8)
0.5	7.330(2)	3.912(3)	9.379(3)	268.9(3)
0.6	7.361(7)	3.914(8)	9.381(7)	270.3(8)
0.8	7.486(6)	3.907(2)	9.329(5)	272.5(7)
1	7.389(3)	3.928(2)	9.449(3)	274.2(2)

Note. Standard deviation is given in parentheses.

a: See Ref 1.

Table 3.7. Lattice Parameters for the $Rb_{1-x}Cs_xNbOB_2O_5$ solid solutions.

x	a (Å)	b (Å)	c (Å)	V (Å^3)
0[a]	7.389(3)	3.928(5)	9.449(3)	274.2(2)
0.2	7.468(5)	3.944(9)	9.411(5)	277.2(4)
0.4	7.472(2)	3.950(2)	9.450(2)	278.8(2)
0.5	7.469(2)	3.956(3)	9.499(2)	280.6(3)
0.6	7.465(4)	3.965(6)	9.508(5)	281.5(8)
0.8	7.555(4)	3.972(7)	9.456(5)	283.7(7)
1.0	7.457(2)	3.992(2)	9.710(5)	289.1(2)

Note. Standard deviation is given in parentheses.

a: see ref 1.

constants of the solid solutions are listed in Table 3.6 and 3.7. The volume/Z-composition plots for $Rb_{1-x}K_xNbOB_2O_5$ and $Rb_{1-x}Cs_xNbOB_2O_5$ are shown in Figure 3.4. The error bars in Figure 3.4 indicate 3σ and the systematic decrease in volume and cell constants as x is varied from 0.1 to 0.9 in $Rb_{1-x}K_xNbOB_2O_5$ indicate that the smaller K ion substitutes the Rb site. It is evident that the end member $KNbOB_2O_5$ forms retaining the crystalline phase of $RbNbOB_2O_5$ and it may have a similar structure. Similarly the solid solution results of $Rb_{1-x}Cs_xNbOB_2O_5$ in Figure 3.4, show a systematic increase in volume and cell constants as Cs substitutes Rb site in the $RbNbOB_2O_5$ structure.

Since birefringence is an important property of nonlinear optical materials to satisfy phase matching condition for SHG processes, we wanted to tune the birefringence by substituting Nb by Ta which is similar in size but heavier. We expected the compound $CsTaOB_2O_5$ to crystallize in the same crystal system and space group as the Nb compound. Although the structure is otherwise similar to the Nb compound, the Ta-centered octahedron of the $CsTaOB_2O_5$ is less distorted. The difference in the axial Ta-O distances is less remarkable than in the Nb compound as summarized in Table 3.5. These results demonstrate structural variability of the pyroborate group in developing materials of differing nonlinearities and birefringence.

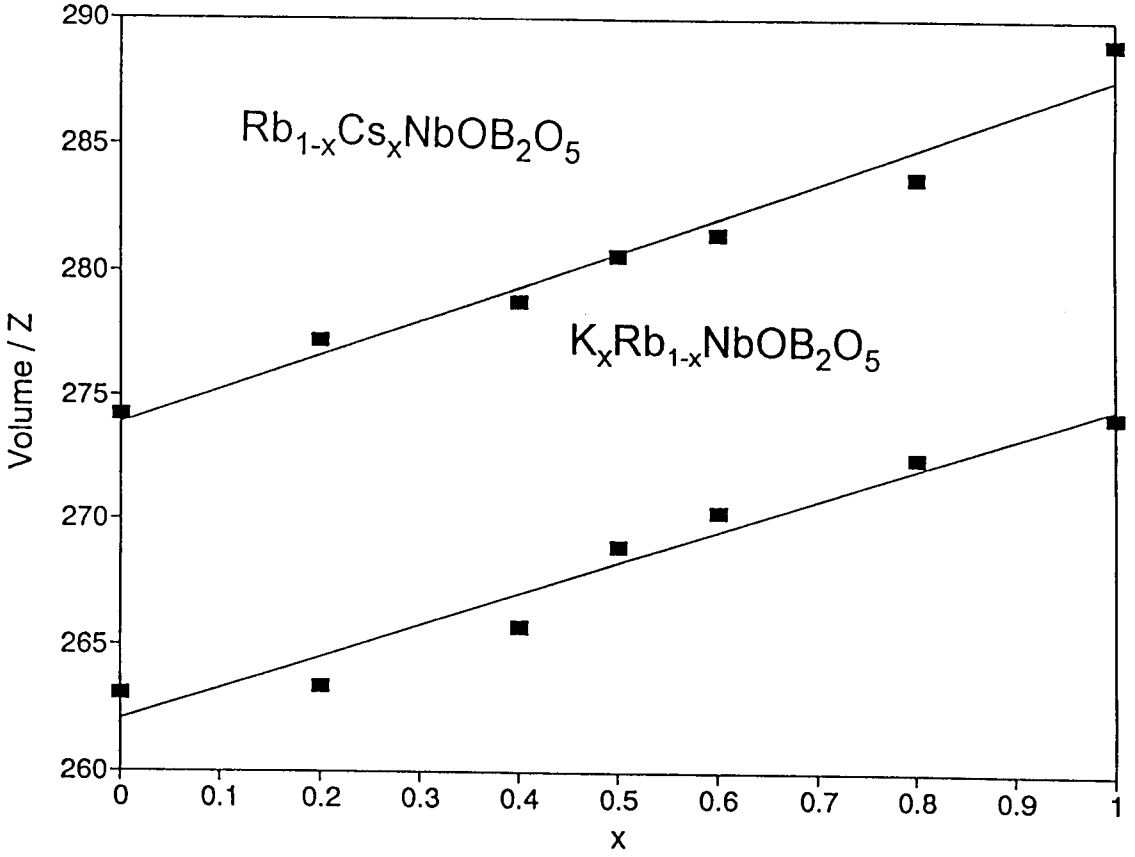

Figure 3.4. Unit cell volume per formula unit for the solid-solution series $K_{1-x}Rb_xNbOB_2O_5$ and $Rb_{1-x}Cs_xNbOB_2O_5$ as a function of composition ($0 \leq x \leq 1$).

The distortion of the pyroborate about the b axis is an important contributor to the net nolinearity of the structure. Apparently, the disposition of the pyroborate plays a crucial role in determining the nonlinearity of the structure. The second order hyperpolarizability component which contributes the most to the second order process is the β_{333} which has $\cos^3\theta$ functional dependence, where θ represents the angle of distortion of B_2O_5 about the b axis. For $KNbOB_2O_5$, the nonlinearity is 64% of the optimum and for $CsNbOB_2O_5$ it is 95% of optimum. Because of its layered structure we predict the Cs compound will exhibit a high birefringence and a significant nonlinearity.

In summary, the crystal chemistry of the pyroborate type of compounds can be tuned to produce materials of desired properties for second harmonic generation. The high nonlinearity and birefingence associated with the $CsNbOB_2O_5$ and $CsTaOB_2O_5$ make them promising candidates for frequency doubling the 1064-nm laser line of Nd:YAG to the 532 nm.

Acknowledgments

This work was supported by the US National Science Foundation, Solid-State Chemistry Program (DMR92-21372).

References

1. Baucher, A., Gasperin, M. *Acta Crystallgr., Sect. B* **1976**, *32*, 2211.

2. Baucher, A., Gasperin, M. *Mater.Res.Bull.* **1975**, 469.

3. Cerville, B., Cesbron, F., Berth, J., Jollies, P. *Acta Crystallgr., Sect. B* **1974**, *30*, 645.

4. Gasperin, M. *Acta Crystallgr., Sect. B* **1974**, *30*, 1181.

5. Chai, B. H. T., University of Central Florida (private communication, June **1993**).

6. Loiacono, G. Crystal Associates (private communication, August **1994**).

7. Texsan: Single Crystal Structure Analysis Software; Molecular Structure Corp Version 5.0.;The Woodlands, TX, **1989**.

8. Sheldrick, G. SHELXS86. In *Crystallographic Computing 3*; Sheldrick, G.; Kruger, C.; Goddard, R.; Eds.; Oxford University Press: New York, **1985**; 175.

9. Walker, N.; Stuart, D. *Acta Crystallgr.*; *Sect. A* **1983**, *39*, 158.

10. Shannon, R. D. *Acta Cryst., Sect. A* **1976**, *32*, 751.

11. Thompson, P. D., Keszler, D. A. *J. Solid. State. Chem.*

12. Wheeler, R. A., Whangbo, M-H., Hughbanks, T., Hoffmann, R., Burdett, J. K., Albright, T. A. *J. Am. Chem. Soc.* **1986**, *107*, 2222.

CHAPTER 4
Structure and Luminescence of $BaCaBO_3F$

Abstract

The crystal structure of the subcell and Bi^{3+}, Ce^{3+}, Eu^{2+}, Tb^{3+}, and Nd^{3+} luminescence of the compound $BaCaBO_3F$ are described. Crystal data: FW = 255.22 amu, $P\bar{6}2m$ (#189), hexagonal, a = 9.0490(8), c = 4.3256(9), V = 306.74(8) $Å^3$, Z = 3, R = 0.060, R_w = 0.075 for 537 averaged reflections. The structure contains Ba and Ca atoms disbursed within and between discrete layers of BO_3 groups and F atoms. The structure of the subcell has been solved, and the material has been determined by precession methods to crystallize in a 3 x 3 x 3 supercell.

Introduction

Following a study of the BaF_2-CaO-B_2O_3 phase system, the structure of a new compound $BaCaBO_3F$ is described. This material crystallizes in a noncentrosymmetric space group and exhibits features that may lead to efficient frequency conversion. Two borates, β-BaB_2O_4 (BBO) and LiB_3O_5 (LBO), are extensively used for frequency conversion of high power laser light.

Experimental

A powder sample of $BaCaBO_3F$ was prepared from the molar quantities of 0.5 $BaCO_3$ (AESAR, 99.9%), 0.5 BaF_2 (AESAR, 99.9%), 1 $CaCO_3$ (ALFA, 99.98%), and 0.55 B_2O_3 (AESAR, 99.9%). The synthesis and crystal growth were performed in an atmosphere of Ar. The mixture of carbonates and B_2O_3 were heated at 973 K for 12 h; then the fluoride was added and the sample was reground and heated at 1273 K for 12 h. A crystal was obtained for X-ray structure analysis from a melt of $BaCaBO_3F$. The melt was contained in a Pt crucible and slowly cooled from 1373 K to 973 K at 6 K/h, and then rapidly cooled at 50 K/h to room temperature. A colorless, transparent crystal of dimensions 0.10 × 0.12 × 0.10 mm was selected and mounted on a glass fiber with epoxy for structure determination. All measurements were made on a Rigaku AFC6R diffractometer with graphite-monochromated Mo Kα radiation. Cell constants and the orientation matrix for data collection were obtained from a least squares refinement with 19 automatically-centered reflections in the range $30 \leq 2\theta \leq 36°$. The cell constants correspond to a haxagonal cell; Laue symmetry 6/mmm was determined on the diffractometer. Intensity data were collected over the range of indices $-14 \leq h \leq 14$, $0 \leq k \leq 14$, $-6 \leq l \leq 6$ by using the ω scan technique to a maximum 2θ value of 70°, and from 2803 measured reflections a total of 511 were observed [$F_o^2 \geq 3\sigma F^2$]. The intensities of three

representative reflections measured after every block of 200 data varied by an average of 2% during the collection.

The structure was solved by using the *TEXSAN* software package.[1] The crystal was found to form in the centerosymmetric space group . The positions of the Ba and Ca atoms were derived from the direct methods program SHELXS, while the remaining atoms B, O, and F were located from difference electron density maps.[2] After a full-matrix least-squares refinement of the model with isotropic displacement coefficients on each atom, an absorption correction was applied (transmission factors = 0.51 -1.29) by using the program DIFABS.[3] The data were averaged (R_{int} = 0.066), and the model was refined with anisotropic displacement coefficients on each atom. Final least squares refinement resulted in the residuals R = 0.060 and R_w = 0.075. The largest peak in the final difference electron density map corresponds to 0.50% of the Ba atom. Crystal data are outlined in Table 4.1. atomic positional and thermal parameters are listed in Table 4.2.

Spectroscopic studies were performed on powder samples nominally doped with 2 mole% of Ce^{3+}, Eu^{3+}, Tb^{3+}, Nd^{3+}, and Bi^{3+}. The preparative procedure was that described above, [A_2O_3 (A = Eu, Tb, Nd, Bi), (99.99%, AESAR)], except that the Ce^{3+} sample [CeO_2, (99.99%, AESAR)], final heating was done in an atmosphere of 25 N_2:1 H_2. Steady-state, room-temperature luminescence spectra were obtained on a computer-controlled right angle

spectrometer. Excitation light from an Oriel 300 W Xe lamp was passed through a 50-cm water filter, focused initially onto the slits of a Cary model-15 prism monochromator, and then onto the sample. Luminescence was collected at a near right angle to excitation, dispersed through an Oriel 22500 1/8 - m monochromator, and detected with a Hamamatsu R636 photomultiplier tube. The signal was collected and amplified with a Keithley model 602 picoammeter and then converted to a digital signal for computer acquisition. Spectrometer control and data acquisition were achieved with computer programs written in this laboratory. The excitation spectrum was corrected by using rhodamine B as a quantum counter. The emission spectrum was corrected with a tungsten lamp that has been calibrated at Eppley Laboratories, Inc.

Table 4.1. Crystal Data and Experimental Conditions for $BaCaBO_3F$.

Diffractomer	Rigaku AFC6R
Radiation	Graphite monochromated Mo Kα (λ = 0.70926 Å)
Formula wt.,	255.22
Unit cell	Hexagonal
a, Å	9.0490(8)
c, Å	4.3256(9)
V, $Å^3$	306.74(8)
Space group	$P\bar{6}2m$ (189)
D_{calc}, g cm^{-3}	4.144
F(000)	342
Z	3
Linear abs. coeff., cm^{-1}	108.30
p factor	0.03
No. unique data with $F_o^2 > 3\sigma(F_o^2)$	511
$R(F_o)$	0.060
$R_w(F_o)$	0.075

Table 4.2. Positional and Thermal Parameters (B_{eq}) for $BaCaBO_3F$.

atom	x	y	z	B_{eq}*
Ba	0	0.7138(1)	1/2	1.90(6)
Ca	0.6160(4)	0.6160	0	1.1(1)
F	0.631(6)	0.6312	1/2	8(2)
O1	1.193(1)	0.689(1)	0	2.3(3)
O2	0.857(5)	0.8566	0	6.6(8)
B1	1/3	2/3	0	3(1)
B2	0	0	0	1.5(7)

Results and Discussion

A view of the contents of the unit cell is given in Figure 4.1. The structure contains one type of Ba and one type of Ca which are 11-coordinate and 7-coordinate, respectively. The structure consists of layers of Ba and F atoms, and Ca and B atoms. Two Ca atoms in adjacent layers are connected by F atoms, thus forming Ca-F-Ca chains along the 100 direction. Selected interatomic distances and angles are listed in Table 4.3. Atom Ba is bound by four O1, four O2, three F in an environment that is best described as a tricapped square antiprism. The Ba and the Ca-centered polyhedra share trigonal faces comprised of two O1 and one F atoms. The Ba atoms within a layer are connected through F atoms. The mutual sharing of the Ba-F atoms forms a hexagonal repeating motif along the 100 plane. The average Ba-O distance is 2.98±0.13 Å, and compare well to Ba-O distances of 2.95 Å for 11-coordinate Ba atoms obtained from the Shannon radii.[4]

The Ca atom is coordinated to two F, four O1, and two O2 atoms. The pentagonal base is comprised of the four O1 and one O2 atoms, and the apex is represented by atom F. The Ca atoms in adjacent layers are connected by F atoms. The Ca-F-Ca bond angle is 178 ± 3° slightly distorted from nonlinearity.

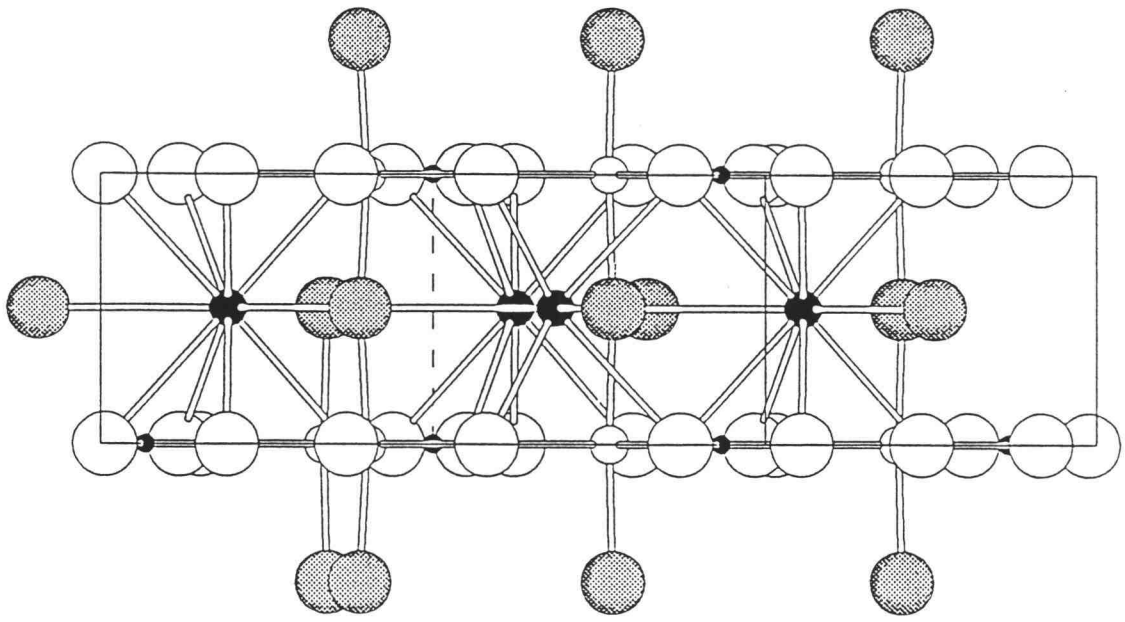

Figure 4.1. Unit cell diagram of $BaCaBO_3F$; view is along the c axis. Medium filled circles represent Ba, open circles represent Ca atoms. Large shaded circles represent F atoms, large open circles represent O atoms.

Table 4.3. Interatomic Distances (Å) and Angles (°) for $BaCaBO_3F$.

Ba-O1 x 4	2.857(7)	O1-Ba-O1	98.4(3)
-O2 x 4	3.1151(8)		134.5(4)
-F x 2	3.11(4)		63.5(4)
-F x 1	3.01(5)	O1-Ba-O2	84.7(2)
			163.5(6)
			124.8(5)
			61.3(5)
		O2-Ba-O2	87.94(3)
			103.6(8)
		F-Ba-F	106.1(7)
			148(1)
		F-Ba-O1	127.8(3)
			66.5(4)
		F-Ba-O2	58.3(6)
			100.5(8)
Ca-O1 x 2	2.40(1)	O1-Ca-O1	77.4(5)
-O1 x 2	2.47(1)		136.4(1)
-O2	2.16(3)		59.0(5)
-F x 2	2.1630(8)	O1-Ca-O2	141.3(2)
			82.3(3)
		F-Ca-F	178(3)
		F-Ca-O1	91(1)
		F-Ca-O2	89(1)
B1-O1 x 3	1.39(1)	O1-B1-O1	120.00
-O2 x 3	1.32(3)	O2-B1-O2	120.00

The average Ca-O bond distance is 2.38±0.13 Å, and it compares well to the Ca-O distances for 7-coordinate Ca atoms in $Ca_5(PO_4)_3F$,[5] 2.37±0.05. The B1 atom is bonded to three O1 and the B2 atom is bonded to three O2 atoms. The average B1-O bond distance is 1.39(1) Å, and the average B2-O distance is 1.32(3) Å. The O-B-O angles are 120° and normal for a 3-coordinate B atom.

The high temperature factors associated with the F and O atoms draw the possibility for the existence of a super cell. Indeed the material $BaCaBO_3F$ was found by precession methods to crystallize in a super cell which is 3 × that of the subcell parameters. Attempts to solve the structure of the super cell are in progress.

The relative orientation of the BO_3 groups are depicted in Figure 4.2. From these orientations, the number density of BO_3 groups, and a microscopic susceptibility β_{333} derived from the value of d_{11} = 1.5 pm/V for $YAl_3(BO_3)_4$, the calculated nonlinearity for the $BaCaBO_3F$ is 0.4 pm/V. The contribution of the Ba-F portion for the nonlinearity is neglected from the calculation. Because the BO_3 groups adopt a coplanar arrangement, the birefringence should be similar to that of BaB_2O_4. For type I phase matching, θ_m may be expected to be between 20 and 30° which would produces a d_{eff} = 0.35 pm/V. The 2% Yb^{3+} doped $BaCaBO_3F$ sample was prepared but due to the lack of crystal growth and optical measurement facilities the work was collaborated with LLNL.

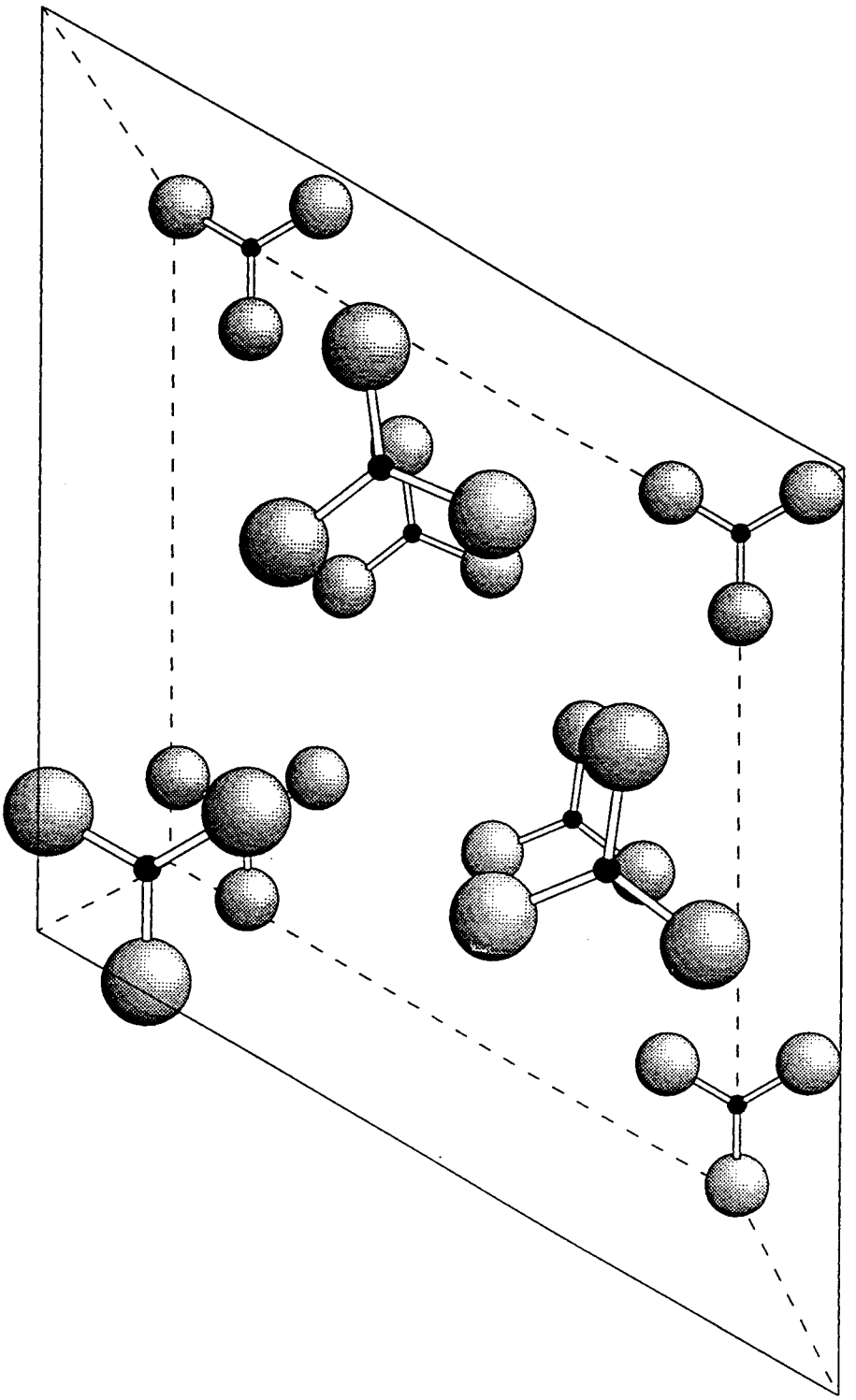

Figure 4.2. Orientation of the BO_3 groups in the unit cell.

The Yb^{3+} : $BaCaBO_3F$ has shown to lase at the LLNL and attempts to utilize it as a self doubling laser are in progress.

The Ce^{3+}: $BaCaBO_3F$ emits in the blue with an emission maximum at 4320 Å (Figure 4.3.). The ground state of the Ce^{3+} ion is split by spin orbit coupling into a $^2F_{5/2}$ and $^2F_{7/2}$ levels. The lowest lying 5d-level is approximately 30,000 cm^{-1} above the ground state. The 4f → 5d transitions being parity allowed have large transition probabilities, and since the 5d orbitals are strongly affected by the crystal field the absorption is a broad band. The emission similarly is broad corresponding to the $^2F_{5/2}$ and $^2F_{7/2}$ states. The doublet character of emission is influenced by temperature and concentration of Ce^{3+} ion.[6]

Eu^{3+} is a commercially valuable luminescent ion for red emitting phosphors in which the red emission is due to the transition from $^5D_0$ → $^7F_2$. The spectroscopic properties of Eu^{3+}-doped phosphors have been discussed by Blasse and co-workers.[7] The composition 2% Eu^{3+} : $BaCaBO_3F$ exhibits an intense emission under ultraviolet excitation (Figure 4.4.). The above transition is by far the most intense transition indicating a noncenterosymmetric environment for the rare earth ion. The life time of the red emission was experimentally measured and was found to be 2 ms. The orange transition $^5D_0$ → $^7F_1$ is much lower in intensity and is allowed by magnetic dipole process. All the other transitions $^5D_0$ → $^7F_0$, $^7F_3$, $^7F_4$, are electric dipole in character and are

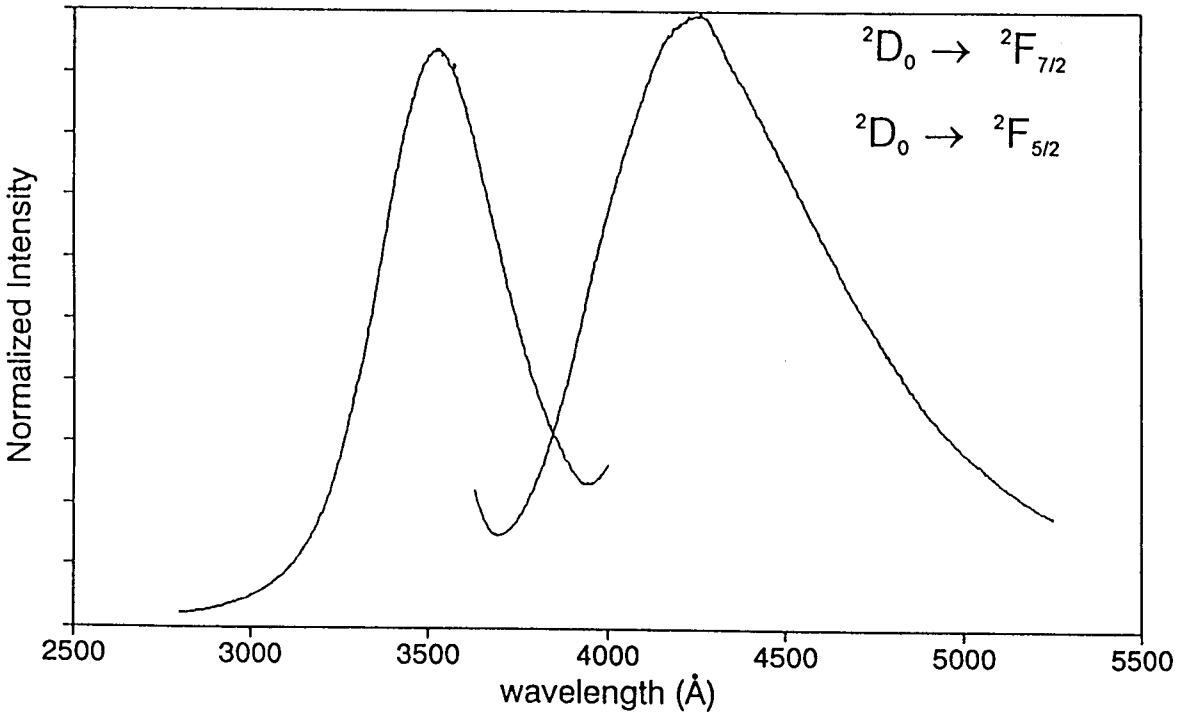

Figure 4.3. Emission and Excitation Spectra of the luminescence of 2% Ce^{3+} : $BaCaBO_3F$ at 298 K.

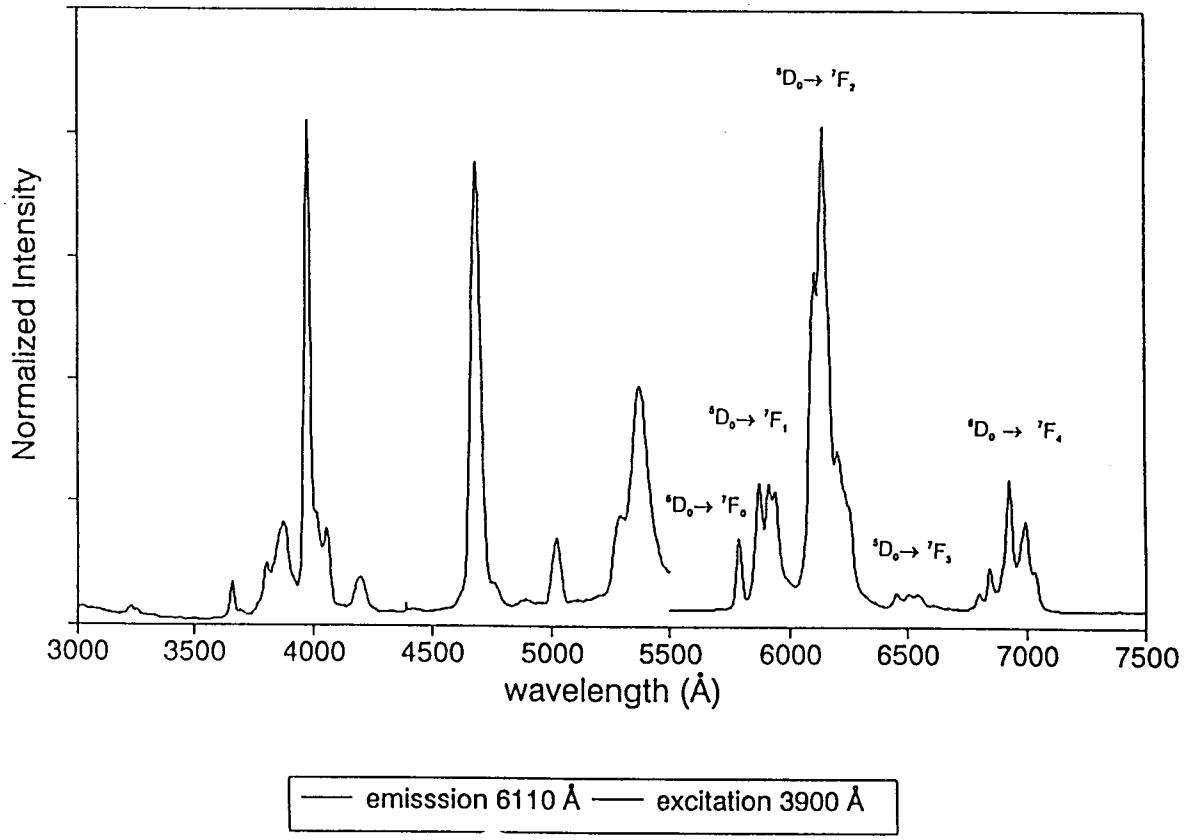

Figure 4.4. Emission and Excitation Spectra of the luminescence of 2% Eu^{3+} : $BaCaBO_3F$ at 298 K.

induced by odd-parity components of crystal field. The Tb^{3+} : $BaCaBO_3F$ exhibits a green emission due to the allowed $^5D \rightarrow {}^4F$ transitions (Figure 4.5.). The LS terms are higher in energy for Tb^{3+} then for Eu^{3+} and consequently luminescence from the $^5D_4$ level to the ^7F_J manifold is in the green. The spectral lines are in agreement with previously reported results.[8] The life time of the green emission was found to be 2 ms.

The Nd^{3+} : $BaCaBO_3F$ exhibits two emission bands centered at 8750 Å and 10640 Å (Figure 4.6.). The transitions correspond to $^4F_{3/2} \rightarrow {}^4I_{9/2}$ and $^4F_{3/2} \rightarrow {}^4I_{11/2}$. The spectroscopic properties of Nd^{3+} in many host materials has been extensively studied particularly Nd^{3+} : $Y_3Al_5O_{12}$ where the transition 1.06 μm emission line is an efficient transition.[9] This spectrum with its sharp lines is typical of the spectra found in rare earth ions. We are particularly interested in the lifetime and emission cross-section of the transition at 900 nm, because it could be used as a source to produce blue light by second harmonic conversion.

The Bi^{3+} : $BaCaBO_3F$ emits as a broad band with the peak centered around 5500 Å (Figure 4.7.). This broad band is due to the allowed transition $^3P_1 \rightarrow {}^1S_o$. The Bi^{3+} is characterized by $6s^2$ ground state configuration. The position of its excitation and emission bands depend largely on the nature of the host lattice. The excitation maximum is at 2900 Å and the emission maximum is at 5520 Å, thus yielding a Stokes shift of 2620 Å. This Stokes shift

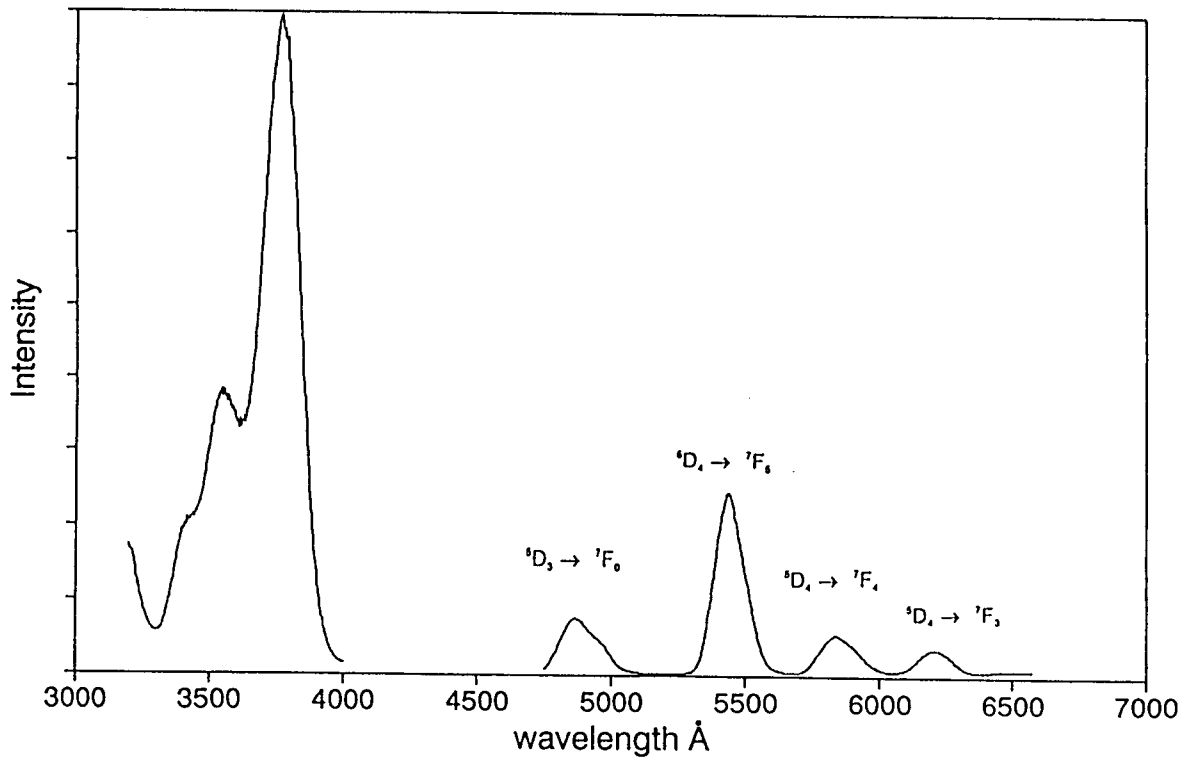

Figure 4.5. Emission and Excitation Spectra of the luminescence of 2% Tb^{3+} : $BaCaBO_3F$ at 298 K.

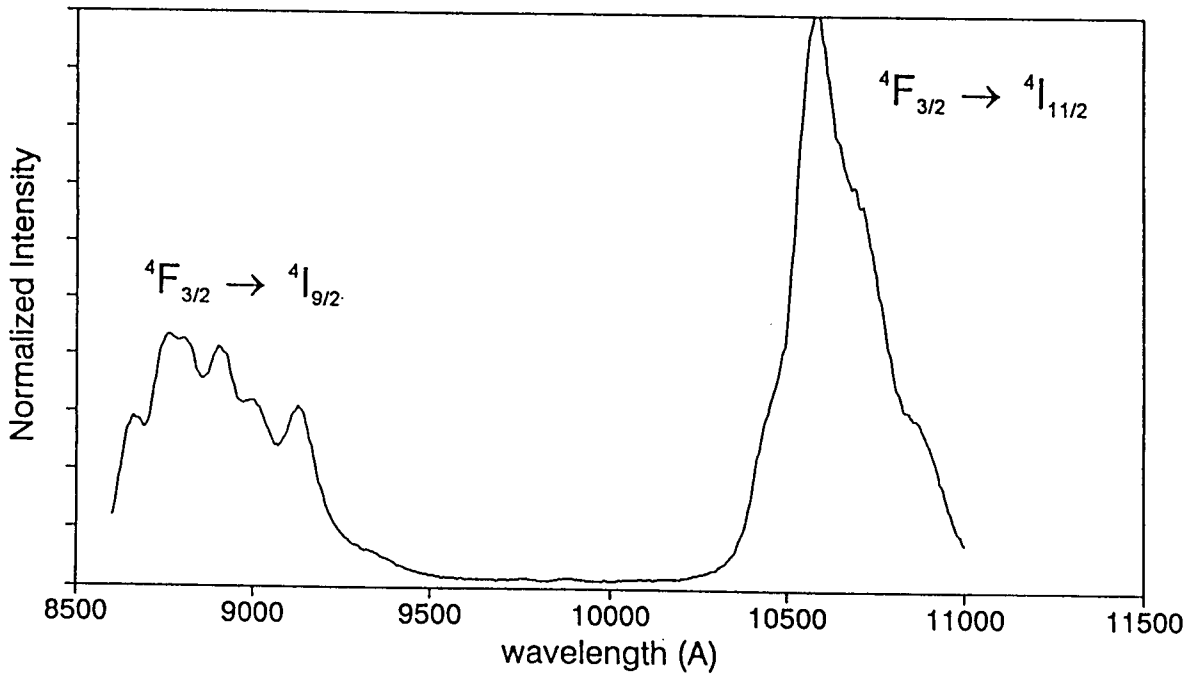

Figure 4.6. Emission and Excitation Spectra of the luminescence of 2% Nd^{3+} : $BaCaBO_3F$ at 298 K.

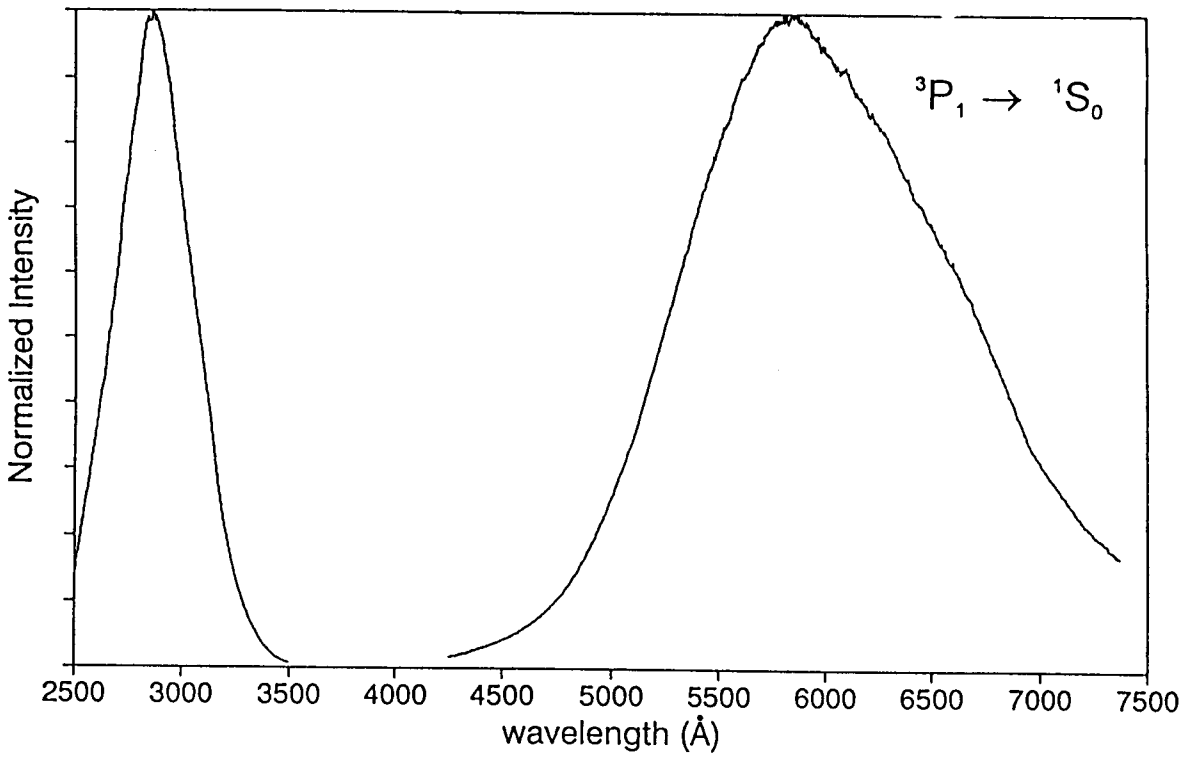

Figure 4.7. Emission and Excitation Spectra of the luminescence of 2% Bi^{3+} : $BaCaBO_3F$ at 298 K.

possibly originates from the fact that the excited state after relaxation is far out of resonance with ions in the ground state. Since excitation energy stays on the Bi^{3+} ion this can be considered as an isolated ion. In the compound Bi_2GeO_{20},[10] Bi^{3+} exhibits a Stokes shift of 1400 Å with the excitation and emission bands at 3550 and 4950 Å respectively.

Acknowledgments

This research was supported by National Science Foundation (DMR92-21372). Acknowledgment is made to the Donors of The Petroleum Research Fund, administered by the American Chemical Society, for partial support of the work.

References

1. TEXSAN: Single Crystal Structure Analysis Software, Version 5.0 **1989**, Molecular Structure Corp., The Woodlands, TX, 77381.

2. Sheldrick, G. SHELXS86. In *Crystallographic Computing 3*; Sheldrick, G.; Kruger,C.; Goddard, R.; Eds.; Oxford University Press: New York, **1985**; pp 175-189.

3. Walker, N.; Stuart, D. *Acta Crystallgr., Sect. A* **1983**, *39*, 158.

4. Shannon, R. D. *Acta Crystallogr., Sect. A* **1976**, *32*, 751.

5. Mackie, P.E., Young, R. A. *J. Appl. Crys.* **1973**, *6*, 26-31.

6. Botden, Th. P. J. *Philips Res. Rept.* **1952**, *7*, 197.

7. Blasse, G. *Philips Technical Review* **1970**, *31*, 309.

8. Saubat, S., Fouassier, C., Hagenmuller, P. *Mater. Res. Bull.* **1981**, *16*, 193.

9. Henderson, B., Imbush, G. F. *Optical Spectroscopy of Inorganic Solids*, Oxford Science Publications, **1989**.

10. Yimmermanns, C. W. M., Blasse, G. *J. Solid State Chem.* **1984**, *52*, 222.

CHAPTER 5
Structure and Solid Solution Study of Noncentrosymmetric Orthoborate Fluorides $Ba_{7-x}Sr_x(BO_3)_3F_5$

Abstract

From a single crystal X-ray diffraction analysis, the compounds $Ba_3Sr_4(BO_3)_3F$ and $Ba_{3.95(2)}Sr_{3.05(3)}(BO_3)_3F_5$ have been determined to crystallize with two formula units per cell in the noncentrosymmetric hexagonal space group $P6_3mc$. Cell parameters for $Ba_3Sr_4(BO_3)_3F$: a = 10.853(1), c = 6.945(2) Å, V = 708.5(2) $Å^3$; Cell parameters for $Ba_{3.95(2)}Sr_{3.05(3)}(BO_3)_3F_5$: a = 10.921 (1), c = 7.017(1) Å, V = 724.8(2) $Å^3$. These compounds are similar in structure to the parent compound $Ba_7(BO_3)_3F_5$. The Sr and Ba-centered polyhedra are interconnected by the fluoride and orthoborate anions to form an intricate 3-dimensional framework. The orthoborate triangles are arranged as a pseudo-hexagonal 6_3 array about the principal axis.

Introduction

The crystal structure and optical properties of $Ba_7(BO_3)_3F_5$ have recently been described by Alekel.[1] Significant second-order nonlinear coefficients have been calculated for the compound and crystals with edge length near 1 cm have been grown. The crystals, however, are highly hygroscopic. To retain the desirable features of the compound and limit its hygroscopicity we have performed a systematic study of the solid solution $Ba_{7-x}Sr_x(BO_3)_3F_5$. The solid solutions were analyzed by powder X-ray diffraction, and the crystal structures of the phases with x = 3 and 4 were examined by using single crystal X-ray diffraction methods.

Experimental

Powders of the alkaline-earth-metal borate fluorides were synthesized by employing high-temperature solid-state methods. Stoichiometric quantities of alkali-metal carbonates (AESAR, >99.9%) were mixed with a 5 mole% excess of B_2O_3, ground under hexane, placed in Pt crucibles, and heated at 923K for 4h to decompose the reagents and initiate the reactions. A stoichiometric amount of barium fluoride (AESAR, 99.9%) was then added to the mixture which was reground and heated for 12h at 1073 K. Powder diffraction data were collected on an automated Philips diffractometer, and peak positions were corrected by using NIST Si standard 640b. The hkl assignment of each reflection was determined by comparison of an indexed pattern of the material $Ba_7(BO_3)_3F_5$. Unit-cell parameters a and c were refined by least-square analysis (POLSQ) with fifteen peaks in the range $22 < \theta < 60°$; results for the solid-solution series are summarized in Table 5.1. Single crystals of $Ba_3Sr_4(BO_3)_3F_5$ were obtained for X-ray structure analysis from a stoichiometric melt. The melt was contained in a Pt crucible and slowly cooled from 1323 K to 973 K at 6 K/h, and then rapidly cooled at 50 K/h to room temperature. Single crystals of $Ba_4Sr_3(BO_3)_3F_5$ were grown by the same procedure. Crystals of approximate dimensions 0.1 x 0.1 x 0.1 mm were selected and mounted on

Table 5.1. Lattice Parameters for the $Ba_{7-x}Sr_x(BO_3)_3F_5$, solid solutions.

x	a (Å)	c (Å)	V (Å)
0[a]	11.208(5)	7.250(2)	788.7(5)
1	11.077(7)	7.150(2)	759.8(2)
2	10.979(4)	7.069(4)	737.9(8)
3	10.893(2)	6.990(3)	718.3(3)
4	10.840(8)	6.983(1)	710.6(8)
5	10.809(2)	6.909(4)	699.9(4)
6	10.809(2)	6.909(4)	699.9(1)

Note. Standard deviation is given in parentheses.

a: See Ref 1.

glass fibers with epoxy for structure determinations. All measurements were made on a Rigaku AFC6R diffractometer with graphite-monochromated Mo Kα radiation. Cell constants and the orientation matrix for data collection were obtained from a least -squares refinement with 20 automatically-centered reflections in the range $30 < 2\theta < 36°$. The cell constants correspond to the hexagonal crystal system; Laue symmetry 6/mmm was determined on the diffractometer. For each crystal, intensity data were collected over the range of indices $-17 < h < 17$, $0 < k < 17$, $-11 < l < 11$ by using the ω scan technique to a maximum 2θ value of 70°. From 6526 measured reflections for $Ba_3Sr_4(BO_3)_3F_5$, a total of 1000 were observed [$F_o^2 \geq 3\sigma F^2$], and from 6480 reflections for $Ba_{3.95(2)}Sr_{3.05(3)}(BO_3)_3F_5$ a total of 890 were observed. The intensities of three representative reflections measured after every block of 200 data varied by an average of 0.2% for $Ba_3Sr_4(BO_3)_3F_5$ and 0.3% for $Ba_{3.95(2)}Sr_{3.05(3)}(BO_3)_3F_5$ during data collection. The structures were solved and refined by using the TEXSAN software package.[2] The crystals were found to form in the noncentrosymmetric space group $P\,6_3\,m\,c$. The positions of the Ba and Sr atoms were derived from the direct methods program SHELXS,[6] while the remaining atoms O, F, and B were located from difference electron density maps. After a full-matrix isotropic refinement of the model[5] absorption corrections were applied by using the program DIFABS[3] (transmission factors

0.90 - 1.10 for $Ba_3Sr_4(BO_3)_3F_5$ and 0.79 - 1.33 for $Ba_{3.95(2)}Sr_{3.05(3)}(BO_3)_3F_5$). The data were averaged (R_{int} = 0.093 for $Ba_3Sr_4(BO_3)_3F_5$ and 0.043 for $Ba_{3.95(2)}Sr_{3.05(3)}(BO_3)_3F_5$). The occupancy of both Ba and Sr sites were refined in the structure $Ba_{3.95(2)}Sr_{3.05(3)}(BO_3)_3F_5$, and it was found that their was a mixed occupancy of Sr in the Ba2 site and Ba in the Sr1 site resulting in a stoichiometry $Ba_{3.95(2)}Sr_{3.05(3)}(BO_3)_3F_5$. Final refinements included anisotropic displacement coefficients on heavy atoms and some of the oxygen atoms, resulted in the residuals R = 0.043 and R_w = 0.056 for the $Ba_3Sr_4(BO_3)_3F_5$ and R = 0.048 and R_w = 0.054 for the $Ba_4Sr_3(BO_3)_3F_5$. The final refinement cycle converged with shift/error = 0.01 for $Ba_3Sr_4(BO_3)_3F_5$ and 0.01 for $Ba_{3.95(2)}Sr_{3.05(3)}(BO_3)_3F_5$ and the maximum and minimum peaks in the final electron density map correspond to 2.37% for $Ba_3Sr_4(BO_3)_3F_5$ and 1.97% for $Ba_{3.95(2)}Sr_{3.05(3)}(BO_3)_3F_5$ of Ba atom. Crystal data are outlined in Table 5.2, and atomic positional and displacement coefficients are listed in Table 5.3. Selected bond distances and angles are given in Table 5.4.

Table 5.2. Crystal data and experimental conditions for $Ba_3Sr_4(BO_3)_3F_5$ and $Ba_{3.95(2)}Sr_{3.05(3)}(BO_3)_3F_5$.

	$Ba_3Sr_4(BO_3)_3F$	$Ba_{3.95(2)}Sr_{3.05(3)}(BO_3)_3F_5$
Diffractomer	Rigaku AFC6R	Rigaku AFC6R
Radiation	Graphite monochromated Mo Kα (λ = 0.70926 Å)	
Formula wt., amu	1033.89	1083.60
Unit cell	Hexagonal	
a, Å	10.853 (1)	10.921(1)
c, Å	6.945 (2)	7.017(1)
V, Å^3	708.5 (2)	724.8(1)
Space group	$P6_3mc$	
D_{calc}, g cm^{-3}	4.846	4.964
F(000)	904	940
Z	2	2
Linear abs. coeff., cm^{-1}	227.98	214.15
No. unique data with with $F_o^2 > 3\sigma(F_o^2)$	1000	890
[a]R (F_o)	0.043	0.048
R_w (F_o)	0.056	0.054

[a] $R = \Sigma \, | \, |F_o| - |F_c| \, | \, / \Sigma \, |F_o|$; $R_w = [\, \Sigma w (\, |F_o| - |F_c| \,)^2 / \Sigma \, w \, |F_o|^2 \,]^{1/2}$.

Table 5.3. Positional and Thermal Parameters (B_{eq}) for $Ba_3Sr_4(BO_3)_3F_5$ and $Ba_{3.95(2)}Sr_{3.05(3)}(BO_3)_3F_5$

	$Ba_3Sr_4(BO_3)_3F_5$				$Ba_{3.95(2)}Sr_{3.05(3)}(BO_3)_3F_5$			
	x	y	z	B_{eq}	x	y	z	B_{eq}
Ba1	0.278(6)	0.1359	0.3705	1.282(4)	0.2756(1)	0.1378	0.3705	1.620(3)
Sr1	0.4706(6)	-0.4706	0.5271(2)	1.53(1)	0.4694(1)	-0.4694(1)	0.5275(4)	2.33(8)
Ba1A					0.4694	-0.4694	0.5275	2.33
Sr2(Ba2)	0.6667	0.3333	0.6238(3)	0.90(3)	0.6667	0.3333	0.626(1)	3.0(2)
Sr2A					0.6666	0.3333	0.626	3.0
F1	0.3333	0.6666	0.520(3)	2.6	0.3333	0.6666	0.514(4)	4.1(8)
F2	0	0	0.208(4)	3.3(5)	0	0	0.182(2)	0
F3	0.589(1)	-0.5894	0.331	9.6(7)	0.583	-0.583	0.344(3)	11.0(3)
O1	0.4066(8)	0.0957(9)	-0.279(1)	1.9(2)	0.403(1)	0.093(1)	-0.278(1)	1.9(3)
O2	0.311(1)	0.1555	-0.0006(2)	2.1(2)	0.313(1)	0.1563	-0.0092	0(1)
B	0.375(1)	0.1876	-0.194	0.90(2)	0.375(2)	0.1874	-0.193(2)	0(1)

Table 5.4. Interatomic distances (Å) and angles (°) for $Ba_3Sr_4(BO_3)_3F_5$ and $Ba_{3.95(2)}Sr_{3.05(3)}(BO_3)_3F_5$.

Ba1-F2 ×2	2.76(1)	2.881(8)	F2-Ba1-O1	88.3(2)	87.1(3)
Ba1-O1 ×2	2.941(9)	2.919(8)	F2-Ba1-O1	77.0(5)	70.9(4)
Ba1-O1 ×2	2.982(7)	2.99(1)	O1-Ba1-O1	136.0(3)	136.0(4)
Ba1-O2	2.64(1)	2.68(1)		82.7(2)	83.3(3)
Ba1-O2 ×2	2.887(8)	2.924(1)	O2-Ba1-O2	122.5(5)	122.3(5)
Sr1-F1	2.584(1)	2.577(2)	O1-Ba1-O2	64.9(3)	64.4(3)
Sr2-F3	2.62(3)	2.61(5)		123.4(2)	125.3(4)
Sr1-F3	2.39(3)	2.43(2)	F1-Sr1-F3	147.5(8)	146.9(8)
Sr1-O1×2	2.644(7)	2.68(1)		62.9(8)	68.1(7)
Sr1-O1×2	2.504(7)	2.54(1)	F1-Sr1-O1	126.1(4)	126.4(5)
Sr1-O1×2	3.043(9)	3.047(4)	F1-Sr1-O2	126.1(4)	126.4(5)
Sr2(Ba2)-F1	2.75(2)	2.72(3)	F3-Sr1-(Ba2)-F3	149.5(6)	141.3(4)
Sr2(Ba2)-O1×3	2.50(3)	2.53(2)	F3-Sr1-(Ba2)-O1	77.6(5)	76.8(3)
Sr2(Ba2)-O1×6	2.791(9)	2.843(8)	F1-Sr2(Ba2)-F3	104.2(3)	100.3(6)

Table 5.4. (continued)

B-O2	1.43(2)	1.42(2)	F3-Sr2(Ba2)-F3	60.2(1)	65.5(6)
			F3-Sr2-(Ba2)-O1	74.5(5)	71.6(3)
				98.8(2)	97.8(3)
				134.9(5)	137.1(4)
			O1-Sr2(Ba2)-O1	150.7(3)	151.2(4)
				114.4(1)	114.6(2)
				49.4(3)	49.3(6)
			O1-B-O1	121(1)	122(1)
			O1-B-O2	119.5(6)	118.8(8)
				119.5(6)	11991)

Results and Discussion

The compounds $Ba_3Sr_4(BO_3)_3F_5$ and $Ba_{3.95(2)}Sr_{3.05(3)}(BO_3)_3F_5$ both crystallize in the hexagonal noncentrosymmetric space group P 6_3mc. Since the two compounds are isostructural, the discussion will be directed to the stoichiometry $Ba_3Sr_4(BO_3)_3F_5$. A labelled diagram of the unit cell is given in Figure 5.1. The Ba and Sr-centered polyhedra interconnect with each other by sharing faces and edges to form a 3-dimensional framework.

The Ba1 atom is 9-coordinately bonded to two F, four O2, and three O1 atoms and is best described as a distorted monocapped cube. The Ba1 polyhedra share O··O··F faces with Sr1 and Sr2 polyhedra. Two adjacent Ba1 polyhedra are connected through adjacent edges of BO_3 triangles. The Sr1 is 9-coordinately bonded to three F and six O2 atoms and occupies a distorted hexagonal base, trigonal base monocapped geometry (Figure 5.2). The hexagonal base is formed by O atoms, the trigonal base is formed by F atoms. The Sr2 is 9-coordinately bonded to four F atoms and six O atoms. The bonding of the atoms around Sr2 results in a distorted monocapped trigonal prism. The Sr2-O1 bond distance 3.043(9) is very long, indicating a weak bonding interaction with metal atom.

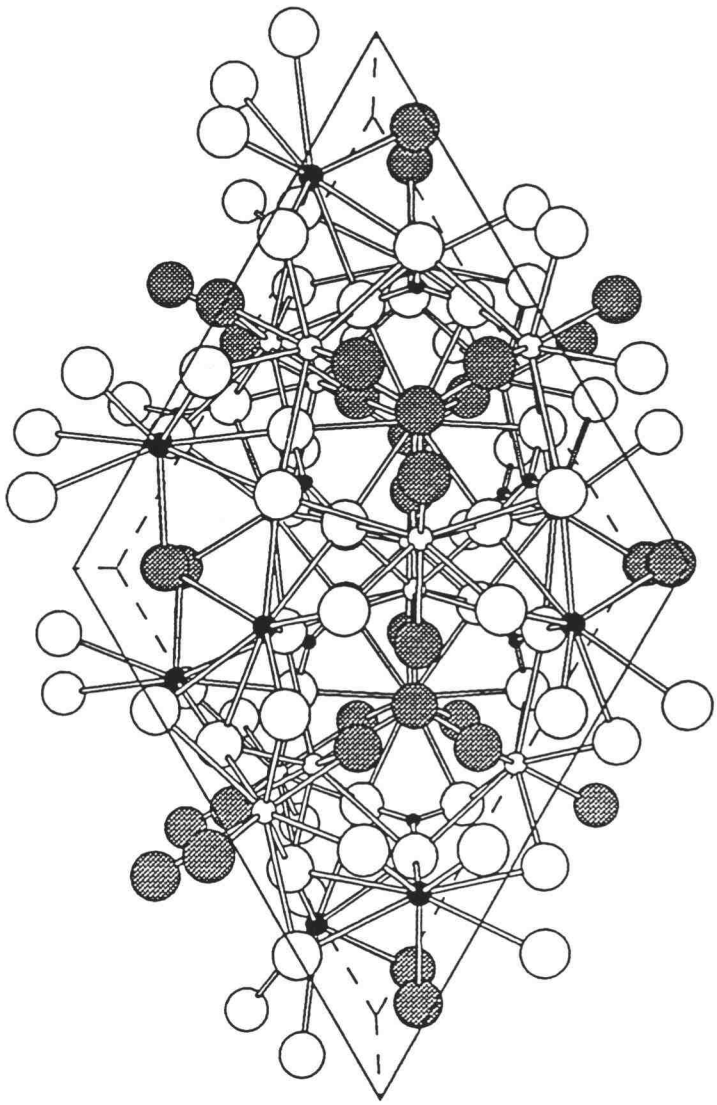

Figure 5.1. A schematic view of the unit cell for $Ba_3Sr_4(BO_3)_3F_5$. The medium filled circles represent Ba atoms, medium light circles represent Sr atoms, small filled circles represent B atoms. Large light circles represent O atoms, large shaded circles represent F atoms.

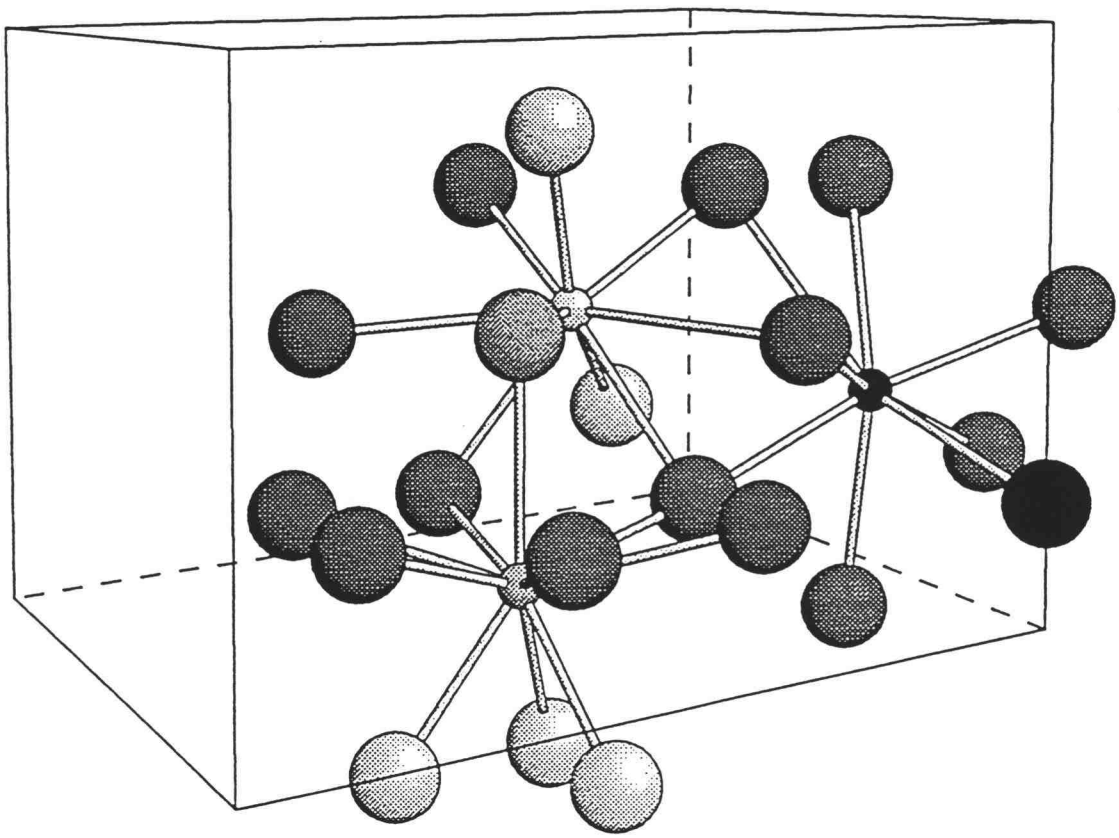

Figure 5.2. The Ba, Sr1 and Sr2 coordination centers in $Ba_3Sr_4(BO_3)_3F_5$. The medium filled circle represents Ba atom, medium shaded circles represent Sr atoms.

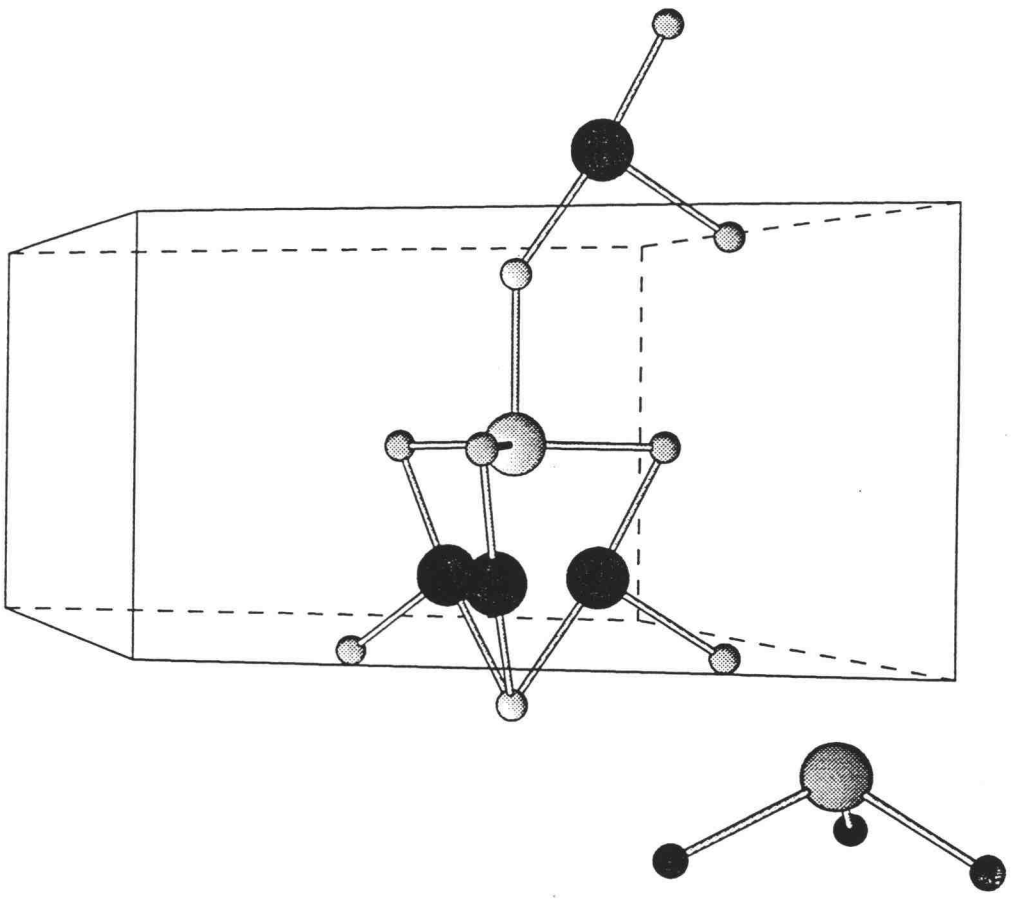

Figure 5.3. Coordination environments for the F atoms in $Ba_3Sr_4(BO_3)_3F_5$.

There are three types of F atoms in the structure (Figure 5.3). The F1 atom is coordinated to four Sr1 atoms in a distorted trigonal base pyramid. The F2 atom is bonded to three Ba1 atoms. The F3 atom is pyramidally bonded to Sr atoms in a T-shaped geometry. The BO_3 groups have bond distances and angles that are unexceptional.

The extent of solubility of Sr in the compound $Ba_7(BO_3)_3F_5$ was determined by performing a solid-solution study of the series $Ba_{7-x}Sr_x(BO_3)_3F_5$ ($0 \leq x \leq 7$). Volume-composition plots are shown in Figure 5.4. The error bars in this Figure indicate 3σ, and the systematic decrease in volume and cell constants as x is varied from 1 to 4 in $Ba_{7-x}Sr_x(BO_3)_3F_5$ indicates that smaller Sr atom substitutes at the Ba sites. The study also indicates that the extent of solubility amounts to x = 4. For x > 4 limit, the equilibrium is established between the $Sr_5(BO_3)_3F$[6] and $Ba_3Sr_4(BO_3)_3F_5$.

The crystal structures for x = 3 and x = 4 in $Ba_{7-x}Sr_x(BO_3)_3F_5$ provide materials that crystallize with a similar atomic positions to those of $Ba_7(BO_3)_3F_5$. The crystal-structure solution for $Ba_{3.95(2)}Sr_{3.05(3)}(BO_3)_3F_5$ revealed the structure to contain more Sr than predicted by synthesis. There is a mixed occupancy of Ba and Sr in sites that were supposed to be primarily Ba and Sr. This results in a composition $Ba_{3.95(2)}Sr_{3.05(3)}(BO_3)_3F_5$. The F3 atom has a high B_{eq} indicating that there may be either a static disorder associated with the site, or there may be a possibility of a super cell in these systems.

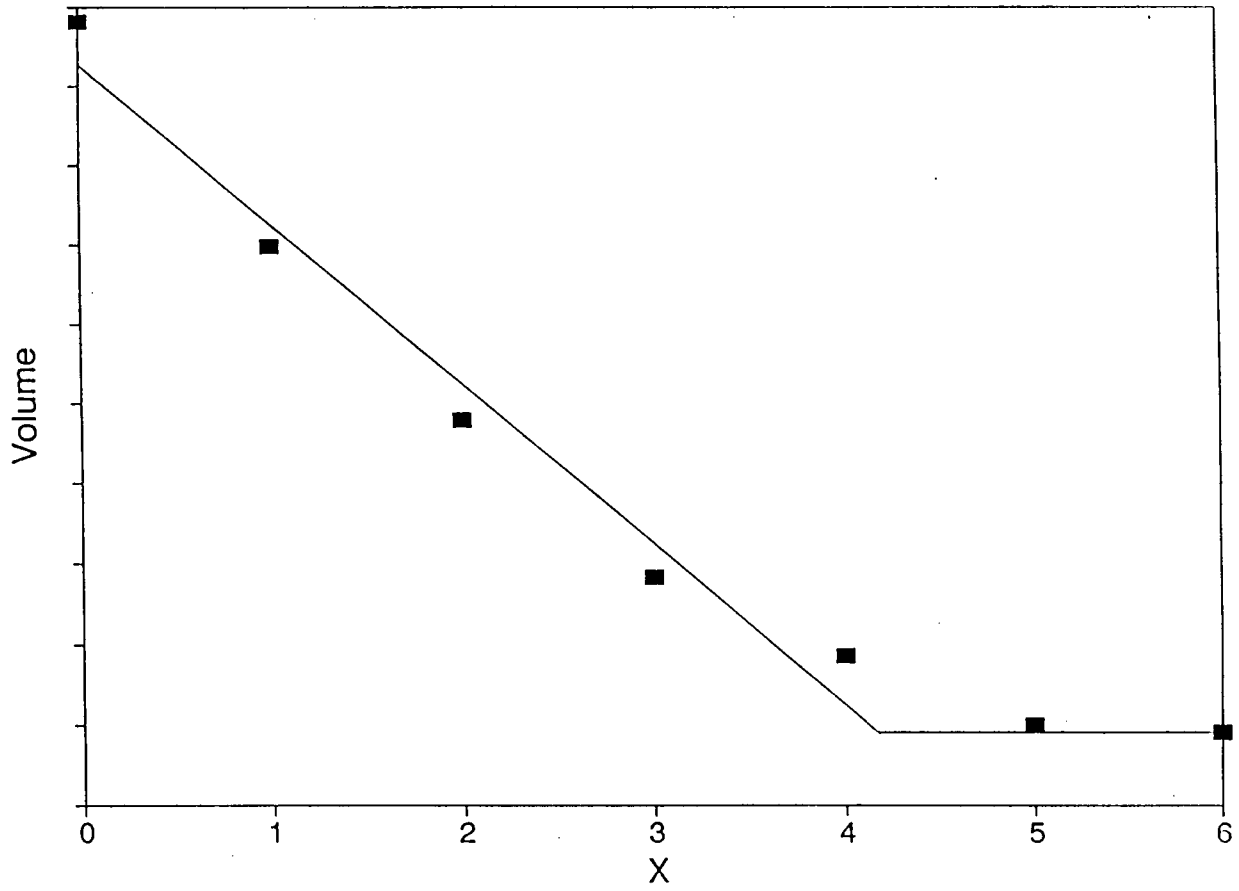

Figure 5.4. Unit cell volume for the solid-solution series as a function of composition ($0 \leq x \leq 6$).

crystal structure are in progress. The orientation of the BO_3 groups about the c axis is an important feature of this compound (Figure 5.5). A chromophore geometry that would maintain a high susceptibility and minimize phase matching and threshold power properties for conversion of IR light[7] is shown in Figure 5.6. Here, the B-O bonds of three orthoborate triangles align along a principal axis . The orientation in the title compound is similar to the idealized geometry except that the BO_3 groups are oriented away from the *c* axis by 40° in comparison with 33° observed for the compound $Ba_7(BO_3)_3F_5$. According to the oxoanion SHG model which predicts a semiquantitative nonlinear susceptibility exclusively on the basis of the atomic structure of the compound, the sum of the BO_3 micropolarizabilities will be less than ideal. With the $\cos^3\theta$ functional dependence of the β_{333} coefficient for a BO_3 planar rotation that is orthogonal to the C_3 axis, as in the title compounds, the calculated susceptibility is 47% ($\cos^3 47°$) in comparison with 59% of optimum exhibited by $Ba_7(BO_3)_3F_5$. By considering the arrangement of the BO_3 groups only, we derive the nonlinear coefficients d_{31} = 0.46 pm/V and d_{33} = 0.8 pm/V for $Ba_3Sr_4(BO_3)_3F_5$ which compare to d_{31} = 0.44 pm/V and d_{33} = 0.6 pm/V for $Ba_7(BO_3)_3F_5$. The d_{33} 's are similar to the nonlinearity of LBO, but the coefficient d_{31} only is operating in phase matching. The lack of coplanarity among all BO_3 groups should produce a small birefringence.

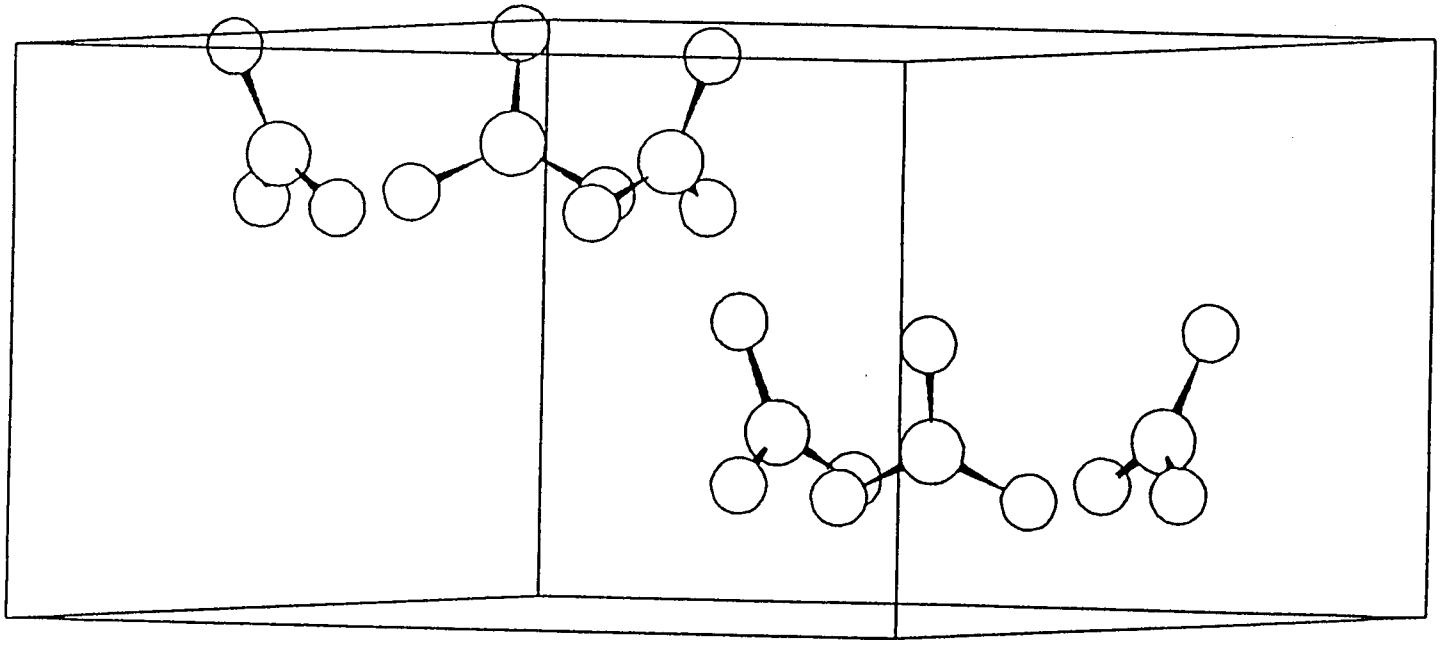

Figure 5.5. The arrangement of BO_3 groups in $Ba_3Sr_4(BO_3)_3F_5$.

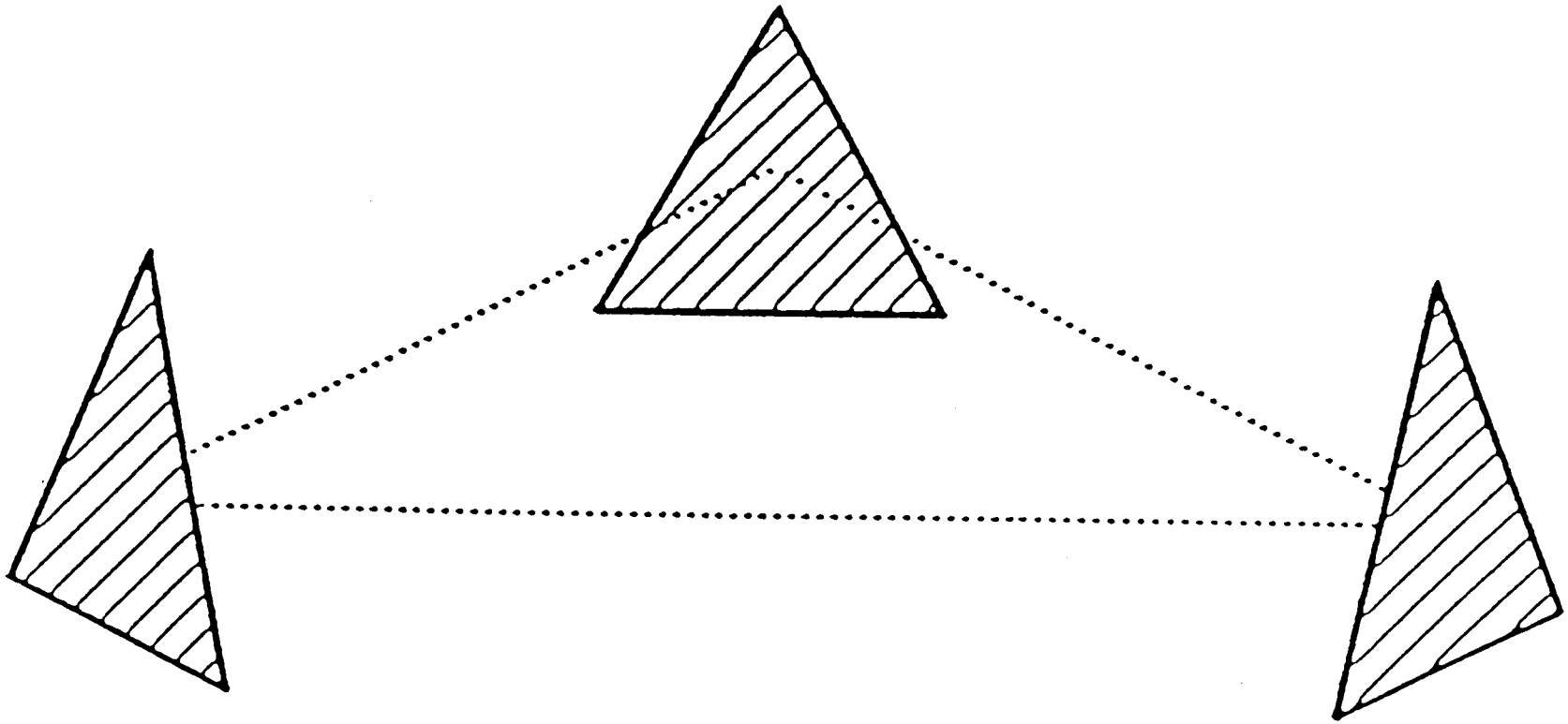

Figure 5.6. A proposed arrangement for BO_3 groups for obtaining high nonlinearity and low birefringence.

Acknowledgments

This research was supported by National Science Foundation (DMR92-21372). Acknowledgment is made to the Donors of The Petroleum Research Fund, administered by the American Chemical Society, for partial support of the work.

References

1. Alekel, T. Ph.D. Thesis Oregon State University **1993**.

2. TEXSAN: Single Crystal Structure Analysis Software, Version 5.0 **1989**. Molecular Structure Corp., The Woodlands, TX, 77381.

3. Sheldrick, G. SHELXS86. In *Crystallographic Computing 3*; Sheldrick, G.; Kruger,C.; Goddard, R.; Eds.; Oxford University Press: New York, 1985; pp 175-189.

4. Walker, N.; Stuart, D. *Acta Crystallgr., Sect. A* **1983**, *39*, 158.

5. Shannon, R. D. *Acta Crystallogr., Sect. A* **1976**, *32*, 751.

6. Alekel, T., Keszler, D. A. *Inorganic Chemistry.*, **1993**, *32*, 101.

7. Schaffers, K. I. Ph.D. Thesis Oregon State University **1993**.

CHAPTER 6
The Polyborates $BaMB_9O_{15}$ (M = Li, Na)

Annapoorna Akella, Jun-Ming Tu, and Douglas Keszler*

Department of Chemistry and

Center for Materials Research

Gilbert Hall 153, Oregon State University

Corvallis, Oregon 97331-4003

In preparation for submission to the *Journal of Solid State Chemistry*

Abstract

The barium alkali-metal borates $BaMB_9O_{15}$ (M = Li, Na) are noncentrosymmetric compounds that are structurally characterized by a complete condensation of B_3O_7 rings, channels extending through this borate framework and occupied by the Ba and Li(Na) atoms. They crystallize with six formula units in the trigonal system, space group R 3c(h). Cell parameters from single crystal X-ray data for $BaLiB_9O_{15}$: a = 10.9595(6), Å; c = 17.035(1), Å, and V = 1772.0(2) $Å^3$; and for $BaNaB_9O_{15}$: a = 11.099(2) Å, c = 17.401(4) Å, and V = 1856.3(7) $Å^3$.

Introduction

Because of both high conversion efficiency and optical damage threshold, the borate LiB_3O_5 (LBO) has found widespread use for the frequency conversion of high-power laser light[1]. The favorable performance of the material has been attributed to the electronic structure and relative orientations of the B_3O_7 rings that make up the condensed structure. As part of our continuing development of the structural chemistry of borates, we describe here the structures of $BaLiB_9O_{15}$ and $BaNaB_9O_{15}$, two derivatives of the $SrLiB_9O_{15}$ structure type.[2] Like LBO, this noncentrosymmetric structure type exhibits a condensation of B_3O_7 rings.

Experimental

Synthesis

Powders of the alkali-metal Ba borates were synthesized by employing high-temperature, solid-state methods. Stoichiometric quantities of the starting reagents, alkali-metal precursors (AESAR, nitrates or carbonates ≥99.9%) $BaCO_3$ (AESAR, ≥99.9%) and B_2O_3 (99.99%), were mixed (a 5 mol % excess B_2O_3 was added to compensate for residual water content), ground under hexane, placed in Pt crucibles, and heated at 873 K for 2 h to decompose the reagents and initiate the reactions. The samples were cooled, reground and then heated for 12 h at 1073 K. Single crystals of $BaLiB_9O_{15}$ were grown in a Pt crucible from a stoichiometric melt that was cooled from 1353 to 1053 K at 8 K/h and then at 60 K/h to room temperature. The crystals of $BaNaB_9O_{15}$ were also grown in a Pt crucible from a melt of molar composition 1 BaO: 0.5 Na_2O: 6.05B_2O_3 that was cooled from 1223 to 973 K and then rapidly to room temperature by simply turning off the power to the furnace.

Crystallographic studies

Crystals of $BaLiB_9O_{15}$ and $BaNaB_9O_{15}$ with edge lengths near 0.1 mm were selected and mounted on glass fibers with epoxy for structure determinations. All measurements were made on a Rigaku AFC6R single crystal diffractometer with graphite-monochromated Mo Kα radiation. Cell

constants and orientation matrices for data collection were obtained from least-squares refinements with 20 automatically-centered reflections in the range 30 $\leq 2\theta \leq$ 36°. Cell constants correspond to the rhombohedral crystal system, and Laue symmetry 3m was determined on the diffractometer. Intensity data were collected over the range of indices $0 \leq h \leq 17$, $-17 \leq k \leq 17$, $-27 \leq l \leq 27$ for the Li compound and $-9 \leq h \leq 9$, $0 \leq k \leq 9$, $-15 \leq l \leq 15$ for the Na compound by using the ω-scan technique to a maximum 2θ value of 75° for $BaLiB_9O_{15}$ and 60° for $BaNaB_9O_{15}$. From 1960 measured reflections for $BaLiB_9O_{15}$, a total of 1308 were observed [$F_o^2 > 3\sigma(F^2)$], and from 1570 reflections for $BaNaB_9O_{15}$ a total of 927 data were observed. The intensities of three representative reflections measured after every block of 200 data varied by an average of 0.2% for $BaLiB_9O_{15}$ and 0.3% for $BaNaB_9O_{15}$.

The structures were solved by using the *TEXSAN* software package[3] Each crystal was found to form in the noncentrosymmetric space group R3c(h). The positions of the Ba atoms were derived from the direct methods program SHELXS,[4] while the remaining atoms Na, O, B, and Li were located from difference electron density maps. After full-matrix isotropic refinements of the models absorption corrections were applied with the program DIFABS[5] (transmission factors = 0.83 - 1.22 for $BaLiB_9O_{15}$ and 0.87 - 1.09 for $BaNaB_9O_{15}$). The data were averaged (R_{int} = 0.073 for $BaLiB_9O_{15}$ and 0.071 for $BaNaB_9O_{15}$), and the models were then refined with anisotropic

displacement coefficients on each atom. Final least-squares refinements resulted in the residuals R = 0.046 and *w* R = 0.058 for $BaLiB_9O_{15}$ and R = 0.037 and w R= 0.043 for $BaNaB_9O_{15}$. The final refinement cycles converged with $\Delta/\sigma = 0.01$ and the maxima and minima in the final electron density maps correspond respectively, to 2.37% and 1.97% of the Ba atom in the Li compound, and 0.49% and 0.66% in the Na compound. Powder diffraction patterns of these materials, obtained with a Philips diffractometer, agree well those generated from the results of the single-crystal studies and the computer program LAZY-PULVERIX.[6] Crystal data are outlined in Table 6.1, and atomic positional and displacement parameters are listed in Table 6.2.

Table 6.1. Crystal data and experimental conditions for $BaMB_9O_{15}$ (M = Li, Na).

	$BaLiB_9O_{15}$	$BaNaB_9O_{15}$
Diffractomer	----------	Rigaku AFC6R ----------
Radiation	Graphite monochromated Mo Kα (λ = 0.70926	
Å)		
Formula wt., u	481.55	497.60
Unit cell	----------	Rhombohedral ----------
a, Å	10.9595(6)	11.099(2)
c, Å	17.035(1)	17.401(4)
V, $Å^3$	1772.0(2)	1856.3(7)
Space group	----------	R3c(h) ----------
D_{calc}, g cm^{-3}	2.707	2.670
F(000)	1344	1392
Z	6	
Linear abs. coeff., cm^{-1}	34.46	33.25
No. unique data with	1308	1383
with $F_o^2 > 3\sigma(F_o^2)$		
$R(F_o)$	0.046	0.037
$R_w(F_o)$	0.058	0.043

Table 6.2. Positional and Thermal Parameters (B_{eq}) for $BaLiB_9O_{15}$ and $BaNaB_9O_{15}$.

	$BaLiB_9O_{15}$				$BaNaB_9O_{15}$			
	x	y	z	B_{eq}	x	y	z	B_{eq}
Ba	0	0	0.4061	1.42(1)	0	0	0.3800	1.13(2)
B1	0.7895(8)	0.7348(8)	0.2177(5)	1.1(1)	0.280(1)	0.069(1)	0.1592(6)	1.4(3)
B2	0.7296(7)	0.8024(7)	0.0953(4)	0.8(1)	0.390(1)	0.118(1)	0.3764(6)	1.4(3)
B3	0.5664(6)	0.5728(6)	0.1580(7)	0.93(5)	0.2307(8)	-0.1068(8)	0.4343(6)	0.6(2)
Li(Na)	0	0	0.672(2)	3(1)	0	0	0.6596(3)	1.4(1)
O1	0.6055(5)	0.6767(5)	0.0980(3)	0.97(7)	0.2583(6)	0.0110(8)	0.3834(6)	0.9(2)
O2	0.4491(8)	0.894(1)	0.1990(4)	1.5(3)	0.1336(8)	0.2367(6)	0.4794(3)	0.8(2)
O3	0.8285(6)	0.8288(6)	0.1599(5)	1.5(2)	0.1838(6)	0.0039(9)	0.0995(4)	1.6(2)
O4	0.5521(6)	0.4440(8)	0.1126(4)	1.2(2)	0.2318(6)	0.110(1)	0.2208(3)	1.4(2)
O5	0.5760(5)	0.9320(5)	0.0432(3)	1.20(8)	-0.2549(7)	-0.0096(7)	0.3209(4)	1.2(2)

$$B_{eq} = 8\frac{\pi^2}{3}\sum_i \sum_j U_{ij} a_i^* a_j^* a_i \cdot a_j$$

Results and Discussion

The structures of $BaMB_9O_{15}$ (M = Li, Na) consist of a 3-dimensional borate framework, 12-coordinate Ba atom and 6-coordinate Li atom in the $BaLiB_9O_{15}$; 9-coordinate Ba atom and 6-coordinate Na atom in the $BaNaB_9O_{15}$. As seen in Figures 6.1., the framework is built from the condensation of B_3O_7 units, that contain channels along the c axis, filled alternately by Ba and Li(Na) atoms. Two compounds are isostructural to $SrLiB_9O_{15}$.

The basic building block of boron framework is B_3O_7 ring, which can be viewed as a planar B_2O_5 group bridged by a tetrahedral BO_4 group. Two O atoms in the B_2O_5 group in the B_3O_7 ring connect to the BO_4 groups of adjacent B_3O_7 rings, while two O atoms in the BO_4 group in the ring link to B_2O_5 groups of neighboring B_3O_7 rings. Therefore, each B_3O_7 ring connects to other four like rings and the B_3O_7 rings are thus fully condensed. The chemical formula of framework can be derived from $B_3O_3O_{4/2} = B_3O_5$. The title compounds may be appropriately expressed as $BaM(B_3O_5)_3$ in terms of the structure. The structures reported containing condensed B_3O_7 rings so far are LiB_3O_5(LBO),[7] CsB_3O_5,[8] TlB_3O_5,[9] and $SrLi(B_3O_5)_3$. The main feature of the compounds containing B_3O_7 rings is their formation in noncentrosymmetric space groups. The acentricity is consistent the chirality of the BO_4 group in the ring.

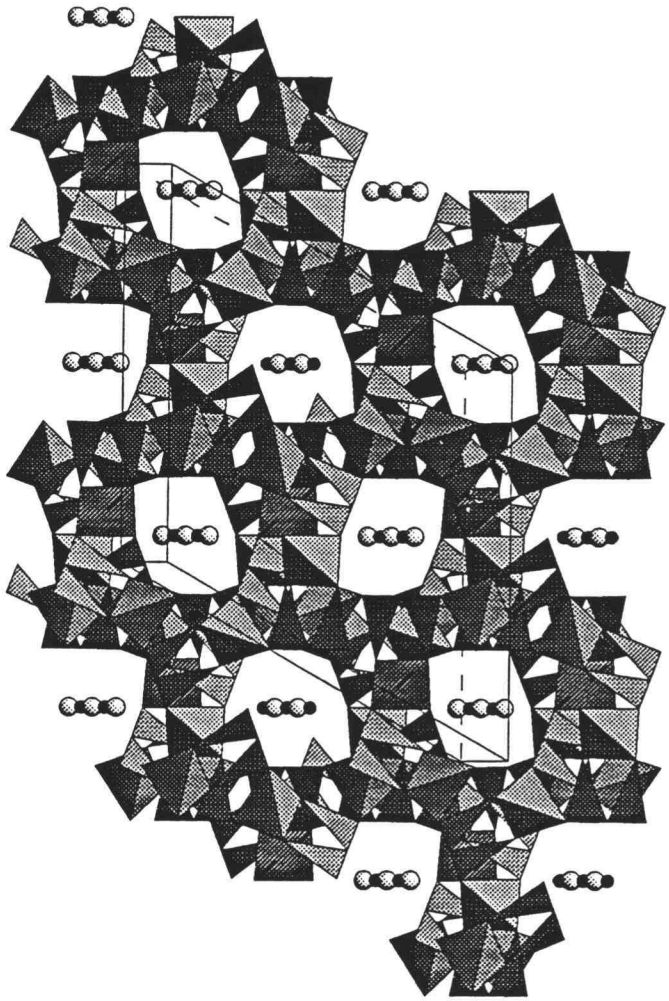

Figure 6.1. Sketch of the three-dimensional borate framework with Ba and Li atoms filling the tunnels, view is along the **c** axis. Triangles are BO_3 groups, tetrahedra BO_4 groups. Lightly shaded circles represent Ba atoms, and filled circles represent Li atoms, here and in Figure 6.2 and 6.3.

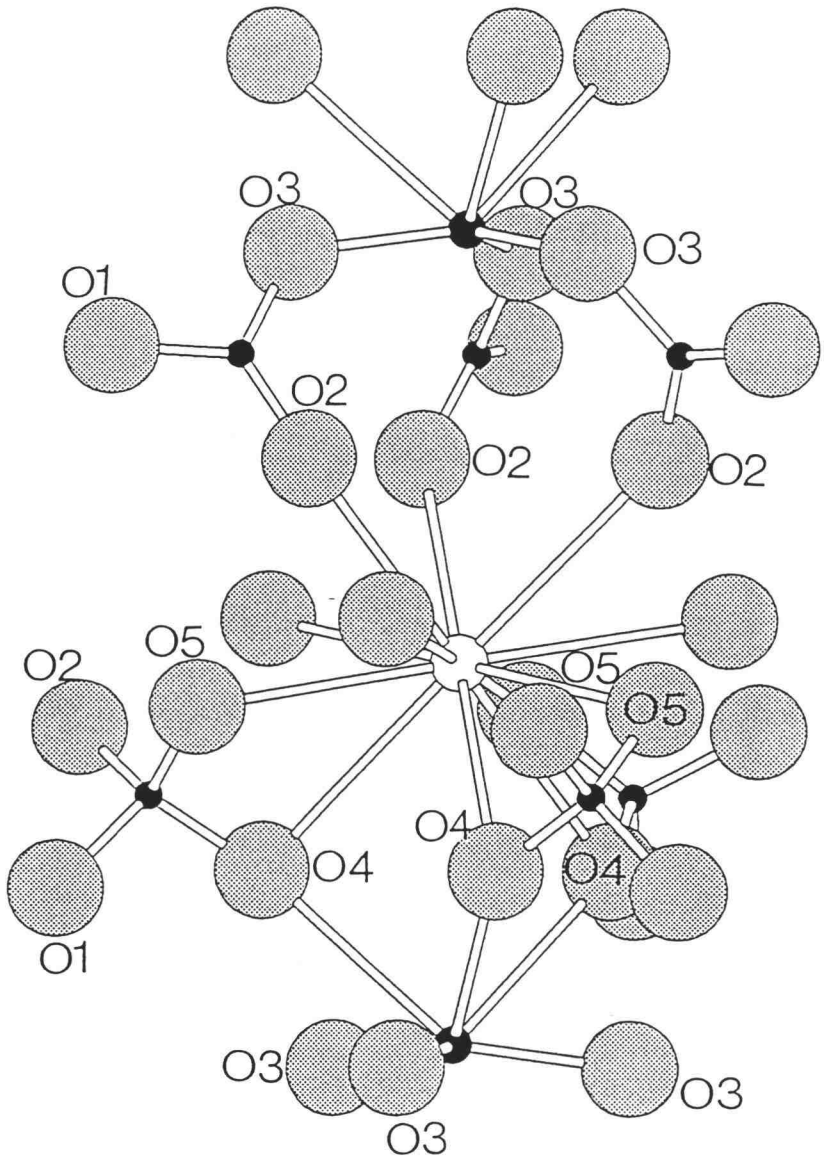

Figure 6.2. Labeled drawing of Ba- and Li-centered polyhedra in $BaLiB_9O_{15}$. Large shaded circles represent O atoms, and small filled circles represent B atoms, here and in Figure 6.3.

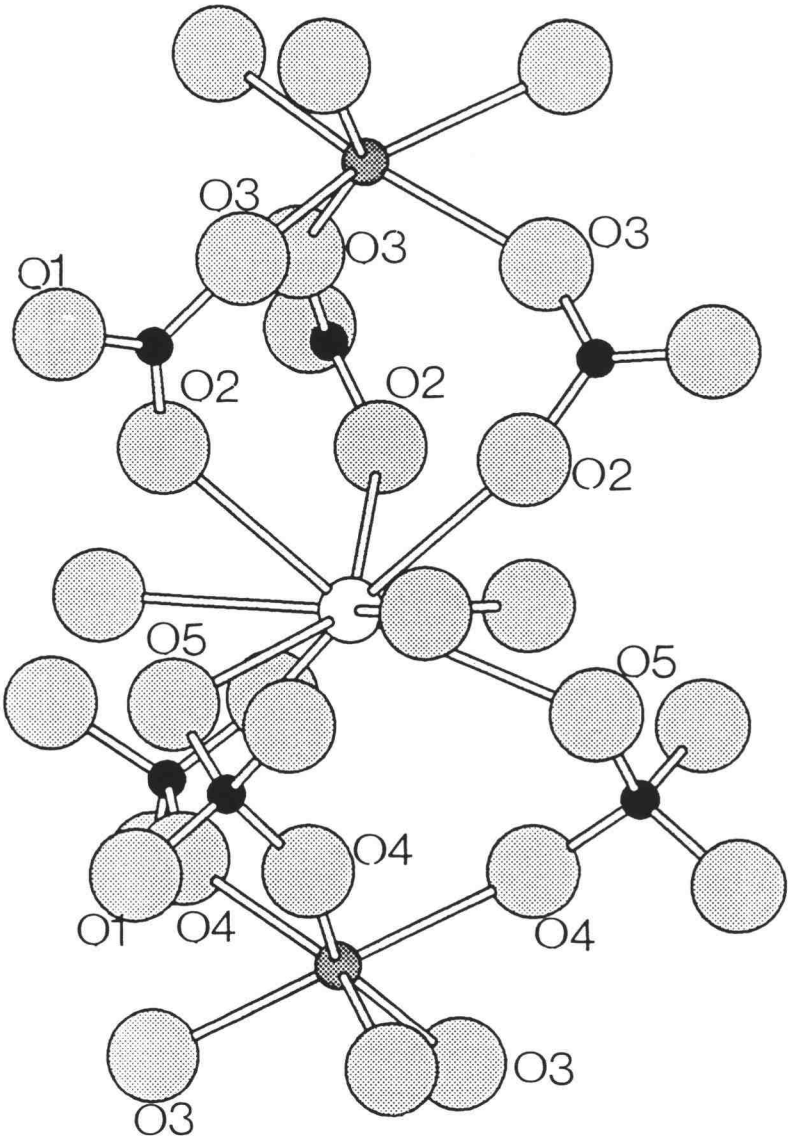

Figure 6.3. Labeled drawing of Ba- and Na-centered polyhedra in $BaNaB_9O_{15}$. Medium filled circles represent Na atoms.

The connectivity of the compound $BaLiB_9O_{15}$ is best appreciated by referring to Figure 6.2. Ba atom is surrounded by twelve O atoms and Li atom by six O atoms. Both the metal atoms lie on a site with C_3 symmetry. The highly distorted Li -centered site shares a face O4··O4··O4 with Ba-centered polyhedron. The Ba- and Li-centered polyhedra are also connected by face and bridged by BO_3 triangles along the c axis.

Selected interatomic distances and angles are summarized in Table 6.3. The bonding distances of Ba-O are in the range of 2.834(4) - 2.961(6) Å averaging at 2.965 ± 0.089 Å, and compare to 3.03 Å for 12-coordinate Ba obtained from crystal radii. The Li atom has three short bonding distances to atom O3 at 1.889(6) Å and three unusually long distances to atom O4 at 2.80(2) Å, in its 3 + 3 coordination environment, compared to the three shorter and longer Li-O distances at 1.98(1) and 2.48(2) Å respectively, in $SrLiB_9O_{15}$. The mean distance of Li-O in $BaLiB_9O_{15}$ is 2.345 ± 0.499 Å, somewhat longer than the length of 2.18 Å calculated for a 6-coordinated Li atom by using crystal radii.[11]

A labeled drawing of environments of the Ba and Na atoms in the structure of $BaNaB_9O_{15}$ is presented in Figure 6.3. Two polyhedra are linked by BO_3 triangles and BO_4 tetrahedra, compared to the edge-sharing in $BaLiB_9O_{15}$. Different connections in these two structures may stem from the coordination of Ba atom. The Ba atom is bound by nine O atoms in a distorted tricapped

Table 6.3. Selected Bond Distances (Å) and Angles (°) for $BaLiB_9O_{15}$ and $BaNaB_9O_{15}$.

	$BaLiB_9O_{15}$	$BaNaB_9O_{15}$		$BaLiB_9O_{15}$	$BaNaB_9O_{15}$
Ba -O1 ×3	2.961(6)	2.809(5)	O1-Ba-O1	117.92(5)	119.95(2)
Ba -O2 ×3	3.047(9)	2.862(6)	O1-Ba-O2	82.4(2)	84.2(3)
Ba -O4 ×3	3.039(8)			46.0(2)	49.1(3)
Ba -O5 ×3	2.838(4)	2.962(6)		121.3(2)	135.8(3)
			O1-Ba-O4	133.7(2)	
				59.0(2)	
			O1-Ba-O5	64.9(2)	62.8(2)
				60.1(2)	62.3(2)
			O2-Ba-O2	75.7(3)	87.3(2)
			O2-Ba-O4	104.6(2)	
				179.6(2)	
				104.6(2)	
			O2-Ba-O5	59.5(2)	61.7(2)

Table 6.3. (continued)

	$BaLiB_9O_{15}$	$BaNaB_9O_{15}$		$BaLiB_9O_{15}$	$BaNaB_9O_{15}$
			O4-Ba-O5	120.1(2)	
				79.3(2)	
			O4-Ba-O4	75.1(2)	
			O4-Ba-O5	120.1(2)	
				79.3(2)	
				120.1(2)	
			O5-Ba-O5	116.9(1)	108.6(1)
				59.0(2)	
Li(Na) -O3 ×3	1.889(6)	2.283(6)	O3-Li(Na)-O3	118.7(4)	100.7(2)
Li(Na) -O4 ×3	2.80(2)	2.470(6)	O3-Li(Na)-O4	94.5(6)	103.6(4)
			O3-Li(Na)-O4	136(1)	150.8(4)
			O3-Li(Na)-O4	54.2(5)	59.0(2)
B1-O3	1.33(1)	1.40(1)	O3-B1-O4	114.5(6)	115.6(8)

Table 6.3. (continued)

	$BaLiB_9O_{15}$	$BaNaB_9O_{15}$		$BaLiB_9O_{15}$	$BaNaB_9O_{15}$
B1-O4	1.39(1)	1.37(1)	O3-B1-O5	123.5(6)	120.2(8)
-O5	1.345(8)	1.37(1)	O4-B1-O5	119.5(7)	124.2(9)
B2-O1	1.370(6)	1.35(1)	O1-B2-O2	123.1(6)	120.9(9)
-O2	1.32(1)	1.36(1)	O1-B2-O3	116.1(2)	121.2(9)
-O3	1.46(1)	1.36(1)	O2-B2-O3	119.7(6)	117.9(8)
B3-O1	1.42(1)	1.48(1)	O1-B3-O2	111.8(7)	104.1(7)
-O2	1.41(1)	1.51(1)	O1-B3-O4	102.9(7)	109.1(8)
-O4	1.54(1)	1.45(1)	O1-B3-O5	112.6(4)	114.4(6)
-O5	1.51(1)	1.46(1)	O2-B3-O4	115.7(5)	114.3(6)
			O2-B3-O5	114.6(8)	109.2(7)

trigonal prismatic environment, which is similar to that of Sr atom in $SrLiB_9O_{15}$. The Ba-O distances vary from 2.809(5) to 2.962(6) Å averaging at 2.878 ± 0.067 Å. This compares to 2.85 ± 0.10 Å for the 9-coordinate Ba atom in the structure of $BaNaBO_3$.[12] The Na atom occupies a distorted trigonal prismatic site. The mean distance, 2.376 ± 0.102 Å compares to the 6-coordinate Na-centered environments in $BaNaBO_3$, Na1-O = 2.446 ± 0.063 Å, and Na2-O = 2.423 ± 0.100 Å.

There are three crystallographically distinct B atoms; atoms B1 and B2 are in triangular mode, and B3 is in a tetrahedral mode. The distances and angles for the B-O interactions are normal.

Acknowledgments

This work was supported by the US National Science Foundation, Solid-State Chemistry Program (DMR92-21372).

References

1. Chen, C., Wu, Y., Li, Y. *J. Crystal Growth* **1990**, *99*, 790.

2. Schaffers, K. I., Keszler, D. A. *Chem. Mat.* to be submitted.

3. TEXSAN, Structure Analysis Package, Molecular Structure Corp., MSC (3200A, Research Forest Drive, the Woodlands, TX 77381. International Tables for X-ray Crystallography. Vol. IV. Birmingham: Kynoch Press **1974**.

4. Sheldrick, G. M. In Crystallographic Computing 3; Sheldrick, G. M., Krüger, C., Godard, R., Eds.; Oxford Univ. Press, Oxford, U. K., **1985**, 175.

5. Walker, M., Stuart, D. *Acta Crystallogr., Sect.A,* **1983**, *39*, 158.

6. Yvon, K., Jeitschko, W., Parthe, E. *J. Appl. Crystallogr.*, **1977**,*10*, 73.

7. Kurtz, S. W., Perry, T. T., *J. Appl. Phys.* **1968**, *39*, 3798.

8. Krogh-Moe, J., *Acta Crystallogr., Sect.B,* **1974**, *30*, 1178.

9. Chen, C., Wu, Y., Jiang, A., Wu, B., You, G., Li, R., Lin, S. *J. Opt. Soc. Am. Sect.* B, **1989**, *6(4)*,616.

10. Akella, A. Ph. D. Thesis, Oregon State University **1994**.

11. Shannon, R. D. *Acta Crystallogr., Sect.*A, **1976**, **32**, 751.

12. Tu, J. M., Keszler, D. A. *Acta Crystallogr., Sect. C* **1994,** in press.

CHAPTER 7
Structures of Aminoguanidinum Salts

$C_2H_8N_4O_3$: N-Carboxy Aminoguanidinium Hydrate Inner Salt, Formerly Known as Aminoguanidinium Bicarbonate

Annapoorna Akella and Douglas A. Keszler*

Department of Chemistry and

Center for Advanced Materials Research

Oregon State University

Gilbert 153

Corvallis, Oregon 97331-4003

Acta Crystallogr., Sect. C, **1994** in press.

Abstract

The structure of aminoguanidinium bicarbonate, $(H_2N)_2CNH(NH_2).H_2CO_3$, has been determined by single crystal X-ray methods. The unique feature of this compound is that it crystallizes as the N-carboxy aminoguanidinium along with a molecule of water. As the molecular formula suggests it does not exist as the bicarbonate in the crystal instead it exists as an inner salt. The O2 atom of the N-carboxy unit intermolecularly bonds to the hydrogen atoms of the water and to the neighboring aminoguanidinium molecules.

Comment

While searching for guanidinium based optical materials, we have determined the structure of commercially available aminoguanidinium bicarbonate. The aminoguanidinium structures studied to date are the chloride,[1] dihydrogenphosphate,[3] sulfate,[2] formate, nitrate and tartarate,[4] each prepared from the title compound. These compounds exhibit multiple H-bonds due to the high density of hetero atoms in the structure.

The crystals were formed by slow evaporation of an aqueous solution of commercially available aminoguanidinium bicarbonate (ALDRICH, 99.9%). Bond lengths and angles are listed in Table 7.2; details of hydrogen bonding are listed in Table 7.3. A packing diagram of the centerosymmetric title compound is depicted in Fig 7.1. The unique feature of the crystal structure of the title compound is that it does not exist as the bicarbonate salt as had previously been assumed. The structure instead contains an N-carboxy substituent on the aminoguanidinium unit which cocrystallizes with a molecule of water. The presence of the water molecule in the crystal accounts for the reported molecular formula. The molecular formula of the title compound, and of aminoguanidinium bicarbonate are identical and cannot be distinguished by elemental anlysis. The bonding of the N4 atom with the C2 to form the N-carboxy bond in the title compound resembles the binding of CO_2 to biotin, an

essential growth factor present in minute amounts in all living cells.[5] Biotin plays an indispensable role in numerous naturally occurring carboxylation reactions.

The aminoguanidinium moiety is nearly planar with bond angles and C-N distances similar to those found in other guanidinium or substituted guanidinium salts. The hydrogen atoms were located in the difference synthesis maps and were refined isotropically. There appear to be two O1-N (2.90), two O1-O2 (2.75), two O3-N (2.88) and one O2-N hydrogen bonds.

Acknowledgments

This work was supported by the donors of the Petroleum Research Fund, administered by the American Chemical Society, for partial support of this research.

References

1. Mullen, D. & Hellner, E. (1978). *Acta Cryst.*, **B34**. 2789-2794.

2. Bryden, J. H., (1957). *Acta Cryst.* 10, 677-680.

3. Adams, J. M. (1977). *Acta Cryst.* **B33**. 1513-1515.

4. Akella, A. & Keszler, D. A. (1994). *Acta Cryst.* submitted for publication. Zubay, G. Biochemistry Macmillan Publishing Company: New York, II Edition 1988.

Table 7.1. Atomic parameters for aminoguanidinium bicarbonate.

Atom	x	y	z	B_{eq}
O1	0.4566(1)	-0.5687(3)	0.8674(2)	3.30(5)
O2	0.2999(4)	0.1365(2)	0.7231(1)	3.17(5)
O3	0.0861(1)	-0.0150(3)	0.65531(8)	3.07(5)
N1	0.2520(2)	-0.1394(3)	0.8954(1)	2.82(5)
N2	0.1384(2)	0.2187(3)	0.9750(1)	2.99(6)
N3	0.3313(2)	-0.0084(3)	1.0548(1)	2.97(1)
N4	0.1501(2)	-0.1230(3)	0.8147(1)	2.97(6)
C1	0.1820(2)	0.0046(3)	0.7260(1)	2.42(6)
C2	0.2386(2)	0.0249(3)	0.9755(1)	2.35(5)
H1	0.398(3)	-0.682(6)	0.819(2)	6.2(6)
H2	0.077(2)	-0.234(3)	0.811(1)	3.5(4)
H3	0.319(2)	-0.268(4)	0.897(1)	3.8(4)
H4	0.398(2)	-0.148(5)	1.060(2)	4.4(4)
H5	0.070(2)	0.241(4)	0.923(2)	4.2(5)
H6	0.530(3)	-0.508(5)	0.836(2)	5.4(6)
H7	0.320(2)	0.105(5)	1.110(2)	4.3(5)
H8	0.124(2)	0.319(4)	1.032(2)	4.1(5)

$$B_{eq} = 8\frac{\pi^2}{3}\sum_i\sum_j U_{ij} a_i^* a_j^* \mathbf{a}_i \cdot \mathbf{a}_j$$

Table 7.2. Interatomic Distances (Å) and Angles (°) for aminoguanidinium bicarbonate.

O1-C1	1.220(3)	O2-C1-O3	125.9(1)
O2-C1	1.254(2)	O2-C1-N4	118.5(1)
N1-N4	1.385(2)	N1-N4-C1	115.5(1)
N1-C2	1.337(2)	N1-N4-H2	121.3(3)
N1-H2	0.88(2)	N1-C2-N3	120(1)
N2-C2	1.326(2)	H3-N2-N2	121.0(1)
N2-H4	0.91(2)	N3-C2-N2	118.3(2)
N2-H7	0.93(2)	C2-N2-H4	120.7(2)
N3-H5	0.91(2)	C2-N2-H7	123(1)
N3-C2	1.314(2)	H4-N2-H7	117(1)
N3-H8	0.91(2)	C2-N3-H5	123(1)
N4-C1	1.373(2)	C2-N3-H8	120(1)
N4-N1	1.385(2)	H5-N3-H8	116(2)
N4-H2	0.86(2)	C1-N4-H2	116(1)
O1-H6	0.86(2)	N4-N1-C2	119.4(1)
		N4-N1-H3	120(1)
		C2-N1-H3	120(1)
		H1-O1-H6	107(2)
		O2-C1-N4	118.5(1)

Table 7.3. Hydrogen-bonding geometry (Å).

O1-O2	2.73(1)
O1-O2	2.77(2)
O1-N1	2.84(2)
O1-N2	2.97(3)
O2-N2	2.89(1)
O3-N3	2.85(2)
O3-N3	2.92(2)

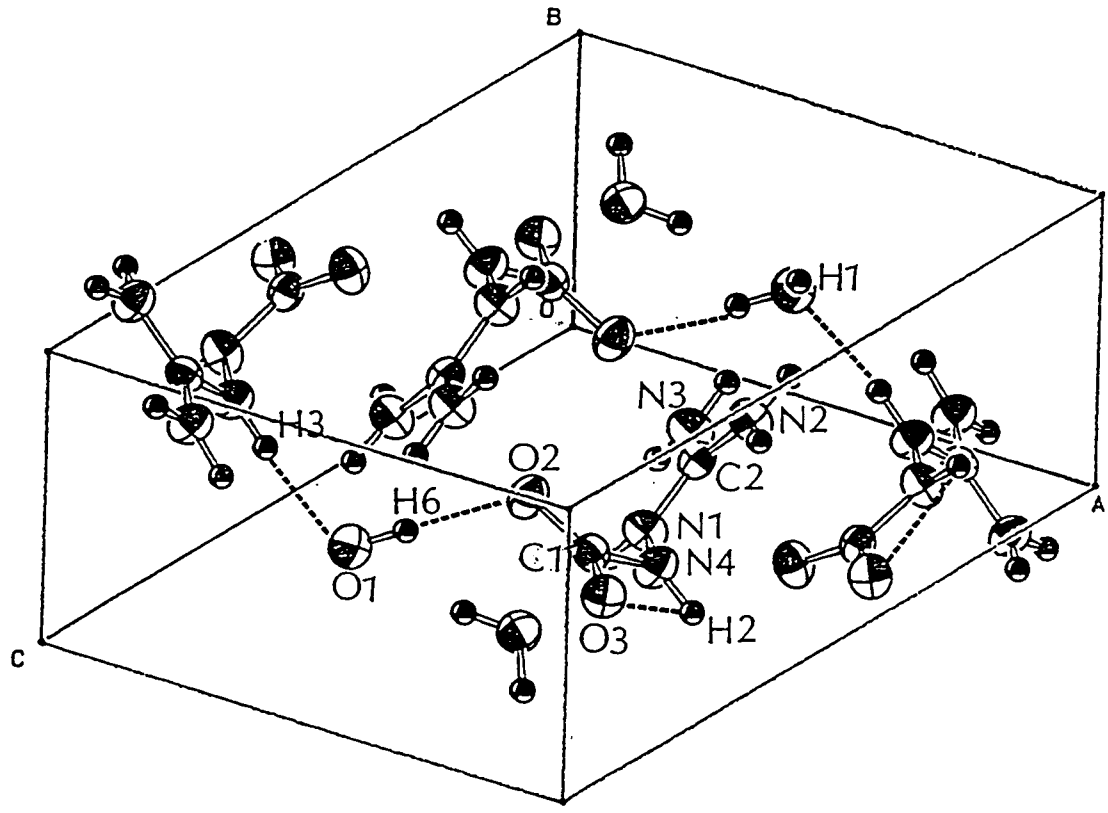

Figure 7.1. Unit cell packing diagram of aminoguanidinium bicarbonate

Table 7.4. Experimental details for the structure solution of aminoguanidinium bicarbonate.

EXPERIMENTAL DETAILS	
Compound	aminoguanidinium bicarbonate
CRYSTAL DATA	
Chemical formula $C_2H_8N_4O_3$	Crystal system Monoclinic
M_r 136.11	Space group P $2_1/c$
a (Å) 9.193(2)	α (°)
b (Å) 4.8371(6)	β (°) 93.10(1)
c (Å) 13.248(2)	γ (°)
Z 4	D_m (Mg m^{-3})
V (Å^3) 588.3(2)	D_x (Mg m^{-3}) 1.537
Radiation Mo Kα	No. of reflections for lattice parameters 20
Wavelength (Å) 0.71069	θ range for lattice parameters (°) $28 \leq 2\theta \leq 34$
Absorption coefficient (mm^{-1}) 0.130	Temperature 296
Crystal source: Grown from an aqueous solution of aminiguanidinium bicarbonate.	
Crystal color Colorless	Crystal description block
Crystal size (mm) 0.1 × 0.1× 0.2	
DATA COLLECTION	
Diffractometer type Rigaku AFC6R	Collection method ω-2θ
No. of reflections measured 2007	R_{int} 0.050
No. of independent reflections 1900	θ_{max}(°) 30
No. of observed reflections 1263	No. of standard reflections (and interval) 3 standards:{3,2,-2;0,2,-5;2,2,-4}
Criterion for observed $F_o^2 \geq 3\sigma(F_o^2)$	Variation of standards 1.9% in intensity
h_{min} 0	h_{max} 12

Table 7.4. (Continued).

EXPERIMENTAL DETAILS (*continued*)			
k_{min}	0	k_{max}	6
l_{min}	-18	l_{max}	18
REFINEMENT			
Treatment of hydrogen atoms (circle approximate entry, or describe in box below) refall refxyz refU nonref		*F*, F^2 or *I* F	
R	0.047	No. of parameters refined	114
wR	0.057	No. of reflections used in refinement	12
S	2.08	Weighing scheme $\Sigma w (\|F_o\| - \|F_c\|)^2$ $w = 1/\sigma(F_o)$; $\sigma(F_o^2)$*	
$(\Delta/\sigma)_{max}$	0.01	$(\Delta/\rho)_{min}$ (e Å^{-3})	-0.24
Extinction correction method (if applied)		$(\Delta/\rho)_{max}$(e Å^{-3})	0.28

*$\sigma(F_o^2) = [C + {}^1/_4(t_c/t_b)^2(b_1+b_2)+(pxI)^2]^{1/2}$
C = total # of counts per peak
t_c = time spent counting peak intensity
t_b = time spent counting one side of the background
b_1 = high-angle background counts
b_2 = low-angle background counts
p = fudge factor or p-factor
I = $C-{}^1/_2(t_c/t_b)(b_1+b_2)$

DIFABS: Walker,N., & Stuart, D., (1983). *Acta Cryst* **A39**, 158-166.
TEXSAN Single Crystal Structure Analysis Software Version 5.0, (1989). Molecular Structure Corporation, 3200a Research Forest Drive, Woodlands, TX 77381, U.S.A.

Structure of Aminoguanidinium Formate

Annapoorna Akella and Douglas A. Keszler

Department of Chemistry and

Center for Advanced Materials Research

Oregon State University

Gilbert 153

Corvallis, Oregon 97331-4003

Submitted to *Acta Crystallogr., Sect C.*

Abstract

The structure of aminoguanidinium formate, $(H_2N)_2CNH(NH_2)\cdot H_2CO_2$, has been determined by single crystal X-ray methods. The compound crystallizes in the monoclinic system and space group $P2_1/c$. The O1 and O2 atoms of the formate intermolecularly bond to the hydrogen atoms of the aminoguanidinium fragment.

Comment

In pursuit of new, noncenterosymmetric guanidinium and formate based nonlinear optical materials we have prepared the compound aminoguanidinium formate. There has been considerable interest in simple guanidinium salts in the last two decades.[1-3] These salts contain multiple hydrogen bonds to oxygen atoms, each O atom accepting three hydrogen atoms. The aminoguanidinium compounds studied structurally to date are the chloride,[5] dihydrogenphosphate,[6] and sulfate.[4] Since the aminoguanidinium ion contains seven H atoms per moiety, it is capable of forming H-bonds with the formate ion. This hydrogen bonding ability is potentially useful in crystal engineering of compounds containing H_2O_2 of crystallization.[1-2]

The crystals were formed by slow evaporation of a solution prepared by a stoichiometric addition of aminoguanidinium bicarbonate (ALDRICH, 99.9%) to formic acid. Bond lengths and angles are listed in Table 7.6.; details of hydrogen bonding are listed in Table 7.7. A packing diagram of the centerosymmetric title compound is depicted in Fig 7.2. The formate ions are related by a 2-fold screw axis along the a axis. The aminoguanidinium moiety is nearly planar with bond angles and C-N distances similar to those found in other guanidinium or substituted guanidinium salts. The hydrogen atoms were located in the difference synthesis maps and were refined isotropically.

There appears to be three O1-N hydrogen bonds (2.90) and two O2-N (2.82) hydrogen bonds. This work was supported by the donors of the Petroleum Research Fund, administered by the American Chemical Society, for partial support of this research.

References

1. Adams, J. M. & Pritchard, R. G. (1976). *Acta Cryst.* B**32**. 2438-2440.

2. Adams, J. M., Pritchard, R. G. & Thomas, J. M. (1976). *Chem. Commun.* 358-359.

3. Adams, J.M. & Small, R. W. H. (1974). *Acta Cryst.* B**30**, 2191-2193.

4. Mullen, D. & Mellner, E. (1978). *Acta Cryst.*, B**34**. 2789-2794.

5. Bryden, J. H., (1957). *Acta Cryst.* 10, 677.

6. Adams, J. M. (1977). *Acta Cryst.* B**33**. 1513-1515.

Table 7.5. Atomic parameters for aminoguanidinium formate

Atom	x	y	z	B_{eq}
O1	0.5347(4)	0.1780(2)	0.4360(2)	4.90(9)
O2	0.7432(4)	0.1268(2)	0.6202(1)	4.38(9)
N1	0.7963(4)	0.1261(2)	0.0654(2)	3.49(8)
N2	1.15556(2)	0.1410(2)	0.2132(2)	4.0(1)
N3	0.8811(4)	-0.0219(2)	0.2115(2)	3.31(8)
N4	0.6653(5)	-0.0889(2)	0.1539(2)	3.6(1)
C1	0.9434(4)	0.0817(2)	0.1627(2)	2.76(8)
C2	0.6924(6)	0.1176(2)	0.5031(2)	4.2(1)
H1	0.662(6)	0.087(3)	0.035(3)	5.0(7)
H2	0.864(6)	0.195(3)	0.029(3)	5.2(7)
H3	1.193(6)	0.216(3)	0.179(3)	6.1(8)
H4	0.984(5)	-0.046(2)	0.270(2)	3.8(6)
H5	0.556(7)	-0.10393)	0.207(3)	7(1)
H6	0.571(6)	-0.161(3)	0.127(2)	5.3(7)
H7	0.791(8)	0.039(4)	0.462(3)	10(1)
H8	1.250(5)	0.115(2)	0.280(3)	4.7(6)

$$B_{eq} = 8\frac{\pi^2}{3}\sum_i \sum_j U_{ij} a_i^* a_j^* a_i \cdot a_j$$

Table 7.6. Interatomic Distances (Å) and Angles (°) for aminoguanidinium formate.

O1-C2	1.226(3)	O1-C2-O2	127.5(2)
O1-C2	1.241(3)	C1-N1-H2	118(2)
N1-C1	1.317(3)	H1-N1-H2	117(2)
N1-H1	0.85(3)	C1-N2-H3	125(3)
N1-H2	0.94(3)	C1-N2-H8	118(2)
N2-C1	1.322(3)	H3-N2-H8	121(2)
N2-H3	0.94(3)	N4-N3-C1	120(2)
N2-H8	0.87(3)	N4-N3-H4	199.7(2)
N3-N4	1.409(3)	C1-N3-H4	124(2)
N3-C1	1.325(3)	N3-N4-H5	116(2)
N3-H4	0.82(2)	N3-N4-H6	108(2)
N4-H5	0.80(3)	H5-N4-H6	105(2)
N4-H6	0.96(3)	N1-C1-N2	110(2)
C2-H7	1.11(2)	N1-C1-N3	119.8(2)

Table 7.7. Hydrogen-bonding geometry (Å).

O1-O2	2.21
O1-N1	2.87
O1-N2	2.93
O1-N4	2.96
O2-N1	2.88
O2-N3	2.75
N1-N2	2.28
N1-N3	2.29
N1-N4	2.70
N2-N3	2.28

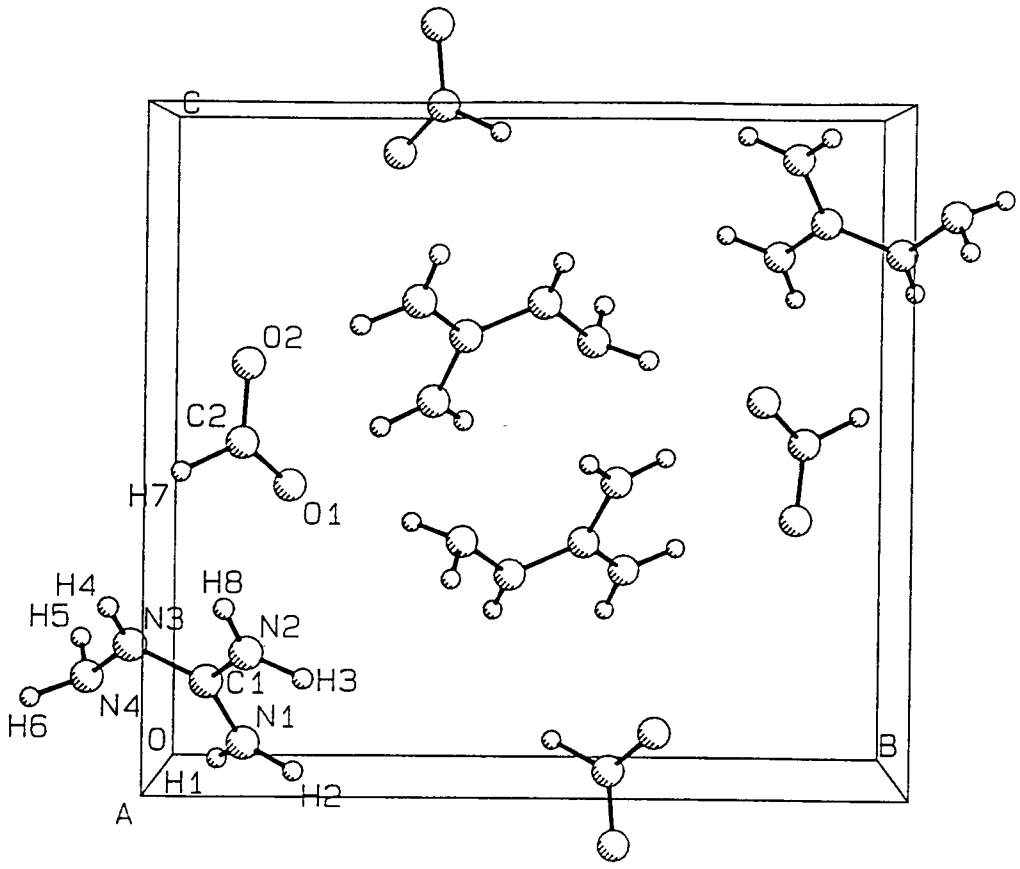

Figure 7.2. Packing Diagram for aminoguanidinium formate

Table 7.8. Experimental details for the structure solution of aminoguanidinium formate.

EXPERIMENTAL DETAILS	
Compound	aminoguanidinium bicarbonate
CRYSTAL DATA	
Chemical formula $C_2H_8N_4O_3$	Crystal system Monoclinic
M_r 136.11	Space group P 2_1 /c
a (Å) 9.193(2)	α (°)
b (Å) 4.8371(6)	β (°) 93.10(1)
c (Å) 13.248(2)	γ (°)
Z 4	D_m (Mg m^{-3})
V (Å^3) 588.3(2)	D_x (Mg m^{-3}) 1.537
Radiation Mo Kα	No. of reflections for lattice parameters 20
Wavelength (Å) 0.71069	θ range for lattice parameters (°) 28 ≤ 2θ ≤ 34
Absorption coefficient (mm^{-1}) 1.30	Temperature 296
Crystal source: Grown from an aqueous solution of the aminiguanidinium bicarbonate.	
Crystal color Colorless	Crystal description block
Crystal size (mm) 0.1) × 0.1) × 0.2	
DATA COLLECTION	
Diffractometer type Rigaku AFC6R	Collection method ω-2θ
No. of reflections measured 2007	R_{int} 0.050
No. of independent reflections 1900	θ_{max}(°) 30
No. of observed reflections 1263	No. of standard reflections (and interval) 3 standards:{3,2,-2;0,2,-5;2,2,-4}
Criterion for observed $F_o^2 \geq 3\sigma(F_o^2)$	Variation of standards 1.9% in intensity
h_{min} 0	h_{max} 12
k_{min} 0	k_{max} 6
l_{min} -18	l_{max} 18

Table 7.8. (continued)

EXPERIMENTAL DETAILS (*continued*)	
REFINEMENT	
Treatment of hydrogen atoms (circle approximate entry, or describe in box below) refall refxyz refU nonref	*F*, F^2 or *I* F
R 0.047	No. of parameters refined 114
wR 0.057	No. of reflections used in refinement 1263
S 2.08	Weighing scheme $\Sigma w (\lvert F_o \rvert - \lvert F_c \rvert)^2$ $w = 1/\sigma(F_o)$; $\sigma(F_o^2)$*
$(\Delta/\sigma)_{max}$ 0.01	$(\Delta/\rho)_{min}$ (e Å^{-3}) -0.24
Extinction correction method (if applied)	$(\Delta/\rho)_{max}$(e Å^{-3}) 0.28
Primary- and secondary-extinction values	Source of atomic scattering factors International Tables for X-ray Crystallography

*$\sigma(F_o^2) = [C + {}^1/_4(t_c/t_b)^2(b_1+b_2)+(pxI)^2]^{1/2}$

C = total # of counts per peak
t_c = time spent counting peak intensity
t_b = time spent counting one side of the background
b_1 = high-angle background counts
b_2 = low-angle background counts
p = fudge factor or p-factor
I = $C - {}^1/_2 (t_c/t_b)(b_1+b_2)$

DIFABS: Walker,N., & Stuart, D., (1983). *Acta Cryst* **A39**, 158-166.

TEXSAN Single Crystal Structure Analysis Software Version 5.0, (1989). Molecular Structure Corporation, 3200a Research Forest Drive, Woodlands, TX 77381, U.S.A.

Structure of Aminoguanidinium Nitrate

Annapoorna Akella and Douglas A. Keszler

Department of Chemistry and

Center for Advanced Materials Research

Oregon State University Gilbert 153

Corvallis, Oregon 97331-4003

Submitted to *Acta Crystallogr., Sect. C* **1994**.

Abstract

The structure of aminoguanidinium nitrate, $CH_7N_5O_3$, has been determined by single crystal X-ray methods. The structure is a salt like complex containing discrete aminoguanidinium and nitrate ions. The O1 and O3 atoms of the nitrate group intermolecularly bond to the H atoms of the aminoguanidinium ion.

Comment

As part of a program to synthesize new optical materials having significant birefringence, we have prepared the compound aminoguanidinium nitrate. Several guanidinium salts have been studied during the last two decades,[1,4] and the chloride,[3] dihydrogenphosphate,[4] and sulfate,[2] have been structurally characterized. In the oxoanion salts multiple hydrogen bonds to O atoms are present, each O atom accepting three H atoms. Similar H - bond interactions are observed in the structure reported here.

The crystals were formed by slow evaporation of a solution prepared by a stoichiometric addition of aminoguanidinium hydrochloride (ALDRICH, 99.9%) to a sodium nitrate (ALDRICH, 99.9%) solution. A packing diagram of the structure is depicted in Fig 7.3; bond lengths and angles are listed in Table 7.10. The aminoguanidinium moiety is nearly planar with bond angles and C-N distances similar to those found in other guanidinium or substituted guanidinium salts; the N1-C1-N3-N4 torsion angle is 4.02(3)°. The H atoms were located in the difference electron density maps and were refined with isotropic displacement coefficients. Details of hydrogen bonding are listed in Table 7.11. Three O1··N hydrogen bonds and two O2··N hydrogen bonds link the aminoguanidinium and nitrate groups. The nitrate and aminoguanidinium moieties are approximately coplanar. Within the same plane nitrate groups are

linked through H bonds to the N atoms of gunidinium portin of the molecule. Above and below this plane the groups are intermolecularly bonded through the H atoms of the amino group (atoms N4, H6, and H7).

Acknowledgment is made to the Donors of the Petroleum Research Fund, administered by the American Chemical Society, for support of this research.

References

1. Adams, J.M. & Small, R. W. H. (1974). *Acta Cryst.* B**30**, 2191-2193.

2. Mullen, D. & Hellner, E. (1978). *Acta Cryst.*, B**34**. 2789-2794.

3. Bryden, J. H., (1957). *Acta Cryst.* 10, 677.

4. Adams, J. M. (1977). *Acta Cryst.* B**33**. 1513-1515.

Table 7.9. Atomic parameters for aminoguanidinium nitrate.

Atom	x	y	z	B_{eq}
O1	0.8178(2)	0.4752(2)	0.2681(2)	4.82(4)
O2	0.6710(2)	0.4385(2)	-0.1057(2)	4.36(4)
O3	0.5573(2)	0.2153(2)	0.0154(3)	4.74(4)
N1	0.0380(2)	-0.1698(2)	-0.8063(3)	3.88(4)
N2	0.2316(2)	-0.1301(2)	-0.4248(3)	4.61(5)
N3	0.2980(2)	0.1237(2)	-0.5409(3)	3.81(4)
N4	0.2462(2)	0.2045(2)	-0.7091(3)	4.00(4)
N5	0.6820(2)	0.3772(2)	0.0583(2)	3.35(3)
C1	0.1875(2)	-0.0603(2)	-0.5925(3)	3.21(4)
H1	-0.036(3)	-0.0286(3)	-0.834(4)	4.6(4)
H2	0.007(3)	-0.128(3)	-0.901(4)	4.1(4)
H3	0.396(3)	0.192(3)	-0.406(5)	5.3(5)
H4	0.338(3)	-0.062(3)	-0.286(5)	6.5(6)
H5	0.172(3)	-0.254(3)	-0.474(4)	4.7(4)
H6	0.352(3)	0.240(3)	-0.768(5)	6.4(5)
H7	0.230(3)	0.328(3)	-0.617(5)	6.3(5)

$$B_{eq} = 8\frac{\pi^2}{3}\sum_i\sum_j U_{ij} a_i^* a_j^* \mathbf{a}_i \cdot \mathbf{a}_j$$

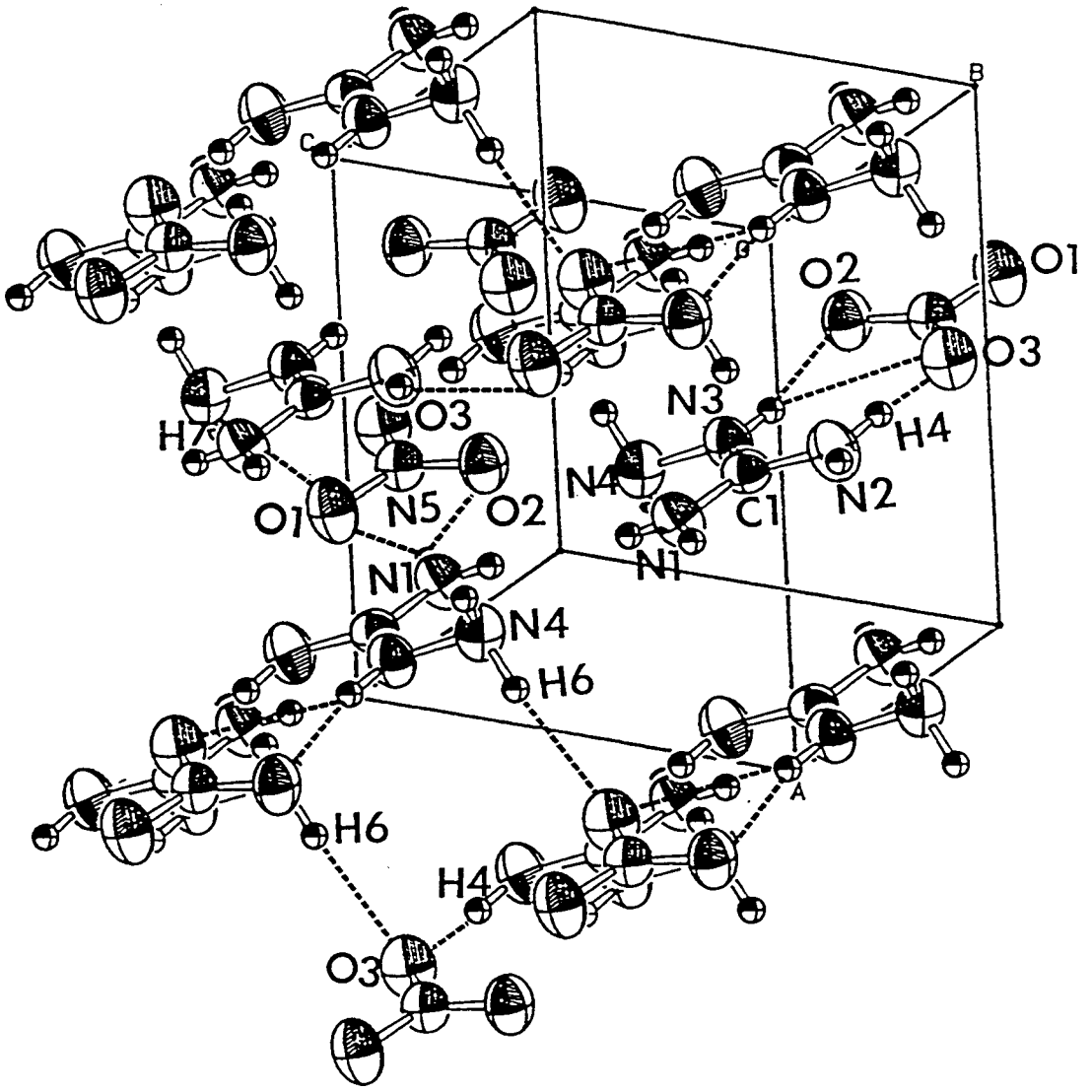

Figure 7.3. Packing diagram for aminoguanidinium nitrate.

Table 7.10. Interatomic Distances (Å) and Angles (°) for aminoguanidinium nitrate.

O1-N5	1.248(2)	O1-N5-O3	119.2(2)
O2-N5	1.232(2)	O1-N5-O2	120.8(1)
O3-N5	1.246(2)	O3-N5-O2	120.1(1)
N1-C1	1.312(2)	N1-C1-N3	120.4(2)
N1-H1	0.860(5)	N1-C1-N2	121.1(1)
N1-H2	0.770(5)	N3-C1-N2	118.6(1)
N2-C1	1.320(3)	N3-N4-H7	108.3(1)
N2-H4	0.884(1)	N3-N4-H6	110.3(3)
N2-H5	0.851(5)	N4-N3-C1	119.5(1)
N3-N4	1.399(3)	N4-N3-H3	120.4(6)
N3-C1	1.328(2)	H7-N4-H6	105.4(2)
N3-H3	0.839(1)	C1-N1-H1	119.4(4)
N4-H6	0.939(1)	C1-N1-H2	121.4(1)
N4-H7	0.975(2)	H1-N1-H2	118.7(2)
		C1-N2-H4	112.1(2)
		C1-N2-H5	116.2(1)
		C1-N3-H3	120.1(2)
		H4-N2-H5	119.8(6)

Table 7.11. Hydrogen Bonding Distances (Å)

O1...N1	3.038(2)
O1...N2	3.088(2)
O1...N4	3.153(3)
O3...N2	2.983(2)
O3...N2	2.972(2)
O3...N4	3.104(2)

Table 7.12. Experimental Details for the solution of title compound.

EXPERIMENTAL DETAILS			
Compound		aminoguanidinium nitrate	
CRYSTAL DATA			
Chemical formula	$CH_7N_5O_3$	Crystal system	Triclinic
M_r	134.11	Space group	P -1
a (Å)	7.341(1)	α (°)	110.47(2)
b (Å)	7.722(2)	β (°)	102.64(2)
c (Å)	6.024(1)	γ (°)	104.87(2)
Z	2	D_m (Mg m^{-3})	
V (Å^3)	290.7(1)	D_x (Mg m^{-3})	1.589
Radiation	Mo Kα	No. of reflections for lattice parameters	20
Wavelength (Å)	0.71069	θ range for lattice parameters (°)	$20 \le 2\theta \le 28$
Absorption coefficient (mm^{-1})	0.137	Temperature	296
Crystal source: Grown from a stoichiometric mixture of aminoguanidinium hydrochloride and sodium nitrate in water.			
Crystal color	Colorless	Crystal description	block
Crystal size (mm)	0.1 × 0.1× 0.2		
DATA COLLECTION			
Diffractometer type	Rigaku AFC6R	Collection method	ω-2θ
No. of reflections measured	3384	R_{int}	0.076
No. of independent reflections	1692	θ_{max}(°)	30
No. of observed reflections	1126	No. of standard reflections (and interval)	3 standards:{-1,-2,3;1,2,-3;1,1,2}
Criterion for observed	$F_o^2 \ge 3\sigma(F_o^2)$	Variation of standards	1.9% in intensity
h_{min}	-10	h_{max}	10
k_{min}	-10	k_{max}	10
l_{min}	-8	l_{max}	8

Table 7.12. (continued)

EXPERIMENTAL DETAILS (*continued*)	
REFINEMENT	
Treatment of hydrogen atoms (circle approximate entry, or describe in box below) refall refxyz refU nonref	*F*, F^2 or *I* F
R 0.044	No. of parameters refined 110
wR 0.054	No. of reflections used in refinement 1126
S 1.44	Weighing scheme $\Sigma w (\|F_o\| - F_c\|)^2$ $w = 1/\sigma(F_o)$; $\sigma(F_o^2)$*
$(\Delta/\sigma)_{max}$ 0.01	$(\Delta/\rho)_{min}$ (e Å^{-3}) -0.40
Extinction correction method (if applied) TEXSAN	$(\Delta/\rho)_{max}$(e Å^{-3}) 0.27
Primary- and secondary-extinction values 0.24119(4)E-5	Source of atomic scattering factors International Tables for X-ray Crystallography

*$\sigma(F_o^2) = [C + {}^1/_4(t_c/t_b)^2(b_1+b_2)+(pxI)^2]^{1/2}$

C = total # of counts per peak
t_c = time spent counting peak intensity
t_b = time spent counting one side of the background
b_1 = high-angle background counts
b_2 = low-angle background counts
p = fudge factor or p-factor
I = $C - {}^1/_2 (t_c/t_b)(b_1+b_2)$

DIFABS: Walker,N., & Stuart, D., (1983). *Acta Cryst* **A39**, 158-166.

TEXSAN Single Crystal Structure Analysis Software Version 5.0, (1989). Molecular Structure Corporation, 3200a Research Forest Drive, Woodlands, TX 77381, U.S.A.

Structure of Aminoguanidinium Tartarate Monohydrate

Annapoorna Akella and Douglas A. Keszler

Department of Chemistry and

Center for Advanced Materials Research

Oregon State University

Gilbert 153

Corvallis, Oregon 97331-4003

Submitted to *Acta Crystallogr., Sect. C,* **1994** in press.

Abstract

The structure of aminoguanidinium tartarate monohydrate, has been determined by single crystal X-ray methods. The structure is a salt like complex containing discrete aminoguanidinium and tartarate ions and a water residue. The O atoms of the tartarate ion and water intermolecularly bond to the H atoms of the aminoguanidinium ion.

Comment

In search of new guanidinium based nonlinear optical materials, we have prepared the noncenterosymmetric compound aminoguanidinium tartarate. The aminoguanidinium compounds structurally characterized to date are the dihydrogenphosphate,[1] chloride,[2] sulfate,[3] formate and nitrate.[4] The corresponding guanidinium tartarate has been reported,[1] but not structurally characterized.

The planarity of the aminoguanidinum moiety is disrupted by the presence of the the amino group; interatomic distances and angles (see Table 7.14) are similar to those previously reported for other guanidinium and tartarate compounds. The compound crystallizes with a molecule of water in the unit cell. Because of the high density of heteroatoms in the structure, multiple hydrogen bonds are observed. The system of hydrogen bonds among the water molecule the tartarate and aminoguanidinium groups is depicted in Fig. 7.4. There are multiple hydrogen bonds between the O atoms of the water and tartarate and the hydrogen atoms of the aminoguanidinium (see Table 7.15). The O2··H14, O3··H14, O3··H10, and O4··H8 hydrogen bonds link the amninoguanidinium and the tartarate residue. Atom O7 of the water molecule bridges the tartarate and aminoguanidinium via atoms H2 and H6.

Acknowledgment is made to the Donors of the Petroleum Research Fund, administered by the American Chemical Society, for support of this research.

References

1. Adams, J. M. (1977). *Acta Cryst.* **B33**. 1513-1515.

2. Bryden, J. H., (1957). *Acta Cryst.* 10, 677.

3. Mullen, D. & Hellner, E. (1978). *Acta Cryst.*, **B34**. 2789-2794.

4. Akella, A. & Keszler, D. A. (1994) *Acta Cryst.* B submitted for publication.

Table 7.13. Atomic parameters for aminoguanidinium tartarate monohydrate.

Atom	x	y	z	B_{eq}
O1	0.6119(3)	0.0961(2)	0.0947(4)	2.3(1)
O2	0.6242(4)	0.2547(2)	0.0850(4)	3.3(1)
O3	0.6007(4)	0.2666(2)	0.4631(4)	2.4(1)
O4	0.8523(3)	0.1904(2)	0.3906(4)	2.2(1)
O5	0.6447(3)	0.0838(2)	0.7367(4)	2.4(1)
O6	0.8466(3)	0.1510(2)	0.7518(4)	2.8(1)
O7	0.9312(3)	0.0915(3)	0.0924(5)	2.8(1)
N1	0.2920(4)	1.1387(3)	0.2166(7)	3.3(2)
N2	0.2016(4)	1.0624(3)	0.2014(6)	3.1(2)
N3	0.3770(4)	0.9588(3)	0.2171(7)	3.1(2)
N4	0.1621(4)	0.9033(3)	0.2015(7)	3.4(2)
C1	0.2488(4)	0.9750(3)	0.2061(6)	2.4(2)
C2	0.6163(4)	0.1823(3)	0.1709(6)	2.1(2)
C3	0.6124(4)	0.1755(3)	0.3840(5)	1.7(1)
C4	0.7444(4)	0.1333(3)	0.4516(5)	1.7(1)
C5	0.7471(4)	0.1238(3)	0.6447(5)	1.9(1)
H1	0.072(4)	0.918(3)	0.215(7)	2.0(1)
H2	0.110(5)	1.076(3)	0.157(7)	3.0(1)
H3	0.749(5)	0.071(3)	0.407(6)	4.0(1)
H4	0.535(4)	0.136(3)	0.412(6)	1.3(8)
H5	0.897(8)	0.130(5)	-0.03(1)	10(2)

$$B_{eq} = 8\frac{\pi^2}{3}\sum_i \sum_j U_{ij} a_i^* a_j^* a_i \cdot a_j$$

Table 7.13. (continued)

Atom	x	y	z	B_{eq}
H6	0.886(5)	0.171(3)	0.285(8)	3(1)
H7	0.517(5)	0.280(3)	0.489(7)	3(1)
H8	0.187(5)	0.846(3)	0.201(8)	4(1)
H9	0.620(6)	0.097(4)	-0.02(1)	6(1)
H10	0.260(8)	1.188(5)	0.33(1)	9(2)
H11	0.283(6)	1.175(4)	0.120(8)	5(2)
H12	0.898(8)	0.038(5)	0.11(1)	11(3)
H13	0.431(5)	1.005(3)	0.214(8)	4(1)
H14	0.412(7)	0.894(5)	0.23(1)	9(2)

Table 7.14. Interatomic Distances (Å) and Angles (°) for aminoguanidinium tartarate monohydrate.

O1-C2	1.335(5)	O1-C2-O2	125.0(4)
O1-H9	0.86(6)	O1-C2-C3	110.4(3)
O2-C2	1.199(5)	O2-C2-C3	124.5(4)
O3-C3	1.412(5)	O3-C3-C2	110.2(3)
O3-H7	0.88(5)	C1-N3-H14	121(4)
O4-C4	1.418(5)	O3-C3-C4	107.5(3)
O4-H6	0.87(5)	O3-C3-H4	112(2)
O5-C5	1.279(5)	C2-C3-C4	108.5(3)
O6-C5	1.237(5)	C2-C3-H4	105(2)
O7-H5	1.09(8)	C4-C3-H4	113(2)
O7-H12	0.83(8)	O4-C4-C3	109.8(3)
N1-N2	1.412(5)	O4-C4-C5	110.1(4)
N1-H10	1.12(7)	O4-C4-H3	113(2)
N1-H11	0.87(6)	C3-C4-C5	111.4(4)
N2-C1	1.323(5)	C3-C4-H3	108(2)
N2-H2	0.99(5)	C5-C4-H3	105(2)
N3-C1	1.306(6)	O5-C5-O6	125.5(4)
N3-H13	0.85(5)	O5-C5-C4	115.2(4)
N3-H14	0.99(7)	O6-C5-C4	119.2(4)
N4-C1	1.335(6)	C2-O1-H9	113(4)
N4-H1	0.93(4)	C3-O3-H7	111(3)
N4-H8	0.86(5)	C4-O4-H6	112(3)
C2-C3	1.528(5)	H5-O7-H12	115(7)
C3-C4	1.529(6)	N2-N1-H10	110(4)
C3-H4	0.98(4)	N2-N1-H11	109(5)

Table 7.14. (continued)

C4-H5	1.530(6)	H10-N1-H11	101(5)
C4-H3	0.99(3)	N1-N2-C1	119(4)
C4-C5	1.530(5)	N1-N2-H2	118(4)
C4-H3	0.94(5)	C1-N2-H2	121(3)
		C1-N3-H13	119(3)
		H13-N3-H14	120(5)
		C1-N4-H1	118(3)
		C1-N4-H8	122(4)
		H1-N4-H8	120(5)
		N2-C1-N3	120.8(4)
		N2-C1-N4	118.4(5)
		N3-C1-N4	121.1(4)

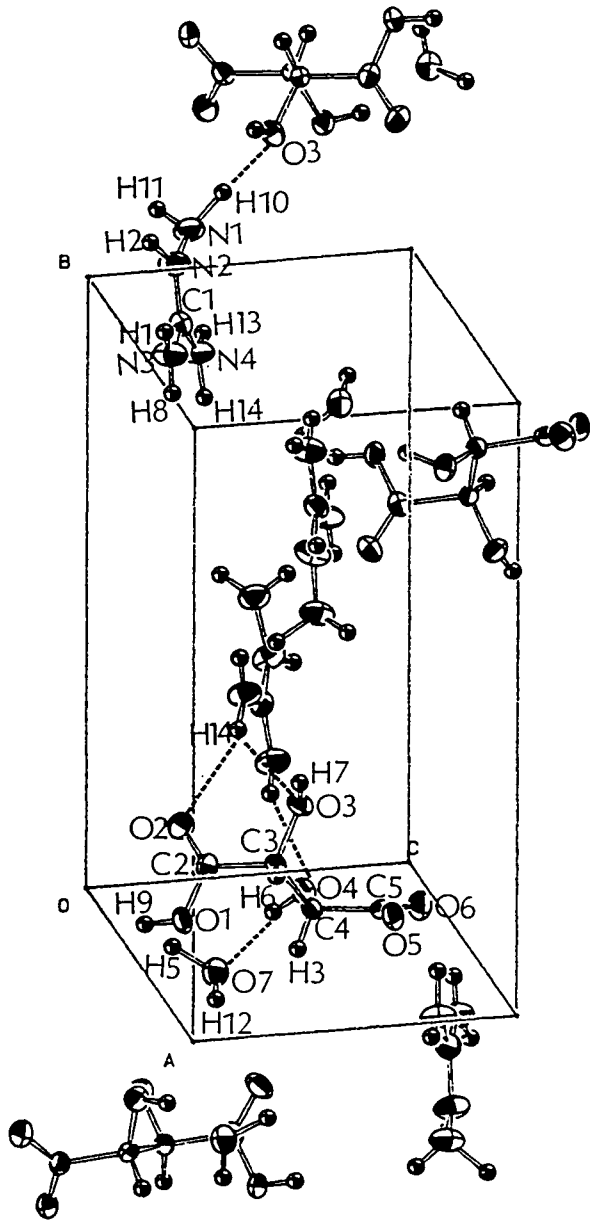

Figure 7.4. Structure and hydrogen bonding of the title compound.

Table 7.15. Hydrogen bonding details (Å).

O2...N1	3.10(4)
O3...N3	3.01(3)
O4...N4	3.08(5)
O4...O7	2.67(2)
O5...O7	2.78(2)
O5...N4	3.08(2)
O7...N2	2.85(2)

Table 7.16. Experimental Details for the solution of title compound.

EXPERIMENTAL DETAILS			
Compound		aminoguanidinium tartarate monohydrate	
CRYSTAL DATA			
Chemical formula	$C_5H_{14}N_4O_7$	Crystal system	Orthorhombic
M_r	218.13	Space group	$P2_12_12_1$
a (Å)	10.013(2)	α (°)	
b (Å)	14.137(2)	β (°)	92.38(2)
c (Å)	7.153(1)	γ (°)	
Z	4	D_m (Mg m^{-3})	
V (Å^3)	1012.5(3)	D_x (Mg m^{-3})	1.431
Radiation	Mo Kα	No. of reflections for lattice parameters	20
Wavelength (Å)	0.71069	θ range for lattice parameters (°)	$30 \le 2\theta \le 36$
Absorption coefficient (mm^{-1})	0.124	Temperature	296
Crystal source: Grown from a stoichiometric mixture of aminoguanidinium bicarbonate and tartaric acid in water.			
Crystal color	Colorless	Crystal description	block
Crystal size (mm) 0.1 × 0.1 × 0.1			
DATA COLLECTION			
Diffractometer type	Rigaku AFC6R	Collection method	ω-2θ
No. of reflections measured	2941	R_{int}	0.055
No. of independent reflections	1578	θ_{max}(°)	30
No. of observed reflections	1092	No. of standard reflections (and interval)	3 standards:{0,4,0;0,1,2;-4,0,0}
Criterion for observed	$F_o^2 \ge 3\sigma(F_o^2)$	Variation of standards	1.9% in intensity
h_{min}	0	h_{max}	14
k_{min}	0	k_{max}	19

Table 7.16. (continued)

EXPERIMENTAL DETAILS (*continued*)	
l_{min} -10	l_{max} 10
REFINEMENT	
Treatment of hydrogen atoms (circle approximate entry, or describe in box below) refall refxyz refU nonref	*F*, F^2 or *I* F
R 0.047	No. of parameters refined 197
wR 0.052	No. of reflections used in refinement 1092
S 1.76	Weighing scheme $\Sigma w (\lvert F_o \rvert - F_c \rvert)^2$ $w = 1/\sigma(F_o)$; $\sigma(F_o^2)$*
$(\Delta/\sigma)_{max}$ 0.01	$(\Delta/\rho)_{min}$ (e Å^{-3}) -0.25
Extinction correction method (if applied) TEXSAN	$(\Delta/\rho)_{max}$(e Å^{-3}) 0.32
Primary- and secondary-extinction values	Source of atomic scattering factors International Tables for X-ray Crystallography

*$\sigma(F_o^2) = [C + {}^1/_4(t_c/t_b)^2(b_1+b_2)+(pxI)^2]^{1/2}$

C = total # of counts per peak
t_c = time spent counting peak intensity
t_b = time spent counting one side of the background
b_1 = high-angle background counts
b_2 = low-angle background counts
p = fudge factor or p-factor
I = $C-{}^1/_2 (t_c/t_b)(b_1+b_2)$

DIFABS: Walker,N., & Stuart, D., (1983). *Acta Cryst* **A39**, 158-166.

TEXSAN Single Crystal Structure Analysis Software Version 5.0, (1989). Molecular Structure Corporation, 3200a Research Forest Drive, Woodlands, TX 77381, U.S.A.

CHAPTER 8
Structure and Eu^{2+} Luminescence of Dibarium Magnesium Orthoborate

Annapoorna Akella and Douglas A. Keszler

Department of Chemistry and

Center for Advanced Materials Research,

Gilbert Hall 153, Oregon State University,

Corvallis, Oregon 97331-4003

Submitted to *Materials Research Bulletin*

Abstract

The Structure of the mixed alkaline-earth orthoborate $Ba_2Mg(BO_3)_2$ has been established as a buetschliite type with single - crystal X-ray diffraction methods. Crystal data: a = 5.343(2), c = 16.520(3) Å, V = 408.4(2) $Å^3$, Z = 3, space group = R -3 m. A Eu^{2+} -doped powder exhibits a luminescence peak at 6085 Å and a Stokes shift of ~ 11,000 cm^{-1}.

Materials Index: barium, magnesium, orthoborate.

Introduction

The ion Eu^{2+} is commonly used as the emission center in blue emitting phosphors.[1] Depending on the crystal-field and structural environment about the ion however, its emission can occur at longer wavelengths, even in the red portion of the visible spectrum. Such a long wavelength emission (near 620 nm) has been reported,[2] in a Eu^{2+} -doped sample of the compound $Ba_2LiB_5O_{10}$.[3] This emission is especially unusual with respect to the large Stokes shift (~ 11,000 cm^{-1}) that is observed without a strong thermal quenching. This shift has been attributed to an off-center displacement of the Eu^{2+} ion at the irregular and large Ba^{2+} dopant site.

To determine if the large Stokes shift observed for Eu^{2+} : $Ba_2LiB_5O_{10}$ could be reproduced in other materials, we have examined the structural and optical characteristics of Eu^{2+} : $Ba_2Mg(BO_3)_2$. The Ba - Mg borate was first reported by Verstegen,[4] who proposed that it adopted the structure of the mineral buetschliite. This structure affords an anisotropic environment of a distorted hexagonal base, trigonal base about the Ba atom. Consequently, a large Stokes shift might be anticipated for a Eu^{2+} dopant. We have observed such a shift, and the details of the single crystal structure of $Ba_2Mg(BO_3)_2$ and the Eu^{2+} luminescence data are presented here.

Experimental

A powder sample of $Ba_2Mg(BO_3)_2$ was prepared from the molar quantities of 2 $BaCO_3$ (AESAR, 99.9%), 1 B_2O_3 (ALFA, 99.98%), and 1 $Mg(NO_3)_2.6H_2O$ (AESAR, 99.9%). The mixture of carbonate, nitrate and B_2O_3 was heated at 873 K for 1/2 h; then the sample was reground and heated at 1273 K for 12 h. A crystal was obtained for X-ray structure analysis from a melt of composition 1 BaF_2 : 1 BaO: 1 MgO : 0.55 B_2O_3. The melt was contained in a Pt crucible and slowly cooled from 1273 K to 873 K at 6 K/h, and then rapidly cooled at 50 K/h to room temperature. A colorless, transparent crystal of dimensions 0.12 × 0.15 × 0.12 mm was selected and mounted on a glass fiber with epoxy for structure determination. All measurements were made on a Rigaku AFC6R diffractometer with graphite-monochromated Mo Kα radiation. Cell constants and the orientation matrix for data collection were obtained from a least-squares refinement with 19 automatically-centered reflections in the range $30 \leq 2\theta \leq 36°$. The cell constants correspond to a hexagonal cell; Laue symmetry -3m was determined on the diffractometer. Intensity data were collected over the range of indices $-8 \leq h \leq 8$, $0 \leq k \leq 8$, $-24 \leq l \leq 24$ by using the ω scan technique to a maximum 2θ value of 65°, and from 1070 measured reflections a total of 213 unique data were observed [$F_o^2 \geq 3\sigma F^2$]. The intensities of three representative reflections measured after every block of 200

data varied by an average of 2% during the collection. The structure was solved by using the TEXSAN software package.[5] The crystal was found to form in the centerosymmetric space group R-3m(h). The positions of the Ba and Mg atoms were derived from the direct methods program SHELXS,[6] while the remaining atoms were located from difference electron density maps. After a full-matrix least-squares refinement of the model with isotropic displacement coefficients on each atom, an absorption correction was applied (transmission factors = 0.85 -1.17) by using the program DIFABS.[7] The data were averaged (R_{int} = 0.063), and the model was refined with anisotropic displacement coefficients on each atom. Final least squares refinement resulted in the residuals R = 0.029 and R_w = 0.037. The largest peak in the final difference electron density map corresponds to 0.38% of the Ba atom. Crystal data, atomic parameters, and anisotropic displacement coefficients are listed in Table 8.1.

Spectroscopic studies were performed on powder samples nominally doped with 2 mole% Eu^{2+}. The preparative procedure was that described above [Eu_2O_3 (99.99%, MOLYCORP)], except the final heating was done in an atmosphere of 25 N_2 : 1 H_2. Steady-state room temperature luminescence spectra were obtained on a computer-controlled right angle spectrometer. Excitation provided by an Oriel 300 W Xe lamp was passed through a 50-cm water filter and focused onto the slits of a Cary model-15 prism monochromator.

Excitation was focussed onto the sample. Luminescence was collected at a near-right angle to excitation, dispersed through an Oriel 22500 1/8 m monochromator, and detected with a Hamamatsu R636 photomultiplier tube. The signal was collected and amplified with a Keithley model 602 picoammeter and then converted to a digital signal for computer acquisition. Spectrometer control and data acquisition were achieved with computer programs written in this laboratory. Excitation spectra were corrected by using rhodamine B as a quantum counter. Emission spectra were corrected for the throughput of the detection system with a tungsten lamp that has been calibrated at Eppley Laboratory, Inc.

TABLE 8.1.

Crystallographic Data and Atomic Parameters for $Ba_2Mg(BO_3)_2$

Space group R-3m (h), (No. 166), Z = 3, formula wt. 416.58 amu, μ = 144.53 cm^{-1} a = 5.343 (2), c = 16.520 (3) Å, ρ_{calc} = 5.080 g cm^{-3}, R = 0.029, R_w = 0.037

	site symmetry	x	y	z	B_{eq}
Ba	D_{3d}	0	0	0.22414(3)	0.86(2)
Mg	C_{3v}	0	0	0	0.8(1)
B	C_{3v}	0	0	0.4099(6)	0.6(2)
O	C_s	0.1841(5)	-0.1841	0.0765(3)	1.09(4)

Atom	U11	U22	U33	U12	U13	U23
Ba	0.0107(3)	0.0107	0.0114(3)	0.0053	0	0
Mg	0.010(2)	0.010	0.009(2)	0.005	0	0
B	0.015(4)	0.015(4)	-0.001(3)	0.003	0	0
O	0.014(2)	0.014	0.014(2)	0.008(2)	-0.0020(7)	0.0020

Results and Discussion

Crystal Structure Description

The structure of the title compound is that of the mineral buetschliite, $K_2Ca(CO_3)_2$.[8] Layers of flat orthoborate groups, a common feature of simple borate structures, extend orthogonal to the crystallographic c axis (Fig. 8.1). Interleaved between these layers are double sheets of Ba atoms and single sheets of Mg atoms. The Ba atom is bound by parallel bases of distorted hexagons and triangles, while the Mg atom occupies a distorted octahedral environment.

Selected interatomic distances are listed in Table 8.2. The nine Ba-O bond distances range from 2.731(1)-2.976(5) Å, avg. = 2.81 ± 0.12 Å; the six O atoms lying on the distorted hexagonal plane are bonded to the Ba atom at a distance of 2.731(1) Å, and the three O atoms lying on the trigonal base are located at a distance of 2.976(5) Å (Fig. 8.2). These distances are in good agreement with Ba-O distances of 2.857(4) - 3.018(7) for $Ba_2Ca(BO_3)_2$,[9] 2.710(7)-2.969(6) Å for $Ba_3In(BO_3)_3$,[10] and 2.65(2)-3.15(1) for $Ba_3Sc(BO_3)_3$.[11] Adjacent Ba atoms are linked via triangular O faces of the 9-vertex polyhedra. The polyhedron also shares its smallest trigonal face with the Mg-centered octahedron. The six O atoms around the Mg atom distort slightly from an ideal octahedron; O-Mg-O angles deviate from orthogonality by less than 2°, and the

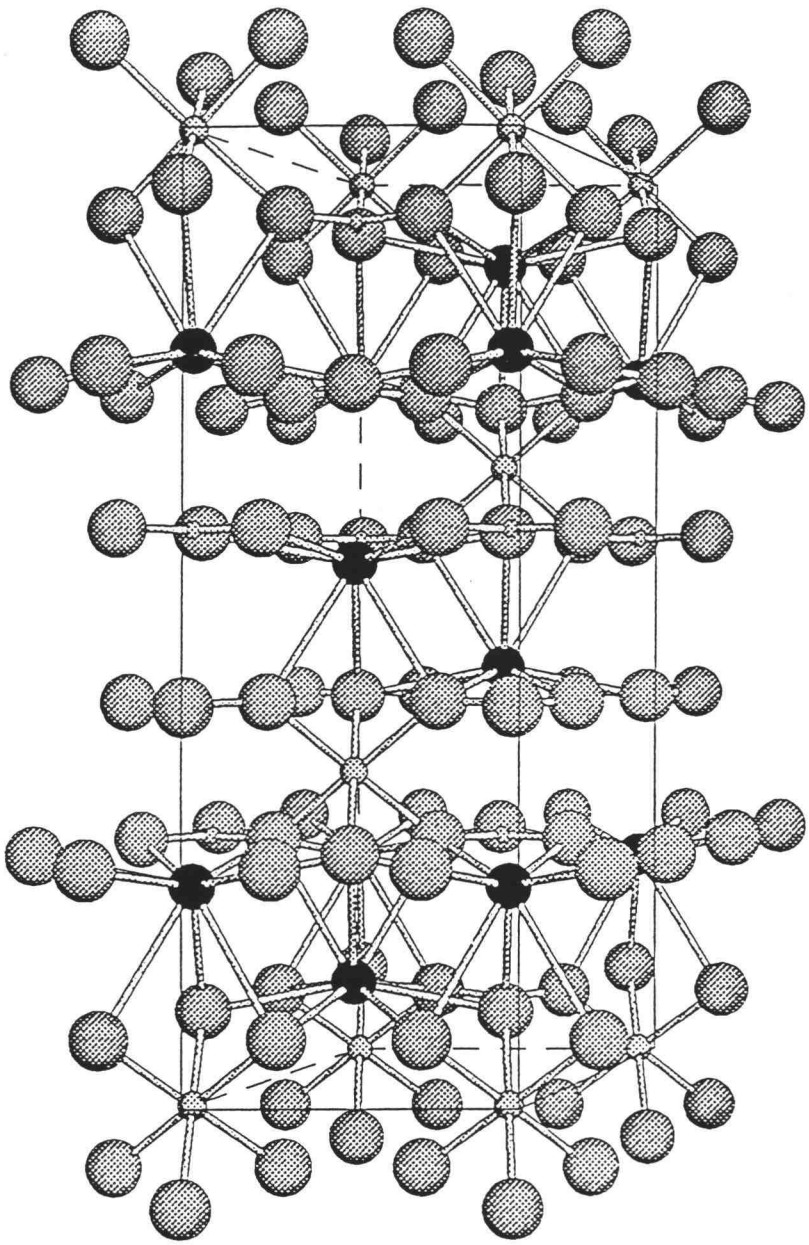

Figure 8.1. Sketch of the unit cell of $Ba_2Mg(BO_3)_2$ as viewed orthogonal to the *c* axis. The large shaded circles represent O atoms, the filled circles represent the Ba atoms, and the small open circles represent the Mg atoms.

Table 8.2. Selected Interatomic Distances (Å) and Angles (°) for $Ba_2Mg(BO_3)_2$

Ba-O (× 3)	2.976(5)	O-Ba-O	70.1(1)
Ba-O (× 6)	2.731(1)		59.5(1)
			101.32(9)
			78.14(4)
			129.10(6)
			65.0(2)
			115.0(1)
			145.06(6)
Mg -O (× 6)	2.121(4)	O-Mg-O	88.2(2)
B-O	1.381(5)	O-B-O	120

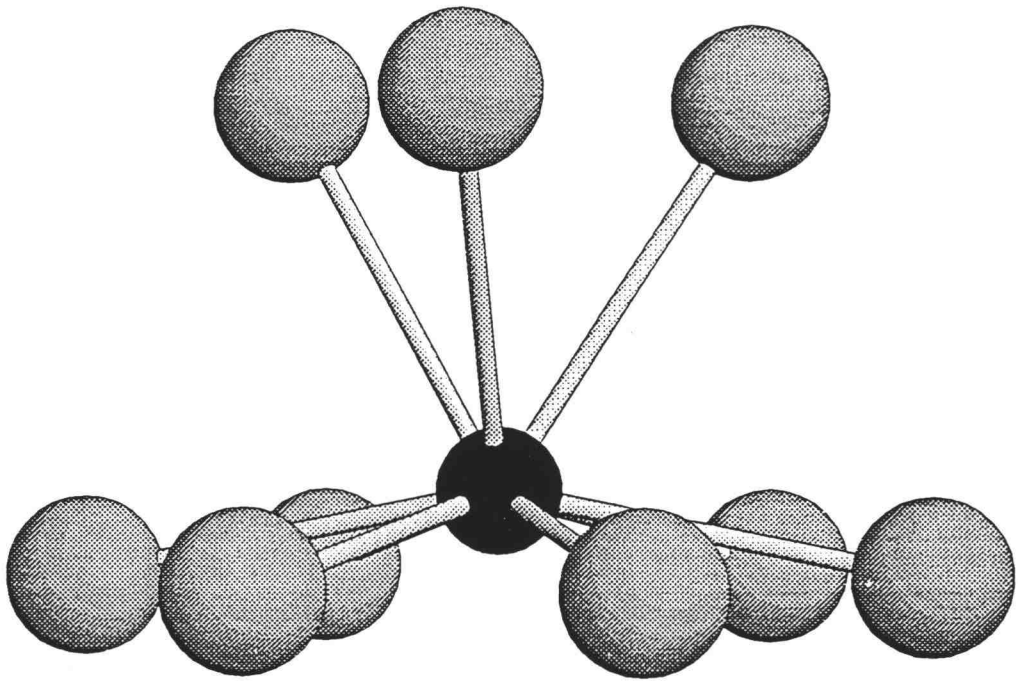

Figure 8.2. Sketch of the coordination environment about the Ba atom. Medium filled circle represents the Ba atom, larger circles represent O atoms.

Mg-O distance is 2.121(4). This distance compares well to the average Mg-O distance of 2.2(1) Å for $Mg_2B_2O_5$[12] and $LaMgB_5O_{10}$[13] and 2.1Å calculated from crystal radii,[14] all for a 6-coordinate Mg. Mg atoms within the same plane are bridged by BO_3 groups; as a result, there are no common O vertices shared between the octahedra. The BO_3 anion has trigonal symmetry; and the B-O distance is normal.

Luminescence

The composition $Ba_{1.98}Eu_{0.02}Mg(BO_3)_2$ exhibits intense emission under ultraviolet excitation. The positions of the excitation and emission maxima for the Eu^{2+} sample are 3590 and 6085 Å, respectively. It is evident that the long emission wavelength does not arise from a low-energy position of the excited state, since the ultraviolet absorption is typical of those Eu^{2+} centers that emit blue light. The Stokes shift is approximately 11,000 cm^{-1}, a value similar to that observed by Dirksen and Blasse, for Eu^{2+} : $Ba_2LiB_5O_{10}$ which emits at 6200 Å with a Stokes shift of 11000 cm^{-1}. The broad emission can be assigned to the allowed transition $4f^65d^1 \rightarrow 4f^7$. The large Stokes shift likely results from the nature of the Ba site on which the Eu^{2+} ion resides. As noted above, the Ba site is nine coordinate with three long and six short Ba-O bond lengths. Because the dopant site is highly anisotropic and the radius of the Eu^{2+} ion is only 90 % of that of the Ba^{2+} ion, severe distortion and strain may be expected

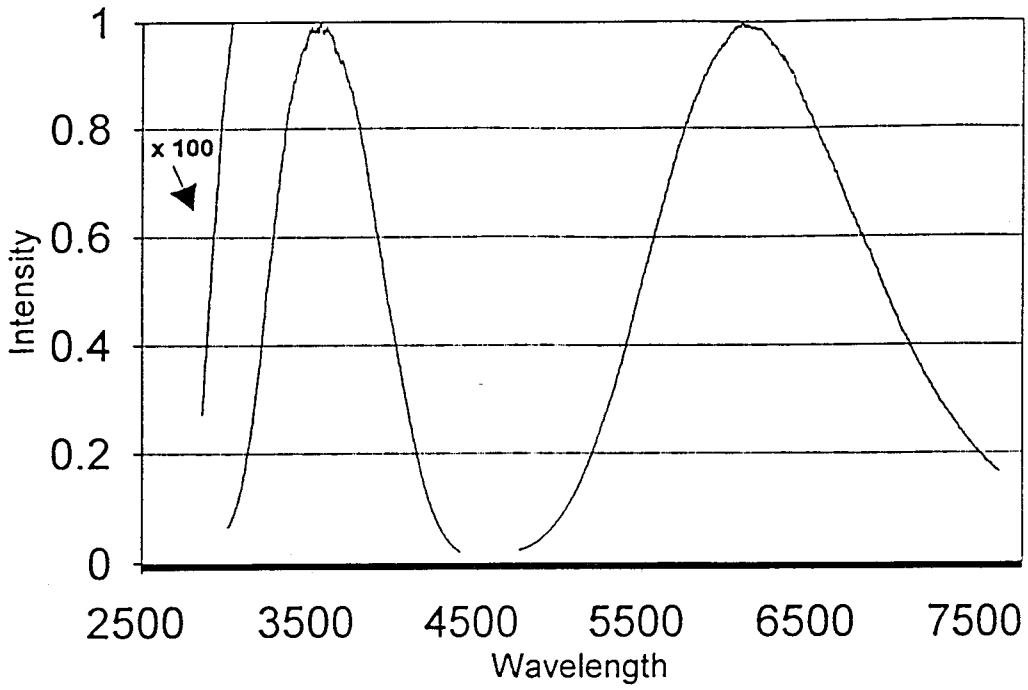

Figure 8.3. Emission and excitation spectra of the luminescence of $Ba_{1.98}Eu_{0.02}Mg(BO_3)_2$ at 298K. The intensity is given in arbitrary units, and the wavelength is given in Å. Luminescence was visible to the eye with an excitation wavelength as short as 2400 Å.

for the Eu^{2+} ground state structural configuration. On excitation, an expected, considerable reorientation of this configuration would lead to sizable observed Stokes shift. A similar model has been proposed for the doped compound Eu^{2+} : $Ba_2LiB_5O_{10}$ where the Eu^{2+} substitutes for the Ba^{2+} ion in an anisotropic site with Ba - O distances ranging from 2.644(2) to 3.020(2) Å.

Studies are ongoing to more fully develop and characterize the unusual optical and structural properties of these materials.

Conclusions

The Stokes shift observed for the emission of Eu^{2+} when doped into $Ba_2Mg(BO_3)_2$ likely results from the anisotropic coordination environment associated with the Ba site. In contrast to previously reported examples, here we can correlate the observed Stokes shift with a systematic variation of short and long bond lengths around the Ba dopant site.

Acknowledgments

This research was supported by National Science Foundation (DMR92-21372). Acknowledgment is made to the Donors of The Petroleum Research Fund, administered by the American Chemical Society, for partial support of the work.

References

1. Weller, T. *J. Lumin.* **1991**, *48 & 49*, 49.

2. Dirksen, G. J., Blasse, G. *J. Solid State Chem.* **1991**, *92*, 591.

3. Smith, R. W., Keszler, D. A. Mater. Res. Bull. **1989**, *24*, 725.

4. Verstegen, J. M. P. J. *J. Electrochem. Soc.* **1974**, *121*, 1631.

5. TEXSAN: Single Crystal Structure Analysis Software; Molecular Structure Corp.,Version 5.0.;The Woodlands, TX, **1989**.

6. Sheldrick, G. SHELXS86. In *Crystallographic Computing 3*; Sheldrick, G.; Kruger,C.; Goddard, R.; Eds.; Oxford University Press: New York, **1985**; 175.

7. Walker, N.; Stuart, D. *Acta Crystallgr., Sect. A* **1983**, *39*, 158.

8. Pabst, A. *American Mineralogi*st. **1974**, *59*, 353.

9. Akella, A., Keszler, D. A. *Main Group Metal Chemistry* **1994**, in press.

10. Cox, J. R. Ph.D. Dissertation, Oregon State University **1993**.

11. Cox, J. R., Huang, J. H., Keszler, D. A. *Chem. Mat.* **1993**, in press.

12. Takeuchi, Y. *Acta Crystallogr.* **1952**, *5*, 574.

13. Saubat, B., Vlasse, M., Fouassier, C. *J. Solid State. Chem.* **1980**, 34, 271.

14. Shannon, R. D. *Acta Crystallogr., Sect. A* **1976**, 32, 751.

CHAPTER 9
Crystal Structure of the Borate $Ba_2Ca(BO_3)_2$

Annapoorna Akella and Douglas A. Keszler*

Department of Chemistry,

Oregon State University,

Gilbert Hall 153,

Corvallis, Oregon 97331-4003, USA.

Main Group Metal Chemistry, in press.

Abstract

The borate $Ba_2Ca(BO_3)_2$ has been prepared and its structure determined by single crystal X-ray diffraction methods. It crystallizes in the monoclinic space group C2/m (#12) with a = 9.362(2), b = 5.432(2), c = 6.635(2) Å, β = 119.38(1)°, and V = 302.6(1) $Å^3$. The structure was determined from 762 unique reflections and refined to the final residues R = 0.040 and R_w = 0.049. The structure is built from BO_3 triangles, distorted CaO_6 octahedra, and distorted BaO_9 polyhedra. It is composed of calcium-borate layers that are interwoven by a 3-dimensional Ba-centered polyhedral framework.

Introduction

The compounds $Ba_2Ca(BO_3)_2$ and $Sr_2Mg(BO_3)_2$ were first described by Verstegen in a report on the characteristics of Tb^{3+} luminescence in borates having the formula $X_2Y(BO_3)_2$ where X = Ba, Sr, Ca and Y = Ca, Mg.[1] Powder X-ray diffraction data on the Ba-Ca and Sr-Mg compounds were supportive of a structural arrangement that resembled that of the trigonal mineral buetschliite, but in a crystal system of lower symmetry. As part of our effort to develop the structural chemistry and optical properties of new borates, we describe here the unique crystal structure of $Ba_2Ca(BO_3)_2$, a material that is isostructural to the Sr-Mg analogue.[2] Our findings are entirely consistent with the work and proposals of Verstegen.

Results

A labelled drawing of the unit cell of $Ba_2Ca(BO_3)_2$ is provided in Figure 9.1. The structure may be described in one way as a 3-dimensional framework of BaO_9 polyhedra that is interposed by distorted CaO_6 octahedra and BO_3 triangles. Here, the BaO_9 polyhedra share rectangular faces, edges, and vertices to form a framework that contains tunnels extending along the **b** axis (Figure 9.2). Sites within these tunnels are occupied by the Ca and B atoms. Another description emphasizes the distorted calcite-like Ca borate layers that are present in the structure (Figure 9.3). These layers stack approximately along the direction [104] and are interleaved by a double layer of Ba atoms (Figure 9.3).

Selected interatomic distances and angles are listed in Table 9.1. The environment about the Ba atom is best described as a distorted tricapped trigonal prism. Two adjacent BaO_9 polyhedra share rectangular faces comprised of four O2 atoms at the corners with an O2-O2-O2 angle of 90° (Figure 9.2). The Ba-O distances range from 2.857(4) to 3.018(7) Å with an average distance of 2.84±0.08 Å. These distances are in good agreement with Ba-O distances of 2.710(7) - 2.969(6) Å for $Ba_3In(BO_3)_3$[3] and 2.65(2) - 3.15(1) Å for $Ba_3Sc(BO_3)_3$,[4] all for a 9-coordinate Ba atom.

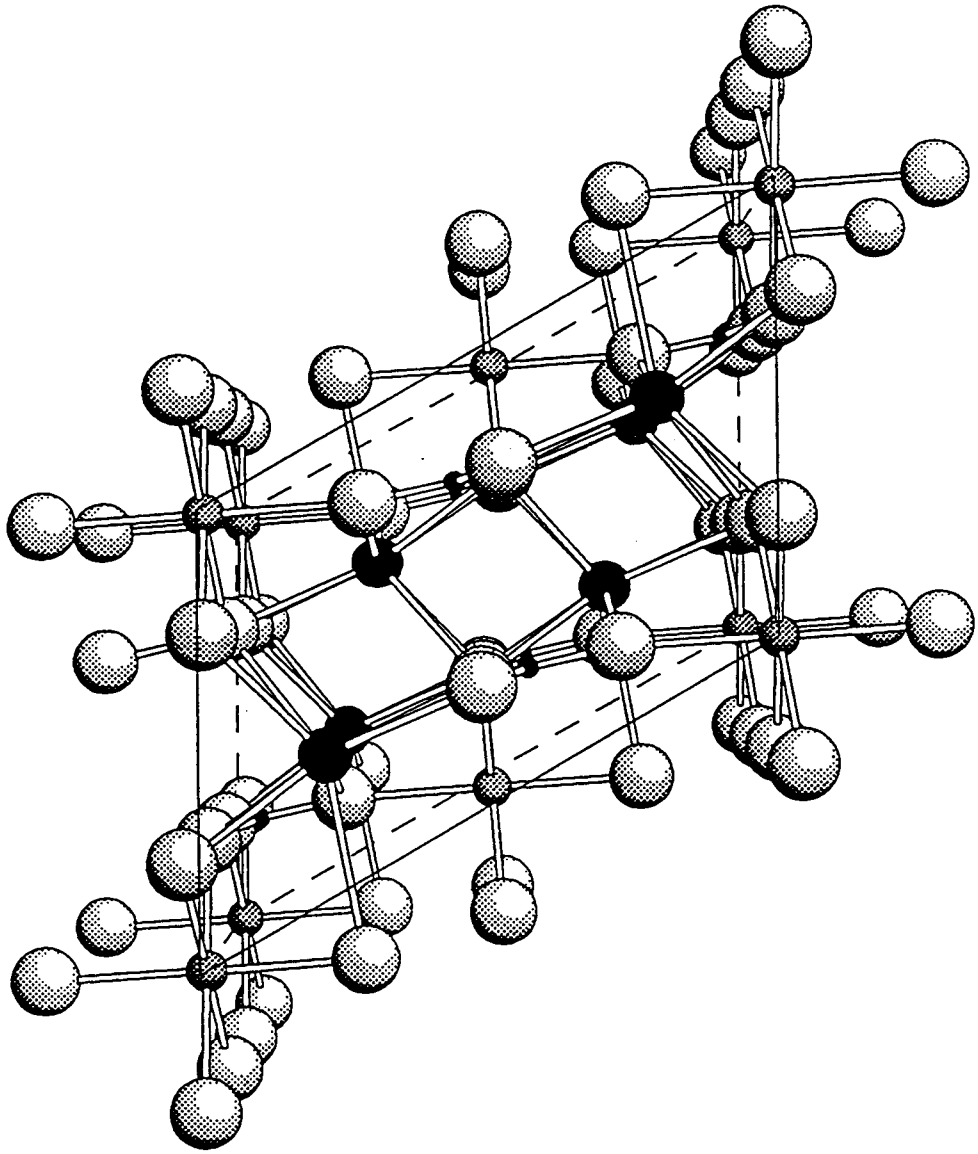

Figure 9.1. Unit-cell diagram; view is along the *b* axis. Large shaded circles represent O atoms, small dark circles represent B atoms, small shaded circles represent Ca atoms, and medium dark circles represent Ba atoms, here, and in ensuing figures.

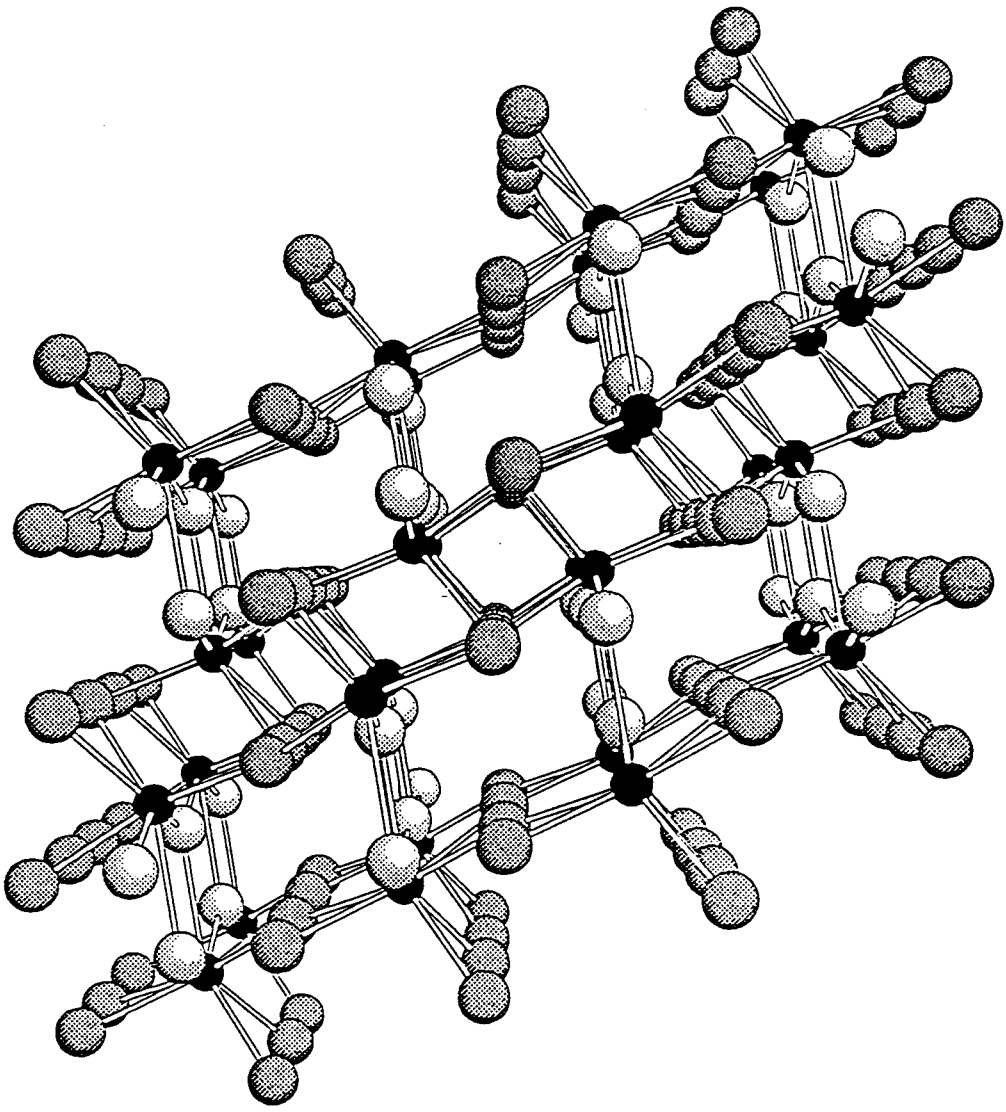

Figure 9.2. Framework resulting from condensation of BaO_9 polyhedra.

Table 9.1. Bond distances (Å) and angles (°) in $Ba_2Ca(BO_3)_2$

Ba - O1 × 1	3.018(7)	O1 - Ba -O1	72.2(1)
Ba - O1 × 2	2.854(2)		144.2(3)
Ba - O2 × 2	2.804(5)	O1 - Ba - O2	101.7(2)
Ba - O2 × 2	2.759(5)		136.4(1)
Ba - O2 × 2	2.857(4)		69.5(1)
			70.8(2)
			135.7(1)
			72.9(1)
			50.1(2)
			112.8(2)
			119.9(2)
		O2 - Ba - O2	90.5(1)
			120.45(3)
			167.7(2)
			51.6(2)
			64.1(2)
			101.8(1)
			118.09(7)
Ca - O1 × 2	2.338(6)	O2 - Ca - O2	98.0(2)
Ca - O2 × 4	2.309(5)		82.0(2)
		O1 - Ca - O2	91.2(2)
			88.8(2)
B - O1 × 1	1.37(1)	O1 - B - O2	120.4(4)
B - O2 × 2	1.394(7)	O2 - B - O2	118.9(8)

Two adjacent Ba-centered polyhedra share vertices through two opposing O1 atoms forming chains along the b direction. The Ba-centered and Ca-centered polyhedra share a triangular face consisting of one O1 and two O2 atoms. The Ca atom occupies a distorted octahedral environment having C_{2h} site symmetry. The Ca atom is bonded to four O2 atoms equatorially with a bond distance of 2.309(5) Å and two O1 atoms axially with a bond distance of 2.338(6) Å. As seen in Figure 3, the Ca-centered octahedra are isolated from each other by the Ba-centered polyhedra and the BO_3 groups. The BO_3 anions deviate slightly from trigonal symmetry; O-B-O angles are 120.4(4) and 118.9(8)°. The B atom binds one O1 and two O2 atoms at distances of 1.37(1) and 1.394(7) Å, respectively. The distances are typical when compared to similar interactions in $ScBO_3$,[5] 1.3752(5), and $SrBe_2(BO_3)_2$,[6] 1.37(1), and a distance of 1.40 Å calculated from crystal radii.[7]

Experimental Section

Synthesis. A powder sample of $Ba_2Ca(BO_3)_2$ was prepared by grinding a molar ratio of 2 $BaCO_3$ (CERAC, 99.9%), 1 $CaCO_3$ (AESAR, 99.9%), and 1.05 B_2O_3 (ALFA, 99.98%) under hexane to a fine powder followed by heating at 973 K in a Pt crucible for 1 h. The mixture was reground and heated at 1273 K for 24 h. A crystal was obtained for X-ray structure analysis from a melt of composition 0.5 $BaCl_2$: 0.5 BaO : 1 CaO : 0.55 B_2O_3. The melt was contained

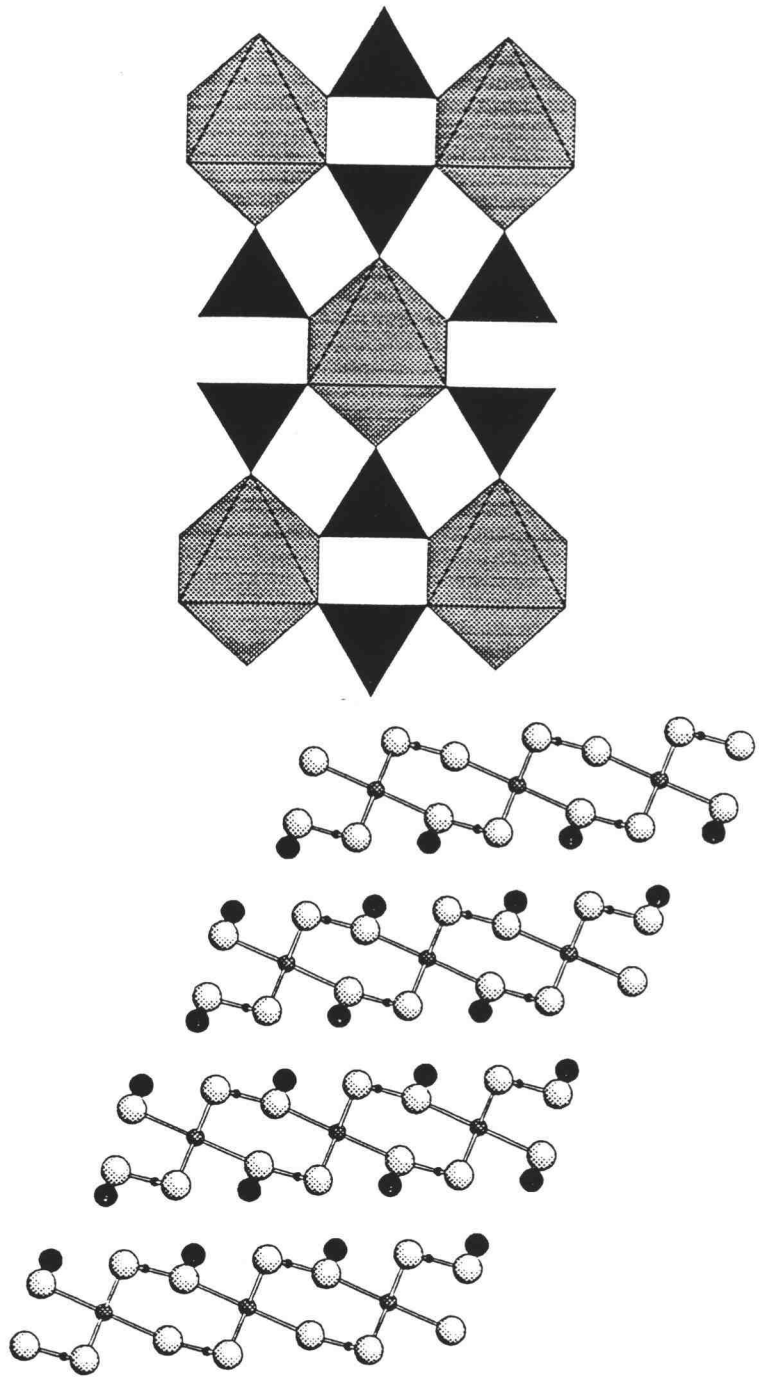

Figure 9.3. Top: Polyhedral view along [104] of Ca- and B-centered polyhedra. Bottom: Layered stacking of calcium borate layers (view is along the b axis).

in a Pt crucible and slowly cooled from 1273 K to 873 K at 6 K/h, and then rapidly cooled at 50 K/h to room temperature.

Crystallographic Study. A colorless, transparent crystal of dimensions 0.12 × 0.15 × 0.10 mm was selected and mounted on a glass fiber with epoxy for structure determination. All measurements were made on a Rigaku AFC6R diffractometer with graphite-monochromated Mo Kα radiation. Cell constants and the orientation matrix for data collection were obtained from a least-squares refinement with 20 automatically-centered reflections in the range $30 \leq 2\theta \leq 36°$. The cell constants correspond to a monoclinic cell, and Laue symmetry 2/m was determined on the diffractometer. Intensity data were collected over the range of indices $0 \leq h \leq 15$, $0 \leq k \leq 8$, $-10 \leq l \leq 10$ by using the ω scan technique to a maximum 2θ value of 70°; from 760 measured reflections a total of 664 were observed [$F_o^2 \geq 3\sigma F_o^2$]. The intensities of three representative reflections measured after every block of 200 data varied by an average of 2% during the collection. The structure was solved by using the *TEXSAN* crystallographic software package.[8] The compound was found to form in the centerosymmetric space group C2/m. The positions of the Ba and Ca atoms were derived from the direct methods program SHELXS, while the remaining atoms were located from difference electron density maps.[9] After a full-matrix least-squares refinement of the model with isotropic displacement

coefficients on each atom, an absorption correction was applied by using the program DIFABS (transmission factors = 0.76 -1.28).[10] The data were averaged (R_{int} = 0.059), and the model was refined with anisotropic thermal displacement coefficients on each atom. Final least-squares refinement resulted in the residuals R = 0.040 and R_w = 0.049. The largest peak in the final difference electron density map corresponds to 1.12% of the Ba atom. Crystal data and atomic parameters and are given in Tables 9.2 and 9.3, respectively.

Acknowledgments

This research was supported by National Science Foundation (DMR92-21372). Acknowledgment is made to the Donors of The Petroleum Research Fund, administered by the American Chemical Society, for partial support of the work.

Table 9.2. Crystal data and experimental conditions for $Ba_2Ca(BO_3)_2$.

Diffractometer	Rigaku AFC6R
Radiation	Graphitemonochromated Mo Kα (λ = 0.71069 Å)
Formula wt., u	432.36
Unit cell	Monoclinic
a, Å	9.636(2)
b, Å	5.432(1)
c, Å	6.635(2)
β, °	119.38(1)
V, Å^3	302.6(1)
Space group	C2/m
ρ_{calc}, g cm^{-3}	4.745
F(000)	380
Z	2
Linear abs. coeff., cm^{-1}	137.35
No. unique data with $F_o^2 > 3\sigma(F_o^2)$	726
R (F_o)	0.040
R_w (F_o)	0.049

Table 9.3. Positional parameters and equivalent displacement coefficients (B_{eq}) for $Ba_2Ca(BO_3)_2$; estimated standard deviations are given in parentheses.

		x	y	z	B_{eq}
Ba	m	0.21117(5)	0	0.68315(8)	0.85(2)
B	m	-0.063(1)	1/2	0.248(1)	0.6(2)
Ca	2/m	0	0	0	0.66(5)
O1	m	-0.2220(7)	1/2	0.178(1)	1.0(2)
O2		0.0180(5)	0.2790(8)	0.2743(7)	0.9(1)

$$B_{eq} = 8\frac{\pi^2}{3}\sum_i\sum_j U_{ij} a_i^* a_j^* a_i \cdot a_j$$

References

1. Verstegen, J. M. P. J. *J. Electrochem. Soc.* **121** (1974), 1631.

2. Sarkar, S., Schaffers, K. I., Keszler, D. A., unpublished results.

3. Cox, J. R., Ph.D. Dissertation, Oregon State University (1993).

4. Cox, J. R., Huang, J. H., Keszler, D. A. *Chem. Mat.* (1993), in press.

5. Sun, H., Keszler, D. A. *Acta Crystallogr., Sect. C*, **44** (1988), 1505.

6. Schaffers, K. I., Keszler, D. A. *J. Solid State Chem.*, **85** (1990), 270.

7. Shannon, R. D. *Acta Crystallogr., Sect. A* **32**, (1976), 751.

8. Molecular Structure Corporation, *TEXSAN*, Structure Analysis Package, MSC (3200A Research Forest Drive, Woodlands, TX 77381).

9. Sheldrick, G. M. in "*Crystallographic Computing 3*" (Sheldrick, G.M., Kruger, C., Goddard, R.), pp 175-189, Oxford Univ. Press, Oxford (1985).

10. Walker, N., Stuart. D. *Acta Crystallogr., Sect A, 39* (1983), 158.

CHAPTER 10
The Buetschliite Derivative $K_2Zr(BO_3)_2$

Annapoorna Akella and Douglas A. Keszler

Department of Chemistry and

Center for Advanced Materials Research,

Gilbert Hall 153, Oregon State University,

Corvallis, Oregon 97331-4003

Inorg. Chem. **1994**, *33*, 1554.

Abstract

The Buetschliite derivative $K_2Zr(BO_3)_2$ has been synthesized and structurally characterized by single-crystal X-ray diffraction techniques. The borate forms in the centerosymmetric trigonal space group R-3m(h) with cell parameters a = 5.283 (8) Å, c = 17.518 (2) Å, and Z = 3. One crystallographically distinct K-centered hexagonal base-trigonal base O environment exists in the structure. The Zr atom is six coordinate and its immediate O environment deviates only slightly from an ideal octahedral geometry.

Introduction

The minerals Eitelite, $Na_2Mg(CO_3)_2$, and Buetschliite, $K_2Ca_2(CO_3)_2$, have been known since the early 1970's when synthetic forms were prepared and their structures determined by Pabst.[1,2] Each structure contains cations dispersed between sheets of planar CO_3 groups. Buetschliite is related to the parent Eitelite by rotation of the CO_3 groups about the C_3 axis.

From a phase study of the K-Zr borate system, we have identified the new compound $K_2Zr(BO_3)_2$ which is isoelectronic and isostructural to Buetschliite. Because such layered compounds can exhibit significant birefringence, we have determined the structure of the material and measured its refractive indices.

Experimental Section

Synthesis. A powder sample of $K_2Zr(BO_3)_2$ was prepared from the molar ratio of 1 $ZrOCl_2{\cdot}8H_2O$ (AESAR, 99.9%), 2 B_2O_3 (ALFA, 99.98%), and 4 KF (AESAR, 99.9%). The mixture of oxide chloride and B_2O_3 was heated at 873 K for 1/2 h followed by addition of KF; then the sample was ground and heated at 1000 K for 12 h. Residual K compounds were removed by washing the sample in H_2O. Crystals were grown for X-ray structure analysis by melting the sample in excess KF flux in a Pt crucible at 1073 K, slowly cooling at 6 K/h to 500 K, and

rapidly cooling at 50 K/h to room temperature. The KF flux was dissolved in hotwater, providing crystals of hexagonal morphology.

Crystallographic Study. A colorless, transparent crystal of dimensions 0.12 × 0.15 × 0.08 mm was selected and mounted on a glass fiber with epoxy for structure determination. All measurements were made on a Rigaku AFC6R single crystal diffractometer with graphite-monochromated Mo Kα radiation. Cell constants and the orientation matrix for data collection were obtained from a least squares refinement with 19 automatically-centered reflections in the range $30 \leq 2\theta \leq 36°$. The cell constants correspond to a hexagonal cell; Laue symmetry -3m was determined on the diffractometer. Intensity data were collected over the range of indices $-8 \leq h \leq 8$, $0 \leq k \leq 8$, $-28 \leq l \leq 28$ by using the ω scan technique to a maximum 2θ value of 70°, and from 1395 measured reflections a total of 1305 were observed [$F_o^2 > 3\sigma F^2$]. The intensities of three representative reflections measured after every block of 200 data varied by an average of 2% during the collection.

The structure was solved by using the *TEXSAN* software package.[3] The crystal was found to form in the centerosymmetric space group R-3m(h). The positions of the K and Zr atoms were derived from the direct methods program SHELXS, while the remaining atoms O and B were located from difference electron density maps.[4] After a full-matrix isotropic refinement of the

model an absorption correction was applied (transmission factors 0.594-1.00) by using the program DIFABS.[5] The data were averaged (R_{int} = 0.112), and the model was refined with anisotropic thermal displacement coefficients on each atom. Final least squares refinement resulted in the residuals R=0.022 and *w* R=0.028. The largest peak in the final difference electron density map corresponds to 0.36% of the Zr atom. Crystal data are outlined in Table 10.1., and atomic positional and thermal parameters are listed in Tables 10.2, and 10.3.

Table 10.1. Crystallographic Data for $K_2Zr(BO_3)_2$.

chem formula	$K_2Zr(BO_3)_2$
fw, u	287.03
crystal system	Trigonal
space group	R-3m (h), (No. 166)
a, Å	5.283 (8)
c, Å	17.518 (2)
V, $Å^3$	423.35 (1)
Z	3
ρ_{calc}, g cm^{-3}	3.377
radiation	Mo Kα[a]
temp, K	298
linear abs.coeff μ, cm^{-1}	33.57
transm.factors	0.594 -1.00
R, R_w[b]	0.022, 0.028

[a] Graphite monochromated; λ = 0.71069 Å. [b] $R = \Sigma \, | \, |F_o| - |F_c| \, | \, / \, \Sigma \, |F_o|$;

$R_w = [\, \Sigma w \, (|F_o|^2 - |F_c|^2)^2 \, / \, \Sigma \, w \, |F_o|^4 \,]^{1/2}$.

Table 10.2. Positional and Thermal Parameters (B_{eq}) for $K_2Zr(BO_3)_2$.

	site symmetry	x	y	z	B_{eq} (Å^2)
K	C_{3v}	0	0	0.20963(4)	0.70(1)
Zr	D_{3d}	0	0	0	0.70(1)
O	C_s	0.1827(1)	0.3654	0.07089(7)	1.10(1)
B	C_{3v}	1/3	2/3	0.0700(2)	0.75(5)

$$B_{eq}=(\frac{8\pi^2}{3})\sum_i\sum_j U_{ij}a_i^*a_j^*a_i.a_j$$

Table 10.3. Anisotropic displacement coefficients for $K_2Zr(BO_3)_2$.

Atom	U11	U22	U33	U12	U13	U23
Zr	0.0086(2)	0.0086	0.0093(2)	0.0043	0	0
K	0.0147(2)	0.0147	0.0164	0.0074	0	0
O	0.0111(5)	0.0111	0.0160(4)	0.0028(8)	0.0024(4)	-0.0024
B	0.0099(8)	0.0099	0.009(1)	0.005	0	0

Table 10.4. Selected Interatomic Distances (Å) and Angles (°) for $K_2Zr(BO_3)_2$.

Zr -O (× 6)	2.083(1)	O-Zr-O	88.09(5)
K-O (× 3)	2.950(1)	O-K-O	78.14(4)
K-O (× 6)	2.8025(6)		58.79(4)
			107.56(3)
			78.14(4)
			136.03(2)
			62.21(5)
			50.41(5)
			109.67(3)
			140.95(5)
B-O	1.378(1)	O-B-O	119.99(1)

Results and Discussion

The structure of the title compound is that of the mineral Buetschliite. Layers of flat orthoborate groups extend orthogonal to the crystallographic c axis (Figure 10.1.), a standard feature of simple borate structures. Interleaved between these layers are double sheets of K atoms and single sheets of Zr atoms.

The chemically and crystallographically distinct K atom is nine coordinate, providing a prototypical example of a hexagonal base-trigonal base environment (Figure 10.2.) that we have found to be a common feature of borate structures containing large alkaline-earth metals.[6,7] The average K-O bond length is 2.85(7) Å; the six O atoms lying on the distorted hexagonal plane are bonded to the K atom at a distance of 2.8025(6) Å, and the three O atoms lying on the trigonal base are located at a distance of 2.950(6) Å. Adjacent K atoms are linked via triangular O faces of the 9-vertex polyhedra. The polyhedron also shares its smallest trigonal face with the Zr-centered octahedron.

The six O atoms around the Zr atom distort slightly from an ideal octahedron; O-Zr-O angles deviate from orthogonality by less than 2°, and the Zr-O distance is normal. The Zr atoms within the same plane are bridged by BO_3 groups, as a result, there are no common O vertices shared between the

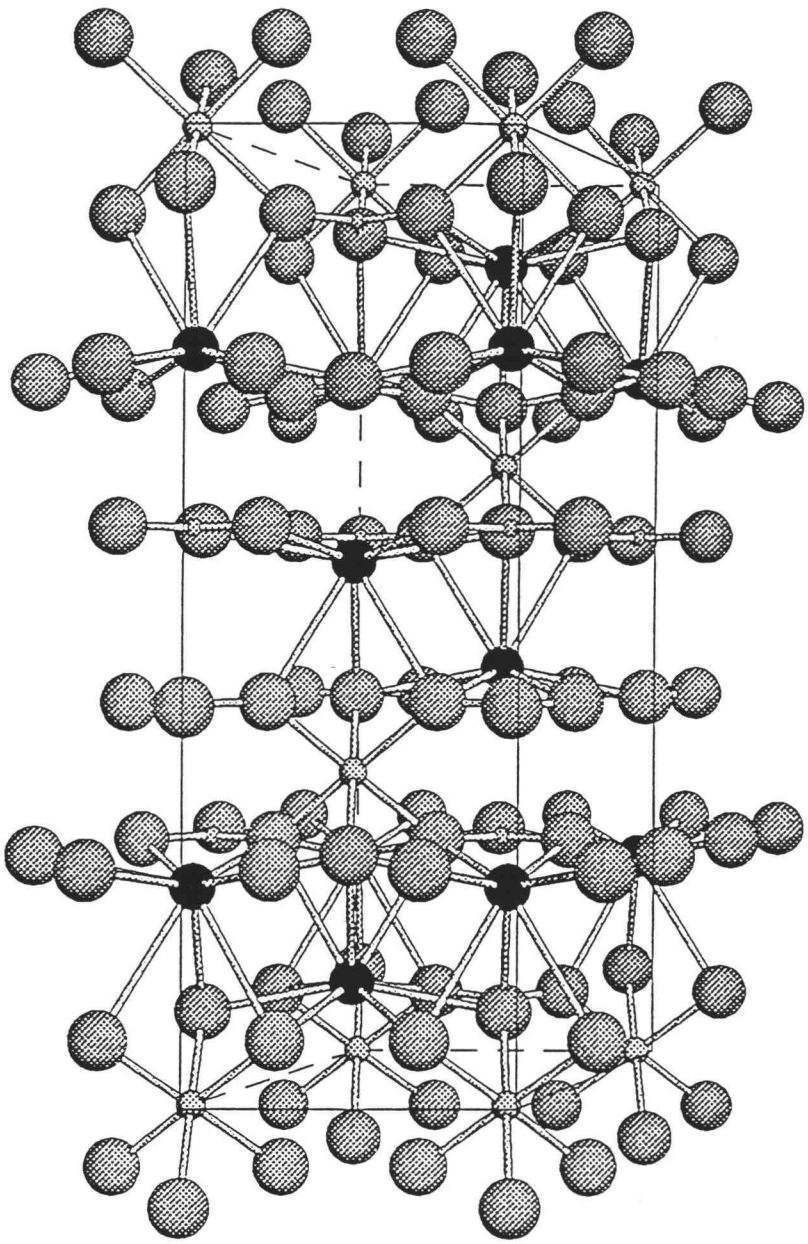

Figure 10.1. Sketch of the unit cell of $K_2Zr(BO_3)_2$ as viewed orthogonal to the *c* axis. The large shaded circles represent O atoms, the dark circles represent the K atoms and the small grey circles represent the Zr atoms.

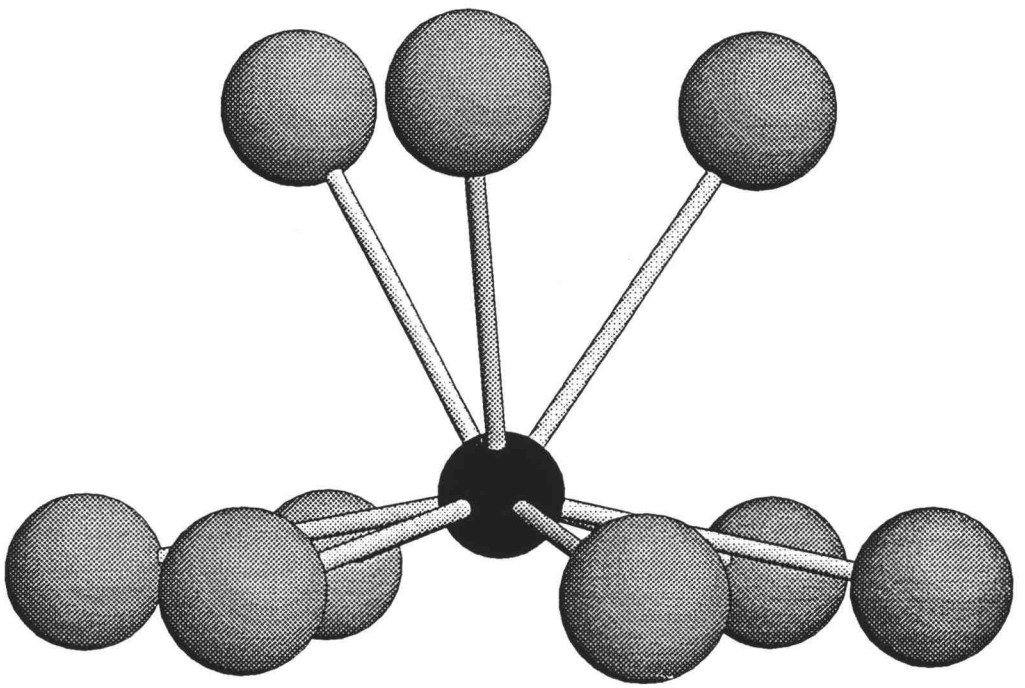

Figure 10.2. Sketch of the coordination environment about the K atom. Small dark circle represents the K atom, larger circles represent O atoms.

Zr-centered octahedra. The distances and angles in the BO_3 trigonal planes are unexceptional. Crystalline $K_2Zr(BO)_3$ exhibits uniaxial negative birefringence. The refractive indices of the crystals as determined by the oil-dispersion technique are $\omega = 1.773(1)$ and $\epsilon = 1.747(3)$, and the birefringence $\omega-\epsilon = 0.026$.[8] These values may be compared with those of Buetschliite $\omega = 1.600$, $\epsilon = 1.462$, and $\omega-\epsilon = 0.138$.

By using the Gladstone-Dale relationship, $(n-1)/\rho = K$, the X-ray results, and tabulated values of specific refractivities (k),[9] average refractive indices [$n = (2\omega+\epsilon) / 3$] may be computed. For $K_2Zr(BO_3)_2$ $n_{obsd} = 1.76$ and $n_{calcd} = 1.70$, while for Buetschliite $n_{obsd} = 1.53$ and $n_{calcd} = 1.55$. The larger index for the Zr compound arises primarily from the presence of the Zr atom and a density that is 30% greater than that of Buetschliite. Presumably, in making a contribution of nearly 45% to the refractive energy that is largely isotropic, the ZrO_2 component also leads to the reduced birefringence.

Acknowledgments

This work was supported by the US National Science Foundation, Solid-State Chemistry Program (DMR-9221372). DAK thanks the Alfred P. Sloan Foundation for a fellowship. Tables listing complete crystallographic and data collection information and anisotropic displacement coefficients (2 pages).

References

1. Pabst, A. *American Mineralogist.* **1973**, *58*, 211-217.

2. Pabst, A. *American Mineralogist.* **1974**, *59*, 353-358.

3. Texsan: Single Crystal Structure Analysis Software; Molecular Structure Corp Version 5.0.;The Woodlands, TX, **1989**.

4. Sheldrick, G. SHELXS86. In *Crystallographic Computing 3*; Sheldrick, G.; Kruger,C.; Goddard, R.; Eds.; Oxford University Press: New York, **1985**; pp 175-189.

5. Walker, N.; Stuart, D. *Acta Crystallgr.*; *Sect. A* **1983**, *39*, 158-166.

6. Alekel, T.A.; Ph.D. Dissertation, Oregon State Univ., 1993.

7. Cox, J.A.; Keszler, D.A. Unpublished results.

8. Bloss,F.D. *An Introduction to the Methods of Optical Crystallography*, Holt, Rinehart and Winston: New York, **1961**; pp 294.

9. Mandarino, J.A. *Can. J. Mineral.* **1976**, *14*, 498-502.

CHAPTER 11
Structure and Eu^{3+} Luminescence of $Sr_4Ge_2O_7F_2$

Annapoorna Akella and Douglas A. Keszler

Department of Chemistry and

Center for Advanced Materials Research

Oregon State University

Gilbert Hall 153

Corvallis, Oregon 97331-4003

In preparation for submission to *Chemistry of Materials*

Abstract

The structure and Eu^{3+} luminescence of the compound $Sr_4Ge_2O_7F_2$ is described. Crystal data: FW = 645.65 amu, P $2_1/c$ (#14), monoclinic, a = 8.024(1), b = 11.224(1), c = 11.547(2) Å, β = 109.79(1)°, V = 978.6(3) $Å^3$, Z = 2, R = 0.046, R_w = 0.051 for 4342 averaged reflections. The structure contains layers of edge shared Sr-centered polyhedra connected by pyrogermanate groups Ge_2O_7. There are four crystallographically distinct Sr atoms, one 6-coordinate, two 7-coordinate, and one 8- coordinate.

Introduction

Alkaline-earth metal germanate fluorides have not been known in literature, here we present the crystal structure of the first alkaline-earth metal germanate fluoride. Our interest in oxoanion fluorides stems from our perception that, addition of fluoride to a matrix lowers the melting point and viscosity of a melt. We speculate that the presence of a fluoride around an alkaline-metal site may provide anisotropic sites, which could potentially exhibit unusual optical properties when doped with luminescent ions. The rare earth ion Eu^{3+} when doped in the title compound provides an unuusual luminescence with a peak of maximum intensity at 7000 Å. Typically peaks at 5900 Å (orange) or 6200 Å (red) are the most intense peaks for Eu^{3+} luminescence. We attribute this unusual luminescence to the greatly distorted Sr sites the dopant occupies.

Experimental

A powder sample of $Sr_4Ge_2O_7F_2$ was prepared by heating the molar quantities of 3 $SrCO_3$ (AESAR, 99.9%), 2 GeO_2 (ALFA, 99.98%), and 1 SrF_2 (AESAR, 99.9%) in an atmosphere of Ar. A crystal was obtained by slowly cooling a stoichiometric melt in a Pt crucible from 1223 K to 873 K at 6 K/h, and then rapidly cooled at 50 K/h to room temperature. The melt was contained in a Pt crucible and slowly cooled from 1223 K to 873K at 6 K/h, and then rapidly

at 50 K/h to room temperature. A colorless, transparent crystal of dimensions 0.10 × 0.12 × 0.10 mm was selected and mounted on a glass fiber with epoxy for structure determination. All measurements were made on a Rigaku AFC6R diffractometer with graphite-monochromated Mo Kα radiation. Cell constants and the orientation matrix for data collection were obtained from a least squares refinement with 19 automatically-centered reflections in the range 30 ≤ 2θ ≤ 36°. The cell constants correspond to a monoclinic cell; Laue symmetry 2/m was determined on the diffractometer. Intensity data were collected over the range of indices $0 \le h \le 12$, $0 \le k \le 18$, $-18 \le l \le 18$ by using the ω scan technique to a maximum 2θ value of 70°, and from 4592 measured reflections a total of 2489 were observed [$F_o^2 \ge 3\sigma F^2$]. The intensities of three representative reflections measured after every block of 200 data varied by an average of 2% during the collection.

The structure was solved by using the *TEXSAN* software package.[4] The crystal was found to form in the centerosymmetric space group . The positions of the Sr and Ge atoms were derived from the direct methods program SHELXS,[5] while the remaining atoms O and F were located from difference electron density maps. After a full-matrix least-squares refinement of the model with isotropic displacement coefficients on each atom, an absorption correction was applied (transmission factors = 0.80 -1.47) by using the program DIFABS.[6] The data were averaged (R_{int} = 0.054), and the model

was refined with anisotropic displacement coefficients on each atom. Final least squares refinement resulted in the residuals R = 0.046 and R_w = 0.051. The largest peak in the final difference electron density map corresponds to 0.88% of the Sr atom. Crystal data are outlined in Table 11.1.; atomic positional and thermal parameters are listed in Table 11.2.

The luminescence measurement was performed on a powder sample nominally doped with 2 mole% Eu^{3+}. The preparative procedure was that described above [Eu_2O_3 (99.99%, MOLYCORP)], except 2 mole % KNO_3 was added for charge compensation. Steady-state, room-temperature luminescence spectra were obtained on a computer-controlled right angle spectrometer. Excitation provided by an Oriel 300-W Xe lamp was passed through a 50-cm water filter, focused onto the slits of a Cary model-15 prism monochromator, and subsequently onto the sample. Luminescence was collected at a near-right angle to excitation, dispersed through an Oriel 22500 1/8 - m monochromator, and detected with a Hamamatsu R636 photomultiplier tube. The signal was collected and amplified with a Keithley model 602 picoammeter then converted to a digital signal for computer acquisition. Spectrometer control and data acquisition were achieved with computer programs written in this laboratory.

The excitation spectrum was corrected by using rhodamine B as a quantum counter. The emission spectrum was corrected with a tungsten lamp that has been calibrated at Eppley Laboratories.

TABLE 11.1. Crystallographic Data for $Sr_4Ge_2O_7F_2$

chem formula	$Sr_4Ge_2O_7F_2$
fw, u	645.65
crystal system	Monoclinic
space group	$P2_1/c$ (#14)
a, Å	8.024(1)
b, Å	11.224(1)
c, Å	11.547(2)
V, Å^3	978.6(3)
β, °	109.79(1)
Z	4
ρ_{calc}, g cm^{-3}	4.382
radiation	Mo Kα[a]
temp, K	298
linear abs. coeff μ, cm^{-1}	270.26
transm. factors	0.81 - 1.41
R, R_w[b]	0.046, 0.051

[a] Graphite monochromated; λ = 0.71069 Å. [b] $R = \Sigma \, | \, |F_o| - |F_c| \, | \, / \, \Sigma \, |F_o|$; $R_w = [\, \Sigma w (\, |F_o| - |F_c| \,)^2 \, / \, \Sigma \, w \, |F_o|^2 \,]^{1/2}$.

TABLE 11.2. Positional and Equivalent Displacement Parameters (B_{eq}) for $Sr_4Ge_2O_7F_2$

	x	y	z	B_{eq}
Sr1	0.4690(1)	0.08110(7)	0.68322(7)	0.34(2)
Sr2	0.3365(1)	-0.13231(7)	0.91678(8)	0.46(3)
Sr3	0.8310(1)	-0.13400(7)	0.92273(7)	0.36(3)
Sr4	-0.0289(1)	0.09323(7)	0.69941(7)	0.36(2)
Ge1	0.1530(1)	-0.19424(9)	0.62417(8)	0.30(3)
Ge2	0.2730(1)	0.19652(9)	0.36749(8)	0.37(3)
F1	0.0750(7)	-0.0069(5)	0.9011(4)	0.5(2)
F2	0.5738(8)	-0.0005(5)	0.8974(5)	0.8(2)
O1	0.2721(9)	0.2142(6)	0.7461(5)	0.6(2)
O2	0.7211(9)	0.2157(6)	0.7567(6)	0.6(1)
O3	0.200(1)	-0.0488(6)	0.6683(6)	1.0(1)
O4	0.135(1)	-0.2673(6)	0.9750(6)	0.8(2)
O5	0.9358(9)	-0.2662(6)	0.1232(6)	0.8(2)
O6	0.4084(9)	0.2366(6)	0.5121(6)	0.7(2)
O7	0.720(1)	-0.0498(6)	0.6750(7)	0.9(2)

Results and Discussion

A view of the contents of the unit cell is given in Figure 11.1. The structure contains four types of Sr, one 6-coordinate, two 7-coordinate, and one 8- coordinate, two crystallographically distinct 4- coordinate Ge atoms. The Sr-centered polyhedra share faces, edges and vertices to form a three-dimensional framework that contains pyro tetrahedral interstices occupied by Ge atoms (Figure 11.2). As indicated by the stoichiometry, the Ge_2O_7 groups result from corner sharing of Ge-centered tetrahedra (Figure 11.3).

Selected interatomic distances and angles are listed in Table11.3. Atom Sr1 is bound by one each of atoms O1, O2, O3, O6, O7, and F2 in a distorted octahedral geometry. Atom Sr2 is bound by one each of atoms O2, O3, O4 and O6, and F1 and two F2 atoms in an environment best described as a distorted monocapped octahedron. Atom Sr3 is bound to one each of atoms O1, O4, O5, O6, O7, and F2 and two F1 atoms in an environment best described as a distorted dodecahedron. The Sr4 atom is bonded to one each of atoms O1, O2, O3, O4, O5, O7 and F1 in a distorted monocapped octahedral geometry. The Sr1 atom shares an edge (O1··O3) with Sr4, an edge (O2..O6) with Sr2 and corners (F2 and O6) with Sr3, and Ge2. The Sr1 atoms are isolated from each other. The atom Sr2 shares edges (O2··O6, F2··O6, O2··O3, O2··O3), with Sr1, Sr3 and Sr4 and Ge1 atoms. Two adjacent

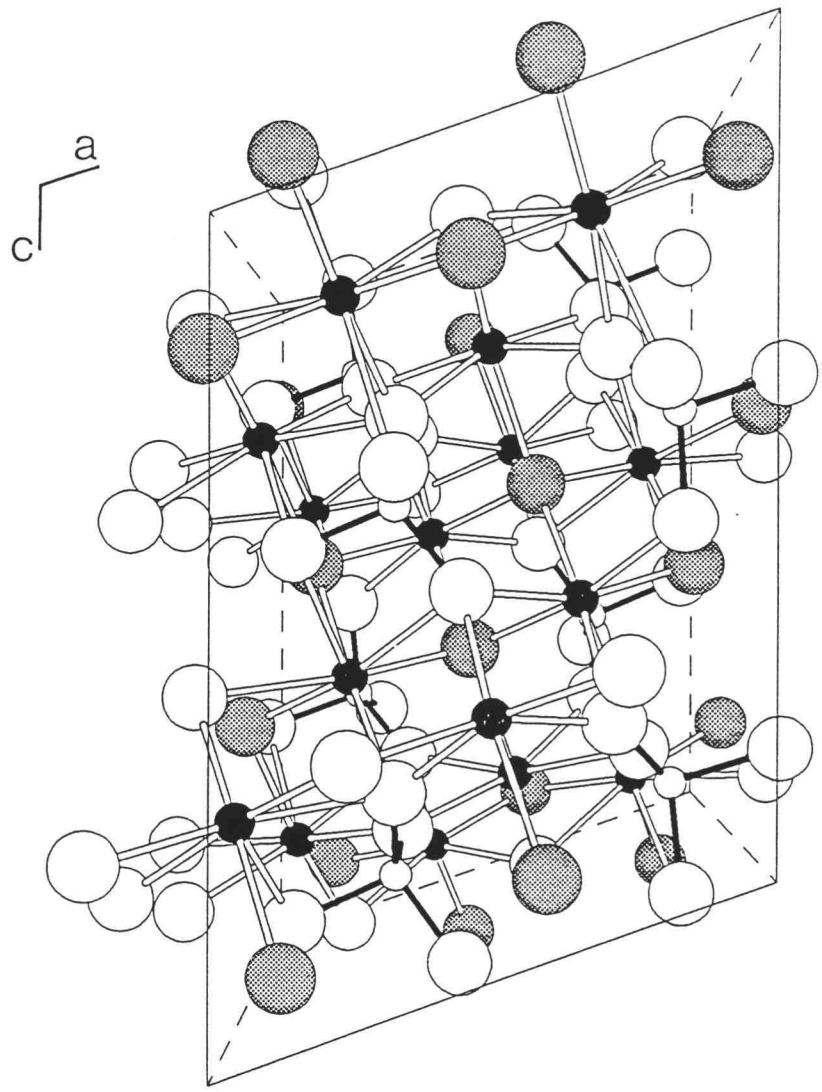

Figure 11.1. Unit cell diagram of $Sr_4Ge_2O_7F_2$; view is along the *b* axis. Large, shaded circles represent F atoms, and large, open circles represent O atoms. Small, filled circles represent Sr atoms, small open circles represent Ge atoms.

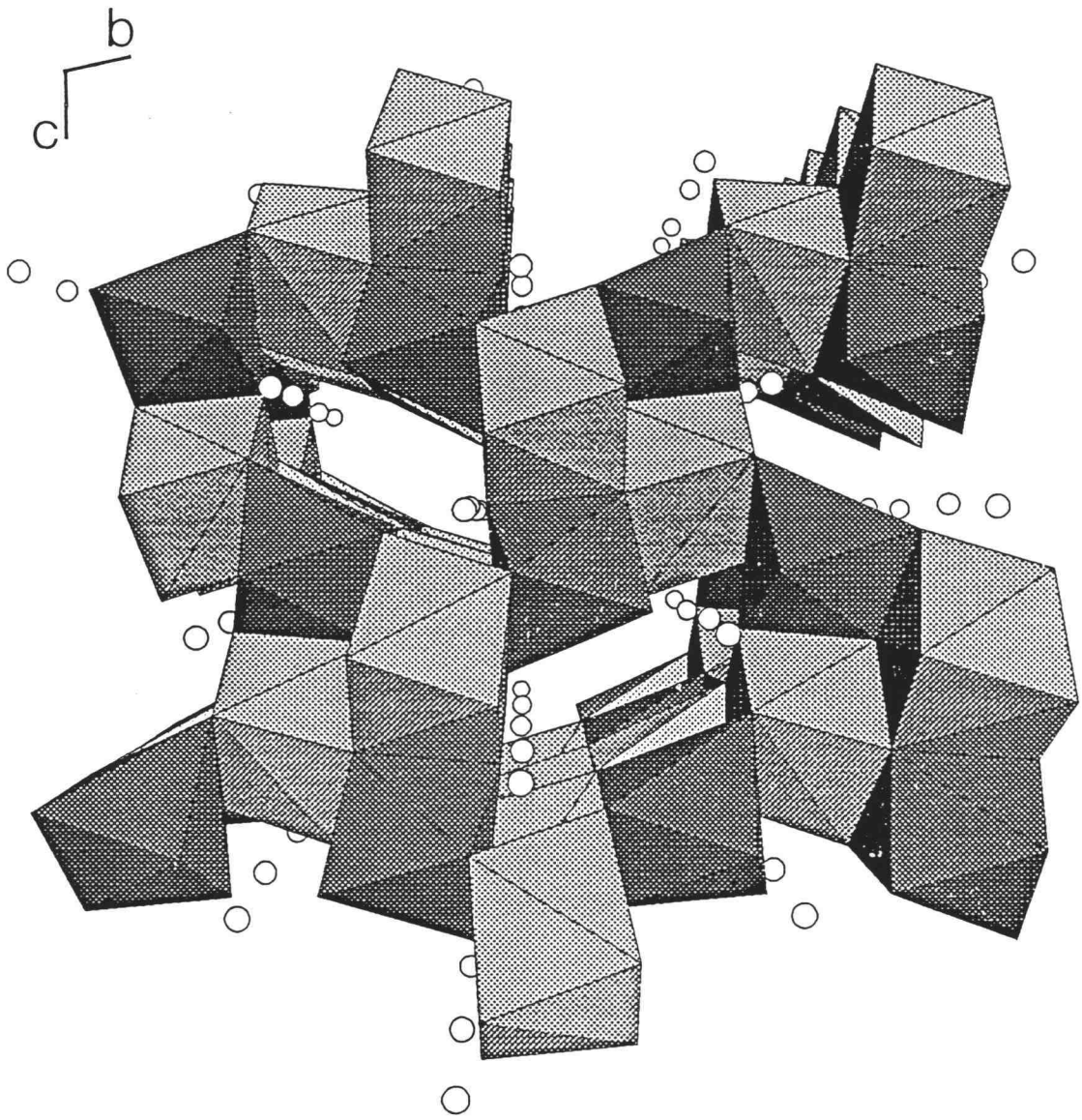

Figure 11.2. Framework resulting from condensation of Sr polyhedra. Small, open circles represent Ge atoms.

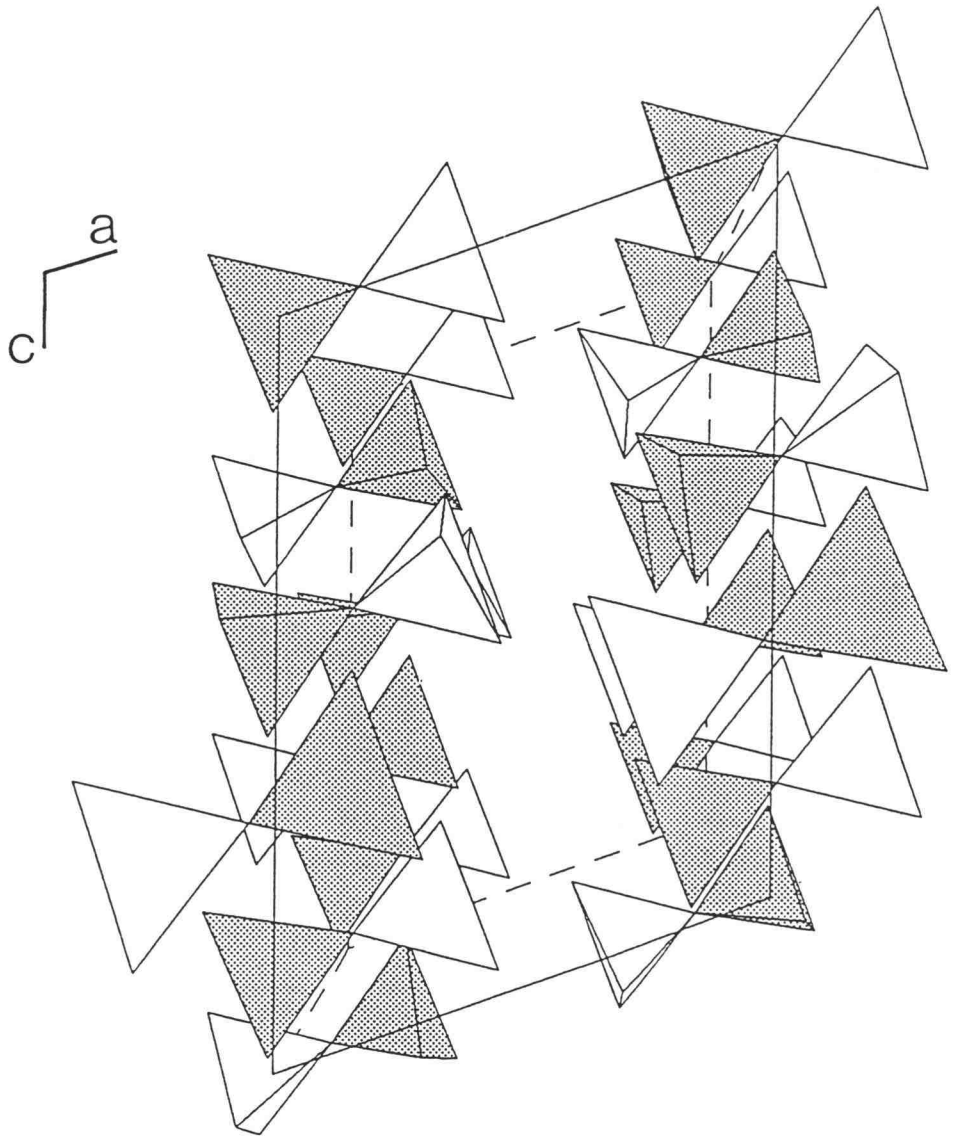

Figure 11.3. Polyhedral view along the [100] direction of the Ge-centered polyhedra. Shaded tetrahedra represent $Ge1O_4$ and light tetrahedra represent $Ge2O_4$.

TABLE 11.3. Interatomic Distances (Å) and Angles (°) for $Sr_4Ge_2O_7F_2$.

Sr1-O1	2.446(7)	O1-Sr1-O2	93.4(2)
-O2	2.441(8)	O1-Sr1-O3	75.7(2)
-O3	2.569(8)	O1-Sr1-O6	80.9(2)
-O6	2.562(7)	O1-Sr1-O7	165.2(2)
-O7	2.522(8)	O2-Sr1-O3	163.4(2)
-F2	2.498(6)	O2-Sr1-O6	76.0(2)
		O3-Sr1-O7	109.7(2)
		O6-Sr1-O7	108.3(2)
		F2-Sr1-O1	87.7(2)
		F2-Sr1-O2	85.62)
		F2-Sr1-O6	157.6(2)
		F2-Sr1-O7	79.7(2)
Sr2 -O2	2.546(7)	O2-Sr2-O3	61.6(2)
-O3	2.864(8)	O2-Sr2-O4	81.0(2)
-O4	2.474(8)	O2-Sr2-O6	76.7(2)
-O6	2.416(8)	O3-Sr2-O4	114.2(2)
-F1	2.476(6)	O3-Sr2-O6	122.2(2)
-F2	2.479(7)	F1-Sr2-F2	107.8(2)
-F2	2.506(6)	F1-Sr2-O2	113.3(2)
		F1-Sr2-O3	73.1(2)
		F1-Sr2-O4	75.9(2)
		F2-Sr2-F2	73.4(2)
		F2-Sr2-O2	105.7(2)
		F2-Sr2-O3	76.1(2)

TABLE 11.3. (continued)

		F2-Sr2-O4	169.6(2)
		F2-Sr2-O6	79.0(2)
Sr3 -O1	2.516(7)	O1-Sr3-O4	80.7(2)
-O4	2.753(8)	O1-Sr3-O5	102.7(2)
-O5	2.635(8)	O1--Sr3-O6	76.8(2)
-O6	2.709(7)	O1-Sr3-O7	62.7(2)
-O7	2.850(8)	O4-Sr3-O5	60.3(2)
-F1	2.510(6)	O4-Sr3-O6	108.0(2)
-F1	2.487(6)	O4-Sr3-O7	110.7(2)
-F2	2.495(7)	O5-Sr3-O6	60.0(2)
		O5-Sr3-O7	116.5(2)
		F1-Sr3-F1	72.1(2)
		F1-Sr3-F2	107.0(2)
		F1-Sr3-O1	112.0(5)
		F1-Sr3-O4	70.5(2)
		F1-Sr3-O5	112.5(2)
		F1-Sr3-O6	99.0(2)
		F2-Sr3-O1	105.9(2)
		F2-Sr3-O4	173.4(2)
		F2-Sr3-O5	116.6(2)
		F2-Sr3-O6	73.4(2)
		F2-Sr3-O7	73.6(2)

TABLE 11.3. (continued)

Sr4 -O1	2.664(7)	O1-Sr4-O2	113.1(2)
-O2	2.695(8)	O1-Sr4-O3	72.5(2)
-O3	2.539(8)	O1--Sr4-O4	83.4(2)
-O4	2.466(8)	O1-Sr4-O5	59.2(2)
-O5	2.742(8)	O4-Sr4-O7	105.5(2)
-O7	2.510(8)	O2-Sr4-O3	170.7(2)
-F1	2.459(6)	O2-Sr4-O4	78.2(2)
		O2-Sr4-O5	59.5(2)
		O2-Sr4-O7	73.7(2)
		O3-Sr4-O4	110.3(2)
		O3-Sr4-O5	121.6(3)
		O3-Sr4-O7	99.9(2)
		O4-Sr4-O5	99.5(2)
		O5-Sr4-O7	122.8(2)
		F1-Sr4-O1	92.5(2)
		F1-Sr4-O2	92.7(2)
		F1-Sr4-O3	79.4(2)
		F1-Sr4-O4	167.5(2)
		F1-Sr4-O5	72.4(2)
		F1-Sr4-O7	79.4(2)

TABLE 11.3. (continued)

			F1-Sr4-O7	79.4(2)
Ge1	-O2	1.728(8)	O2-Ge1-O3	108.0(4)
	-O3	1.712(8)	O2-Ge1-O4	118.5(4)
	-O4	1.727(7)	O2-Ge1-O5	99.7(3)
	-O5	1.799(8)	O3-Ge1-O4	117.9(4)
			O3-Ge1-O5	110.3(4)
			O4-Ge1-O5	100.3(4)
Ge2	-O1	1.727(7)	O1-Ge2-O5	100.1(3)
	-O5	1.759(8)	O1-Ge2-O6	117.2(3)
	-O6	1.722(7)	O1-Ge2-O7	108.5(3)
	-O7	1.730(8)	O5-Ge2-O6	100.4(4)
			O5-Ge2-O7	111.2(4)
			O6-Ge2-O7	117.6(4)

Sr2 share an edge (F2··F2) which are further bonded to Sr1 on both sides. Atom Sr3 shares and edge (O1··O7) with Ge2 and edges (O1··O6, F2··F1, F2··O6 and F1··O7) with Sr1, Sr2 and Sr4 atoms. Two adjacent Sr3 atoms are connected by Ge2-centered tetrahedron. The Sr4 atoms shares edges O5··O1 with Ge2, O1··O3 and O2··O7 with Sr1, O4··O1 and O7··F1 with Sr3. Two adjacent Sr4 polyhedra are isolated and bridged by the Ge_2O_7 group. The average Sr1-O distance is 2.51 ± 0.06 Å, which compares to the Sr-O distance of 2.53 for 6-coordinate Sr, obtained from the Shannon radii.[7] The average Sr2-O distance is 2.57 ± 0.19 Å, and the average Sr4-O distance is 2.60 ± 0.11 Å, which compare to the Sr-O distance of 2.64 ± 0.08 for a 7-coordinate Sr atom in $Sr_2ScLiB_4O_{10}$ and 2.59 Å obtained from crystal radii.[8] The average Sr3-O distance is 2.69 ± 0.12 Å, which compares well to a Sr-O distance of 2.67 ± 0.17, for 8-coordinate Sr atoms in $SrKB_5O_9$,[9] and 2.64 Å obtained from crystal radii. The average Sr1-F bond distance for Sr1 is 2.498(6), which compares well to 2.49 Å for a 6-coordinate Sr atom obtained from Shannon radii. The average Sr-F distance for Sr2 is 2.487 ± 0.016 Å, and the average Sr-F distance for Sr4 is 2.459 ± 0.006, which compares well to 2.52 Å for a 7-coordinate Sr atom obtained from the Shannon radii. The average Sr-F distance for Sr3 is 2.49 ± 0.011 Å, and compares well to 2.57 Å for an eight coordinate Sr atom obtained from Shannon radii.

The Ge1 atom is connected to one each of atoms O2, O3, O4, and O5 and the Ge2 atom is bonded to one each of atoms O1, O5, O6, and O7 atoms to form slightly distorted tetrahedra. The Ge1-centered tetrahedra are isolated from each other. instead they connect to the Ge2-centered tetrahedra through an O5 atom to form vertex-sharing dimers Ge_2O_7 (Figure 11.3). The average Ge1-O bond distance is 1.741 ± 0.039 Å, and the average Ge2-O bond distance is 1.734 ± 0.0167 Å; each compares to the Ge-O distance of 1.79 Å for $SrGeO_3$.[10] All O-Ge-O angles are near the tetrahedral value, except the Ge1-O5-Ge2 is 151.6(4). The Ge1-O5-Ge2 angle indicates that the Ge1- and Ge2-centered tetrahedra are in an approximately eclipsed conformation with respect to each other.

The bond-valence method[11-12] was used to calculate the valences of all the atoms in the structure. The fluorine atoms both have a valence within 10 % of standard integral values, indicating that they have been correctly identified in the structure analysis. All the other atoms have calculated valences within 5 % of standard integral values, except for atoms O3 and O7 where valences of 1.8, indicate lack of bonding electron density, and atoms O5 and Ge2 where valences of 2.3 and 4.2 , indicate excess of bonding electron density.

Eu^{3+} Luminescence

Luminescence of the Eu^{3+} ion in a crystalline material is generally associated with transitions from the excited state $^5D_0$ to ground-state levels of the ^7F_J manifold. In general, the more intense emission features are associated with the $^5D_0 \rightarrow {}^7F_1$ transition near 5900 Å (orange) and $^5D_0 \rightarrow {}^7F_2$ transition near 6200 Å (red). The transitions of the type $^5D_0 \rightarrow {}^7F_2$, $^7F_4$, $^7F_6$ follow electric-dipole selection rules while transitions of the type $^5D_0 \rightarrow {}^7F_0$, $^7F_3$, $^7F_5$ follow magnetic-dipole selection rules. If the Eu^{3+} ion occupies a site lacking a center of symmetry, the electric-dipole transitions are expected to predominate, and as noted above, the strongest of these is usually the J = 0 → 2 transition. In the spectrum of $Eu_{0.02}K_{0.02}Sr_{3.96}Ge_2O_7F_2$ (Figure 11.4), however, we observe the most intense peak corresponding to the J = 0 → 4 transition near 7000 Å. This result is, at least, consistent with the lack of a center of symmetry at any of the Sr dopant sites.

Studies are ongoing to more fully characterize the optical characteristics of Eu^{3+} and other ions in this host.

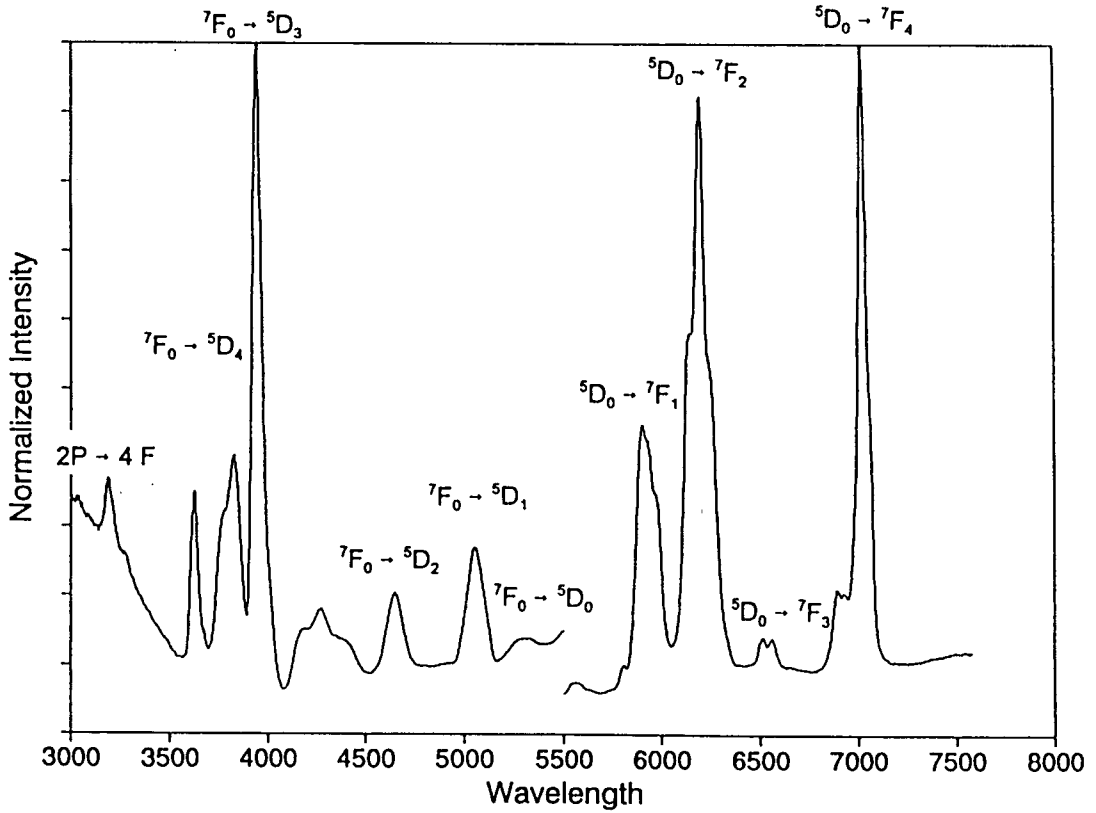

Figure 11.4. Emission and excitation spectra of the luminescence of $Eu_{0.02}K_{0.02}Sr_{3.96}Ge_2O_7F_2$ at 298 K (λ_{exc} = 3940 Å for emission and λ_{em} = 7000 Å for excitation).

Acknowledgments

This research was supported by National Science Foundation (DMR92-21372). Acknowledgment is made to the Donors of The Petroleum Research Fund, administered by the American Chemical Society, for partial support of the work.

References

1. Siverman, S. M.; Balmer, M. K. *J. Am. Ceram. Soc.* **1971**, *54*, 98.

2. Burrus, H. L.; Nicholson, K. P.; Rooksby, H. P. *J. Lumin.* **1971**, *3*, 467.

3. Wanmaker, W. L.; Verriet, J. G. *Philips Res. Rep.* **1973**, *28*, 80.

4. TEXSAN: Single Crystal Structure Analysis Software, Version 5.0 **1989**. Molecular Structure Corp., The Woodlands, TX, 77381.

5. Sheldrick, G. SHELXS86. In *Crystallographic Computing 3*; Sheldrick, G.; Kruger,C.; Goddard, R.; Eds.; Oxford University Press: New York, 1985; pp 175-189.

6. Walker, N.; Stuart, D. *Acta Crystallgr., Sect. A* **1983**, *39*, 158.

7. Shannon, R. D. *Acta Crystallogr., Sect. A* **1976**, *32*, 751.

8. Thompson, P. D., Keszler, D. A. *Solid State Ionics* **1989**, *32/33*, 521.

9. Tu, J., Keszler, D. A. unpublished results.

10. Nadezhina, T. N., Pobedimskaya, E. A., Ilyukhin, V.V., Belov, N. V. *Sov. Phys. Crystallogr.* **1981**, *26*, 168.

11. Schlager, M., Hoppe, R. *Z. Anorg. Allg. Chem.* **1993**, *619*, 976.

12. O'Keefe, M., Hansen, S. *J. Am. Chem. Soc.* **1988**, *110*, 1506.

CHAPTER 12
Sr_2LiSiO_4F : Synthesis, Structure, and Eu^{2+} Luminescence

Annapoorna Akella and Douglas A. Keszler

Department of Chemistry and

Center for Advanced Materials Research

Oregon State University, Gilbert Hall 153

Corvallis, Oregon 97331-4003

Submitted to *Chemistry of Materials*

Abstract

The structure and Eu^{2+} luminescence of the compound Sr_2LiSiO_4F are described. Crystal data: FW = 293.26, $P2_1/m$ (#11), monoclinic, a = 6.5825(9), b = 5.4158(8), c = 6.9266(6) Å, β = 112.525(8)°, V = 228.09(5) $Å^3$, Z = 2, R = 0.049, R_w = 0.058 for 760 averaged reflections. The structure contains two crystallographically distinct Sr atoms, both are 10 -coordinate and bound by eight O atoms and two F atoms. The Li atom occupies a distorted square pyramid and the Si atom a slightly distorted tetrahedron. When doped with the lanthanide ion Eu^{2+}, the compound exhibits a bright green emission with a maximum intensity at 531 nm.

Introduction

Inorganic oxoanion halides have for some time been of technological use and interest as fluorescent lamp phosphors,[1] laser hosts,[2] and X-ray storage media.[3] Despite this utility, synthetic examples of such materials remain rather uncommon. In this contribution we describe the preparation and structure of the new compound Sr_2LiSiO_4F. It is to our knowledge the first synthetic example of an alkaline-earth silicate fluoride to be structurally characterized by single-crystal X-ray methods.

We have been attracted to the synthesis of oxoanion halides, in general, by the possibility of observing unusual optical properties as well as moderately low, congruent melting points. The latter feature, of course, is desirable for the growth of large single crystals. Below we present data on an uncommon green Eu^{2+} luminescence from the title compound and its melting characteristics.

Experimental

A powder sample of Sr_2LiSiO_4F was prepared from the molar quantities of 2 $SrCO_3$ (AESAR, 99.9%), 1 SiO_2 (ALFA, 99.98%), and 1 LiF (AESAR, 99.9%). The mixture of carbonate and SiO_2 was heated at 873 K for 1 h; then the fluoride was added and the sample was reground and heated in a Pt crucible at 1273 K for 12 h under an Ar atmosphere. A crystal was obtained for X-ray structure analysis from a stoichiometric melt. The melt was contained in

a Pt crucible and slowly cooled from 1223 to 873K at 6 K/h, and then rapidly cooled at 50 K/h to room temperature. A colorless, transparent crystal of dimensions 0.10 × 0.12 × 0.10 mm was selected and mounted on a glass fiber with epoxy for structure determination. All measurements were made on a Rigaku AFC6R diffractometer with graphite-monochromated Mo Kα radiation. Cell constants and the orientation matrix for data collection were obtained from a least squares refinement with 19 automatically-centered reflections in the range $30 \leq 2\theta \leq 36°$. The cell constants correspond to a monoclinic cell; Laue symmetry 2/m was determined on the diffractometer. Intensity data were collected over the range of indices $0 \leq h \leq 10$, $0 \leq k \leq 8$, $-11 \leq l \leq 11$ by using the ω scan technique to a maximum 2θ value of 70°; from 1070 measured reflections a total of 760 were observed [$F_o^2 \geq 3\sigma F^2$]. The intensities of three representative reflections measured after every block of 200 data varied by an average of 2% during the collection.

The structure was solved by using the *TEXSAN* software package.[4] The crystal was found to form in the centerosymmetric space group $P2_1/m$. The positions of the Sr and Si atoms were derived from the direct methods program SHELXS,[5] while the remaining atoms F, O, and Li were located from difference electron density maps. After a full-matrix least-squares refinement of the model with isotropic displacement coefficients on each atom, an absorption correction was applied by using the program DIFABS (transmission factors = 0.51 -1.29).[6]

The data were averaged (R_{int} = 0.066), and the model was refined with anisotropic displacement coefficients on each atom. Final least squares refinement resulted in the residuals R = 0.049 and R_w = 0.058. The largest peak in the final difference electron density map corresponds to 0.38% of the Sr1 atom. Crystal data are outlined in Table 12.1; atomic parameters are listed in Table 12.2.

The luminescence measurement was performed on a powder sample nominally doped with 2 mole% Eu^{2+}. The preparative procedure was that described above [Eu_2O_3 (99.99%, MOLYCORP)], except for the final heating where the sample was placed in an atmosphere of 25 N_2:1 H_2. Steady-state, room-temperature luminescence spectra were obtained on a computer-controlled right angle spectrometer. Excitation light from an Oriel 300-W Xe lamp was passed through a 50-cm water filter, focused initially onto the slits of a Cary model-15 prism monochromator, and then onto the sample. Luminescence was collected at a near right angle to excitation, dispersed through an Oriel 22500 1/8-m monochromator, and detected with a Hamamatsu R636 photomultiplier tube. The signal was collected and amplified with a Keithley model 602 picoammeter and then converted to a digital signal for computer acquisition. Spectrometer control and data acquisition were achieved with computer programs written in this laboratory.

The excitation spectrum was corrected by using rhodamine B as a quantum counter. The emission spectrum was corrected with a tungsten lamp that has been calibrated at Eppley Laboratories, Inc.

TABLE 12.1. Crystallographic Data for Sr_2LiSiO_4F

chem formula	Sr_2LiSiO_4F
fw, u	293.26
crystal system	Monoclinic
space group	$P2_1/m$ (#11)
a, Å	6.5825(9)
b, Å	5.4158(8)
c, Å	6.9266(6)
V, $Å^3$	228.09(5)
β, °	112.525(8)
Z	2
ρ_{calc}, g cm^{-3}	4.270
radiation	Mo Kα[a]
temp, K	298
linear abs. coeff μ, cm^{-1}	228.82
transm. factors	0.51 -1.29
R, R_w[b]	0.049, 0.058

[a] Graphite monochromated; λ = 0.71069 Å. [b] $R = \Sigma \, | \, |F_o| - |F_c| \, | \, / \, \Sigma \, |F_o|$; $R_w = [\, \Sigma w (\, |F_o| - |F_c| \,)^2 / \Sigma \, w \, |F_o|^2 \,]^{1/2}$.

TABLE 12.2. Positional and Equivalent Displacement Parameters (B_{eq}) for Sr_2LiSiO_4F.

	site symmetry	x	y	z	B_{eq}
Sr1	m	0.1597(2)	1/4	0.3722(1)	0.50(3)
Sr2	m	0.6342(2)	1/4	0.8985(1)	0.57(3)
Si	m	0.6547(5)	1/4	0.3351(4)	0.29(8)
F	$\bar{1}$	0	0	0	1.0(2)
O1	m	0.405(1)	1/4	0.158(1)	0.7(2)
O2		0.2252(8)	-0.009(1)	0.7117(8)	0.9(2)
O3	m	0.665(1)	1/4	0.572(1)	1.2(3)
Li	m	0.141(3)	1/4	-0.125(3)	1.1(7)

Results and Discussion

A view of the contents of the unit cell is given in Figure 12.1. The structure contains two types of 10-coordinate Sr atoms, a 5-coordinate Li atom, and a 4-coordinate Si atom. The Sr-centered polyhedra share faces and vertices to form a three-dimensional framework that contains distorted square pyrimidal and tetrahedral interstices occupied by the Li and Si atoms, respectively (Figure 12.2). The Li - and Si - centered polyhedra share vertices to form a thick, two-dimensional substructure that extends parallel to the plane (100). As indicated by the formula, the SiO_4 groups are isolated one from the other, while the Li-centered square pyramids are linked through the F atoms (Figure 12.3). Atom Sr1 is bound by one O1, four O2, three O3, and two F atoms in an environment that is best described as a distorted bicapped square antiprism. Atom Sr2 is bound by three O1, four O2, one O3, and two F atoms in an environment that is best described as a distorted bicapped dodecahedron. The uniqueness of each of these polyhedra may be appreciated by considering their associations with the other metal atoms in the structure. Both are surrounded by four Si atoms, but the Sr1-centered site shares only edges O2··O2, O1··O3, and O2··O3 (×2), while the Sr2-centered polyhedron shares vertex O3, edge O1··O2(×2), and face O1··O2··O2. Similarly, both polyhedra share O and F atoms with four adjacent Li atoms, but

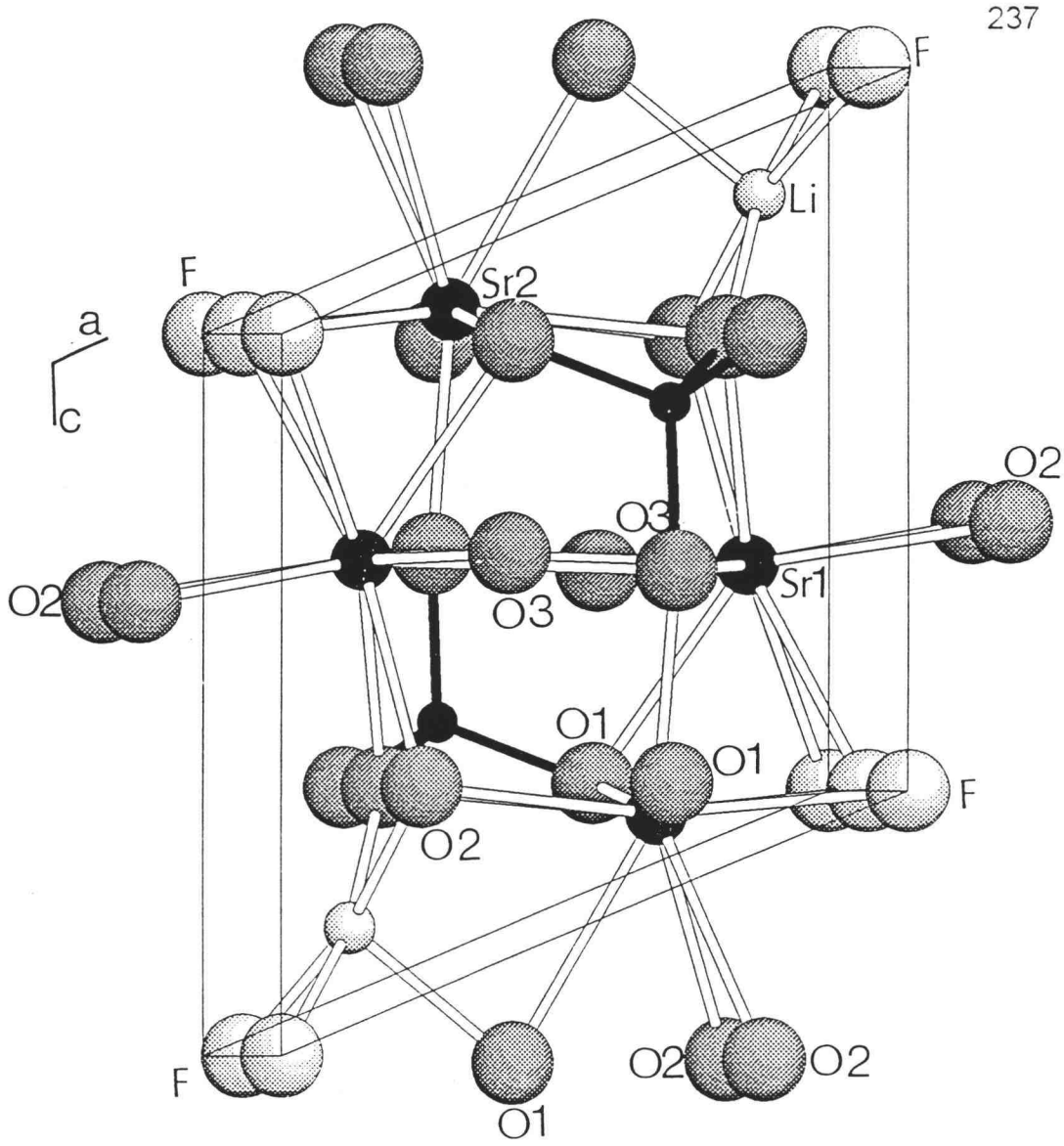

Figure 12.1. Unit cell diagram of Sr_2LiSiO_4F as viewed along the *b* axis. Here, and in ensuing figures, large circles represent O and F atoms; O atoms are more heavily shaded. Large filled circles represent Sr atoms, and small filled circles represent Si atoms. Medium, lightly shaded circles represent Li atoms.

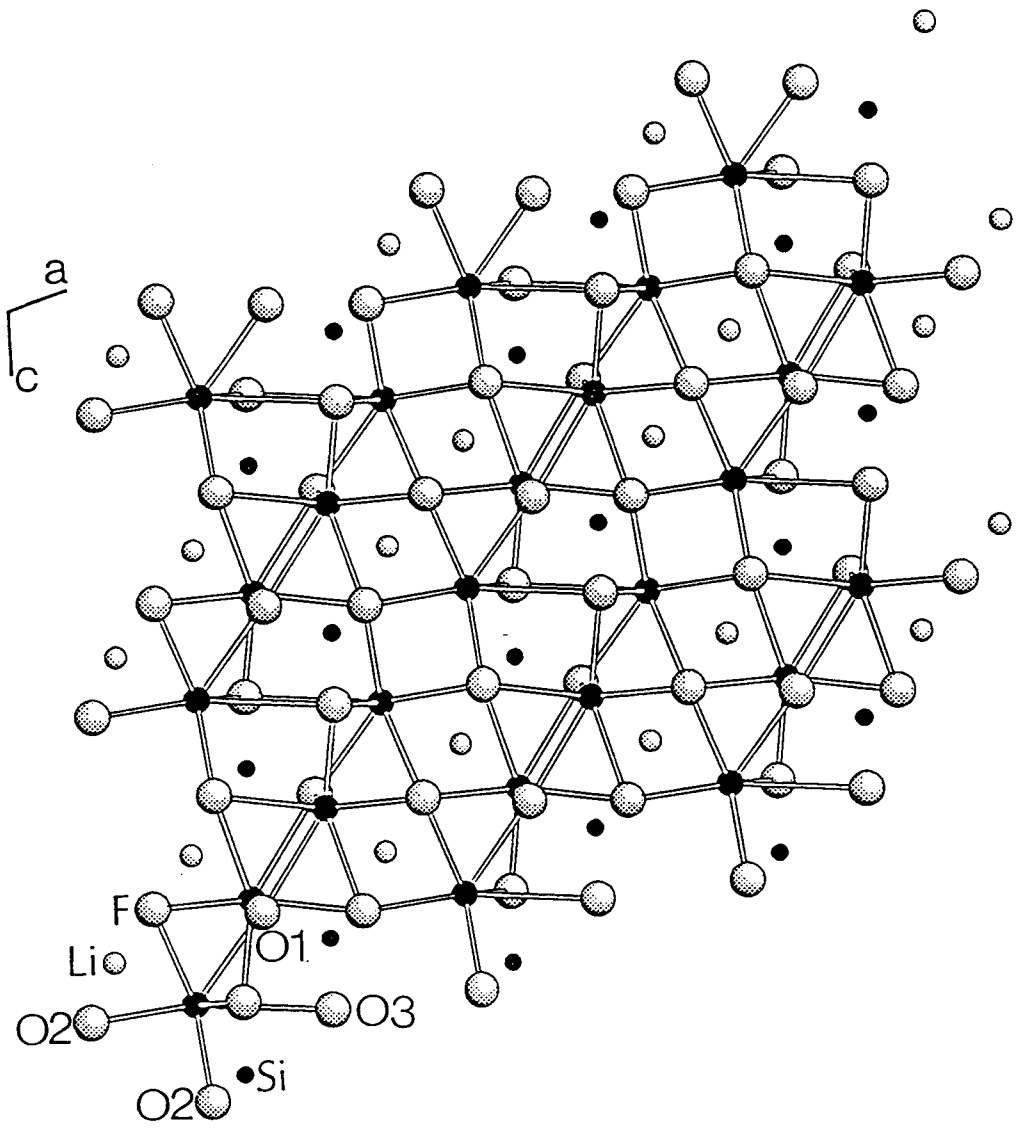

Figure 12.2. Framework resulting from condensation of Sr polyhedra.

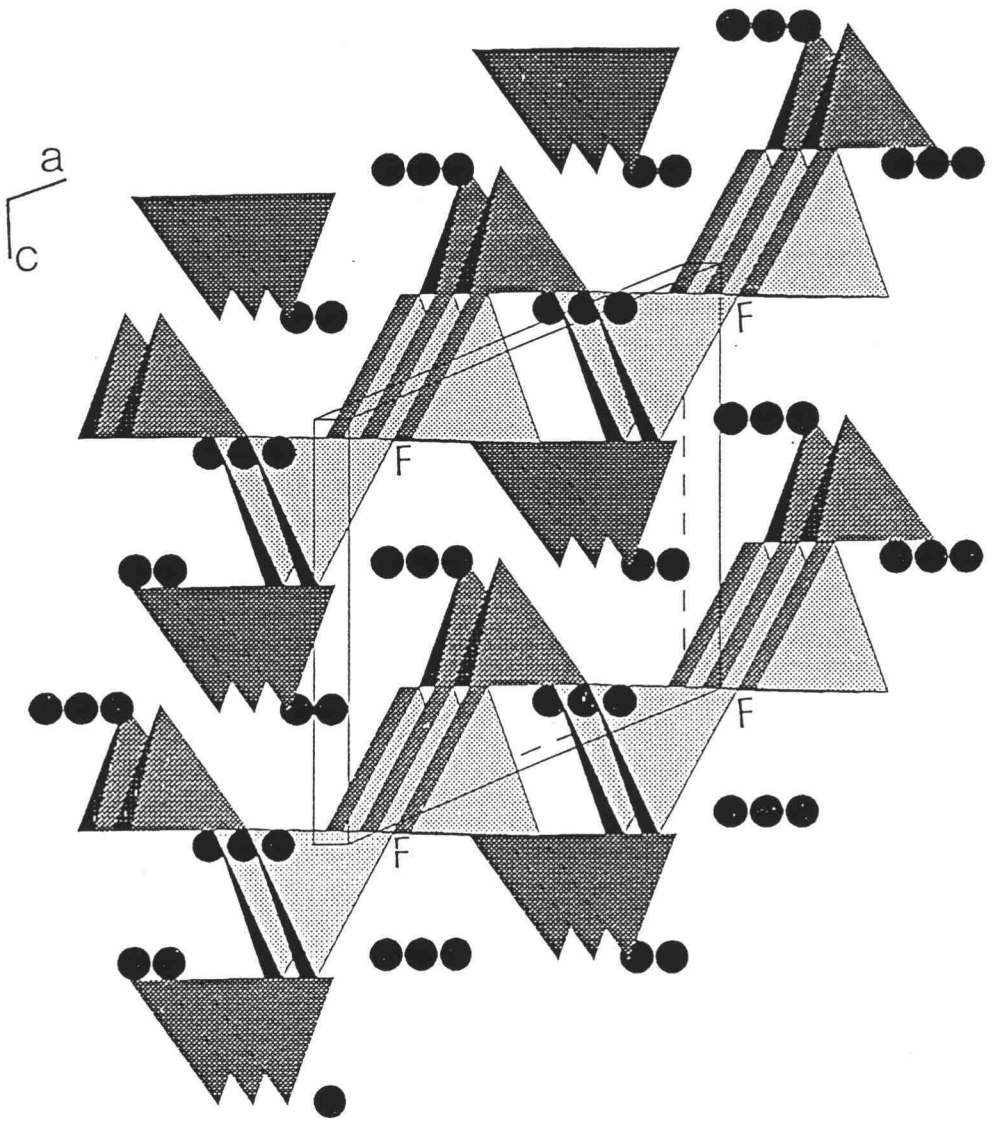

Figure 12.3. Polyhedral view of Si- and Li-centered polyhedra. Heavily shaded polyhedra represent SiO_4 groups and lightly shaded polyhedra represent LiO_3F_2 groups.in a different manner.

The Sr1 -centered site shares edges O2··O2 and O2··F(×2) and the face F··F··O1, and the Sr2 -centered site shares edge F··F and faces O1··O2··F(×2) and O2··O2··O1. The Sr1 environment is bound by 17 neighboring Sr atoms - 8 Sr1 and 9 Sr2 - while the Sr2 environment is bound by 15 Sr atoms - 9 Sr1 and 6 Sr2. The details of the connectivities of these polyhedra through vertices, triangular faces, and quadrilateral faces are summarized in Table 12.3.

Interatomic distances and angles are listed in Table 12.4. The average Sr1-O, 2.77 ± 0.18 Å, and Sr2-O distances, 2.74 ± 0.17 Å, compare to Sr-O distances of 2.711 ± 0.05 Å and 2.859 ± 0.07 Å for 10-coordinate Sr atoms in α'-Sr_2SiO_4.[7] The Sr-F bond distances for Sr1, 2.7404(8), and Sr2, 2.6132(9) Å, compare to the value of 2.67 Å obtained from Shannon radii.[8]

The Li atom is coordinated to one O1, two F, and two O2 atoms. The rectangular base of the pyramid is comprised of the F and O2 atoms, and the apex is represented by atom O1. A displacement of the Li atom above the plane of the base toward the apex is indicated by the angle F-Li-O2 = 169.4(9)°. The average Li-O distance, 2.03 ± 0.03 Å, compares to the Li-O distances for 5-coordinate Li atoms in $SrLiBO_3$,[9] 2.06 ± 0.10 Å, and $BaLiBO_3$,[10] 2.05 ± 0.11 Å.

Table 12.3. Shared polyhedral vertices and faces for Sr-and Sr2-centered polyhedra.

centered polyhedron	shared vertex or face	bound atom
Sr1	F (×2)	Sr1
	O3 (×2)	
	O2··O3 (×2)	
	O3··O3 (×2)	
Sr2	O1	Sr1
(Sr1)	O2 (×4)	(Sr2)
	O1··O3··F (×2)	
	O2··O2··O3	
	O2··O2··F··F	
Sr2	O1 (×2)	Sr2
	F (×2)	
	O1··O2··O2··F	
	O1··O2··O1··O2	

TABLE 12.4. Selected Interatomic Distances (Å) and Angles (°) for Sr_2LiSiO_4F.

Sr1-O1	2.575(9)	O1-Sr1-O2	126.2(2)
-O2 × 2	2.627(5)		128.1(2)
-O2 × 2	2.708(5)	O1-Sr1-O3	76.7(2)
-O3 × 2	2.912(3)		56.7(2)
-O3 × 1	3.071(8)	O2-Sr1-O3	57.6(2)
-F × 2	2.7404(8)		117.2(2)
			149.1(2)
			82.6(2)
			140.2(2)
		F-Sr1-O1	63.7(1)
		F-Sr1-O2	116.7(1)
			167.9(1)
			92.6(1)
			64.5(1)
			112.5(1)
		O2-Sr1-O2	64.5(2)
			105.58(9)
			75.7(1)
		O3-Sr1-O3	68.5(1)
			136.8(3)
		F-Sr1-F	59.21(2)
Sr2-O1 × 2	2.734(1)	O1-Sr2-O2	125.1(2)
-O1 × 1	2.756(9)		69.9(2)
-O2 × 2	2.817(5)		113.5(2)

Table 12.4. (continued)

-O2 × 2	2.866(5)		55.3(2)
-O3 × 1	2.343(9)	O1-Sr2-O3	84.2(2)
Sr2-F × 2	2.6132(9)	O1-Sr2-O3	86.9(4)
			69.9(2)
		F-Sr2-O1	125.3(2)
			120.2(1)
		F-Sr2-O2	92.9(2)
			169.7(1)
		F-Sr2-O3	81.3(2)
		O1-Sr2-O1	164.1(3)
			92.8(2)
		O2-Sr2-O2	124.47(8)
			96.5(1)
		F-Sr2-F	62.41(2)
Si-O1	1.631(7)	O1-Si-O2	106.2(3)
-O2 ×2	1.621(6)	O1-Si-O3	113.5(5)
-O3	1.619(9)	O2-Si-O2	107.2(5)
		O2-Si-O3	111.7(3)
Li-O1	2.06(2)	O1-Li-O2	102.7(7)
-O2 ×2	2.01(2)	F-Li-O1	87.2(7)
-F ×2	2.01(2)	F-Li-O2	92.5(2)
			169.4(9)
		O2-Li-O2	88.4(8)
		F-Li-F	84.6(9)

The Si atom binds to one O1, one O3, and two O2 atoms. The average Si-O distance, 1.623 ± 0.005 Å, is normal, and all O-Si-O angles are near the tetrahedral value.

The bond valence method[11-12] was used to calculate a valence of 1.0 for the F atom; it appears that this atom has been correctly identified in the structure analysis. All other atoms have calculated valences within 3% of standard integral values, except for atoms Sr1 and O3 where valences of 1.8 and 1.9, respectively, indicate a lack of bonding electron density.

From quenching experiments, we have found that the compound completely melts at 940° C. Prior to melting the compound undergoes a phase change at 900° C.

The composition $Sr_{1.98}Eu_{0.02}LiSiO_4F$ exhibits an intense green emission under ultraviolet excitation (Figure 12.4). Excitation and emission maxima occur at 348 and 531 nm, respectively. The position of the excitation band is similar to those observed for many blue emitting Eu^{2+} phosphors, and it is consistent with the weak crystal field to be expected for a 10-coordinate silicate fluoride site. The broad emission peak is attributable to the allowed transition $4f^6 5d^1 \rightarrow 4f^7$. Obviously, the long wavelength emission results from a sizable Stokes shift rather than a low-energy position of the excited state. This large shift may be related to the rather anisotropic O, F environment of the dopant sites. The room temperature spectrum provides little information concerning

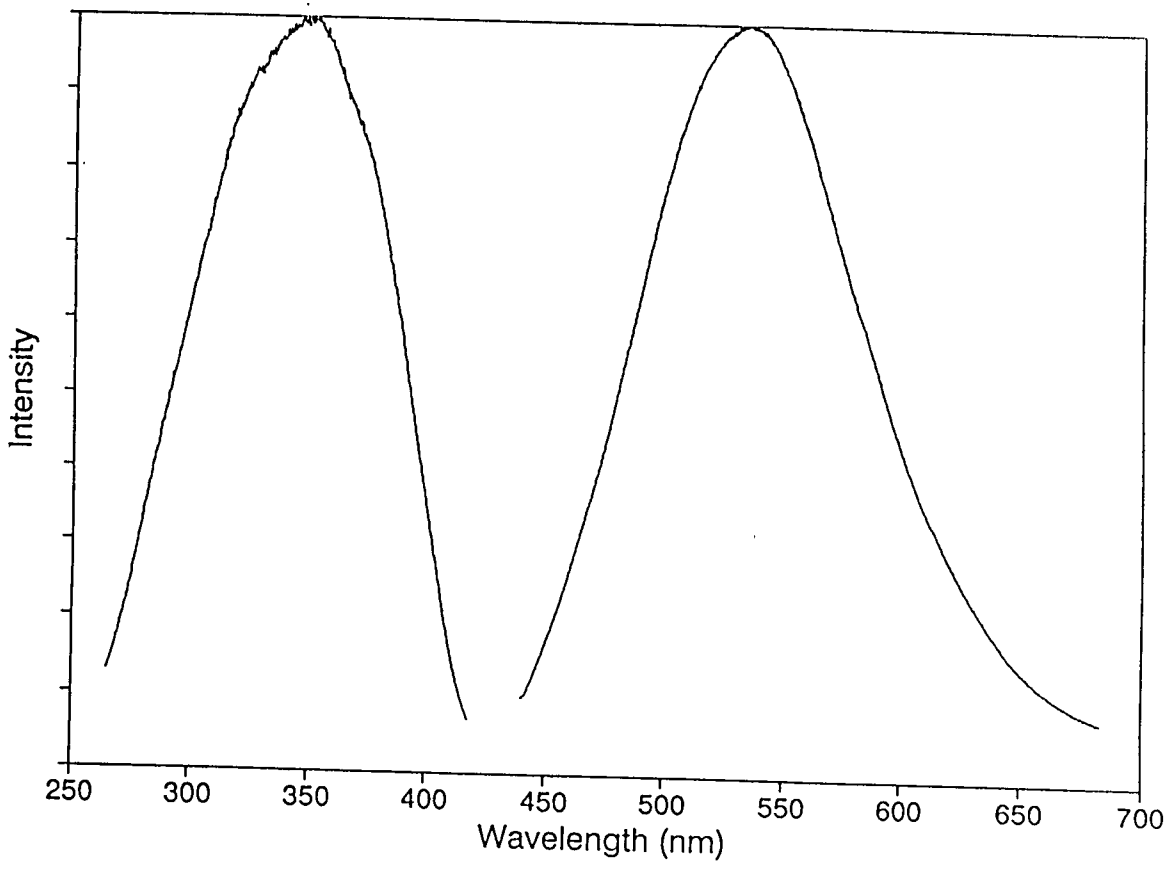

Figure 12.4. Emission and excitation spectra of the luminescence of $Sr_{1.98}Eu_{0.02}LiSiO_4F$ at 298 K. λ_{exc} = 348 nm for emission and λ_{em} = 531 nm for excitation.

the distribution of Eu^{2+} ions over the two nonequivalent Sr dopant sites. While the sites are structurally distinct, they are likely to be electronically comparable. Similar Eu^{2+} excitation and emission characteristics may be expected from each site, leading to the symmetric peaks observed in the spectrum (Figure 4). Of course the presence of a single, luminescent center cannot be excluded. Wanmaker and Verriet[3] have reported similar behavior for Eu^{2+}: $Ca_3SiO_4Cl_2$ which emits at 510 nm,[3] and Nicholson and Burrus have also reported[2] 500-nm emission from the formulation Eu^{2+}: $Sr_2Si_3O_8Cl_4$.

Work is ongoing to more fully characterize the phase change and luminescence properties asociated with this new host.

Acknowledgments

This research was supported by the National Science Foundation (DMR92-21372). Acknowledgment is also made to the Donors of The Petroleum Research Fund, administered by the American Chemical Society, for partial support of the work.

References

1. Siverman, S. M., Balmer, M. K. *J. Am. Ceram. Soc.* **1971**, *54*, 98.

2. Burrus, H. L., Nicholson, K. P., Rooksby, H. P. *J. Lumin.* **1971**, *3*, 467.

3. Wanmaker, W. L.; Verriet, J. G. *Philips Res. Rep.* **1973**, *28*, 80.

4. TEXSAN: Single Crystal Structure Analysis Software, Version 5.0 **1989,** Molecular Structure Corp., The Woodlands, TX, 77381.

5. Sheldrick, G. SHELXS86. In *Crystallographic Computing 3*; Sheldrick, G.; Kruger,C., Goddard, R., Eds.; Oxford University Press: New York, 1985; pp 175.

6. Walker, N., Stuart, D. *Acta Crystallgr., Sect. A* **1983**, *39*, 158.

7 Catti, M., Gazzoni, G., Ivaldi, G., Zanini, G. *Acta Crystallogr., Sect B* **1983**, *39*, 674.

8. Shannon, R. D. *Acta Crystallogr., Sect. A* **1976**, *32*, 751.

9. Tu, J.; Keszler, D. A. unpublished results.

10. Schlager, M., Hoppe, R. *Z. Anorg. Allg. Chem.* **1993**, *619*, 976.

11. Brown, I. D., Altermatt, D. *Acta Crystallogr., Sect B* **1985**, *41*, 244.

12. O'Keefe, M., Hansen, S. *J. Am. Chem. Soc.* **1988**, *110*, 1506.

CHAPTER 13
Structure and Eu^{2+} Luminescence of $Li_4SrCa(SiO_4)_2$

Annapoorna Akella and Douglas A. Keszler

Department of Chemistry and Center for

Advanced Materials Research

Oregon State University

Gilbert Hall 153

Corvallis, Oregon 97331-4003

In preparation for submission to *Inorganic Chemistry*

Abstract

The structure and Eu^{2+} luminescence of the compound $Li_4SrCa(SiO_4)_2$ is described. Crystal data: FW = 339.63, P bca (#57), orthorhombic, a = 4.983(2), b = 9.930(2), c = 14.057(2) Å, V = 695.5(4) $Å^3$, Z = 4, R = 0.056, R_w = 0.063 for 996 averaged reflections. The structure contains layers consisting of corner shared Li- centered polyhedra connected by Si-centered tetrahedra with Sr atoms lying between them. There are one crystallographically distinct Sr and Ca atoms, which are 10 -and 6- coordinate. The rare earth ion Eu^{2+} when doped in $Li_4SrCa(SiO_4)_2$ exhibits an intense blue emission with an emission maximum at 430 nm.

Introduction

Inorganic silicates such as Mn^{2+}:Zn_2SiO_4 and Tb^{3+}:Y_2SiO_5 have been used technologically as green emitting phosphors in projection television tubes.[1-2] The ultraviolet emission from Eu(II) phosphors has several applications, e.g., in insect traps, photocopy machines, and for promoting tanning of the skin.

The Eu(II) ion has been useful in providing efficient absorption and emission in several structures, mostly based on Sr compounds. The ionic radii of Sr(II) and Eu(II) are 0.113 and 0.117 nm, respectively, and therefore substitution of Eu(II) in Sr compounds readily occurs. One commercially important Eu(II)-activated phosphor is $Sr_5(PO_4)_3Cl$:Eu(II), a strontium chlorapatite, and its maximum emission occurs at 450 nm. Other efficient phosphors include $Sr_2P_2O_7$:Eu(II) (415 nm) and $Ba_2MgSi_2O_7$:Eu(II) (510) nm. In this contribution we describe the structure of the new compound, $Li_4SrCa(SiO_4)_2$, structurally characterized by single-crystal X-ray methods. We also present data on the intense blue Eu^{2+} luminescence from this host that has an emission wavelength maximum at 437 nm.

Experimental Section

Synthesis

A powder sample of $Li_4SrCa(SiO_4)_2$ was prepared from the molar quantities of 2 Li_2CO_3 (AESAR, 99.9%), 1 $SrCO_3$ (AESAR, 99.9%), 1 $CaCO_3$ (AESAR, 99.9%), and 2 SiO_2 (ALFA, 99.98%). The mixture of carbonates and SiO_2 were heated at 873 K for 1 h; then the sample was reground and heated at 1273 K for 12 h. A crystal was obtained for X-ray structure analysis from a stoichiometric melt that was slowly cooled in a Pt crucible from 1280 K to 773 K at 6 K/h, and then rapidly at 50 K/h to room temperature.

Crystallographic Study

A colorless, transparent crystal of dimensions 0.12 × 0.12 × 0.15 mm was selected and mounted on a glass fiber with epoxy for structure determination. All measurements were made on a Rigaku AFC6R diffractometer with graphite-monochromated Mo Kα radiation. Cell constants and the orientation matrix for data collection were obtained from a least squares refinement with 19 automatically-centered reflections in the range $30 \leq 2\theta \leq 36°$. The cell constants correspond to an orthorhombic cell; Laue symmetry mmm was determined on the diffractometer. Intensity data were collected over the range of indices $0 \leq h \leq 16$, $0 \leq k \leq 23$, $-8 \leq l \leq 8$ by using the ω scan technique to a maximum 2θ value of 73°, and from 3686 measured

reflections a total of 996 were observed [$F_o^2 \geq 3\sigma F^2$]. The intensities of three representative reflections measured after every block of 200 data varied by an average of 2% during the collection.

The structure was solved by using the *TEXSAN* software package.[3] The crystal was found to form in the centerosymmetric space group P bca. The positions of the Sr, Ca and Si atoms were derived from the direct methods program SHELXS,[4] while the remaining atoms O and B were located from difference electron density maps. After a full-matrix least-squares refinement of the model with isotropic displacement coefficients on each atom, an absorption correction was applied by using the program DIFABS[5] (transmission factors = 0.87 -1.11). The data were averaged (R_{int} = 0.10), and the model was refined with anisotropic displacement coefficients on each atom. Final least squares refinement resulted in the residuals R = 0.049 and R_w = 0.058. The largest peak in the final difference electron density map corresponds to 0.59% of the Sr atom. Crystal data are outlined in Table 13.1.; atomic positional and thermal parameters are listed in Table 13.2.

A luminescence measurement was performed on a powder sample nominally doped with 2 mole% Eu^{2+}. The preparative procedure was that described above [Eu_2O_3 (99.99%, MOLYCORP)], except the final heating was done in an atmosphere of 25 N_2 :1 H_2. Steady-state, room temperature luminescence spectra were obtained on a computer-controlled right angle

spectrometer. Excitation provided by an Oriel 300-W Xe lamp was passed through a 50-cm water filter and focused onto the slits of a Cary model-15 prism monochromator. Excitation was focused onto the sample, and luminescence was collected at a near-right angle to excitation, dispersed through an Oriel 22500 1/8-m monochromator, and detected with a Hamamatsu R636 photomultiplier tube. The signal was collected and amplified with a Keithley model 602 picoammeter and then converted to a digital signal for computer acquisition. Spectrometer control and data acquisition were achieved with computer programs written in this laboratory. The excitation spectrum was corrected by using rhodamine B as a quantum counter. The emission spectrum was corrected with a tungsten lamp that has been calibrated at Eppley Laboratories, Inc.

Table 13.1. Crystallographic Data for $Li_4SrCa(SiO_4)_2$.

chem formula	$Li_4SrCa(SiO_4)_2$
fw, u	339.63
crystal system	Orthorhombic
space group	P b c a(No. 57)
a, Å	4.983(1)
b, Å	9.930(2)
c, Å	14.057(2)
V, $Å^3$	695.5 (4)
Z	4
ρ_{calc}, g cm^{-3}	3.377
radiation	Mo Kα[a]
temp, K	298
linear abs.coeff μ, cm^{-1}	85.89
transm.factors	0.87 -1.11
R, R_w[b]	0.056, 0.063

[a] Graphite monochromated; λ = 0.71069 Å. [b] $R = \Sigma \, | \, |F_o| - |F_c| \, | \, / \, \Sigma \, |F_o|$;

$R_w = [\, \Sigma w \, (|F_o|^2 - |F_c|^2)^2 \, / \, \Sigma w \, |F_o|^4 \,]^{1/2}$.

Table 13.2. Positional and Equivalent Displacement Parameters (B_{eq}) for $Li_4SrCa(SiO_4)_2$

	site symmetry	x	y	z	B_{eq} (Å^2)
Sr	m	0.0553(2)	0.23147(8)	3/4	0.72(3)
Ca	C_2	1/2	0	1/2	0.43(5)
Si1	m	0.4732(4)	-0.025392)	3/4	0.31(7)
Si2	C_2	0.0174(4)	1/4	0	0.36(7)
O1	m	-0.421(1)	-0.3128(6)	3/4	0.5(2)
O2	m	-0.203(1)	-0.0001(6)	3/4	0.6(2)
O3		0.3338(8)	0.0448(4)	0.6558(3)	0.5(1)
O4		0.2090(8)	0.3350(4)	0.9274(3)	0.6(1)
O5		-0.1782(9)	0.1503(4)	0.5616(3)	0.6(2)
Li1		-0.041(2)	-0.022(9)	0.8731(7)	0.1(1)
Li2		0.33333	0.66666	0.0700(2)	0.75(5)

$$B_{eq} = (\frac{8\pi^2}{3}) \sum_i \sum_j U_{ij} a_i^* a_j^* a_i . a_j$$

Results and Discussion

A view of the contents of the unit cell is given in Figure 13.1. The structure contains a 10-coordinate Sr atom, 6-coordinate Ca atom, a 4-coordinate Li atom, and a 4-coordinate Si atom. It contains layers of CaO_6 octahedra and SiO_4 tetrahedra bridged by Li_2O_7 polyhedra. By sharing edges, two Sr-centered polyhedra are bridged by Si-centered tetrahedra. The Si-centered tetrahedra and Ca-centered octahedra share vertices to form a three-dimensional framework that contains channels occupied by the Sr and Li atoms (Figure 13.2). Corner shared Li -centered polyhedra form a thick, two-dimensional substructure that extends in the plane (100) with the Ca and Si atoms lying between successive layers (Figure 13.3). The SiO_4 groups are isolated, one from the other.

Selected interatomic distances and angles are listed in Table 13.3. The Sr atom is 10-coordinate and is bound by two each of atoms O1, O2, O3, O4 and O5 in an environment that is best described as a bicapped square anti prism geometry. The Sr-centered polyhedron shares a triangular face comprised of atoms O1, O3, and O4 with the Li2-centered tetrahedron. The Sr-centered polyhedron shares edges O2··O4 with Li1 and O3··O5 with Ca. The Si-centered tetrahedra share an edge O1··O2 with the Sr-centered polyhedron. The corner shared Li_2O_7 units share faces with Sr-centered polyhedra on either

TABLE 13.3. Selected Interatomic Distances (Å) and Angles (°) for $Li_4SrCa(SiO_4)_2$.

Sr -O1	2.505(6)	O1-Sr-O1	144.0(2)
-O1	2.734(6)	O1-Sr-O2	79.6(2)
-O2	2.635(6)		86.6(2)
-O2	2.766(6)	O1-Sr-O3	135.8(1)
-O3 × 2	2.667(4)	O1-Sr-O4	98.1(1)
-O4 × 2	2.804(4)	O1-Sr-O5	73.7(1)
-O5 × 2	3.003(4)	O2-Sr-O2	166.2(1)
		O2-Sr-O3	69.4(1)
		O2-Sr-O4	116.95(8)
		O2-Sr-O5	64.95(8)
		O3-Sr-O3	59.5(2)
		O3-Sr-O4	70.8(1)
		O3-Sr-O5	116.9(1)
		O4-Sr-O4	125.6(2)
		O4-Sr-O5	171.3(1)
		O5-Sr-O5	123.8(2)
Ca -O3 × 2	2.384(4)	O3-Ca-O3	180
-O4 × 2	2.414(2)	O3-Ca-O4	93.0(2)
-O5 × 2	2.355(4)		87.0(1)
		O3-Ca-O5	77.3(1)
		O4-Ca-O4	180
		O4-Ca-O5	97.7(1)
		O5-Ca-O5	180
Si1 -O1	1.629(6)	O1-Si1-O2	108.1(3)

Table 13.3. (continued)

Si1 -O2	1.633(6)	O1-Si1-O3	110.4(2)
-O3 × 2	1.649(4)	O2-Si1-O3	110.6(2)
		O3-Si1-O3	106.8(3)
Si2 -O4 × 2	1.632(4)	O4-Si2-O4	108.4(3)
-O5 × 2	1.637(4)	O4-Si2-O5	109.3(2)
		O4-Si2-O5	111.5(2)
		O5-Si2-O5	106.9(3)
Li1 -O2	1.91(1)	O2-Li1-O3	102.3(5)
-O3	1.966(9)	O2-Li1-O4	100.4(4)
-O4	1.98(1)	O2-Li1-O5	106.0(5)
-O5	1.90(1)	O3-Li1-O5	104.7(4)
		O4-Li1-O5	108.2(5)
Li2 -O1	1.95(1)	O1-Li2-O3	106.6(5)
-O3	2.06(1)	O1-Li2-O4	101.9(5)
-O4	2.05(1)	O3-Li2-O4	101.0(5)
-O5	1.91(1)	O3-Li2-O5	96.5(5)

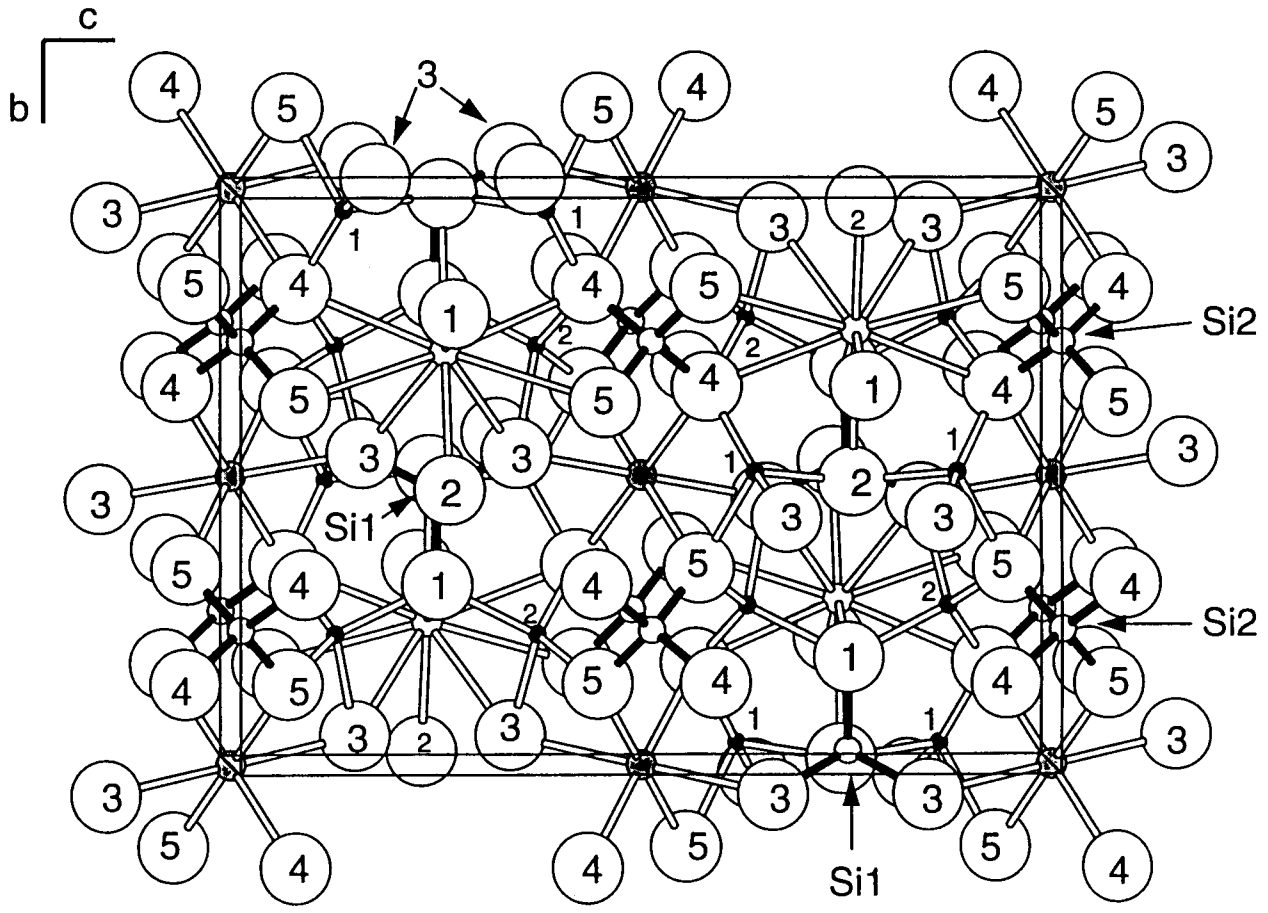

Figure 13.1. Unit cell diagram of $Li_4SrCa(SiO_4)_2$; view is along the *a* axis. Large open circles represent O atoms, small open circles represent Sr atoms, medium shaded circles represent Ca atoms, small filled circles represent Li atoms, small open circles represent Si atoms.

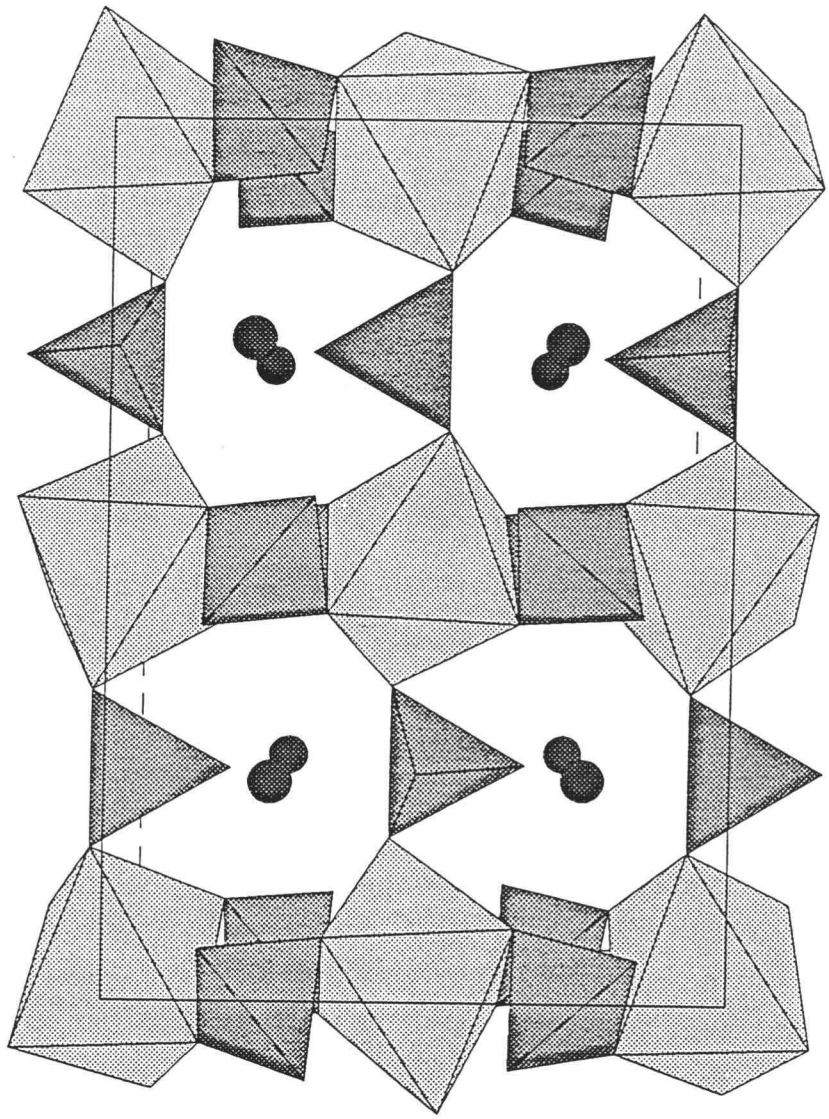

Figure 13.2. Polyhedral view of Ca- and Si-centered polyhedra. Dark polyhedra represent SiO_4 and shaded polyhedra represent Ca-centered polyhedra. Dark circles represent Sr atoms.

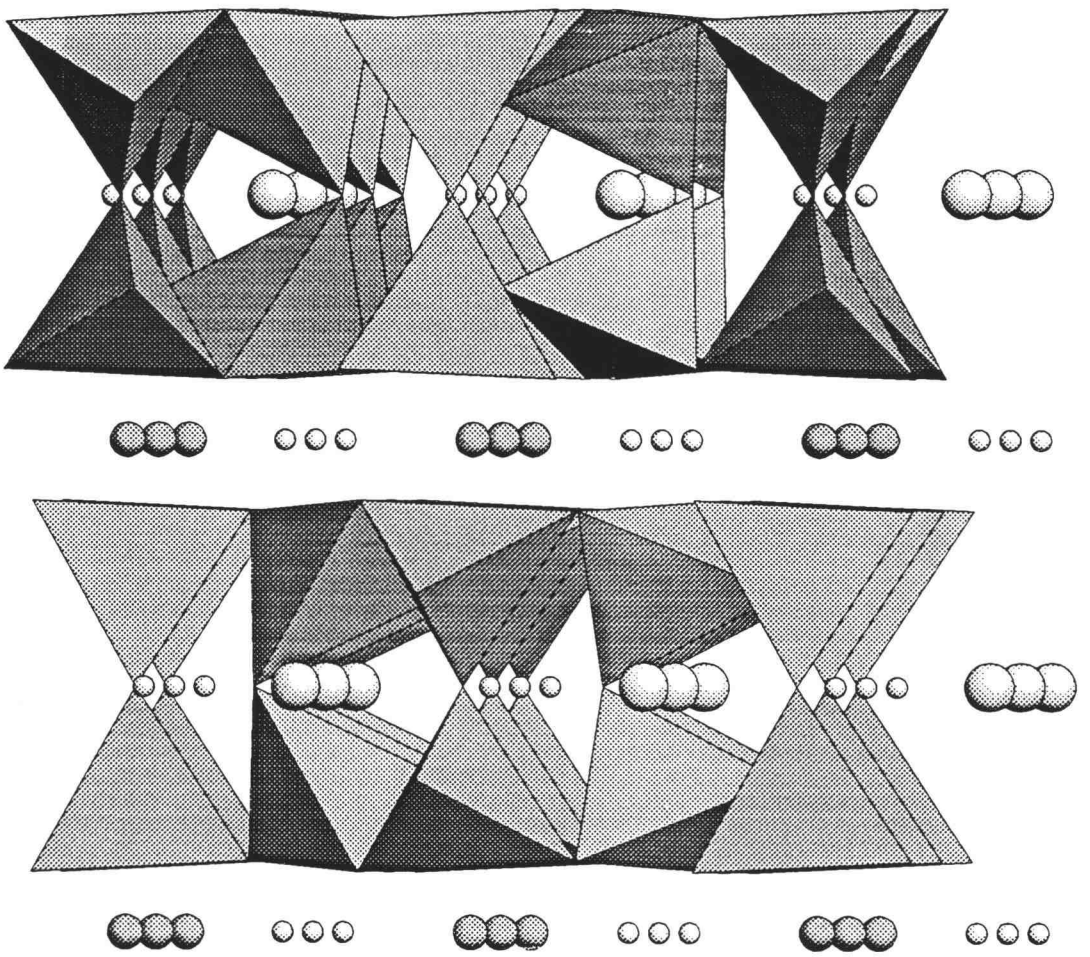

Figure 13.3. Polyhedral view of Li_2O_7 groups. Large circles represent Sr atoms, medium shaded circles represent Ca atoms, small circles represent Si atoms.

sides. Two adjacent Sr-centered polyhedra are bridged by Si1 tetrahedra; the Si1 shares edges O3··O3 and O2··O1 with Sr-centered polyhedra. The average Sr-O distance is 2.76 ± 0.16 Å, which compare to Sr-O distances of 2.711 and 2.859 Å for 10-coordinate Sr atoms in α'-Sr_2SiO_4.[6]

The Ca atom is coordinated to two each of atoms O3, O4, and O5 forming an octahedral geometry. The Ca atom shares corners O4 with Si2, Li2 and Sr atoms. Two adjacent Si2-centered tetrahedra are bridged by a Ca-centered octahedran where the edge O4..O5 serves as the bridge. Two adjacent Ca octahedra are bridged by Si1 tetrahedra through an O3 atom, otherwise the CaO_6 octahedra are isolated from each other. Thus the structure consists of layers of CaO_6 octahedra and $Si2O_4$ tetrahedra bridged by $Li1_2O_7$ polyhedra and $Si1O_4$ tetrahedra. The average Ca-O distance is 2.384 ± 0.026 Å, which compares to Ca-O distances of 2.30 - 2.44 Å for 6-coordinate Ca atoms in Ca_2SiO_4.[7]

There are two crystallographically distinct Li atoms, both are 4-coordinate. The Li1 atom is bound to one each of atoms O2, O3, O4 and O5 and the Li2 atom is bound to one each of atoms O1, O3, O4 and O5. The O2 and the O1 atoms serve as a corner for the corner sharing of the Li1- and Li2-centered tetrahedra to form the respective Li_2O_7 polyhedra. The Li1 atom shares a triangular face comprised of O1, O3 and O4 with Sr-centered polyhedron and Li2 shares an edge O2··O4 with Sr atom. The Li1 and Li2

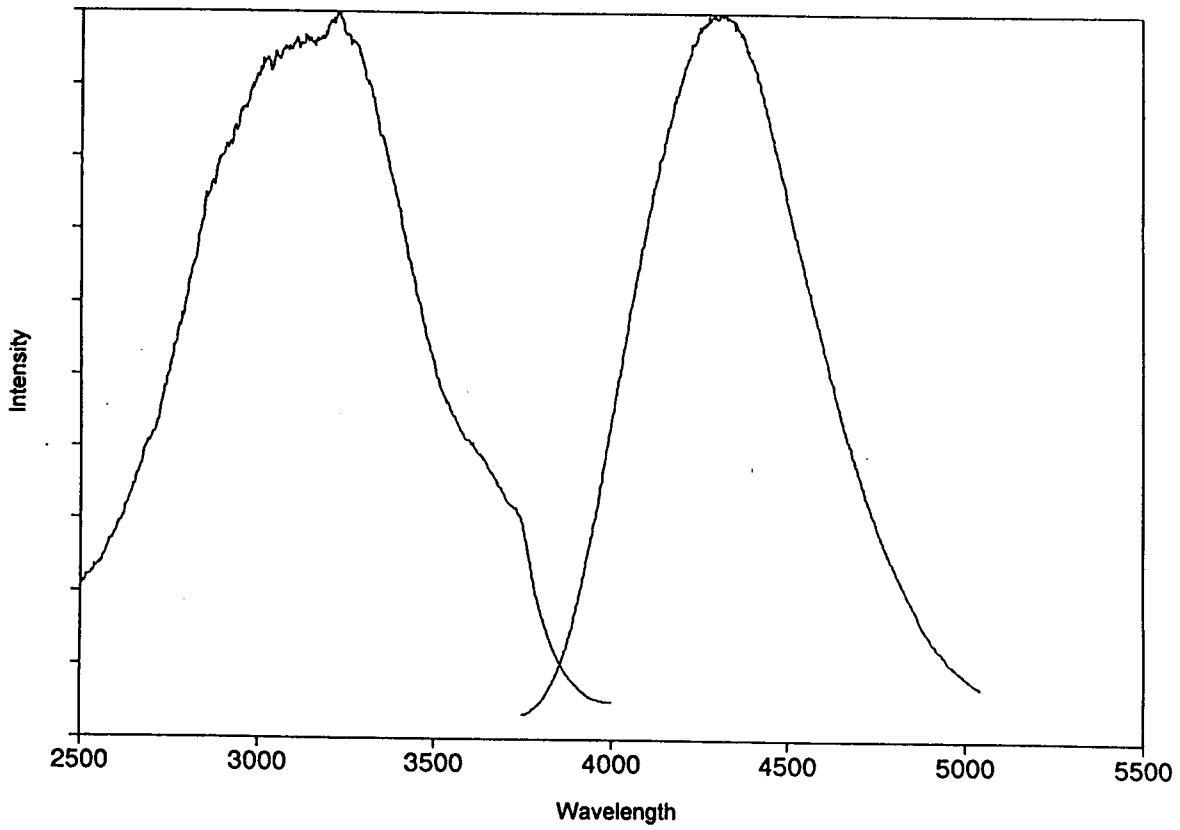

Figure 13.4. Emission and Excitation Spectra of the luminescence of $Li_4Sr_{1.98}Eu_{0.02}Ca(SiO_4)_2$ at 298 K.

polyhedra share corners to form chains that extend along the direction [010], and two such chains are bridged by SiO_4 and CaO_6 groups. The average Li1-O bond distance is 1.94 ± 0.04 Å, and the average Li2-O bond distance is 1.99 ± 0.07, and it compares well to the Li-O distances for 4-coordinate Li atoms in Li_2CaSiO_4,[8] 1.969 ± 0.014 Å, and Li_2O,[9] 1.997 Å.

There are two distinct Si atoms in the unit cell. The atom Si1 is bonded to one O1, one O2, and two O3 atoms. The atom Si2 is bonded to two O4 and two O5 atoms. The SiO_4 groups are isolated from each other. The average Si1-O bond distance is 1.640 ± 0.010, and the average Si2-O bond distance is 1.635 ± 0.003 both are normal, and all O-Si-O angles are near the tetrahedral value.

The composition $Li_4Sr_{1.98}Eu_{0.02}Ca(SiO_4)_2$ exhibits an intense emission under ultraviolet excitation. Excitation and emission maxima occur at 335 and 430 nm, respectively. The transition that can be assigned to the emission is the allowed transition $4f^65d^1 \rightarrow 4f^7$. The emission spectra are typically broad bands because of vibronic coupling with the host environment through the 5 d orbitals of the excited state. The position and shape of the 5d → 4f emission curve varies with crystal field strength and coupling of the ion with the host. Eu^{2+} has been shown to emit in a wide range from the uv to red.[10-11] The typical trend observed with Eu^{2+} is that as the crystal field strength of the host increases, the luminescence decreases in energy.[12] Typically Eu^{2+} when

substituting greater coordination sites tends to emit at higher energies. In the title compound, it appears that the Eu^{2+} ion is predominantly occupying the 10-coordinate Sr site.

Acknowledgments

This research was supported by National Science Foundation (DMR92-21372). Acknowledgment is made to the Donors of The Petroleum Research Fund, administered by the American Chemical Society, for partial support of the work.

References

1 Kotera, Y. *J. Jpn. Soc. Color. Mater.*, **1985**, *58*, 80.

2. Blasse, G., *Mater. Chem. Phys.* **1987**, 253.

3. TEXSAN: Single Crystal Structure Analysis Software, Version 5.0 **1989**. Molecular Structure Corp., The Woodlands, TX, 77381.

4. Sheldrick, G. SHELXS86. In *Crystallographic Computing 3*; Sheldrick, G.; Kruger,C.; Goddard, R.; Eds.; Oxford University Press: New York, **1985**; pp 175-189.

5. Walker, N.; Stuart, D. *Acta Crystallgr., Sect. A* **1983**, *39*, 158.

6 Catti, M.; Gazzoni, G.; Ivaldi, G.; Zanini, G. *Acta Crystallogr. Sect B* **1983**, *39*, 674.

7. Udagawa, S., Urabe, K., Natsume, M., Yano, T. *Cement Concr. Res.*, **1980**, *10*, 139-144.

8. Gard, J. A., West, A. R. *J. Solid State Chem.* 7, **1973**, 422-427.

9. Zintl, E., Harder, A., Dauth, B. Z. *Electrochem.*, **1934**, *40*, 588.

10. K.I. Schaffers, T.A. Reynolds, D. A. Keszler, *Inorganic Chemistry.*

11. G. J. Dirksen, G. Blasse J. Solid State Chem., **1991**, *92*, 591.

12. C. Fouassier, B. Latourrette, J. Portier, P. Hagenmuller *Mat. Res. Bull.*, **1976**, *11*, 993.

BIBLIOGRAPHY

Adams, J. M. *Acta Crystallogr., B* **1977**, *33*, 1513-1515.

Adams, J. M.; Pritchard, R. G. *Acta Crystallogr. B* **1976**, *32*, 2438-2440.

Adams, J. M., Pritchard, R. G. & Thomas, J. M. *Chem. Commun.* **1974**, 358-359.

Adams, J.M.; Small, R. W. H. *Acta Cryst. B* **1974**, *30*, 2191-2193.

Akella, A.; Keszler, D. A. *Acta Cryst. B* **1994a**, submitted for publication.

Akella, A.; Keszler, D. A. *Acta Cryst. B* **1994b**, submitted for publication.

Akella, A. Ph. D. Thesis, Oregon State University **1994**.

Akella, A., Keszler, D. A. *Main Group Metal Chemistry* **1994**, in press.

Alekel, T. A., Keszler, D. A. *J. Solid State Chem.*, in press.

Alekel, T. A., Keszler, D. A. *Inorganic Chemistry.*, **1993**, *32*, 101.

Ballman, A. A. *Amer. Mineral.* **1962**, 47, 1380; Fon, Y. X., Schlecht, R.,

Baucher, A., Gasperin, M. *Acta Crystallgr., Sect. B* **1976** *32*, 2211.

Baucher, A., Gasperin, M. *Mater.Res.Bull.* **1975** 469.

Blasse, G. *Philips Technical Review* **1970**, *31*, 309.

Blasse, G., *Mater. Chem. Phys.* **1987**, 253.

Bloss,F.D. *An Introduction to the Methods of Optical Crystallography*, Holt, Rinehart and Winston: New York, **1961**; pp 294.

Botden, Th. P. J. *Philips Res. Rept.* **1952**, *7*, 197.

Brown, I. D., Altermatt, D. *Acta Crystallogr., Sect B* **1985**, *41*, 244.

Bryden, J. H., *Acta Crystallogr.* **1957**, *10*, 677-680.

Burrus, H. L.; Nicholson, K. P.; Rooksby, H. P. *J. Lumin.* **1971**, *3*, 467.

C. Fouassier, B. Latourrette, J. Portier, P. Hagenmuller *Mat. Res. Bull.*, **1976**, *11,* 993.

Catti, M., Gazzoni, G., Ivaldi, G., Zanini, G. *Acta Crystallogr., Sect B* **1983**, *39*, 674.

Cerville, B., Cesbron, F., Berthou, J., Jolles, P. *Acta Crystallgr., Sect. B* **1974** *30*, 645.

Chai, B. H. T., University of Central Florida (private communication, June **1993**).

Chen, C. T. Sci. Sinica **1979,** *22*, 756; Chen, C. T., Liu, G. Z. *Ann. Rev. Mater. Sci.* **1986,** *16*, 203.

Chen, C., Wu, B., Jiang, A., You, G. *Sci. Sin., Ser B* **1985**, *28*, 235.

Chen, C., Wu, Y., Jiang, A., Wu, B., You, G., Li, R., Lin, S. *J. Opt. Soc. Am. Sect.* B, **1989**, *6(4)*,616.

Chen, C., Wu, Y., Jiang, B., Wu, B., You, G., Li, R., Lin, S. *J. Opt. Soc. Am. B* **1989**, *6*, 616.

Chen, C., Wu, Y., Li, Y. *J. Crystal Growth* **1990**, *99*, 790.

Cox, J. R. Ph.D. Dissertation, Oregon State University **1993**.

Cox, J. R., Huang, J. H., Keszler, D. A. *Chem. Mat.* **1993**, in press.

Cox, J.A.; Keszler, D.A. Unpublished results.

Crystal data for $Ba_3Sr_4(BO_3)_3F_5$: Rigaku AFC6R diffractometer, a = 10.853(1), c = 6.945 Å, V = 708.5 Å^3, space group $P6_3mc$, 1000 unique data, R = 0.043, wR = 0.056.

Crystal data for $Ba_7(BO_3)_3F_5$: Rigaku AFC6R diffractometer, a = 11.208(5), c = 7.250(2) Å, V = 788.7 (5) Å3, space group P31c, 745 unique data, R = 0.052, wR = 0.068.

Crystal data for $BaCaBO_3F$: Rigaku AFC6R diffractometer, a = 9.049(1), c = 4.326(1) Å, V = 306.74(8) $Å^3$, space group P-62m, 511 unique data, R = 0.062, wR = 0.075.

Crystal data for $CsNbOB_2O_5$: Rigaku AFC6R diffractometer, a = 7.527(2), b = 3.988(1), V = 291.7 Å3, space group $Pmn2_1$, 862 unique data, R = 0.023, wR = 0.029.

Crystal data for $CsTaOB_2O_5$: Rigaku AFC6R diffractometer, a = 7.548(1), b = 3.906(1), c = 9.771 (1) Å, V = 288.11(9) $Å^3$, space group $Pmn2_1$, R = 0.057, wR = 0.071.

Crystal data for $SrLi(B_3O_5)_3$: Rigaku AFC6R diffractometer, a = 10.610(1), c = 17,538(2)Å, V = 1709.9(4) $Å^3$, space group R3c, 433 unique data, R = 0.051, wR = 0.067.

Dirksen, G. J., Blasse, G. *J. Solid State Chem.* **1991**, *92*, 591.

Eckardt, R. C., Masuda, H., Fan, Y. X., Byer, R. L. *IEEE J. Quantum Electron.* **1990**, *26*, 922.

Eimerl, D., Davis, L., Velsko, S., Graham, E. K., Zalkin, A. *J. Appl. Phys.* **1987**, *62*, 1968.

Nikogosyan, D. N. *Appl. Phys. A* **1991**, *52*, 359.

Eimerl, D., Velsko, S., Davis, L., Wang, F. *Prog. Cryst. Growth Charact.* **1990,** *20*, 59.

For K derivative: Chai, B. H. T. University of Central Florida (private communcation).

Franken, P., Hill, A., Peters, C., Weinreich, G. *Phys. Rev. Lett.* **1961**, *7*, 118.

G. J. Dirksen, G. Blasse J. Solid State Chem., **1991**, *92*, 591.

Gard, J. A., West, A. R. *J. Solid State Chem.* 7, **1973**, 422-427.

Gasperin, M. *Acta Crystallgr., Sect. B* **1974** *30*, 1181.

Henderson, B., Imbush, G. F. *Optical Spectroscopy of Inorganic Solids*, Oxford Science Publications, **1989**.

International Tables for X-ray Crystallography. Vol. IV. Birmingham: Kynoch Press **1974**.

Itoh, K., Marumo, F., Kuwano, Y. *J. Cryst. Growth* **1990**, *106*, 728; Kouta, H.,

Kuwano, Y., Ito, K., Marumo, F. *J. Cryst. Growth* **1991,** *114*, 676.

Schaffers, K. I., T.A. Reynolds, D. A. Keszler, *Inorganic Chemistry.*

König, H., Hoppe, R., Z. Anorg. Allg. Chem. **1978**, *434*, 71.

Kotera, Y. *J. Jpn. Soc. Color. Mater.*, **1985**, *58*, 80.

Krogh-Moe, J. *Acta Crystallogr.*, Sect. B **1973,** *30*, 1025.

Krogh-Moe, J., *Acta Crystallogr., Sect.B,* **1974**, *30*, 1178.

Kurtz, S. W., Perry, T. T., *J. Appl. Phys.* **1968**, *39*, 3798.

Loiacono, G. Crystal Associates (private communication, August **1994**).

Mackie, P.E., Young, R. A. *J. Appl. Crys.* **1973**, *6*, 26-31.

Mandarino, J.A. *Can. J. Mineral.* **1976**, *14*, 498-502.

Molecular Structure Corporation, *TEXSAN*, Structure Analysis Package, MSC (3200A Research Forest Drive, Woodlands, TX 77381).

Mullen, D. & Hellner, E. *Acta Crystallogr.* B **1978**, *34*, 2789-2794.

Nadezhina, T. N., Pobedimskaya, E. A., Ilyukhin, V.V., Belov, N. V. *Sov. Phys. Crystallogr.* **1981**, *26*, 168.

O'Keefe, M., Hansen, S. *J. Am. Chem. Soc.* **1988**, *110*, 1506.

Pabst, A. *American Mineralogist.* **1973**, *58*, 211-217.

Pabst, A. *American Mineralogist.* **1974**, *59*, 353-358.

Qin, M. W., Luo, D., Jiang, A. D., Huang,Y. C. Technical Digest, *Advanced Solid-State Lasers*, **1992**, 311.

Sarkar, S., Schaffers, K. I., Keszler, D. A., unpublished results.

Saubat, B., Vlasse, M., Fouassier, C. *J. Solid State. Chem.* **1980**, 34, 271.

Saubat, S., Fouassier, C., Hagenmuller, P. *Mater. Res. Bull.* **1981**, *16*, 193.

Schaffers, K. I. Ph.D. Thesis Oregon State University **1993**.

Schaffers, K. I., Keszler, D. A. *Chem. Mat.* to be submitted.

Schaffers, K. I., Keszler, D. A. *J. Solid State Chem.*, **1990**, *85*, 270.

Schlager, M., Hoppe, R. *Z. Anorg. Allg. Chem.* **1993**, *619*, 976.

Shannon, R. D. *Acta Crystallogr., Sect. A* , **1976**, *32*, 751.

Sheldrick, G. M. in "*Crystallographic Computing 3*" (Sheldrick, G.M., Kruger, C., Goddard, R.), pp 175-189, Oxford Univ. Press, Oxford **1985**.

Walker, N.; Stuart, D. *Acta Crystallgr., Sect. A* **1983**, *39*, 158.

Siverman, S. M., Balmer, M. K. *J. Am. Ceram. Soc.* **1971**, *54*, 98.

Smith, R. W., Keszler, D. A. *Mater. Res. Bull.* **1989**, *24*, 725.

Sun, H., Keszler, D. A. *Acta Crystallogr., Sect. C*, **44** (1988), 1505.

Takeuchi, Y. *Acta Crystallogr.* **1952**, *5*, 574.

Thompson, P. D., Huang, J., Smith, R. W., Keszler, D. A. *J. Solid State Chem.* **1991**, *95*, 126.

Thompson, P. D., Keszler, D. A. *J. Solid. State. Chem.*

Thompson, P. D., Keszler, D. A. *Solid State Ionics* **1989**, *32/33*, 521.

Touboul, M. *Compt. Rend., Sect. C* **1973,** *277*, 1025; Gasperin, M., *Acta Crystallogr., Sect. B* **1974,** *30*, 1181.

Tu, J. M., Keszler, D. A. *Acta Crystallogr., Sect. C* **1994,** in press.

Tu, J., Keszler, D. A. unpublished results.

Udagawa, S., Urabe, K., Natsume, M., Yano, T. *Cement Concr. Res.*, **1980**, *10*, 139-144.

Velsko, S. P. in Materials for Nonlinear Optics: Chemical Perspecties, ACS Symposium Series No. 455, edited by Marder, S., Sohn, J., Stucky, G. (Washington DC: Am. Chem. Soc., **1991**) 343.

Verstegen, J. M. P. J. *J. Electrochem. Soc.* **1974**, *121*, 1631.

Walker, N.; Stuart, D. *Acta Crystallgr.*; *Sect. A* **1983**, *39*, 158.

Wanmaker, W. L.; Verriet, J. G. *Philips Res. Rep.* **1973**, *28*, 80.

Weber, M. J. *CRC Handbook of Laser Science and Technology*, "Section 1: Nonlinear Optical Materials", Boca Raton, Fla.: CRC Press, **1986**.

Weller, T. *J. Lumin.* **1991**, *48 & 49*, 49.

Wheeler, R. A., Whangbo, M-H., Hughbanks, T., Hoffmann, R., Burdett, J. K., Albright, T. A. *J. Am. Chem. Soc.* **1986** *107*, 2222.

Yimmermanns, C. W. M., Blasse, G. *J. Solid State Chem.* **1984**, *52*, 222.

Yvon, K., Jeitschko, W., Parthe, E. *J. Appl. Crystallogr.*, **1977**,*10*, 73.

Zintl, E., Harder, A., Dauth, B. Z. *Electrochem.*, **1934**, *40*, 588.

Zubay, G. *Biochemistry* Macmillan Publishing Company: New York, II Edition 1988.

APPENDICES

Appendix 1

The Hexagonal Silicate $Li_2BaCaSi_2O_7$: The title compound was discovered during our attempts to prepare the compound $LiBaCaSiO_4F$. Initially when the structure was solved the stoichiometry was assigned as $Li_3BaCaSiO_4F_3$. But this formula was inconsistent with the negative displacement coefficient associated with the Li atom. After refining the multiplicity of the Li atom and examining difference electron-density maps the site was modeled with partial occupancy by both Li and Si. The absence of F is necessary for charge compensation in the structure. The final stoichiometry, which is consistent with microprobe analysis and the X-ray data, is $Li_2BaCaSi_2O_7$. The experimental and crystal parameters are listed in Table A1.1. and the atomic parameters are listed in Table A1.2. The residuals after final least-squares refinement of the anisotropically refined model are R = 0.039 and R_w = 0.052.

A [100] view of the unit cell is depicted in Figure A1.1. The structure contains one 12-coordinate Ba, a 6 coordinate Ca atom, and 4-coordinate Li and Si atoms. The Li site is disordered with Si2. The CaO_6 octahedra are isolated from each other and connected through Li- and Si2 tetrahedra. The BaO_{12} polyhedra share edges.

Table A1.1. Crystallographic Data for $Li_2BaCaSi_2O_7$.

chem formula	$Li_2BaCaSi_2O_7$
fw, u	380.28
crystal system	Hexagonal
space group	$P6_3mc$ (No. 186)
a, Å	6.0737(9)
c, Å	9.9599(9)
V, $Å^3$	318.19 (9)
Z	2
ρ_{calc}, g cm^{-3}	3.969
radiation	Mo Kα[a]
temp, K	298
linear abs.coeff μ, cm^{-1}	1.98
transm.factors	0.87 -1.19
R, R_w[b]	0.039, 0.052

[a] Graphite monochromated; λ = 0.71069 Å. [b] $R = \Sigma \, | \, |F_o| - |F_c| \, | \, / \, \Sigma \, |F_o|$;

$R_w = [\, \Sigma w \, (|F_o|^2 - |F_c|^2)^2 \, / \, \Sigma w \, |F_o|^4 \,]^{1/2}$.

Table A1.2. Positional and Equivalent Displacement Parameters (B_{eq}) for $Li_2BaCaSi_2O_7$.

	x	y	z	B_{eq}
Ba	2/3	1/3	0.8821	1.35(3)
Ca	2/3	1/3	0.5064(4)	0.71(9)
Si1	0	0	0.942(1)	2.2(2)
Si2	0.8338	-0.8338	0.1959	0.71
Li	0.8338(5)	-0.8338	0.1959(8)	0.71(8)
O1	0.5034	-0.5034	0.136(2)	3.1(2)
O2	0.1520(7)	-0.1520	0.871(2)	2.5(4)
O3	0	0	0.117(3)	2.5(5)

$$B_{eq} = (\frac{8\pi^2}{3}) \sum_i \sum_j U_{ij} a_i^* a_j^* a_i . a_j$$

Appendix 2

Phosphate and Vanadate Analogs of $Li_3BaCaSiO_4F_3$: The stoichiometries $Li_3KCaPO_4F_3$, $Li_3KCaVO_4F_3$, and $Li_3BaCaGeO_4F_3$ were prepared with the knowledge that the parent silicate fluoride had the stoichiometry $Li_3BaCaSiO_4F_3$. The actual stoichiometries and structures of the materials remain under investigation in the Keszler lab. Microprobe results indicate that the ratio of K : Ca : P is 1 : 1 :1 for the phosphate derivative. The structural parameters and the probable space groups for these compounds are listed in Table A2.1.

Table A2.1. Structural Parameters for "$Li_3KCaMO_4F_3$" (M = P, V), and "$Li_3BaCaGeO_4F_3$".

	"$Li_3KCaPO_4F_3$"	"$Li_3KCaVO_4F_3$"	"$Li_3BaCaGeO_4F_3$"
Crystal System	hexagonal	hexagonal	rhombohedral
Space Group	P 6_3 m c	P 6_3 m c	P 3_1 2 1
a (Å)	6.078(2)	6.191(2)	5.894(4)
c (Å)	9.895(3)	10.123(3)	22.381(3)
V (Å^3)	316.63(2)	336.06(3)	673.40(3)
Z	2	2	4

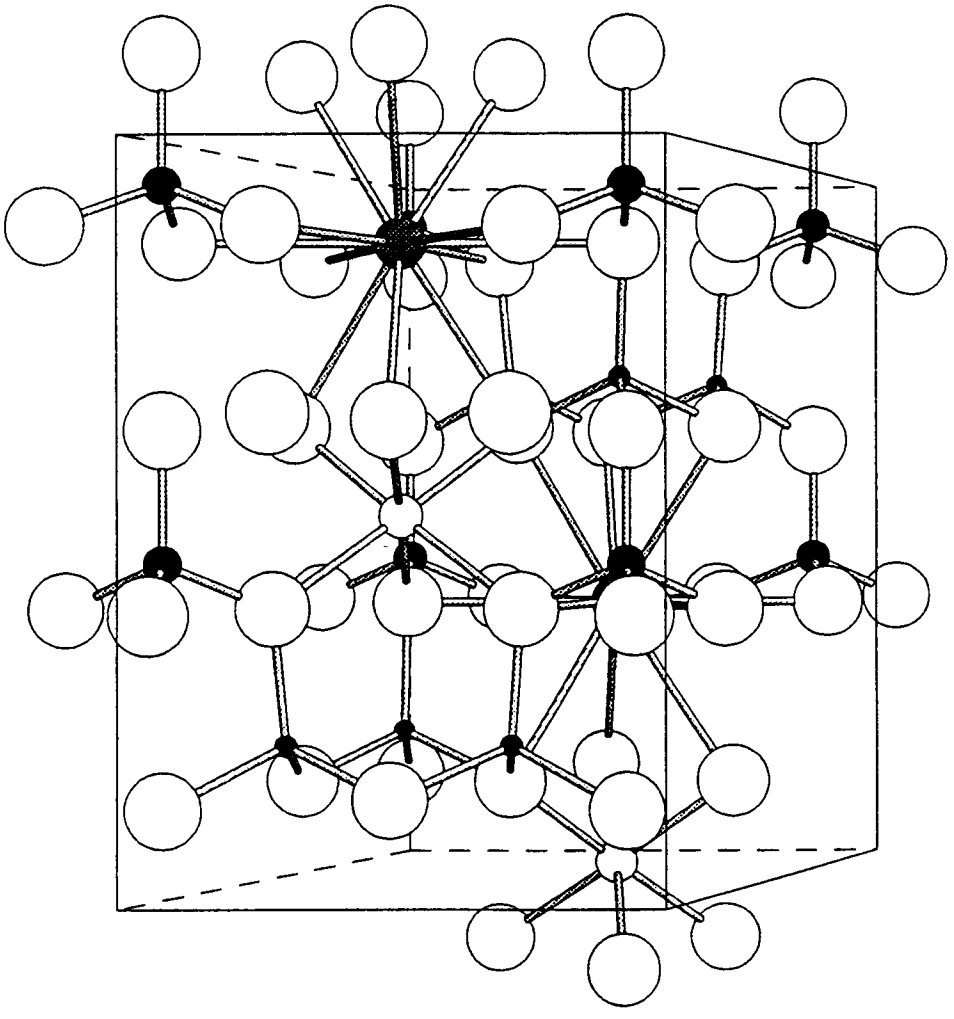

Figure A.1.1. Unit cell diagram of $Li_2BaCaSi_2O_7$; view is orthogonal to the c axis. Medium shaded circles represent Ba atoms, medium open circles represent Ca atoms. Medium filled circles represent Li atoms, small filled represent Si atoms. Large shaded atoms represent O atoms.

CURRICULUM VITAE

ANNAPOORNA AKELLA

Education:

Ph.D. Chemistry, Oregon State University, Corvallis OR. 1992-1994
Major in Solid-State Materials / Inorganic Chemistry

M.S. Organic Chemistry, Oregon State University, Corvallis, OR. Aug 1991
Dissertation: "Macrolactonization of ω-Hydroxy Acyl Xanthates"

M.Sc. Chemistry, University of Hyderabad, Hyderabad, India April 1988
Dissertation: "Quadrupole Antishielding Factors for F^-, Cl^- and Br^- using Ξ a - Theory"

B.Sc. Physical Sciences, Osmania University, Hyderabad, India June 1986

Publications:

Annapoorna Devi; Sen, K. D. "Quadrupole Antishielding Factors for F^-, Cl^- and Br^- using Ξ a - Theory", *Physical Review A*. **1988**.

Keszler, D. A.; Akella, A.; Schaffers, K. I.; Alekel, T. "New Borate Structures For NLO Applications" *Mat. Res. Soc. Symp. Proc.* **1994**, *329*, 15-22.

Akella, A.; Keszler, D. A. "The Buetschliite Derivative $K_2Zr(BO_3)_2$" *Inorganic Chemistry*, **1994**, *33*, 1554.

Akella A.; Keszler, D. A. "Crystal Structure of Aminoguanidinium Formate" *Acta Crystallographica*, submitted.

Akella, A.; Keszler, D. A. "Crystal Structure of

Aminoguanidinium Tartarate" *Acta Crystallographica*, submitted.

Akella, A.; Keszler, D. A. "Structure of Aminoguanidinium Nitrate" *Acta Crystallographica*, submitted.

Akella, A.; Keszler D. A. "Crystal Structure of Aminoguanidinium Bicarbonate" *Acta Crystallographica*, submitted.

Akella, A.; Keszler D. A. "Crystal Structure and Luminescence of the Nonlinear Optical Material $BaCaBO_3F$" *Chemistry of Materials*, in preparation.

Akella, A.; Keszler, D. A. "Crystal chemistry of Nb and Ta Pyroborates " *Journal of Solid State Chemistry*, in preparation.

Akella, A.; Keszler, D. A. "Crystal Structure of the Borate Fluoride $Ba_3Sr_4(BO_3)_3F_5$" *Chemistry of Materials*, in preparation.

Akella, A.; Keszler, D. A. "Sr_2LiSiO_4F"Synthesis, Structure, and Eu^{2+} luminescence". *Chemistry of Materials submitted.*

Akella, A.; Keszler, D. A. "The polyborates $BaMB_9O_{15}$ (M = Li, Na)"*Journal of Solid State Chemistry*, in preparation.

Akella, A.; Keszler, D. A. "Structure and Eu^{2+} luminescence of dibarium magnesium orthoborate" *Material Research Bulletin*, in press.

Akella, A.; Keszler, D. A. "Crystal structure of $Ba_2Ca(BO_3)_2$" *Main Group Metal Chemistry*, in press.

Akella, A.; Keszler, D. A."Structure and Eu^{3+} luminescence of $Sr_4Ge_2O_7F_2$" *Chemistry of Materials*, submitted.

Akella, A.; Keszler, D. A."Structure and Eu^{2+} luminescence of $Li_4SrCa(SiO_4)_2$" *Inorganic Chemistry*, submitted.

Akella, A.; Keszler, D. A."Crystal structures of noncentrosymmetric silicate $Li_2BaCaSi_2O_7$ and the phosphate and vanadate analogs." *Chemistry of Materials*, in preparation.